Fall 2022

Self-Assembling Porous Supramolecular Networks Capable of Post-synthetic Modification With a New Approach to Reticular Design With Semiconductor Potential

Steven A. Sloope

Self-Assembling Porous Supramolecular Networks Capable of Post-Synthetic Modification with a New Approach to Reticular Design with Semiconductor Potential

by

Steven A Sloope

Bachelor of Science
University of South Carolina, 2016

Submitted in Partial Fulfillment of the Requirements

For the Degree of Doctor of Philosophy in

Chemistry

College of Arts and Sciences

University of South Carolina

2022

Accepted by:

John J. Lavigne, Major Professor

Qian Wang, Committee Member

Dmitry V. Peryshkov, Committee Member

Christopher Williams, Committee Member

Cheryl L. Addy, Interim Vice Provost and Dean of the Graduate School

DEDICATION

To my family and friends. Without my mother and father, I could not have been able to even make it to graduate school. Mom and Wayne, you have been absolutely, the most understanding, caring and outwardly helpful and I will fulfill the goals I have told you that I intend. My siblings have also been there for me and there is a lot of you! It can be therapeutic that each and every one of you may come from a different walk of life but have always supported me. I want thank Lawrence, Sara, Catherine, Daniel and Elizabeth. I also cannot leave out Audrey, Anne, Mike, Nick, Savannah, Andrew, and Annabelle. I do need to give a shout out to Daniel for literally being the reason that the first figure in Chapter 5 exists and can only thank you enough for time you spent working on it and all the other things you have done to help me.

I also have another family in the form of my friends. First and foremost, to the good men I met during our tumultuous days. Stephan, Will H., Will M., Rob, Evan, John H., and Jon L. I also want to thank ones I met along the way through you or the friends I met much later in life who still have rooted for me during the good times and the bad. As they say, “It’s not called a PhD for nothing.” In good mention I would like to thank Stephen Davis, Chris Harrison, Brice and Shelley Mann and their families along with those of you at the Scheel establishment for giving me a place to study, write, and grade in a good atmosphere.

ACKNOWLEDGEMENTS

I want to thank Dr. John Lavigne. He allowed me to join his lab which let me realize my love for synthesis and the language that is organic chemistry. I also owe a lot of gratitude to Dr. Wiskur who has been incredibly helpful in many ways. I am very gracious for both of you and consider you to be true friends. I would also like to thank Dr. Wang, Dr. Peryshkov, and Dr. Williams for helping me go through the steps to achieve this goal and to ones who coached me and wrote letters of collaboration for multiple grant proposals, Dr. zur Loye, Dr. Garashchuk (the quantum Mom), and Dr. Greytak. Other professors that had impact were Dr. Shustova, Dr. Berg, Dr. Lovelace, and Dr. Bryson. Anna, Shawna, Erin, Grace, Christian, and James you made this endeavor more bearable. And lastly, I could never forget the undergrad army. Luke, Ian, Priscilla, Hadi, Josh, Cole, and Ashley, I could not have worked on these projects without you. Also, Nathan and Kenzie, it was a joy to have you in lab. I thank each and every one of you for being a part of this.

,

ABSTRACT

In past decades, research in self-assembling supramolecular frameworks have been produced with vast surface area, inherent from their porous nature. Predesigning monomers in a reticular manner allows a framework's structure to be known before self-assembly occurs. This is very helpful since high porosity is sought after for many purposes such as hosting guests within the framework, post-synthetic modifications, sensing and detection, selective catalysis, semiconduction, etc. Methods of design usually focus on forming intrinsic porosity and unfortunately, sometimes the network formed is not as expected and porosity is lost.

In Chapter 1, we discuss novel ways of network formation, their potential pitfalls from reticular design, and the idea of using recyclable materials to form extrinsically porous supramolecular networks. Also included is the introduction of our new approach to solving the issues that arise in reticular design.

Chapters 2, 3, 4 consists of extrinsically porous and robust single crystalline networks formed from the same recyclable diboronate ester and pyridyl linker. Chapter 2 focuses on a coordinated polymer network in which post-synthetic modification is performed using single crystal to single crystal (SCSC) transitions which replace the guests within the host and change the framework's structure. Also included is an investigation of enthalpic binding strength to answer the reversibility seen. Chapter 3 discusses using

these materials to form frameworks having different characteristics and structures arising from solvent driven origins. Chapter 4 also uses these materials in which a crystalline network forms from interdigitating macrocycles. This framework is capable of irreversible SCSC transitions that must occur in a stepwise manner which creates products that cannot be formed with typical procedures.

Chapter 5 presents a new approach to synthesize highly porous supramolecular covalent organic frameworks that are fully conjugated in every direction to have semiconductor potential. This effort for multiscale porosity uses a three-dimensional intrinsically porous bicyclic cage starting material that can dynamically bond to form azodioxide bridges capable of extending electron communication in every direction and expected to be in single crystal form. This approach also comes with guidelines to force the product to follow the reticular design while blocking chances of interpenetration which counters the efforts given for high porosity.

Chapter 6 discusses future directions in research for future graduate student and undergraduate researchers.

TABLE OF CONTENTS

LIST OF TABLES

LIST OF FIGURES

LIST OF SCHEMES

LIST OF SYMBOLS AND ABBREVIATIONS

Å …… Molecular unit of measurement

COF …… Covalent Organic Framework

CP1 …… Coordination Polymer One

CP2 …… Coordination Polymer Two

CP3 …… Coordination Polymer Three

CP4 …… Coordination Polymer Four

DE1 …… Diboronate Ester One

Dram …… Unit of volume

DSC …… Differential Scanning Calorimetry

IPN …… Interpenetrated Network

J …… Joule

mmHg …… Millimeter's mercury

MOF …… Metal Organic Framework

M_S …… Molecular weight

NMR …… Nuclear Magnetic Resonance

PXRD …… Powder X-ray Diffraction

R …… VCP1 retained CP1 crystallinity through benzene vapor absorption

SCSC …… Single Crystal to Single Crystal

TGA …… Thermogravimetric Analysis

V …… CP1 transition to VCP1 through benzene removal

XRD …… X-ray Diffraction

ΔHs …… Enthalpy of binding

ΔH_{sExp} …… Experimental Enthalpy of Binding

$\Delta m_s\%$ …… Experimental mass percent

π …… Pi orbital

CHAPTER 1: SUPRAMOLECULAR POROSITY

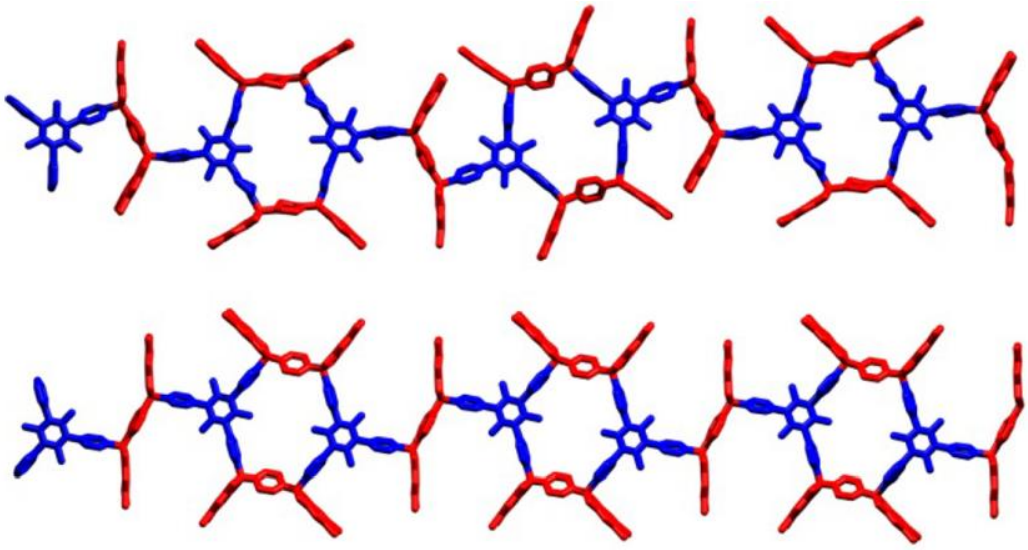

Figure 1.1: The Severin group went through crystal databases to look at bond angles of boron nitrogen coordination adducts. This was to study the effects that different derivatives of boronate esters and pyridyl linkers had on bond angles. This large effort was to synthesize their own compounds that would effectively engineer control whether the crystalline product would be a polymer or a macrocycle. This route proved to not work as expected. Above is a polymer that also contains macrocycles which is the opposite of their goal from their study.[25]

1.1 Overview

In recent decades a large amount of focus has been placed in the creation of supramolecular porous materials due to the versatile properties they can hold. For example, since the late 1700's, zeolites have been known capable of dehydration after being heated to a temperature that forces the precursing water bound guests from the pores they were originally hosted in. Once this occurred, the zeolites were then capable of absorbing a range of small and even dangerous compounds.[1] Though chemistry was

not understood at this time, the first inorganic supramolecular sequestration had been discovered. Furthermore, at present day in the field of inorganic chemistry, zeolites have been used for many applications with another specific example being carbon fuel emissions. In this application, zeolites are capable of effectively breaking down unconsumed organic compounds that are harmful to the environment to a safer form.[2]

Sequestration is traditionally grouped with separation and sensing as motivation for developing materials that have additional applications as a result of their supramolecular porous nature but there are also new focuses such as single crystal to single crystal (SCSC) transitions[3–6]. These transitions can occur to which a guest compound within a crystalline host can be added, removed or even exchanged through a liquid or vapor.[6–8] Other types of these SCSC transitions occur by topochemical polymerizations or stereoselective isomerization, both which are mainly induced by wavelength or heat.[9–12] More recently, application for the porous materials mentioned include stereospecific catalysis in which the pore of a framework where a specific is guest is hosted is then reacted which produces outcomes based on the constraints of the reaction matrix.[13,14] Another utilization of porosity is research on persistent radicals which alone can provide insight on how stereoselective catalysis within a pore occurs giving possible mechanistic insight into how the catalysis occurred.[15,16] This insight could shed light on new designs of porous frameworks that could improve efficiency, selectivity and elucidate new directions for the future.

Reticular design has been used more recently to create self-assembling porous materials in a manner that molecular porosity is controllable and supramolecular networks form in a predictable manner. Organometallic chemists, during the late 1990's, were the first to focus in planning new porous materials for the same applications previously mentioned. These metal organic frameworks (MOFs) are synthesized by capitalizing on a covalently bonded organic linker's ability to coordinate with a metal's three-dimensional orbital geometry which yield high porosity and are often single crystalline. To this day over 90,000 MOFs have been produced and over 500,000 have been predicted.[17] When these MOFs are formed in a robust single crystalline manner, long range order exists infinitesimally allowing characterization to have much less error and isolation can be an ease as opposed to when this is not the case.

In the field of organic chemistry, this same reticular design used to synthesize MOFs has been pursued since the early 2000's in the effort to form covalent organic frameworks (COFs) and supramolecular networks in which hydrogen bonding allows macrocycles to stack upon one another in a manner that a large intrinsic pore is created within the stack.[18,19] For the case of COFs, this effort also yields highly mesoporous materials in which the pore size can be controlled, having a direct effect on surface area.[18] This approach to create these is through derivatives that can self-assemble due to dynamic bonding such that predicted and covalent bonded structure occurs which mirrors the reticular predesign. Though the COF's have a significant weight reduction when compared to MOFs which is inherent without use of metals, unfortunately single crystallinity in COFs is rare.[20,21] With that being said, recent advances have created a few

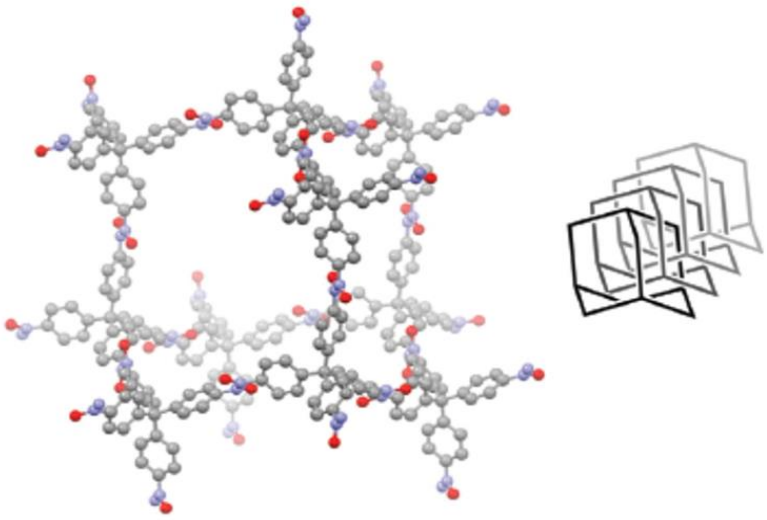

Figure 1.2: The nitroso outfitted macrocyclic adamantine cage that was able to self-assemble into a tree-dimensional COF that was also single crystal. To the right of the cage is view of how the crystal structure existed as an inner penetrated network.[24]

single crystalline COFS but in general. the products are still microcrystalline and x-ray diffraction (XRD) becomes effectively useless in determining the crystal structure.[22–24] Powder x-ray diffraction (PXRD) can be used to elucidate the crystal structure by using simulations from PXRD data. This lack or crystallinity seen in virtually most COFs comes from the nature that the dynamic bonding occurs during the frameworks formation which MOFs are much less prone to having.

The lines can blur when just viewing different approaches and can further overlap when comparing them to other fields of chemistry. For instance, coordinated materials can create crystalline and self-assembling polymers, macrocycles, and a mixture of both. It has also been seen that large effort can go into the design of self-assembling materials in a reticular way that usually is a great method to achieve porous materials, but sometimes the thermodynamics of the system do not allow the expected result if the product obtained is at a lower energy than what had been planned. One specific example

(Figure 1.1) is when the Severin group went through crystal databases to look at bond angles of boron nitrogen coordination adducts.[25] This was to study the effects that different derivatives of boronate esters and pyridyl linkers had on bond angle. This extensive effort was to help them synthesize their own compounds and effectively engineer and control whether the crystalline product would be a two-dimensional network or different cages. This direction proved to not work as expected because they created products that were not intended as well as one that was a mix of intended expectations. One of their results was a polymer that also contains macrocycles and others had open valences located on the pyridyl derivatives used which was the opposite of their goal from their study **(Figure 1.1)**.[25] Another issue with large polymer frameworks is interpenetrated networks (IPN) in which the synthetic goal was to possibly have porosity, but the three dimensional framework(s) assembled in a way that creates bonds that interlace within the originally expected connectivity, essentially filling it.[24] A recent example of this can be seen by the Wuest Group **(Figure1.2)** in which they created adamantine like building blocks that were outfitted with nitroso functional groups that can dynamically bond to form azodioxide bridges. They did achieve the synthesis of three-dimensional COFs that were also single crystal, a feat in itself, but the IPN seen for the COFs created a complete lack of porosity.[24] As Aristotle said, "nature abhors a vacuum." If a large amount of effort was given to design and synthesize new derivatives in the expectation of creating a highly porous framework, it would be quite frustrating to have the opposite occur. This does highlight another pitfall in the reticular method another

question could be asked. If you can't always have what you want, with a different outlook, you might still might find, you get what you need.

Lastly, a newly driven field of research for porous organic supramolecular frameworks is organic electronic and optoelectronic materials porosity in which carbon-based frameworks could pass current efficiently throughout. This is important for the field due to the possibility of doping guest compounds within the pores to change the optoelectronic characteristics of a host. Higher porosity leads to higher dopant density and facile customizability of conductive materials that are lighter weight in the application of higher efficiency OLED's, solar cells, batteries, etc.[5,26–29]

Porosity in these materials can be viewed as many different angles such as intrinsic porosity, extrinsic porosity, and frameworks possessing both at the same time. Intrinsic porosity is usually predesigned in a reticular way and is typically found in two-dimensional or three-dimensional COFs/MOFs, and also macrocycles.[24,30,31] Though reticular driven porosity of any type is usually a planned design, it also may occur with expectation or planning. This is the porosity that can exist by encapsulating a solvent molecule(s), a starting material that did not react but instead became held within the framework during self-assembly or just simply be a void created spontaneously during network formation.[32]

Throughout this text, a discussion will take place that utilizes different views on which direction/synthetic design method chosen could lead to the intended supramolecular porous material. With a thorough examination of research outcomes, intrinsic and extrinsic porosity will be reviewed in a fashion that may not focus on reticular

design. Then reticular chemistry will then be discussed in detail with a possible solution to the pitfalls that can come with it including the one already mentioned.

1.2 Donor Acceptor Coordination Chemistry

In the context of materials design that is seen throughout literature, all that is needed is an electron donor and an electron acceptor for a coordinate bond to occur. This type of chemistry comes in many forms but in general coordination bonds are broadly categorize by an adduct forming between two entities that is reversible and essentially must consist of a Lewis acid and a Lewis base.[33–38] Considering this idea comes from a sophomore understanding of organic chemistry, it should be expected that the literature list could be extensive and virtually endless. The donor-acceptor chemistry that will be discussed moving forward will consist of dynamically bonded and coordinated donor amines and acceptor boronic species.

1.3 Supramolecular Boronates

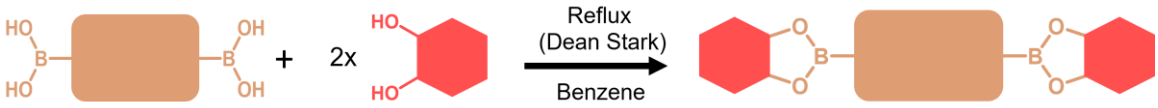

Scheme 1.1: Synthetic scheme of a diboronic acid and two equivalents of catechol forming a diboronate ester through a condensation reaction.

Over time, there has been a growing interest in boron's interactions with other compounds. Due to having only three valence electrons, the neutral form lacks a full octet which leaves a p orbital empty. This electron void allows for many types of interactions to occur once in the presence of a Lewis base. Boron is truly the odd entity of its period to which it can act as a metalloid, leading it to be useful for coordinated (dative) bonding. This is one reason it is widely used in industry and research in fields such as catalysis,

sensing and detection, frustrated Lewis pairs, and facile materials synthesis.

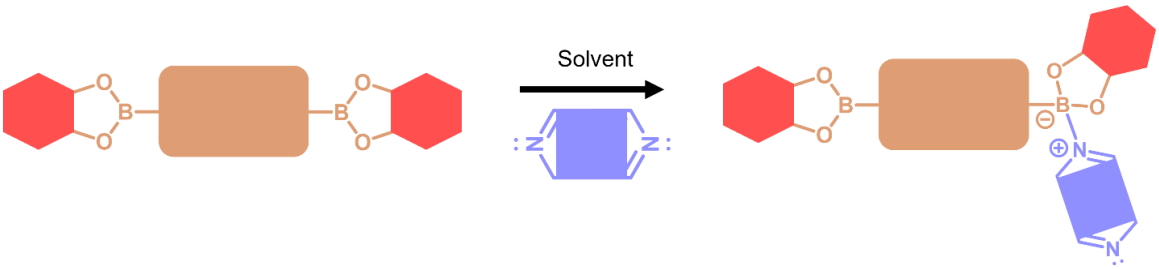

Figure 1.2: Synthetic scheme of a dipyridyl linker interacting with the empty π orbital of one of the boronate esters.

When a boronic acid undergoes a condensation reaction with a diol, a boronate ester is formed. Specifically, when the boronic acid is functionalized on an aromatic and it reacts with a catechol or catechol derivative, the boronate ester allows for extended conjugation between both aromatics it holds together. This means that this type of boronate ester is planar **(Scheme 1.1)**. Even if rings of the ester's aromatics were to be functionalized with other substituents, an electron donor could still bond from either side and since this bond is considered dynamic or reversible, eventually the bonding will occur to which it is the lowest in energy. With an understanding that coordination chemistry is a very large part of boron acid/base chemistry, two specific roles within coordination interactions will be heavily discussed in this text to which one is the donation of electrons from a pyridyl linker to an electron accepting diboronate ester **(Scheme 1.2)**.[25,32–34,39]

1.4 Supramolecular Azodioxide Bridged Frameworks

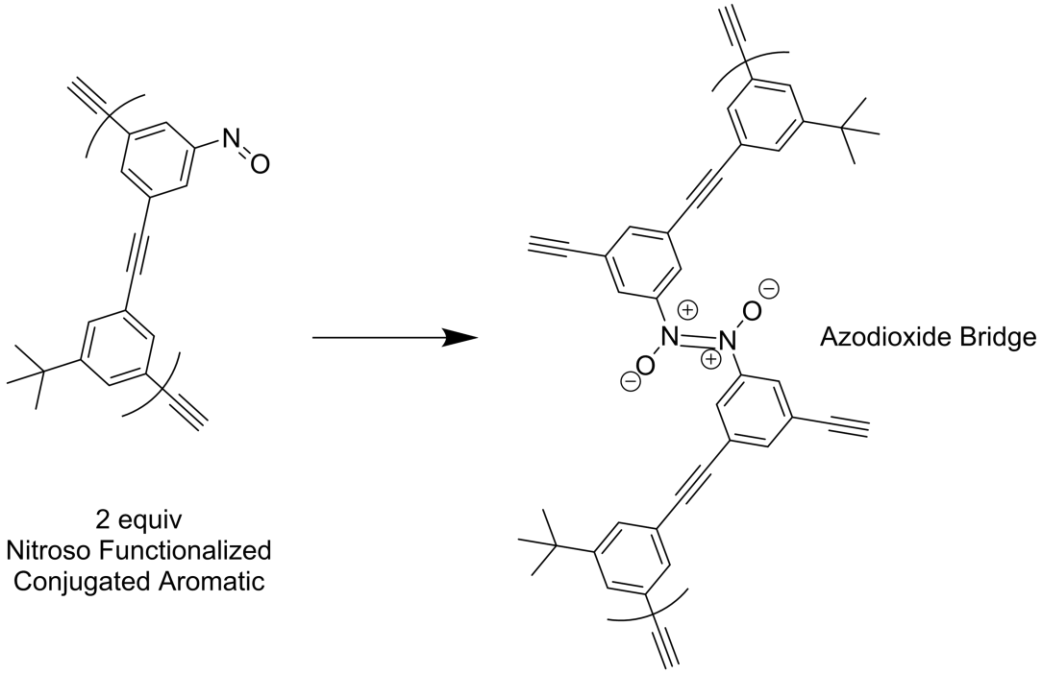

Scheme 1.3: Synthetic scheme of two equivalents a nitroso functionalized derivative that a capable of dynamically bonding to form an azodioxide bridge. This bridge is capable of extending conjugation between the two building blocks.

The second dynamically bonding interaction to be discussed in great detail is of aromatics functionality with nitroso moiety's that are capable dimerizing into azodioxide bridges **(Scheme 1.3)**.[24,40] This functionalization was used by the Wuest Group to create a three-dimensional COF that was also single crystalline.[24] It is of high interest in this text because the azodioxide bridge is capable of extending conjugation throughout a COF if the building blocks were also fully conjugated themselves. In this thought process, a single crystal conjugally linked throughout with azodioxide bridges could have semiconductor potential. Furthermore, if the building blocks were three dimensional it could lead to the possibility of a forming a long sought after fully conjugated three-dimensional organic framework.[30]

1.5 References

(1) Millini, R.; Bellussi, G. Chapter 1. Zeolite Science and Perspectives; 2017; pp 1–36. https://doi.org/10.1039/9781788010610-00001.

(2) Gounder, R.; Moini, A. Automotive NOx Abatement Using Zeolite-Based Technologies. *Reaction Chemistry & Engineering* **2019**, *4* (6), 966–968. https://doi.org/10.1039/C9RE90030F.

(3) Cai, M.; Daniel, S. L.; Lavigne, J. J. Conjugated Bis and Poly(Dioxaborole)s for Optical Sensing of Lewis Bases Based on Main-Chain Perturbations. *Chemical Communications* **2013**, *49* (58), 6504–6506. https://doi.org/10.1039/C3CC41189C.

(4) Maynor, M. S.; Nelson, T. L.; O'Sulliva, C.; Lavigne, J. J. A Food Freshness Sensor Using the Multistate Response from Analyte-Induced Aggregation of a Cross-Reactive Poly(Thiophene). *Organic Letters* **2007**, *9* (17), 3217–3220. https://doi.org/10.1021/ol071065a.

(5) Kwon, E. H.; Kim, M.; Lee, C. Y.; Kim, M.; Park, Y. D. Metal–Organic-Framework-Decorated Carbon Nanofibers with Enhanced Gas Sensitivity When Incorporated into an Organic Semiconductor-Based Gas Sensor. *American Chemical Society Applied Materials & Interfaces* **2022**, *14* (8), 10637–10647. https://doi.org/10.1021/acsami.1c24740.

(6) Xiao, W.; Hu, C.; Ward, M. D. Guest Exchange through Single Crystal–Single Crystal Transformations in a Flexible Hydrogen-Bonded Framework. *Journal of the American Chemical Society* **2014**, *136* (40), 14200–14206. https://doi.org/10.1021/ja507689m.

(7) Sindt, A. J.; Smith, M. D.; Berens, S.; Vasenkov, S.; Bowers, C. R.; Shimizu, L. S. Single-Crystal-to-Single-Crystal Guest Exchange in Columnar Assembled Brominated Triphenylamine Bis-Urea Macrocycles. *Chemical Communications* **2019**, *55* (39), 5619–5622. https://doi.org/10.1039/C9CC01725A.

(8) Nikolayenko, V. I.; Heyns, A.; Barbour, L. J. Threading the Needle: Guest Transport in a Versatile 0D Porous Molecular Crystal. *Chemical Communications* **2017**, *53* (82), 11306–11309. https://doi.org/10.1039/C7CC06676G.

(9) Dou, L.; Zheng, Y.; Shen, X.; Wu, G.; Fields, K.; Hsu, W.-C.; Zhou, H.; Yang, Y.; Wudl, F. Single-Crystal Linear Polymers Through Visible Light–Triggered

Topochemical Quantitative Polymerization. *Science (1979)* **2014**, *343* (6168), 272–277. https://doi.org/10.1126/science.1245875.

(10) Xu, W. L.; Smith, M. D.; Krause, J. A.; Greytak, A. B.; Ma, S.; Read, C. M.; Shimizu, L. S. Single Crystal to Single Crystal Polymerization of a Self-Assembled Diacetylene Macrocycle Affords Columnar Polydiacetylenes. *Crystal Growth & Design* **2014**, *14* (3), 993–1002. https://doi.org/10.1021/cg401380a.

(11) Teo, Y. C.; Lai, H. W. H.; Xia, Y. Synthesis of Ladder Polymers: Developments, Challenges, and Opportunities. *Chemistry – A European Journal* **2017**, *23* (57), 14101–14112. https://doi.org/https://doi.org/10.1002/chem.201702219.

(12) Krishnan, B. P.; Sureshan, K. M. A Spontaneous Single-Crystal-to-Single-Crystal Polymorphic Transition Involving Major Packing Changes. *Journal of the American Chemical Society* **2015**, *137* (4), 1692–1696. https://doi.org/10.1021/ja512697g.

(13) Xu, Y.; Smith, M. D.; Krause, J. A.; Shimizu, L. S. Control of the Intramolecular [2+2] Photocycloaddition in a Bis-Stilbene Macrocycle. *The Journal of Organic Chemistry* **2009**, *74* (13), 4874–4877. https://doi.org/10.1021/jo900443e.

(14) DeHaven, B. A.; Liberatore, H. K.; Greer, A.; Richardson, S. D.; Shimizu, L. S. Probing the Formation of Reactive Oxygen Species by a Porous Self-Assembled Benzophenone Bis-Urea Host. *American Chemical Society Omega* **2019**, *4* (5), 8290–8298. https://doi.org/10.1021/acsomega.9b00831.

(15) Geer, M. F.; Walla, M. D.; Solntsev, K. M.; Strassert, C. A.; Shimizu, L. S. Self-Assembled Benzophenone Bis-Urea Macrocycles Facilitate Selective Oxidations by Singlet Oxygen. *The Journal of Organic Chemistry* **2013**, *78* (11), 5568–5578. https://doi.org/10.1021/jo400685u.

(16) Goodlett, D. W.; Sindt, A. J.; Hossain, M. S.; Merugu, R.; Smith, M. D.; Garashchuk, S.; Gudmundsdottir, A. D.; Shimizu, L. S. From Incident Light to Persistent and Regenerable Radicals of Urea-Assembled Benzophenone Frameworks: A Structural Investigation. *The Journal of Physical Chemistry A* **2021**, *125* (6), 1336–1344. https://doi.org/10.1021/acs.jpca.0c08953.

(17) Moosavi, S. M.; Nandy, A.; Jablonka, K. M.; Ongari, D.; Janet, J. P.; Boyd, P. G.; Lee, Y.; Smit, B.; Kulik, H. J. Understanding the Diversity of the Metal-Organic Framework Ecosystem. *Nature Communications* **2020**, *11* (1), 4068. https://doi.org/10.1038/s41467-020-17755-8.

(18) Sharma, R. K.; Yadav, P.; Yadav, M.; Gupta, R.; Rana, P.; Srivastava, A.; Zbořil, R.; Varma, R. S.; Antonietti, M.; Gawande, M. B. Recent Development of Covalent Organic Frameworks (COFs): Synthesis and Catalytic (Organic-Electro-Photo) Applications. *Materials Horizons* **2020**, *7* (2), 411–454. https://doi.org/10.1039/C9MH00856J.

(19) Ogoshi, T.; Yamagishi, T. Chapter 1. Historical Background of Macrocyclic Compounds; 2015; pp 1–22. https://doi.org/10.1039/9781782622321-00001.

(20) Nguyen, V.; Grünwald, M. Microscopic Origins of Poor Crystallinity in the Synthesis of Covalent Organic Framework COF-5. *Journal of the American Chemical Society* **2018**, *140* (9), 3306–3311. https://doi.org/10.1021/jacs.7b12529.

(21) Li, H.; Chavez, A. D.; Li, H.; Li, H.; Dichtel, W. R.; Bredas, J.-L. Nucleation and Growth of Covalent Organic Frameworks from Solution: The Example of COF-5. *Journal of the American Chemical Society* **2017**, *139* (45), 16310–16318. https://doi.org/10.1021/jacs.7b09169.

(22) Uribe-Romo, F. J.; Hunt, J. R.; Furukawa, H.; Klöck, C.; O'Keeffe, M.; Yaghi, O. M. A Crystalline Imine-Linked 3-D Porous Covalent Organic Framework. *Journal of the American Chemical Society* **2009**, *131* (13), 4570–4571. https://doi.org/10.1021/ja8096256.

(23) Zhang, Y.-B.; Su, J.; Furukawa, H.; Yun, Y.; Gándara, F.; Duong, A.; Zou, X.; Yaghi, O. M. Single-Crystal Structure of a Covalent Organic Framework. *Journal of the American Chemical Society* **2013**, *135* (44), 16336–16339. https://doi.org/10.1021/ja409033p.

(24) Beaudoin, D.; Maris, T.; Wuest, J. D. Constructing Monocrystalline Covalent Organic Networks by Polymerization. *Nature Chemistry* **2013**, *5* (10), 830–834. https://doi.org/10.1038/nchem.1730.

(25) Luisier, N.; Bally, K.; Scopelliti, R.; Fadaei, F. T.; Schenk, K.; Pattison, P.; Solari, E.; Severin, K. Crystal Engineering of Polymeric Structures with Dative

Boron–Nitrogen Bonds: Design Criteria and Limitations. *Crystal Growth & Design* **2016**, *16* (11), 6600–6604. https://doi.org/10.1021/acs.cgd.6b01292.

(26) Terao, J.; Tsuji, Y. New Synthetic Methods of π-Conjugated Inclusion Complexes with High Conductivity. *Journal of Inclusion Phenomena and Macrocyclic Chemistry* **2014**, *80* (3), 165–175. https://doi.org/10.1007/s10847-014-0381-y.

(27) Wang, H.; Shao, Y.; Mei, S.; Lu, Y.; Zhang, M.; Sun, J.; Matyjaszewski, K.; Antonietti, M.; Yuan, J. Polymer-Derived Heteroatom-Doped Porous Carbon Materials. *Chemical Reviews* **2020**, *120* (17), 9363–9419. https://doi.org/10.1021/acs.chemrev.0c00080.

(28) Pingitore, V.; Gugliuzza, A. Fabrication of Porous Semiconductor Interfaces by PH-Driven Assembly of Carbon Nanotubes on Honeycomb Structured Membranes. *The Journal of Physical Chemistry C* **2013**, *117* (50), 26562–26572. https://doi.org/10.1021/jp405969b.

(29) Kumar, P.; Vahidzadeh, E.; Thakur, U. K.; Kar, P.; Alam, K. M.; Goswami, A.; Mahdi, N.; Cui, K.; Bernard, G. M.; Michaelis, V. K.; Shankar, K. C3N5: A Low Bandgap Semiconductor Containing an Azo-Linked Carbon Nitride Framework for Photocatalytic, Photovoltaic and Adsorbent Applications. *Journal of the American Chemical Society* **2019**, *141* (13), 5415–5436. https://doi.org/10.1021/jacs.9b00144.

(30) Wu, Z.; Lee, S.; Moore, J. S. Synthesis of Three-Dimensional Nanoscaffolding. *Journal of the American Chemical Society* **1992**, *114* (22), 8730–8732. https://doi.org/10.1021/ja00048a073.

(31) Tilford, R. W.; Mugavero III, S. J.; Pellechia, P. J.; Lavigne, J. J. Tailoring Microporosity in Covalent Organic Frameworks. *Advanced Materials* **2008**, *20* (14), 2741–2746. https://doi.org/https://doi.org/10.1002/adma.200800030.

(32) Christinat, N.; Croisier, E.; Scopelliti, R.; Cascella, M.; Röthlisberger, U.; Severin, K. Formation of Boronate Ester Polymers with Efficient Intrastrand Charge-Transfer Transitions by Three-Component Reactions. *European Journal of Inorganic Chemistry* **2007**, *2007* (33), 5177–5181. https://doi.org/https://doi.org/10.1002/ejic.200700723.

(33) Rambo, B. M.; Tilford, R. W.; Lanni, L. M.; Liu, J.; Lavigne, J. J. Boronate-Linked Materials: Ranging from Amorphous Assemblies to Highly Structured Networks. In *Macromolecules Containing Metal and Metal-Like Elements*; Abd-El-Aziz, A. S., Carraher Jr., C. E., Pittman Jr., C. U., Zeldin, M., Eds.; John Wiley & Sons, Inc.: Hoboken, NJ, USA, 2009; Vol. 9, pp 255–294. https://doi.org/10.1002/9780470527085.ch6.

(34) Liu, J.; Lavigne, J. J. *Boronic Acids*, Second.; Hall, D. G., Ed.; Wiley-VCH Verlag GmbH & Co. KGaA: Weinheim, Germany, 2011; Vol. 2. https://doi.org/10.1002/9783527639328.

(35) Gao, W.-X.; Feng, H.-J.; Guo, B.-B.; Lu, Y.; Jin, G.-X. Coordination-Directed Construction of Molecular Links. *Chemical Reviews* **2020**, *120* (13), 6288–6325. https://doi.org/10.1021/acs.chemrev.0c00321.

(36) Foo, M. L.; Matsuda, R.; Kitagawa, S. Functional Hybrid Porous Coordination Polymers. *Chemistry of Materials* **2014**, *26* (1), 310–322. https://doi.org/10.1021/cm402136z.

(37) Percástegui, E. G.; Ronson, T. K.; Nitschke, J. R. Design and Applications of Water-Soluble Coordination Cages. *Chemical Reviews* **2020**, *120* (24), 13480–13544. https://doi.org/10.1021/acs.chemrev.0c00672.

(38) Li, X.-Z.; Tian, C.-B.; Sun, Q.-F. Coordination-Directed Self-Assembly of Functional Polynuclear Lanthanide Supramolecular Architectures. *Chemical Reviews* **2022**, *122* (6), 6374–6458. https://doi.org/10.1021/acs.chemrev.1c00602.

(39) Stephens, A. J.; Scopelliti, R.; Tirani, F. F.; Solari, E.; Severin, K. Crystalline Polymers Based on Dative Boron–Nitrogen Bonds and the Quest for Porosity. *American Chemical Society Materials Letters* **2019**, *1* (1), 3–7. https://doi.org/10.1021/acsmaterialslett.9b00054.

(40) Vancik, H.; Simunic-Meznaric, V.; Mestrovic, E.; Halasz, I. Nitrosobenzene Dimerizations as a Model System for Studying Solid-State Reaction Mechanisms. *The Journal of Organic Chemistry* **2004**, *69* (14), 4829–4834. https://doi.org/10.1021/jo049537b.

CHAPTER 2: BENZENE DERIVED COORDINATION POLYMER ONE (CP1

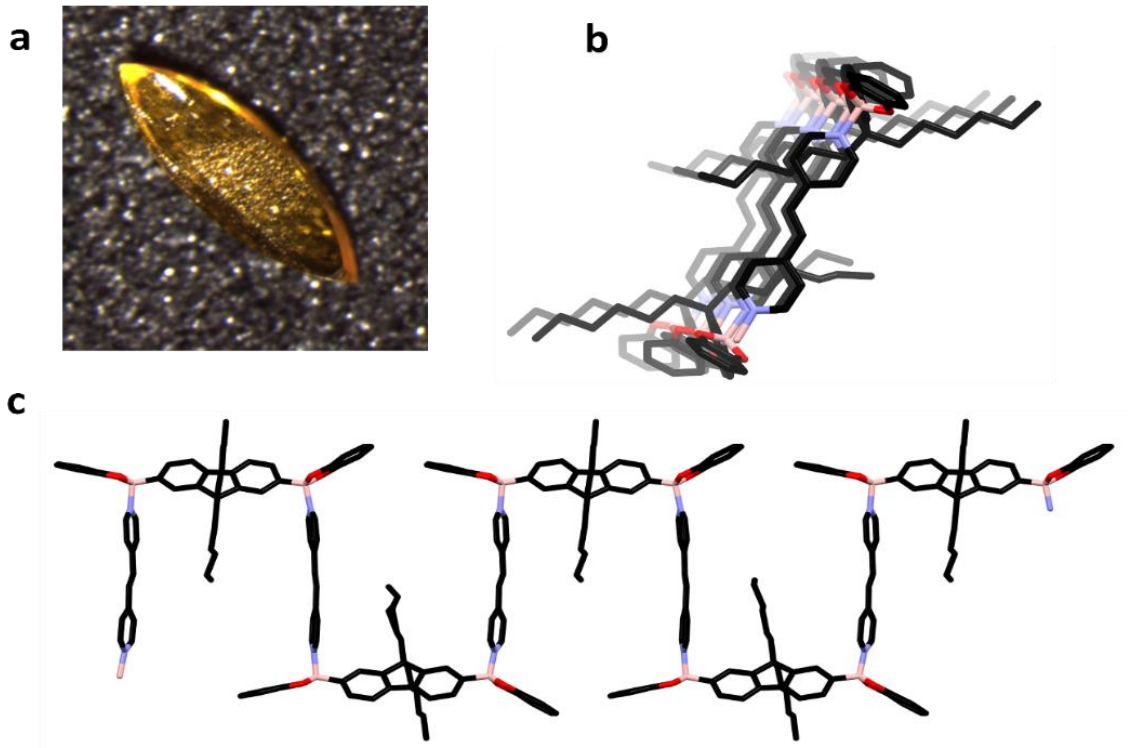

Figure 2.1: Left: Front view of the benzene coordination polymer (CP1) with DE1 linked with dipyridyl ethylene showing its direction alternating symmetrically on its inversion center. Right: Side view of the coordination polymer showing a one-dimensional infinite chain.

2.1: Overview

Boronate esters, a Lewis acid, are interesting due to having an empty p orbital and an unfilled octet when neutral. This allows for a dynamic and reversible dative bond when boron interacts with a nucleophile.[1–4] Pyridine and dipyridyl linkers have been used to study these binding properties and have yielded results that take more detailed analysis because the ester can also being manipulated by its environment.[4–6] The solvent used as

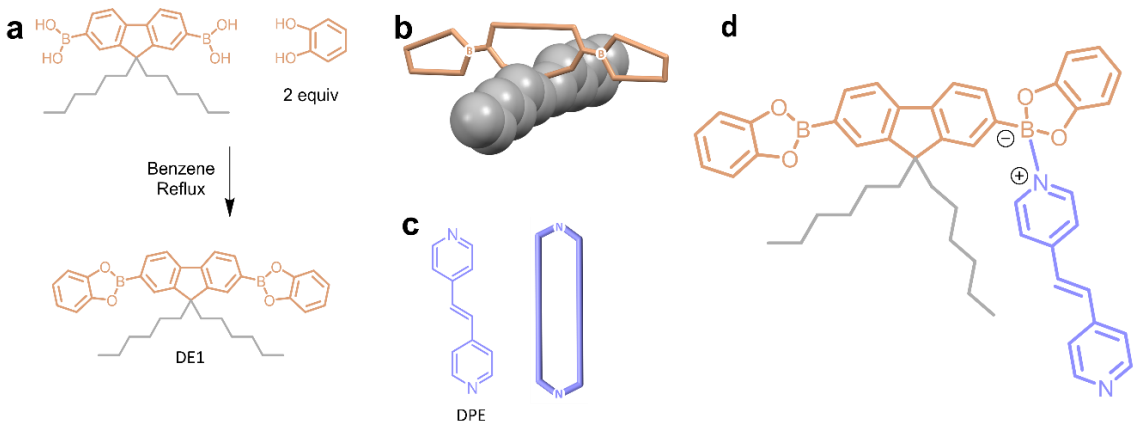

Scheme 2.1: **a.** Synthesis of Diboronate Ester 1 (DE1) using 9,9-dihexylfluorene-2,7-diboronic acid with two equivalents of catechol. **b.** Simplified version of DE1 with the aromatic region having less atoms but showing the rigid aromatic region in orange and the dihexyl chains seen in grey also showing the carbons as spece filled.

the medium for the boronate ester and a pyridyl derivative has shown that it works in collaboration, determining the length of all bonds involved and their angles.[4,5,7] It is expected that not only are the sterics of the individual solvent molecules in the surrounding environment driving these interactions but also their electrostatic potentials. Therefore, if the main enthalpic cost of the creation of these coordinated crystalline products is synthesis of diboronate esters and then dissolving them in solvent with a dipyridyl linker, why not let the thermodynamic cards fall as they may to see what different porous products can be achieved?[6–8] To argue this, if the materials are reusable, the same reactants can be explored with various solvents to see what changes in characteristics occurred because it is not a taxing endeavor to explore.

Herein, we present the idea of encouraging intermolecular interactions in the result of creating the expected unexpected using the fundamental understanding that aliphatics usually cluster with one another while aromatics do the same. To demonstrate this, we have explored these interactions using a two-site functionalized symmetric

diboronate ester synthesized from 9,9-dihexylfluorene-2,7-diboronic acid with catechol via a condensation reaction **(Scheme 2a)**. This diboronate ester has one region of the compound that is a rigid aromatic that has an orthogonal set of aliphatic chains **(Scheme 2b)**. Thus, it is expected that aromatic solvent would interact with very specific parts of the compound leading to even more forces at play than just the ditopic orbital of boronate ester and the tetravalent nature of a diboronate ester. The dihexyl chains would also interact with other chains from ones nearby repeat units if a framework were to occur. This symmetric structure seems that it would help create organization from intermolecular forces within the reaction matrix itself. In this chapter moving forward, a supramolecular boronate network was created yielding a coordinated polymer, CP1, when dipyridyl ethylene (DPE) was used as a linker that was highly crystalline and robust.

2.1.2: Results

Single crystal x-ray diffraction (XRD) showed the compound crystallizes in the monoclinic system. The pattern of systematic absences in the intensity data was consistent with the space group $P2_1/n$, which was confirmed by solution. The asymmetric unit consists of one polymeric $[(C_{37}H_{40}B_2O_4)(C_{12}H_{10}N_2)]$ repeat unit, half each of two benzene molecules located on inversion centers, and another complete benzene molecule.

Computations were also performed to look at the band gap which was found to be 2.014 eV. To make the calculation less taxing, the hexyl chains were replaced with methyls. The basis and method were B3LYP and 6-31G** and calculations were performed using Qchem via the Pople Linux Cluster. Images produced with IQMol.

2.1.3: Discussion

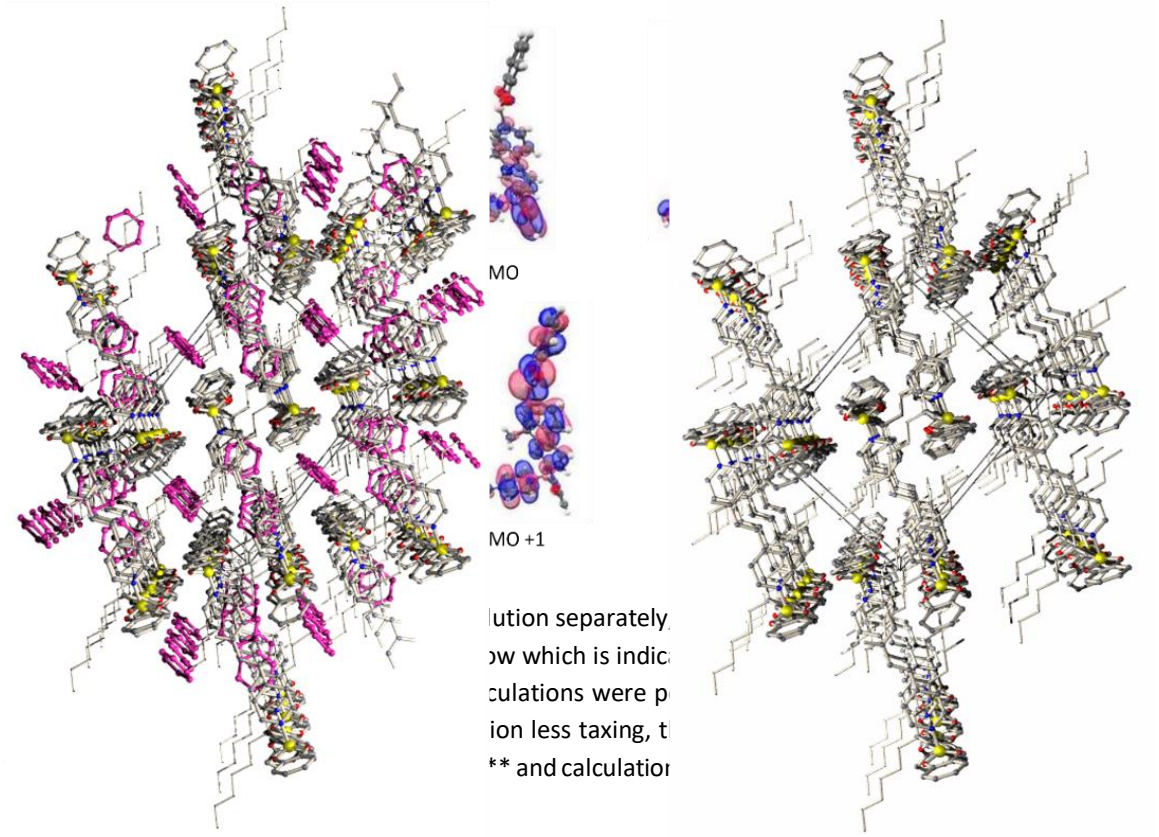

Figure 2.2: **Left:** View down the chain direction (b axis) of several chains. **Right:** The same structure with benzene guest omitted for clarity.

One molar equivalent of DPE and DE1 were heated in benzene until fully dissolved and left to crystallize as (CP1) **(Figure 2.1)**. The resulting product were large and robust single crystals and clusters. The polymer chain is an infinite one-dimensional square wave **(Figure 2.1, Left)** in which the two hexyl aliphatic chains on each diboronate ester interact with hexyl chains located on the adjacent polymer neighbors in both directions **(Figure 2.2)**. This locality shows that the hexyl chains throughout the long-range order of the system act as tethers to which the neighboring repeat units stitch themselves together **(Figure 2.2)**. The hexyl chains can also be seen interacting with other hexyl chains from neighboring fluorene units giving evidence that they did help in the organization process

during crystal structures formation. The aromatic regions of the diboronate ester and dipyridyl linker also interact with one another along with the benzene guests within the host to which is bound by π-π and CH-π bonds.

The location of the benzene guests within are cut in half by the inversion centers of the repeat unit in a way that creates porous channels throughout the crystalline network leading to two questions. The first being, could these pores allow us to change CP1 in such a way to see what happens to the crystal structure if the benzene were to be removed? The other question, could the benzene be exchanged with another guest in a single crystal to single crystal (SCSC) transition that XRD could elucidate? This would be expected to manipulate the host framework and could cause changes to steric strain, bond angles, and optoelectronics.

Something also of interest was that when two monomers were in solution separately, the liquid was clear and colorless. But when mixed, the solution immediately turned yellow which is indicative of a coordination supporting charge transfer. Due to this, calculations were performed to look at the band gap which was found to be 2.014 eV **(Figure 2.3)**.

2.1.4: Experimental

Synthesis of Diboronate Ester One (DE1)

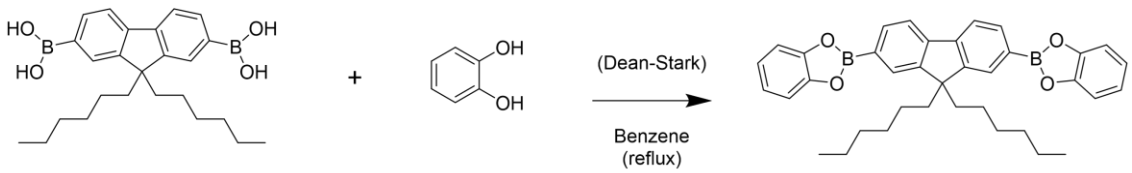

9,9-dihexylfluorene-2,7-diboronic acid | 2 equiv catechol | Boronate Diester 1

Scheme 2.2: 9,9-dihexylfluorene and two equivalents of catechol are refluxed in benzene with a Dean-Stark trap to produce the DE1 through a condensation reaction.

A round bottom flask was charged with 9,9-dihexylfluorene-2,7-diboronic acid (1.0550 g, 2.499 mmol) and catechol (0.5079g, 4.604 mmol), and benzene (600 mL). Heat activated 3Å sieves and 20mL Benzene were added to a Dean Stark trap that was then attached to the reaction flask. Initially reactants did not go into solution but upon heating to reflux the solution became clear and colorless. The reaction was allowed to reflux for 24 hours while stirring under a nitrogen atmosphere. The solution was then purified through hot gravity filtration before isolation in which benzene was removed by rotary evaporation. Short path distillation was performed on the resulting white solid product with reduced pressure sublimation (Kuglerohr) at 110 °C for two hours to remove excess catechol by sublimation (1.23g, 81.6% yield).

^{1}H NMR (300 MHz, CD2Cl2): δ 8.12-8.09 (m, 4H), 7.94-7.91 (d, 2H), 7.37-7.34 (m, 4H), 7.18-7.15 (m, 4H), 2.17-2.12 (m, 4H), 1.09-1.04 (m, 12H), 0.75-0.70 (m, 6H), 0.612 (m, 4H)

Synthesis of Coordination Polymer 1 (CP1)

A round bottom flask was charged with DE1 (1.029 g, 1.804 mmol) and DPE (0.329 g, 1.805 mmol) and dissolved in benzene (100 mL). Crystallization occurred over night and produced large yellow wedges along with crystal clusters (1.328 g, 81%).

2.2: Single Crystal to Single Crystal (SCSC) Transitions of CP1

SCSC transitions have been explored in recent literature with the idea of post-synthetically modifying the characteristics of a synthesized product by utilizing solvents in the liquid or vapor form.[9,10] Other types of SCSC transitions that were not performed are topochemical polymerization within the crystal repeat unit or changing molecular conformation through isomerization which usually occur when initiated with the use of

heat or wavelength.[11,12] Crystals of CP1 were then put in the presence of multiple solvents ranging in characteristics from differences in hybridization, polarity, and steric size/shape. Three solvents were capable of causing an SCSC transition that post-synthetically changed the characteristics of CP1 which involved a liquid transition with styrene as a solvent and a vapor transition with acetonitrile and fluorobenzene.

2.2.1: Styrene Liquid SCSC Transitioned CP1 Crystal

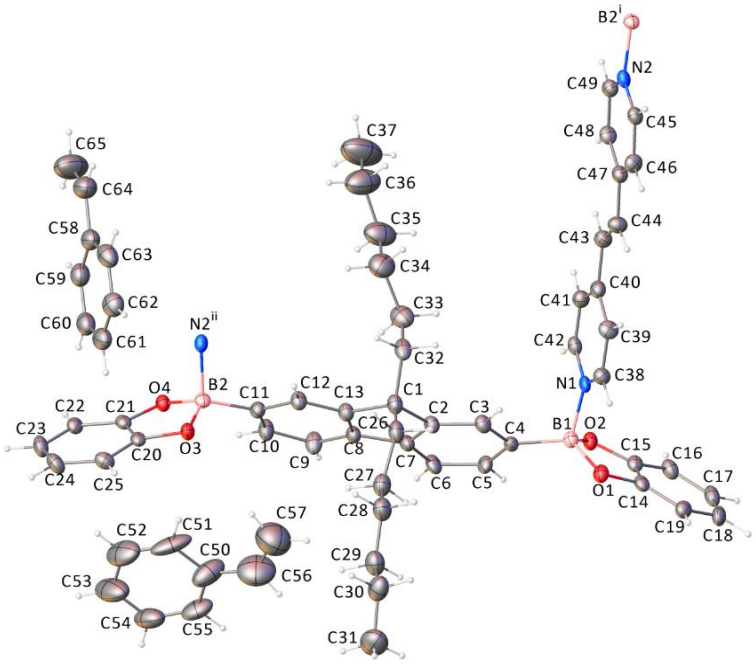

Figure 2.4: Asymmetric unit of the styrene SCSC transitioned CP1crystal, with two additional atoms to complete B2 and N2 bonding environments. Displacement ellipsoids drawn at the 50% probability level. Superscripts denote symmetry-equivalent atoms.

2.2.1.1: Results

The compound crystallizes in the monoclinic system. The pattern of systematic absences in the intensity data was consistent with the space groups $P2_1$ and $P2_1/m$; intensity statistics suggested a non-centrosymmetric structure. A reasonable and stable solution and refinement was obtained in $P2_1$, which was the space group identified by

SHELXT. A check of the finished structure with the ADDSYM program found no missed symmetry elements.[5] The asymmetric unit consists of one $C_{49}H_{50}B_2N_2O_4$ polymeric repeat unit and two crystallographically independent styrene molecules.

2.2.1.2: Discussion

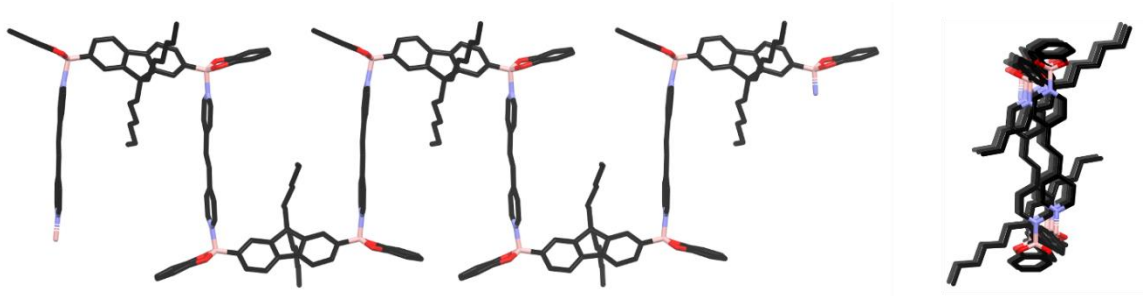

Figure 2.5: Benzene Coordinated Polymer After an SCSC Vapor transition with styrene. Left: Front view of the styrene transitioned coordination polymer with DE1 linked with DPE showing its direction alternating symetrically on its inversion center. Right: Side view of the coordination polymer showing a one dimensional infinite chain.

Initially the intention for use of styrene was to see if an SCSC transition of CP1 would occur and was originally meant to only interact with the crystals as a vapor. An error occurred in which once the vial had been sealed, it was knocked over and the CP1 crystals became submerged in styrene solvent. It was then decided to see if there would be an SCSC solvent transition and the vial was left overnight. When the crystals were given to the crystallographer the next day, a SCSC transition had occurred and the polymer was still intact. This is important because previous work from the Lavigne group shows that styrene does make single crystals with DE1 and DPE but the network is formed by macrocycles and not a coordination polymer. Therefore, since XRD analysis showed that the polymer was still intact with just small changes to the structure itself with the exception that two benzene guests were exchanged, it was proven to be a true SCSC transition which occurred in the solid state and was not a simple recrystallization. The

dihedral angles between the fluorene and DPE for the styrene solvent transitioned CP1 are 106.47° and 107.33° which has slightly less angle strain as seen in CP1 at this juncture, but change seemed negligible. One of these angles can be seen between C4, B1, and N1 **(Figure 2.2, Figure 2.4)**. The respective boron nitrogen bond lengths are 1.661 Å and 1.668 Å. The transition crystals consist of wedges that are yellow in color. The crystal system is monoclinic with a $P2_1$ space group with a repeat unit volume of 2,642.0 $Å^3$ and a density of 1.208 grams per cubic centimeter. When comparing the styrene transition to CP1 in more than just monomer dihedral angles, the density only marginally decreased but the volume significantly was reduced by 47%. This significant change may be due to styrene having the addition of the ethene functional group that benzene does not.

2.2.1.3: Experimental

A one-dram vial was charged with of CP1 crystals with benzene guest (25 mg, 0.057 mmol). The one dram was then placed in a four dram with styrene solvent (7 mL) and capped. The original intention was to only use styrene vapor to find out if an SCSC transition would occur but the vial was accidently knocked over and the CP1 single crystals became submerged in styrene liquid. The single crystals were left overnight in styrene solvent and the next day they were still the same shape as CP1 crystals and translucent but the yellow color was paler in nature than seen when compared to the CP1 single crystal precursor. The sample vial was then sent to the crystallographer for single crystal XRD.

2.2.2: Acetonitrile Vapor SCSC Transitioned CP1 Crystal

2.2.2.1: Results

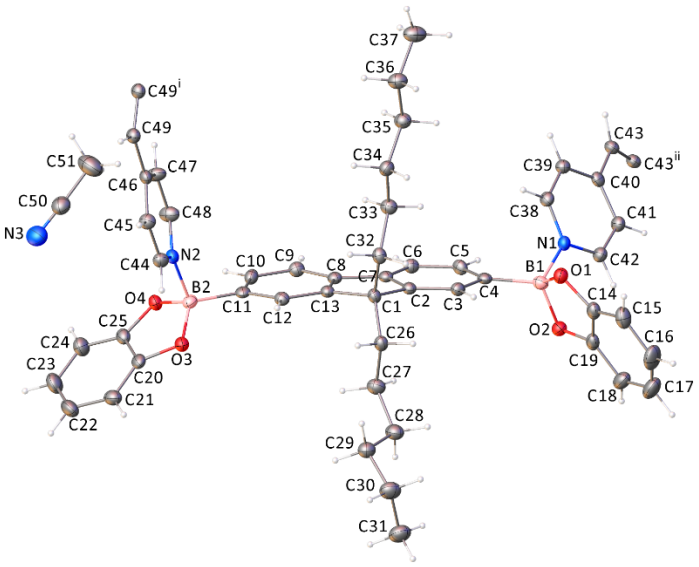

Figure 2.6: Asymmetric unit of the acetonitrile SCSC transitioned CP1 crystal. Displacement ellipsoids drawn at the 50% probability level. DPE ligands on inversion center; two inversion-related atoms shown. Superscripts denote symmetry-equivalent atoms.

XRD was performed on the CP1 crystals sealed within an acetonitrile vapor environment which showed the compound transitioned to the triclinic system. The space group *P*-1 (No. 2) was confirmed by structure solution. The asymmetric unit consists of one [$C_{49}H_{50}B_2N_2O_4$] polymeric repeat unit and one acetonitrile molecule. There are half each of two independent 1,2-dipyridylethene (DPE) ligands within the polymeric repeat unit, each bound to the central $C_{37}H_{40}B_2O_4$ subunit. The (DPE) ligands are located on crystallographic inversion centers.

2.2.2.2: Discussion

Once CP1 had been sealed with acetonitrile within an environment to which the single crystal only was in contact with the acetonitrile's vapor over a two-week period, there was an SCSC transition that occurred but not as expected. The reason the single crystals only had contact with vapor was to ensure that a recrystallization would not occur. The transitioned polymer was still highly crystalline and suitable for XRD analysis

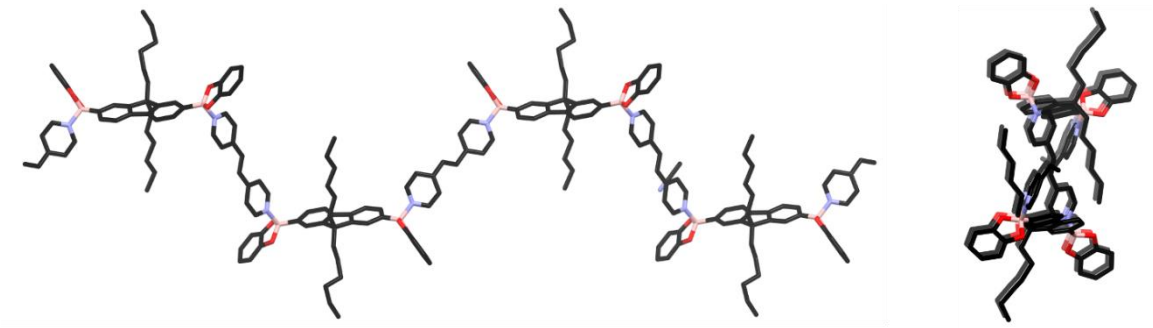

Figure 2.7: Benzene Coordinated Polymer After an SCSC vapor transition with acetonitrile. Left: Front view of the aceto transitioned coordination polymer with DE1 linked with DPE showing its direction alternating symetrically on its inversion center. Right: Side view of the coordination polymer showing a one dimensional infinite chain.

which showed the structure had changed in a more dramatic manner than the liquid styrene SCSC transition mentioned previously. Not only did the square wave change its inversion center **(Figure 2.6, Figure 2.7)**, the original monoclinic crystal system unexpectedly transitioned to crystal became triclinic. For this change to occur it is postulated that over the two-week period, DPE linkers that were dynamically bonded to DE1 were able to break their bonds and perform a nucleophilic exchange to the boron on a DE1 compound linker nearby, effectively causing a chain reaction that continued throughout the system. This chain reaction is expected to have occurred slowly with the reasoning that the crystal was still capable of keeping its translucent character and was still suitable for XRD analysis. Something that was also noticed that will continue as a trend in later chapters is that the solvent vapor also seemed to affect the color of the single crystals leading to the idea that the optoelectronic characteristics were being changed during the transition. Within twenty minutes of CP1 crystals being in the presence of acetonitrile vapor, the color started to change from a translucent yellow to a translucent orange. This color change continued over the two-week period. The boron nitrogen bond angles for the acetonitrile vapor transitioned CP1 are 108.46° and 109.09°

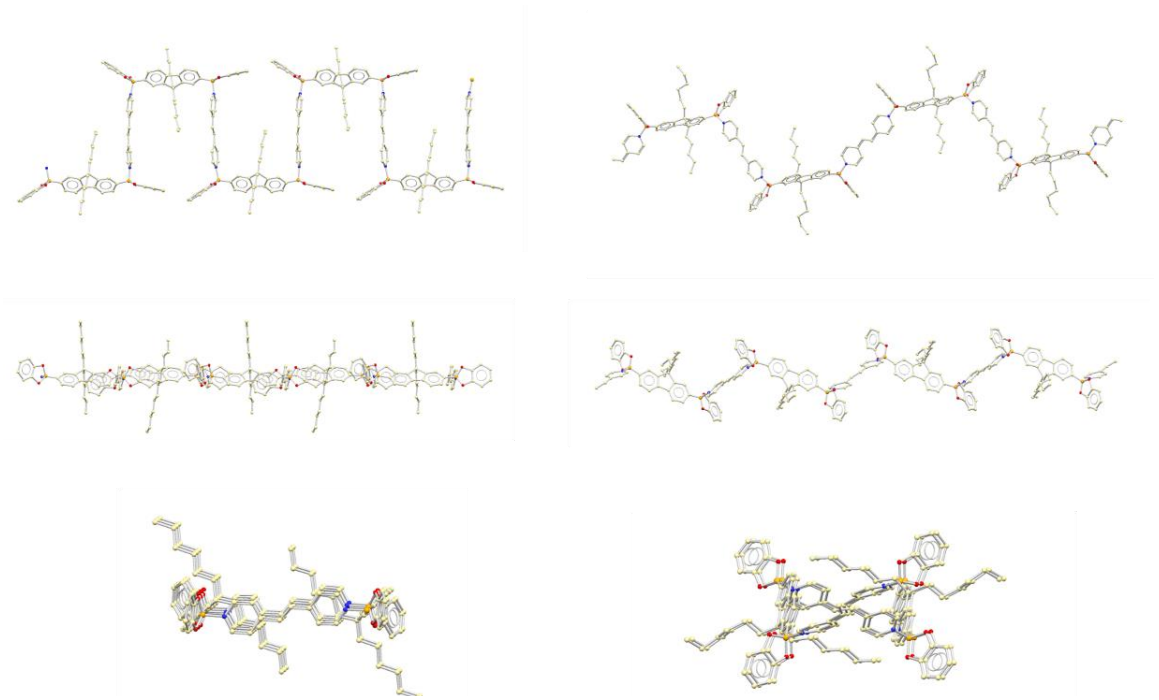

Figure 2.8: Comparison of CP1 (left) the acetonitrile SCSC transitioned coordination polymer (right) When comparing left to right it is seen that a change to the inversion center occurred after the SCSC transition where as the bottom left shows the side view of CP1 that exists as a square wave as opposed to the acetonitrile transitioned structure having more dimensional freedom at the bottom right.

which has much less angle strain as seen in CP1 at this juncture. It seems that however this transition took place, it led to a lower energy bond angle which possibly was the cause for the event to occur, one acetonitrile guest was now present which replace both benzene guests within the structure. One of these angles can be seen between C4, B1, and N1 **(Figure 2.6).** The respective boron nitrogen bond lengths are 1.677 Å and 1.644 Å which shows that as the angle increased the bonds became longer giving them more s character. The transition crystals used in analysis were irregular and are orange in color. The crystal system is triclinic with a P-1 space group with a repeat unit volume of 2135.8 $Å^3$ and a density of 1.234 grams per cubic centimeter. When comparing the acetonitrile transition to CP1 in more than just monomer dihedral angles, the density only marginally increased but the volume significantly was reduced by 51%. This significant change may

be due to the fact that there is only one acetonitrile guest molecule per crystal repeat unit while the original CP1 crystals had two. It is expected that since acetonitrile is much smaller it would cause the volume to lower and is also postulated that the electronegative nature of acetonitrile when compared to benzene may have caused the packing to be much denser than the CP1 crystal precursor.

2.2.2.3: Experimental

A one-dram vial was charged with of CP1 crystals with benzene guest (25 mg, 0.057 mmol). The one dram was then placed in a four dram with acetonitrile solvent (7 mL) and sealed. Acetonitrile vapor was allowed to interact with the CP1 crystals within the four-dram vial. Within twenty minutes the translucent yellow crystals started to turn orange but stayed translucent. Over two weeks the vial was left to sit and the crystals had continued to stay translucent but were much more orange in nature than when compared to the CP1 single crystal precursor. The sample vial was then sent to the crystallographer for single crystal XRD.

2.2.3: Fluorobenzene Vapor SCSC Transitioned CP1 Crystal

2.2.3.1: Results and Discussion

Once CP1 had been sealed within a vial with fluorobenzene in an environment to which the single crystal only was in contact with the solvent's vapor over a two-week period, it resulted in an SCSC transition in which fluorobenzene replaced the benzene guest within the crystal structure. After XRD analysis it was seen that the only real difference between CP1 and the fluorobenzene transitioned single crystals is that the guests were replaced. The structure is virtually the same in which there are two

fluorobenzene guest molecules per crystal repeat unit with no overall changes to the polymer repeat unit's crystal structure. This is expected due to the fact that the difference in size between the fluorine atom on fluorobenzene when compared to the hydrogens on benzene is not very large considering that fluorine is the third smallest element. Therefore, because the structure of CP1 has already been discussed and the only difference is that fluorobenzene has replaced the same location that benzene used to be, no more discussion is needed.

2.2.3.2: Experimental

A one-dram vial was charged with of CP1 crystals with benzene guest (200 mg, 0.046 mmol). The 1-dram was then placed in a 4-dram vial with fluorobenzene solvent (7 mL) and sealed. Fluorobenzene vapor interacted with the CP1 crystals as vapor and the 4-dram vial was left to sit for two weeks. There was no seeable color change for the fluorobenzene transitioned single crystals. The sample vial was then sent to the crystallographer for single crystal XRD.

2.2.4 X-ray Diffraction Data for Solvent/Vapor Coordination Polymer SCSC Transitions of CP1

Structure Label	Benzene Derived Coordination Polymer 1	Styrene Single Crystal to Single Crystal Liquid Transition of Benzene Derived Coordination Polymer	Acetonitrile Single Crystal to Single Crystal Vapor Transition of Benzene Derived Coordination Polymer
Empirical formula	C61H62B2N2O4	C65H66B2N2O4	C51H53B2N3O4
Crystal habit and color	wedge; yellow	wedge, yellow	irregular, orange
Formula weight	908.74	960.81	793.58
Temperature/K	100(2)	100(2)	100(2)
Crystal system	monoclinic	monoclinic	triclinic
Space group	P21/n	P21	P-1
a/Å	13.8410(7)	10.7153(6)	12.1958(7)
b/Å	21.5251(12)	21.4490(13)	12.6787(7)
c/Å	16.8118(9)	11.9226(7)	16.1666(9)
α/°	90	90	106.600(2)
β/°	95.807(2)	105.384(2)	104.804(2)
γ/°	90	90	106.584(2)
Volume/Å3	4983.0(5)	2642.0(3)	2135.8(2)
Z	4	2	2
ρcalcg/cm3	1.211	1.208	1.234
Crystal size/mm3	0.22 × 0.18 × 0.14	0.24 × 0.18 × 0.12	0.16 × 0.1 × 0.08
Reflections collected	160659	54743	52801
Goodness-of-fit on F2	1.029	1.045	1.017
Final R indexes [I>=2σ (I)]	R1 = 0.0549, wR2 = 0.1212	R1 = 0.0525, wR2 = 0.1268	R1 = 0.0471, wR2 = 0.0897
Largest diff. peak/hole / e Å-3	0.65/-0.23	0.44/-0.39	0.25/-0.24
Dihedral angles between the fluorene and dipyridyl ethylene	105.51°, 107.84	106.47°, 107.33°	108.46°, 109.09°
Boron nitrogen bond lengths (Å)	1.670, 1.658	1.661, 1.668	

Table: 2.1 X-ray diffraction data of SCSC transition of CP1 derived in benzene. Also shown is the dihedral bond angles and crystal habit and color. The fluorobenzene vapor transitioned single crystal data from CP1 has been omitted from this table due to it being the same structure.

2.3 Investigation into Benzene Guest Binding Enthalpy Within CP1

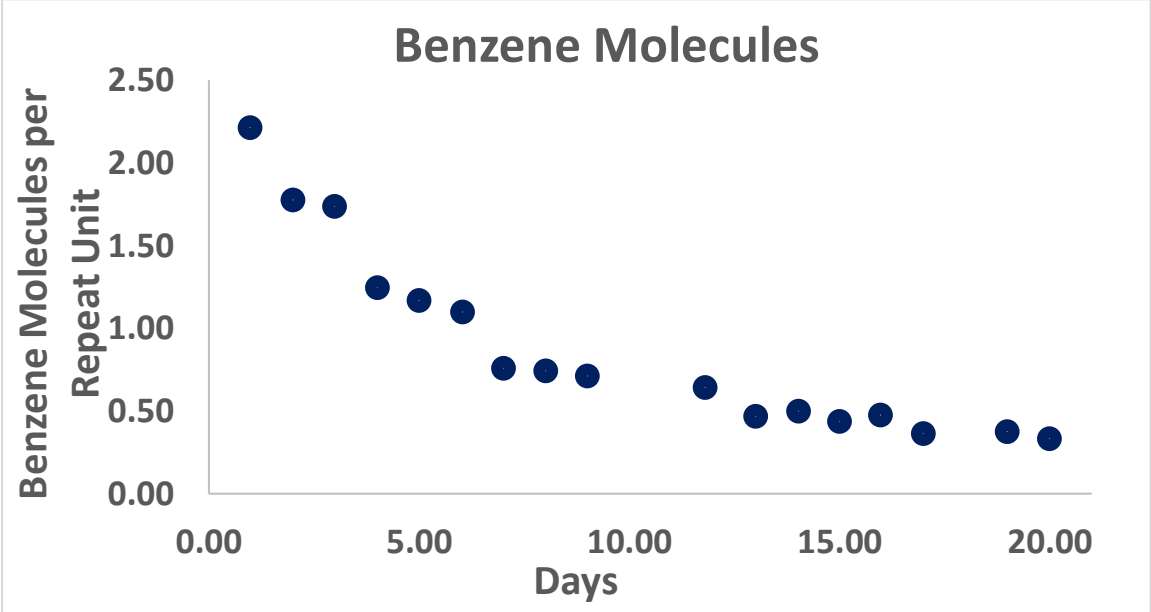

Figure 2.9: Chart showing the amount of benzene gues molecules in CP1 crystal repeat unit while under reduced pressure over time from H-NMR spectra.. It was seen that that the benzene guest was highly bound within the crystal and never seemed to fully vacate without heat being added.

Self-assembling materials are known for their capability of hosting guests within their structures ever since COF's, MOF's, and coordinated materials were being developed in past decades.[13–22] The guest can exist residually from synthesis and could be randomly placed within a crystalline repeat unit. Also, what has been seen earlier in this chapter and in recent research in general is a focus on post synthetic modification whether it be an SCSC transition, conformation change, topochemical polymerization, or sequestration of specific compounds of virtually any kind.[11,12] We have already shown that CP1 single crystals can be post-synthetically modified via an SCSC transitions through liquid or vapor processes that have had a range from small changes on the crystal repeat unit to more drastic. We then decided to take a look at how strongly bound the benzene guest was within CP1 single crystals when not put in a liquid/vapor environment but by

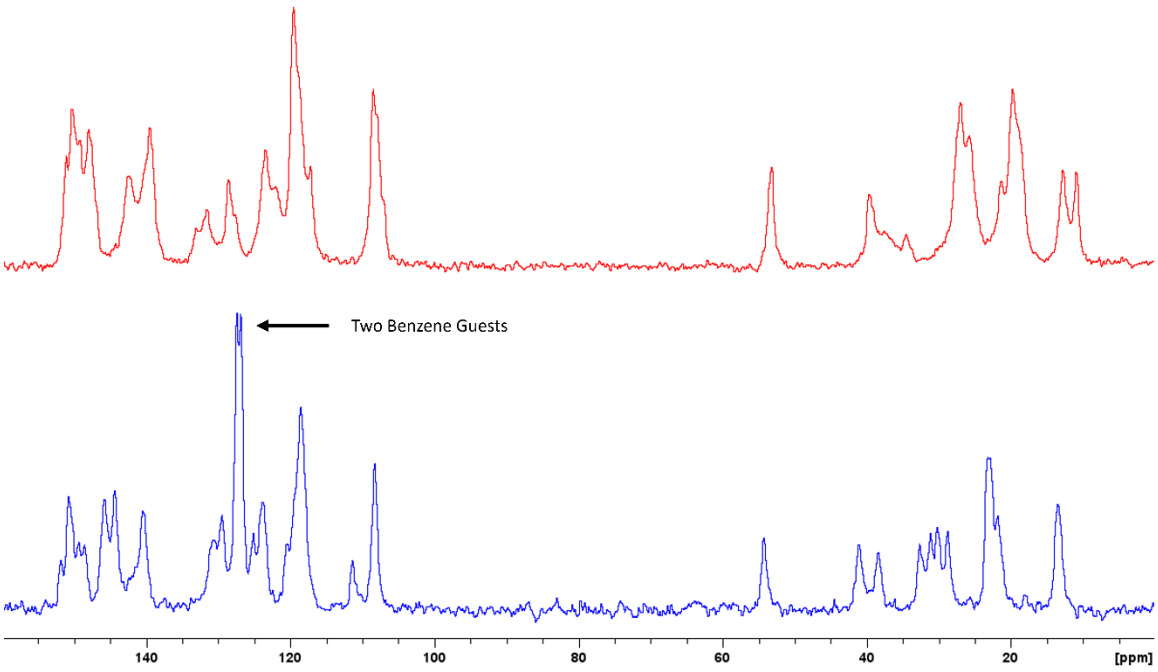

Figure 2.10: Blue: CP1 carbon NMR showing two distinct peaks, giving view of each of the two benzene guests having different intramolecular interactions with their environments. Red: Benzene vacant CP1 carbon NMR showing the benzene peaks do not appear and

other means of removal by changing the physical environment with reduced pressure **(Figure 2.8)**, higher temperature, or both at the same time. Once CP1 had the benzene guest evacuated, carbon NMR was used to find out if the two benzene guests could be seen individually due to both existing in very different environments. It turns out the varying intramolecular forces that bound each benzene guest were so diverse the peaks could be differentiated separately as seen in the CNMR data above **(Figure 2.9)**. The blue spectrum below shows the CP1 carbon NMR and at the top in red shows the guest vacant CP1 which also seems to elucidate small changes to the polymer chains environment which can be seen in slight shits in peaks for the polymer.

2.3.1: Analysis of Benzene Guest Binding Enthalpy with Reduced Pressure and Heat

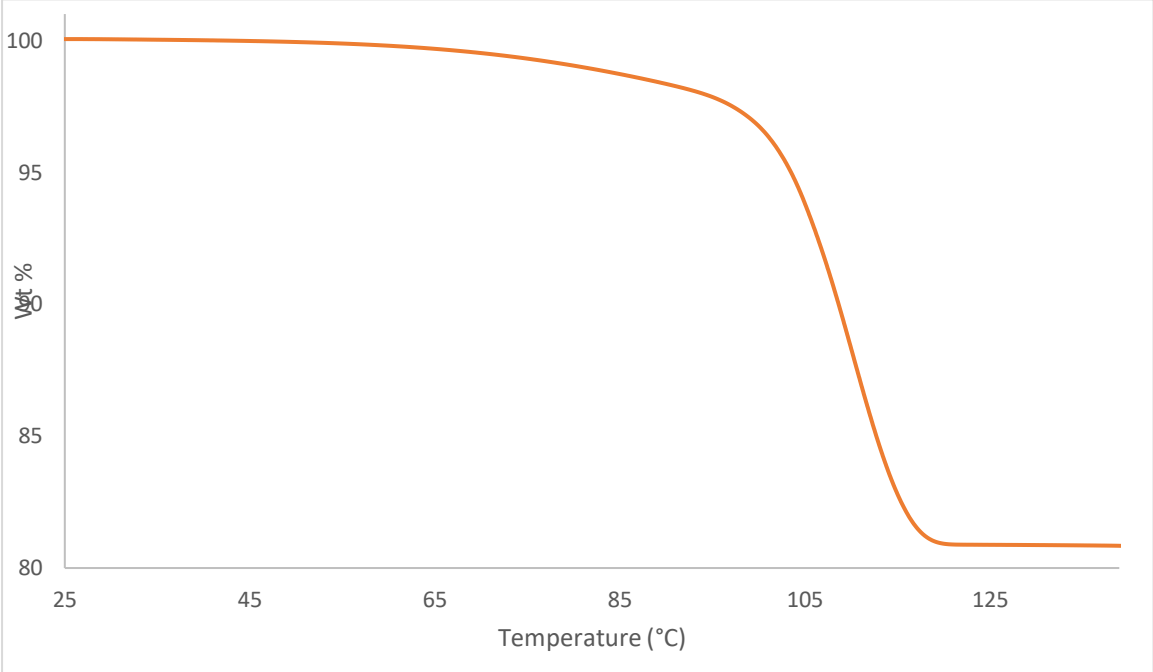

Figure 2.11: Thermogravimetric analysis TGA of single crystals of CP1 in which the loss of weight is seen as the temperature is raised. The mass percent of benzene guest that was forced to vacate was 19.47% which is close to the mass percent of benzene guest per repeat unit based on XRD data which is exactly 17.19%. Iit is expected that the excess percent seen from experimental TGA is benzene molecules bound to the outside surface of the crystals even after they had been placed under reduced pressure before being heated.

Single crystals of CP1 were placed in a vial with reduced pressure for twenty days and the two benzene guests per crystal repeat unit proved to be tightly bound to the system. NMR spectra showed that when even at the twenty-day mark there were still 0.33 molecules of the two original benzene guests per repeat unit left in the system **(Figure 2.8)**. Seeing that the benzene guest seemed to have such a strong binding affinity, it led to the question of exactly how strong were the intermolecular forces holding the aromatic guest to the aromatic system.

Because reduced pressure was simply not enough to fully remove the guest from the CP1 single crystals, we then explored using higher temperature as a measure for forcing the benzene from the system. Thermogravimetric Analysis (TGA) **(Figure 2.11)**

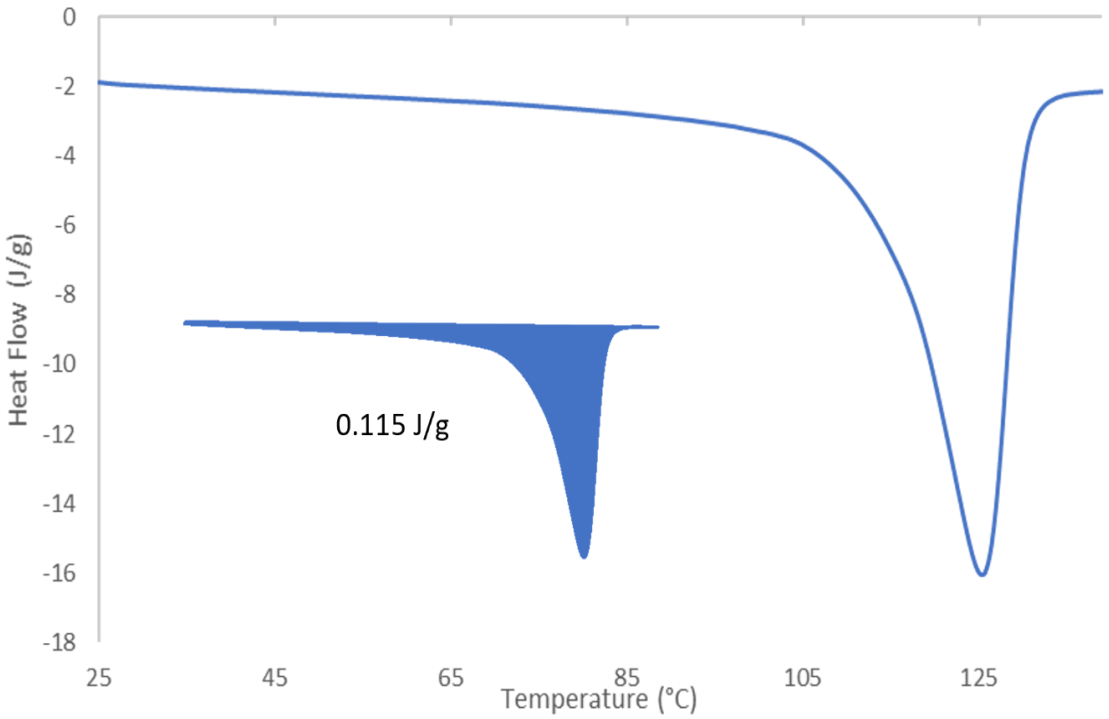

Figure 2.12: Differential Scanning Calorimetry (DSC) was performed to quantitatively measure how much energy it took to for benzene guest molecules from the CP1 host. As temperature was raised over time, and endotherm occurred when the benzene had gotten to a high enough temperature that it was able to be liberated from its guest locations in the crystal repeat unit and egress from the sample of single crystals as a gas.

was used to compare the loss of benzene guest and a loss of weight as the temperature was raised. This measurement also gave mass percent ($\Delta m_s\%$) of experimental benzene lost from the sample to be 19.47%. This percent closely matched the amount of benzene guest within a crystal repeat unit based on XRD data. The exact amount of benzene percent weight per repeat unit is 17.19% and it is expected that the excess percent seen from experimental TGA is benzene molecules bound to the outside surface of the crystals even after they had been placed under reduced pressure before being heated slowly to 125 °C.

Once the mass percent was seen to be acceptable from experimental TGA, we then were curious to know the exact amount of energy that was needed to force the

benzene guest molecules to vacate. Differential Scanning Calorimetry (DSC) **(Figure 2.12)** was then used to measure the experimental enthalpy of binding (ΔH_{sExp}) per gram it takes to desolvate the benzene guest from the polymer host sample. This is done by measuring the integration of the endotherm that occurs once the sample is ramped to 125 °C over time.[23] This data showed that the amount of energy needed to vacate the benzene guest from the sample was 115.0 J/g.

To measure the enthalpy of binding with the data from experimental TGA and DSC, the enthalpy of binding (ΔH_s) of the benzene guests within the structure per repeat unit mole can be calculated. Using the data from DSC when measuring the energy of desolvation (ΔH_{sExp}) and dividing it by the mass percent of benzene egressed during TGA and then multiplied by benzene's molecular weight (M_s), the enthalpy of binding (ΔH_s) can be found.[23] From the experimental, the enthalpy of binding proved to be 46.54 kJ/mol.

$$\Delta H_s = [(\Delta H_{sExp}\ x\ 100)/\ \Delta m_s\%]\ x\ M_s$$

When compared to the enthalpy of vaporization ($\Delta H°_{vap}$), of benzene alone which is 30.8 kJ/mole is clear that the benzene guest enthalpy of binding is significantly higher in the CP1 crystalline form which is expected to be due to the vastly diverse electrostatic environment. The benzene guest is not only bound by π/π and CH/π interactions but instances to which acidic protons are also attracted by oxygens from the boronate esters.[24] In essence the entire structure holds the benzene guests, but the benzene guests also hold the host system together at the same time. It should be noted 1that this

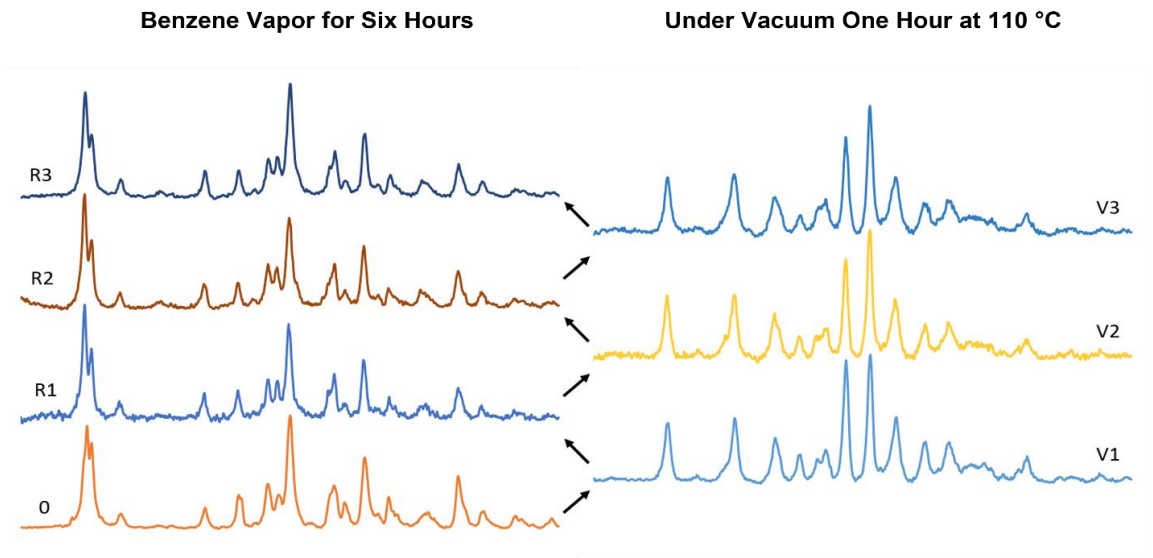

Figure 2.13: Starting with pure CP1 made from benzene solvent, three replicates of removing benzene guest through short path distillation highlighting the large change in crystal structure between CP1 and VCP1 when viewed based on PRXD diffraction data Label 0 is the initial CP1 single crystals. V1, V2, and V3 (right) represent experimental PXRD when VCP1 had transitioned from CP1 and (left) R1, R2, and R3 represent experimental PXRD when VCP1 had reversibly transitioned back to CP1.

enthalpy is not quantitatively comparable to enthalpy of vaporization ($\Delta H°_{vap}$) because the two enthalpies discussed are two completely different systems and environments where one is the enthalpy of binding of benzene within a crystalline coordinated polymer to which guest benzene can be viewed as a solid and the other is the enthalpy of vaporization where the only intermolecular forces are from benzene molecules interacting are only with one another.

2.4: Vacant Coordinated Polymer 1 (VCP1)

Since the enthalpy of binding had been calculated and seen to be higher in energy than expected, the question was then asked if the crystal had transitioned during the formation of vacant CP1 (VCP1). Powder X-Ray Diffraction (PXRD) showed that once all benzene guest had vacated CP1, the diffraction spectra was a much different crystal structure. The theoretical PXRD pattern given from CP1's XRD analysis data did not match

VCP1's experimental PXRD at all which gave evidence that a new, yet unknown, crystal structure had formed.

2.4.1: Reversibility of Benzene Guest Exchange of CP1 and VCP1 Transitions

Since the enthalpy of binding for benzene within CP1 was higher than expected and because the PXRD had shown that a new crystal structure occurs during the transitioning of CP1 to VCP1, we questioned if benzene vapor could find its way back into the pores of VCP1 leading to a reversible process.

2.4.2: Results

When CP1 was heated to 110 °C with reduced pressure (12 mmHg) for an hour the results seen were that CP1 had successfully transitioned to VCP1. PXRD of the starting material before this transition and then after showed that the transition had occurred. This sample of VCP1 was then placed in the presence of benzene vapor in a sealed vial overnight such that the only interaction that VCP1 had with benzene was in the vapor form. The following day the PXRD and NMR showed that the crystal structure of CP1 and had been retained and the material had only taken in two benzene guest molecules as seen from XRD diffraction data. This process was repeated a total of three times with the same sample and it was proven that this process was incredibly reversible **(Figure 2.13)**.

2.4.3: Discussion

The reversibility of this process highlights another post synthetic modification that CP1 can undergo and also gives evidence that VCP1 is certainly capable of benzene intake from its environment whether the resulting goal is to achieve the original crystalline

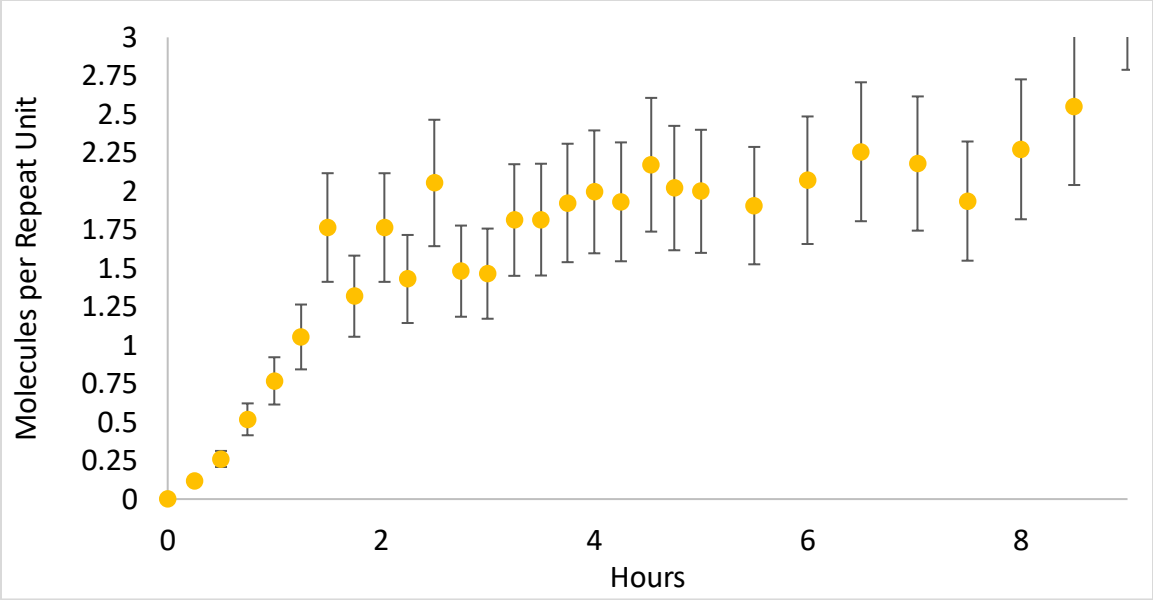

Figure 2.14: The error from loading VCP1 with benzene vapor to transition it back to CP1 three times. Error calculates is rought 20%..

repeat unit or not. Not only can CP1 undergoing SCSC transitions when in the presence of other solvents discussed previously, but is capable of having the benzene guest vacated and then reattaining it repeatedly. The error associated with the vapor loading experiments is roughly about 20 % which shows that efforts could be taken in order to increase the accuracy **(Figure 2.14)**. It seems these dynamically bonded coordination polymers might have a higher propensity toward post-synthetic modification than previously thought. Unfortunately, the actual translucent yellow single crystals became opaque and paler leading to indication that VCP1 had lost single crystallinity which was also proven when put through XRD analysis in which the diffraction pattern showed as rings, proving the sample was now polycrystalline. This meant that XRD analysis for the new crystal structure for VCP1 could not be elucidated with this method. Though this data that could be helpful with understanding how the reversible process occurs, there is other application when considering how carcinogenic benzene is. This could be helpful

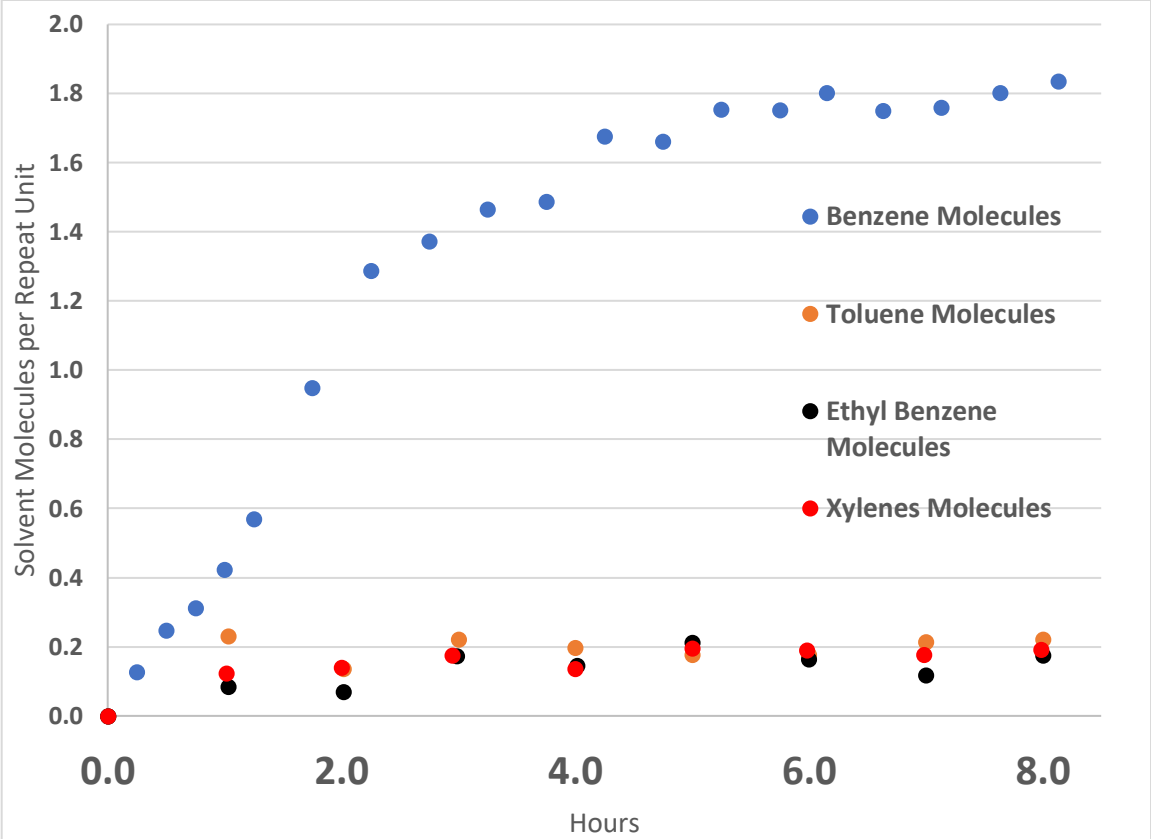

Figure 2.15: When VCP1 was exposed to benzene, toluene, ethyl benzene, and xylenes separtately, it was seen that it was highly selective for only benzene. At most, roughly only 0.2 molecules of toluene, ethyl benzene, and xylenes are absorbed into VCP1 as opposed to benzene that can be almost absorbed within eight hours up to the known two molecules per crystal repeat unit seen previously in reversibility studies and XRD data.

in absorbing benzene for environmental use and could lead to future designs to absorb other compounds. To understand the rate of benzene vapor absorbed by VCP1, a benzene vapor study took place three times. This showed that the two benzene guests per repeat were almost absorbed within eight hours with a 20% margin of error. This error is also expected to have occurred in vapor studies not yet discussed.

2.4.4: Experimental

PXRD was performed on freshly grown CP1 crystals to show the sample was pure in phase. A round bottom flask was charged with CP1 single crystals (1.00 g, 1.10 mmol)

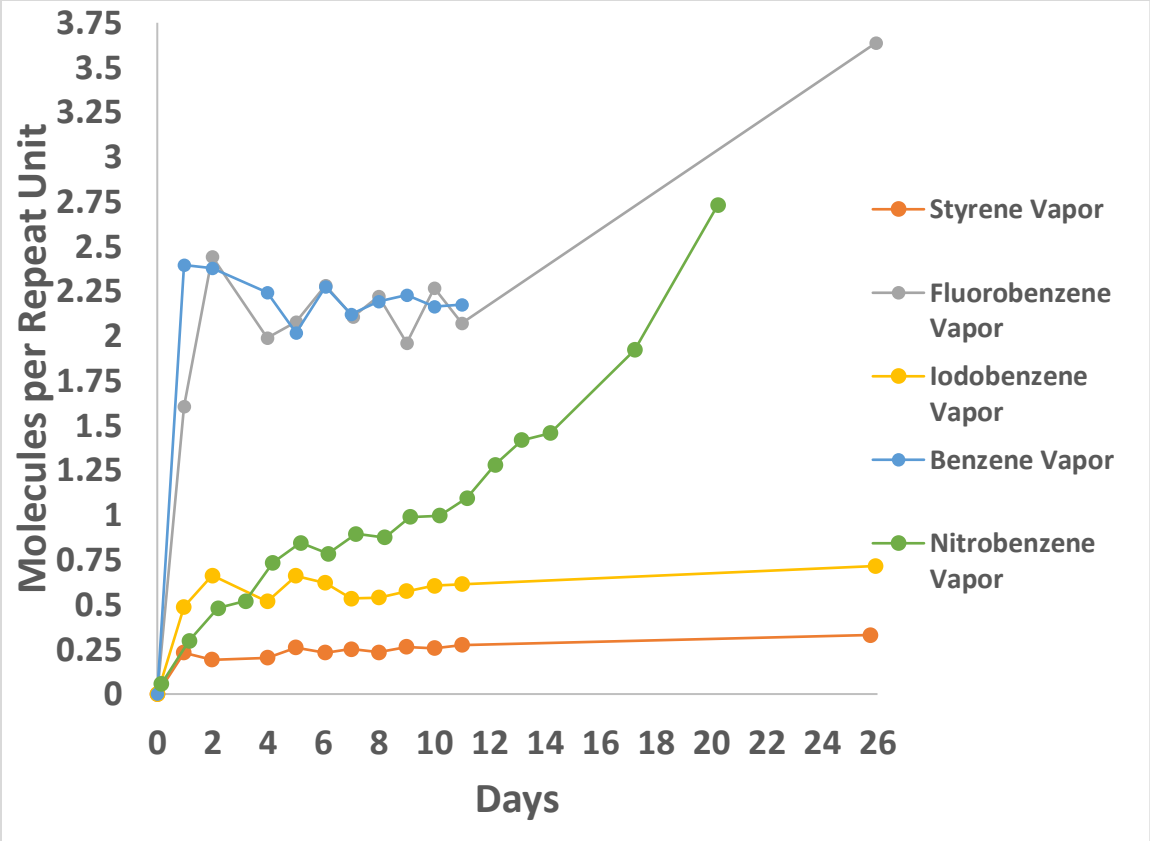

Figure 2.16: When VCP1 was exposed to styrene, fluorobenzene, iodobenzene, benzene, and nitrobenzene vapors separtately, it was seen that it was highly selective for fluorobenzene and benzene. VCP1 seemed much less selective styrene which leveled out at 0.25 molecules per crystal repeat also leveled out for iodobenzene with 0.5 molecules per crystal repeat unit. Nitrobenzene seemed to continue to be absorbed in a more linear way but it is not clear if this was actually being absorbed or if the very low vapor pressure was actually causing it to just condense on tops of the VCP1 crystals.

and placed with reduced pressure (12 mmHg) and heated with short path distillation (Kuglerohr) for one hour at 110 °C. The resulting product was yellow and opaque polycrystalline VCP1. PXRD was performed on the new VCP1 crystals which showed that the crystal transition had occurred. A 1-dram vial was then filled half way with VCP1 crystals and placed in a 4-dram vial containing benzene (5 mL). The sample was left over night. The following morning, NMR and PXRD were performed and it was seen that two benzene guest molecules per repeat unit had been absorbed and that the VCP1 crystals had transitioned back to the original CP1 powder diffraction pattern.

2.5: Vapor Selectivity of Common Carcinogenic Compounds Seen Within the Oil Industry

Once benzene vapor had been seen to cause a reversible process to transition from VCP1 to CP1 and selectively absorb the two benzene molecules per repeat unit, the next question was how selective it was compared to other carcinogenic compounds found in the oil industry.[25]

2.5.1: Results and Discussion

When VCP1 was separately exposed to a benzene, toluene, ethyl benzene, and xylene (BTEX) environment to find over time how much could be absorbed, it was seen that though all had much in common with the exception that all but benzene had small carbon substituent(s), VCP1 was highly selective for benzene **(Figure 2.15)**. When VCP1 was only exposed to the vapor of toluene, ethyl benzene, and xylenes for an eight-hour period, only 0.2 molecules per polymer repeat unit were absorbed which was seen from NMR data. When exposed to benzene vapor, it still followed the trend seen earlier when VCP1 is exposed to benzene vapor.

2.5.2: Experimental

General Procedure for Vapor Studies

Eight 1-dram vials were charged with VCP1 (≈30.0 mg, 0.04 mmol) for each, benzene, toluene, ethyl benzene, and xylenes for a total of 32 samples. One of the eight total vials for each solvent was placed in a 4-dram vial containing one of the four solvents (5 mL) and then sealed. This means that at the same time a VCP1 sample was placed in one 4-dram of benzene, a second sample was placed in a 4-dram of toluene, a third was placed in a 4-dram of ethyl benzene, and a fourth was placed in a 4-dram of xylenes and

the exact times were recorded. This was repeated every fifteen minutes until all VCP1 samples in 1-dram vials were now sealed within 4-dram vials. Once all samples were sealed and exposed to solvents, a period of 15 minutes passed and all samples in the same order of them being sealed, were open and prepared for NMR and again, the exact time each 4-dram was opened, the time was recorded. This method means that all NMR samples that were exposed to vapor in fifteen minutes intervals from a range of fifteen minutes to two hours and were ready for analysis. This was repeated three more times on two-hour intervals which gave an accurate reading from NMR data in which the amount of solvent absorbed for eight hours could be seen in fifteen-minute intervals for each of the four solvents **(Figure 2.15)**.

2.6: Vapor Selectivity of Aryl Halides, Styrene, and Nitrobenzene

Once the selectivity of VCP1's ability to absorb BTEX vapors had been investigated it was decided to look into different aryl halide vapor selectivity with the addition of styrene and nitrobenzene. Styrene was included because though it may have things in common with BTEX compounds, it is also like benzene in the sense that all carbons are sp^2 hybridized while nitrobenzene is the same for carbon and heteroatoms.

2.6.1: Results and Discussion

The selectivity for VCP1's ability to absorb more aromatic compounds **(Figure 2.16)** was further investigated with fluorobenzene due to its being the smallest aryl halide and iodobenzene for being one of the larger. Styrene was also chosen because it has commonality with the BTEX compounds because of its ethylene substituent with the exception that all carbons are sp^2 hybridized, giving it something in common with benzene

alone. Lastly, nitrobenzene was examined because all carbon and heteroatoms are sp^2 hybridized and because the strong electronegativity it holds leading to the question if that might aid or hinder its ability to find itself as a guest within the VCP1 crystal framework. The benzene followed the same trend seen previously and fluorobenzene also had the same outcome. It is expected that because the fluorine on the fluorobenzene is so small, that it was able to act much like a hydrogen on benzene in which it was not inhibited in taking the positions as a guest within the VCP1 and transitioning it to a crystalline structure that is very close to the of CP1. This was also seen in an SCSC transition in which fluorobenzene was able to replace benzene as a guest when CP1 was in the presence of fluorobenzene **(Chapter 2.2.4)**. This transition had a crystalline structure that had so much in common with CP1 that their diffraction pattern was virtually identical when XRD analysis had been performed. Something that should be discussed is that during these vapor studies it took many tries to get data that made sense because early on, there would be large outliers in which solvent vapor that had been absorbed would be much larger then the other experimental trends when measured with NMR. These anomalies were discovered to not be an issue with all VCP1 crystals in the sample dissolving into the solvent used for NMR. When this occurred, it meant that the solvent would take the place of absorbed solvent vapor when the VCP1 crystals not fully dissolved, essentially forcing excess solvent vapor absorbed into the deuterated solution. Due to this issue, the measurement of absorbed vapor would not be correct and often be very high when viewed as an absorbed number of molecules per repeat unit of VCP1. In the case of fluorobenzene, this issue is highlighted **(Figure 2.16)** in fluorobenzene's last data point.

Styrene and iodobenzene were also capable of being absorbed by VCP1 but it was not selective. They leveled off just like toluene, ethyl benzene, and xylenes to which styrene was only absorbed up to 0.25 molecules per crystal repeat unit and iodobenzene absorbed up to 0.5 molecules per repeat unit. Interestingly iodobenzene was capable of being absorbed only as half of one molecule per repeat unit because it may have been able to take a spot as a guest within VCP1 that would be between two repeat units in which half of it is part of the unit cell. Last to be discussed is nitrobenzene that over days seems to stay mostly linear. It is expected if nitrobenzene did get absorbed into VCP1 it was selective with a mostly linear absorption seen.

2.6.2: Experimental

The procedure used for styrene, fluorobenzene, iodobenzene, benzene, and nitrobenzene when investigating the selectivity of VCP1 for absorbing these solvents followed the general procedure previously mentioned when VCP1's selectivity for BTEX was evaluated. The only difference is that the eight 1-dram VCP1 samples used for each solvent were placed in a 4-dram with each solvent daily for a total of eight days and then NMR measurements took place roughly every 24 hours after the last 4-drams were sealed. The NMR measurements were then measured daily.

2.7: Conclusion

It has been seen that that the coordination of DE1 and DPE afforded a highly robust crystalline coordination polymer by merely dissolving them into a solution of benzene then analyzed by XRD. With the structure known it was seen that for every single repeat unit of CP1 there was a total of two benzene guest compounds. CP1 proved to be

similar to other organic system's in literature and was capable of having an SCSC transitions in which benzene was replaced by another solvent molecule that led to post synthetic modification in which the overall crystalline polymer chain's structure ranged between unmodified, slightly, and dramatically modified.[9] Three SCSC transitions occurred in which three solvents were able to exchange the benzene guests in one liquid exchange overnight with styrene, and two separate vapor exchanges with acetonitrile and fluorobenzene over two weeks. The styrene transition **(Figure 2.4)** did have slight changes in which the original CP1 crystal polymer's square wave pattern was retained and the dihedral bond angle at the juncture where DE1 and DPE linkers connected did slightly change. The acetonitrile transition **(Figure 2.6)** seemed to be quite dramatic because the inversion center of the repeat unit changed to have much more dimensional freedom and the crystal system transitioned from monoclinic to triclinic. Lastly, the fluorobenzene transition simply replaced benzene and there was virtually no change to the crystal polymer's repeat unit with the new guest taking the exact locations that benzene had initially.

Furthermore, an effort to understand how strongly bound the benzene guests were within the system took place. It was seen with reduced pressure, the benzene guest within CP1 still existed even after twenty days **(Figure 2.8)** measured by NMR. With the use of solid state carbon NMR, it is clearly seen that both benzene guests are each placed in their own specific environments in when each has their own intramolecular forces confining them to their specific locations in the crystal structure. In order to have a more quantitative answer to this question, CP1 single crystals were studied with TGA and DSC.

TGA **(Figure 2.9)** proved that the amount of benzene guest molecules seen in the crystal repeat unit given from XRD analysis was correct and gave experimental data for the mass percent of benzene within the host framework. This was followed by DSC **(Figure 2.11)** which calculated the amount of energy needed to expel the benzene guest from the CP1 sample. With the use of data from both instruments, the enthalpy of binding was calculated to be 46.54 kJ/mol which when compared to benzene's enthalpy of vaporization, was quite high.[23] During these experiments, CP1 would transition to VCP1 and when PXRD was performed on these samples once the host was vacant of benzene guest. To our surprise, VCP1 had a much different PXRD spectra when compared to the theoretical PXRD given from previous XRD analysis.

In the next step, samples of VCP1 were sealed in vials and exposed to benzene vapor overnight to see if benzene would enter itself back within the crystal repeat unit or just be absorbed in general. It seems the larger than expected enthalpy of binding that was previously calculated had shown to have impact because not only did NMR data give evidence that only two benzenes reentered the VCP1 host, PXRD spectra proved that the transition of CP1 to VCP1 was reversible **(Figure 2.13)** when VCP1 was placed in benzene vapor. The spectra seen after VCP1 was sealed in benzene vapor overnight proved that it matched the original CP1 before the first transition and the theoretical from XRD analysis. Since the transition of CP1 to VCP1 was so reversible, even repeatedly, VCP1 samples were placed within other aromatic solvent vapor environments such as BTEX solvents **(Figure 2.5.1)** which are found within the oil industry and are also carcinogenic.[25] In addition to BTEX vapor studies, other VCP1 samples were placed within fluorobenzene,

iodobenzene, nitrobenzene and styrene **(Figure 2.5.2)** Both of these experimental studies proved that VCP1 was only selective to absorbing benzene and fluorobenzene.2.7:

2.8: References

(1) Cai, M.; Daniel, S. L.; Lavigne, J. J. Conjugated Bis and Poly(Dioxaborole)s for Optical Sensing of Lewis Bases Based on Main-Chain Perturbations. *Chemical Communications* **2013**, *49* (58), 6504–6506. https://doi.org/10.1039/C3CC41189C.

(2) Niu, W.; Smith, M. D.; Lavigne, J. J. Self-Assembling Poly(Dioxaborole)s as Blue-Emissive Materials. *Journal of the American Chemical Society* **2006**, *128* (51), 16466–16467. https://doi.org/10.1021/ja065986c.

(3) Maynor, M. S.; Nelson, T. L.; O'Sulliva, C.; Lavigne, J. J. A Food Freshness Sensor Using the Multistate Response from Analyte-Induced Aggregation of a Cross-Reactive Poly(Thiophene). *Organic Letters* **2007**, *9* (17), 3217–3220. https://doi.org/10.1021/ol071065a.

(4) Rambo, B. M.; Tilford, R. W.; Lanni, L. M.; Liu, J.; Lavigne, J. J. Boronate-Linked Materials: Ranging from Amorphous Assemblies to Highly Structured Networks. In *Macromolecules Containing Metal and Metal-Like Elements*; Abd-El-Aziz, A. S., Carraher Jr., C. E., Pittman Jr., C. U., Zeldin, M., Eds.; John Wiley & Sons, Inc.: Hoboken, NJ, USA, 2009; Vol. 9, pp 255–294. https://doi.org/10.1002/9780470527085.ch6.

(5) Liu, J.; Lavigne, J. J. *Boronic Acids*, Second.; Hall, D. G., Ed.; Wiley-VCH Verlag GmbH & Co. KGaA: Weinheim, Germany, 2011; Vol. 2. https://doi.org/10.1002/9783527639328.

(6) Stephens, A. J.; Scopelliti, R.; Tirani, F. F.; Solari, E.; Severin, K. Crystalline Polymers Based on Dative Boron–Nitrogen Bonds and the Quest for Porosity. *American Chemical Society Materials Letters* **2019**, *1* (1), 3–7. https://doi.org/10.1021/acsmaterialslett.9b00054.

(7) Luisier, N.; Bally, K.; Scopelliti, R.; Fadaei, F. T.; Schenk, K.; Pattison, P.; Solari, E.; Severin, K. Crystal Engineering of Polymeric Structures with Dative Boron–Nitrogen Bonds: Design Criteria and Limitations. *Crystal Growth & Design* **2016**, *16* (11), 6600–6604. https://doi.org/10.1021/acs.cgd.6b01292.

(8) Christinat, N.; Croisier, E.; Scopelliti, R.; Cascella, M.; Röthlisberger, U.; Severin, K. Formation of Boronate Ester Polymers with Efficient Intrastrand Charge-Transfer

Transitions by Three-Component Reactions. *European Journal of Inorganic Chemistry* **2007**, *2007* (33), 5177–5181. https://doi.org/https://doi.org/10.1002/ejic.200700723.

(9) Xiao, W.; Hu, C.; Ward, M. D. Guest Exchange through Single Crystal–Single Crystal Transformations in a Flexible Hydrogen-Bonded Framework. *Journal of the American Chemical Society* **2014**, *136* (40), 14200–14206. https://doi.org/10.1021/ja507689m.

(10) Kittikhunnatham, P.; Som, B.; Rassolov, V.; Stolte, M.; Würthner, F.; Shimizu, L. S.; Greytak, A. B. Fluorescence Polarization Measurements to Probe Alignment of a Bithiophene Dye in One-Dimensional Channels of Self-Assembled Phenylethynylene Bis-Urea Macrocycle Crystals. *The Journal of Physical Chemistry C* **2017**, *121* (33), 18102–18109. https://doi.org/10.1021/acs.jpcc.7b07136.

(11) Xu, W. L.; Smith, M. D.; Krause, J. A.; Greytak, A. B.; Ma, S.; Read, C. M.; Shimizu, L. S. Single Crystal to Single Crystal Polymerization of a Self-Assembled Diacetylene Macrocycle Affords Columnar Polydiacetylenes. *Crystal Growth & Design* **2014**, *14* (3), 993–1002. https://doi.org/10.1021/cg401380a.

(12) Chu, Q.; Swenson, D. C.; MacGillivray, L. R. A Single-Crystal-to-Single-Crystal Transformation Mediated by Argentophilic Forces Converts a Finite Metal Complex into an Infinite Coordination Network. *Angewandte Chemie International Edition* **2005**, *44* (23), 3569–3572. https://doi.org/https://doi.org/10.1002/anie.200500400.

(13) Feng, X.; Ding, X.; Jiang, D. Covalent Organic Frameworks. *Chemical Society Reviews* **2012**, *41* (18), 6010–6022. https://doi.org/10.1039/C2CS35157A.

(14) Tilford, R. W.; Mugavero III, S. J.; Pellechia, P. J.; Lavigne, J. J. Tailoring Microporosity in Covalent Organic Frameworks. *Advanced Materials* **2008**, *20* (14), 2741–2746. https://doi.org/https://doi.org/10.1002/adma.200800030.

(15) Beaudoin, D.; Maris, T.; Wuest, J. D. Constructing Monocrystalline Covalent Organic Networks by Polymerization. *Nature Chemistry* **2013**, *5* (10), 830–834. https://doi.org/10.1038/nchem.1730.

(16) Zhang, Y.-B.; Su, J.; Furukawa, H.; Yun, Y.; Gándara, F.; Duong, A.; Zou, X.; Yaghi, O. M. Single-Crystal Structure of a Covalent Organic Framework. *Journal of the American Chemical Society* **2013**, *135* (44), 16336–16339. https://doi.org/10.1021/ja409033p.

(17) Bojdys, M. J.; Briggs, M. E.; Jones, J. T. A.; Adams, D. J.; Chong, S. Y.; Schmidtmann, M.; Cooper, A. I. Supramolecular Engineering of Intrinsic and Extrinsic

Porosity in Covalent Organic Cages. *Journal of the American Chemical Society* **2011**, *133* (41), 16566–16571. https://doi.org/10.1021/ja2056374.

(18) Kim, S.; Choi, H. C. Recent Advances in Covalent Organic Frameworks for Molecule-Based Two-Dimensional Materials. *American Chemical Society Omega* **2020**, *5* (2), 948–958. https://doi.org/10.1021/acsomega.9b03549.

(19) AU - Karagiaridi, O.; AU - Bury, W.; AU - Sarjeant, A. A.; AU - Hupp, J. T.; AU - Farha, O. K. Synthesis and Characterization of Functionalized Metal-Organic Frameworks. *JoVE* **2014**, No. 91, e52094–e52094. https://doi.org/doi:10.3791/52094.

(20) Rice, A. M.; Dolgopolova, E. A.; Shustova, N. B. Fulleretic Materials: Buckyball- and Buckybowl-Based Crystalline Frameworks. *Chemistry of Materials* **2017**, *29* (17), 7054–7061. https://doi.org/10.1021/acs.chemmater.7b02245.

(21) Rice, A. M.; Leith, G. A.; Ejegbavwo, O. A.; Dolgopolova, E. A.; Shustova, N. B. Heterometallic Metal–Organic Frameworks (MOFs): The Advent of Improving the Energy Landscape. *American Chemical Society Energy Letters* **2019**, *4* (8), 1938–1946. https://doi.org/10.1021/acsenergylett.9b00874.

(22) Uribe-Romo, F. J.; Hunt, J. R.; Furukawa, H.; Klöck, C.; O'Keeffe, M.; Yaghi, O. M. A Crystalline Imine-Linked 3-D Porous Covalent Organic Framework. *Journal of the American Chemical Society* **2009**, *131* (13), 4570–4571. https://doi.org/10.1021/ja8096256.

(23) Chadha, R.; Arora, P.; Saini, A.; Jain, D. S. Solvated Crystalline Forms of Nevirapine: Thermoanalytical and Spectroscopic Studies. *AAPS American Association of Pharmaceutical Scientists* **2010**, *11* (3), 1328–1339. https://doi.org/10.1208/s12249-010-9511-z.

(24) Nishio, M. CH/π Hydrogen Bonds in Crystals. *CrystEngComm* **2004**, *6* (27), 130–158. https://doi.org/10.1039/B313104A.

(25) Avens, H. J.; Unice, K. M.; Sahmel, J.; Gross, S. A.; Keenan, J. J.; Paustenbach, D. J. Analysis and Modeling of Airborne BTEX Concentrations from the Deepwater Horizon Oil Spill. *Environmental Science & Technology* **2011**, *45* (17), 7372–7379. https://doi.org/10.1021/es200963x.

CHAPTER 3: ALL POLYMER STRUCTURES FORMED IN DIFFERENT SOLVENT SOLUTION AND INTRODUCING MACROCYCLE

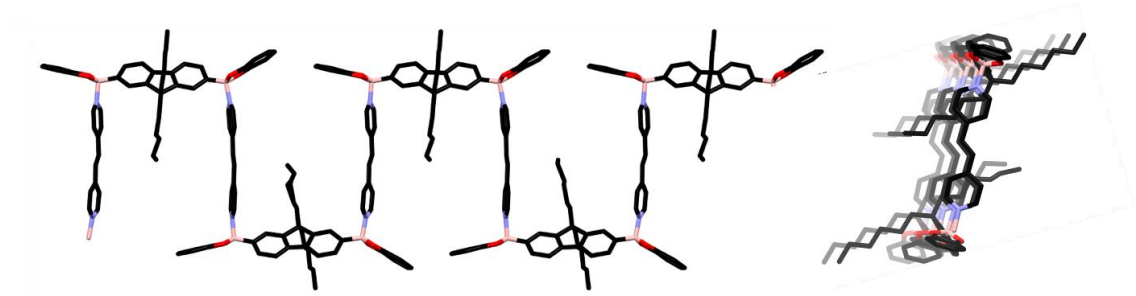

Figure 3.1: Left: Front view of the benzene coordination polymer (CP1) with DE1 linked with dipyridyl ethylene showing its direction alternating symetrically on its inversion center. Right: Side view of the coordination polymer showing a one dimensional infinite chain.

The role of solvent used in crystallization has proven to be critical for a diboronate ester and dipyridyl linker system given the same two starting materials used to create crystalline coordinated polymer networks, the resultant polymer can possess large structural differences based on the solvent used. Single crystal x-ray diffraction is essential in understanding these differences because other spectroscopic techniques give virtually identical results due to identical monomer connectivity for all crystal structures to be discussed. There are many interpretations of how various solvents cause these changes and, at first glance geometry, and steric interactions of the solvent in question would be the dominate answer. But other factors that are believed to cause difference in structure are electronic properties such as polarity and dipole moments of the solvent which can impact the electrostatic interactions with the monomers used. Even when starting materials for both diboronate esters and pyridyl linkers are designed and

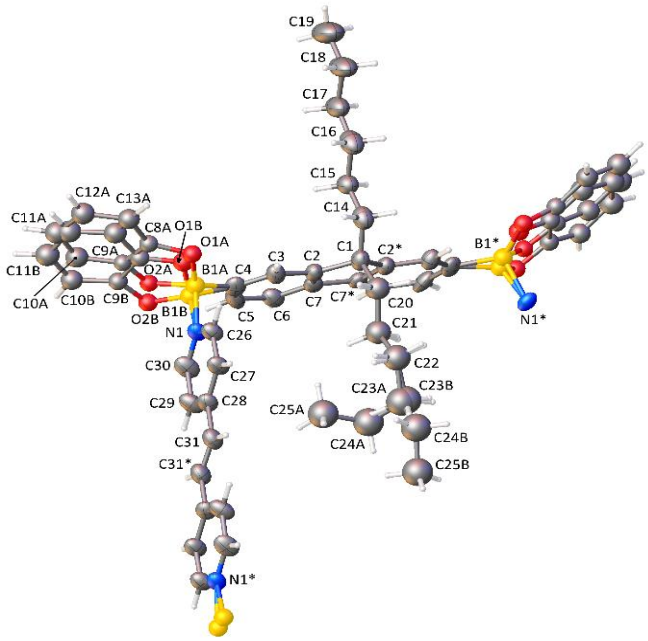

Figure 3.2: Fragment of the polymer repeat unit. Displacement ellipsoids drawn at the 20% probability level. Asterisks denote symmetry-equivalent atoms. The hexyl groups are located on a crystallographic mirror plane; the 1,2-bpe ligand is located on a crystallographic inversion center. Disorder of the $BO_2C_6H_4$ and hexyl groups shown.

synthesized with expectation of specifically creating a polymer or specifically a macrocycle the complex thermodynamics of the reaction matrix often violate this rational thought process.[1–6] This endeavor has shown that the environment must. have a large role even when a large amount of effort is put into trying to minimize the impact. [7,8] Thus, two new derivative diboronate ester monomers will be discussed with one adding more resonance to the system and the second having a strong electron withdrawing group to make the empty p orbital on the two boron's more acidic which would cause a stronger bond with a nucleophile.[9–12] The acidity of the boronate diester also must play a significant role due to it influencing how dynamic the dative bond is which can be due to electron donation, withdrawal, and amount of resonance. The intermolecular and intramolecular forces mentioned above must all be playing a part in how these structures are formed when a nucleophile coordinates with a boronate ester.

3.1: Benzene Coordination Polymer (CP1)

The coordination polymer made in benzene from DE1 and dipyridyl ethylene was discussed in **(Chapter 2)**. Since it is the first of many coordinated polymers discussed, it is reintroduced again to highlight how different each polymer can be solely due to the solvent used to create them. When benzene is used as the solvent the polymer is a one-dimensional chain that exists in a square wave pattern **(Figure 3.1, Figure 3.2)** in which benzene exists as a guest in the crystal structures framework. The dihedral angle between the fluorene and dipyridyl ethylene is 105.51°, and 107.84° which shows that he way the polymer packs causes angle strain at this juncture. The respective bond lengths are 1.670 Å and 1.658 Å which shows a trend that continues in which the larger the dihedral bond angle, the shorter the bond is giving it more s character. One of these angles can be seen between C4, B1, and N1 **(Figure 3.2)**. The dihedral angle of dipyridyl ethylene is evaluated as well due to expectation that it may be partly responsible for the crystal color. This dihedral angle is 173.4° is measured using the nitrogen atoms and the two carbon atoms that form the alkene between the aromatics. CP1 crystals consist of wedges that are yellow in color. The crystal system is monoclinic with a $P2_1/n$ space group with a repeat unit volume of 4,983.0 $Å^3$ and a density of 1.211 grams per cubic centimeter.

3.1.2: Results

XRD was performed on the CP2 crystals and showed that the compound crystallized as large (occasionally > 3 mm) yellow hexagonal plates, which were often clustered together. Several such crystals were surveyed from different reactions and crystal growth attempts, and similar difficulties were encountered in selecting a suitable

data crystal. Despite the large crystal size, diffraction patterns from this material were characterized by very intense low-angle diffraction which degraded rapidly with increasing 2ϑ, resulting in no observable high-angle diffraction above $2\vartheta_{max}$ ~ 40º. This behavior was reproduced from several crystals and at temperatures from 100 K to room temperature. Extensive polymer and solvent disorder in the crystal (described below) is believed to be the reason for these observations.

3.2: Toluene Coordination Polymer (CP2)

3.2.3: Discussion

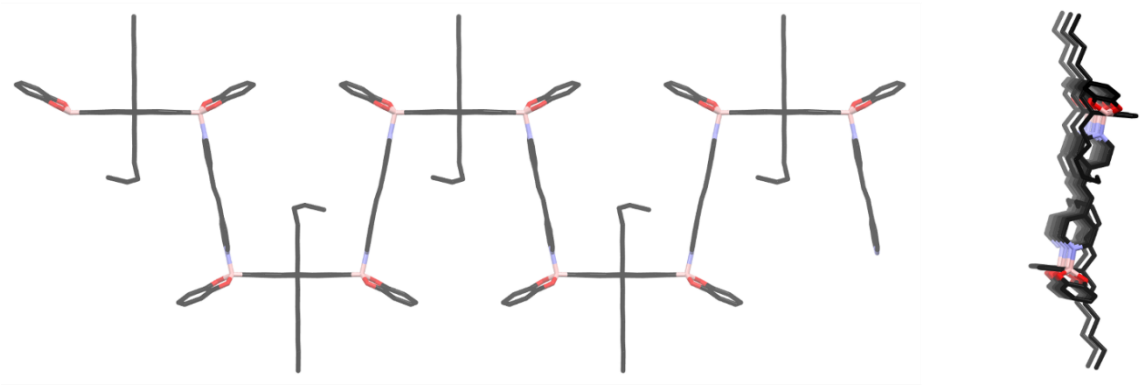

Figure 3.3: Left: Front view of the toluene coordination polymer (CP2) with DE1 linked with dipyridyl ethylene showing its direction alternating symetrically on its inversion center. Right: Side view of the coordination polymer showing a one dimensional infinite chain.

The coordination polymer synthesized in toluene has similarities with CP1 except the for the dihedral angle to which the dipyridyl ethylene linker off of from the diboronate ester **(Figure 3.2)**. When this angle is viewed from the front for CP1 **(Figure 3.3, Left)**, it is much more of a square wave patter with angles forming box like pincers. This same

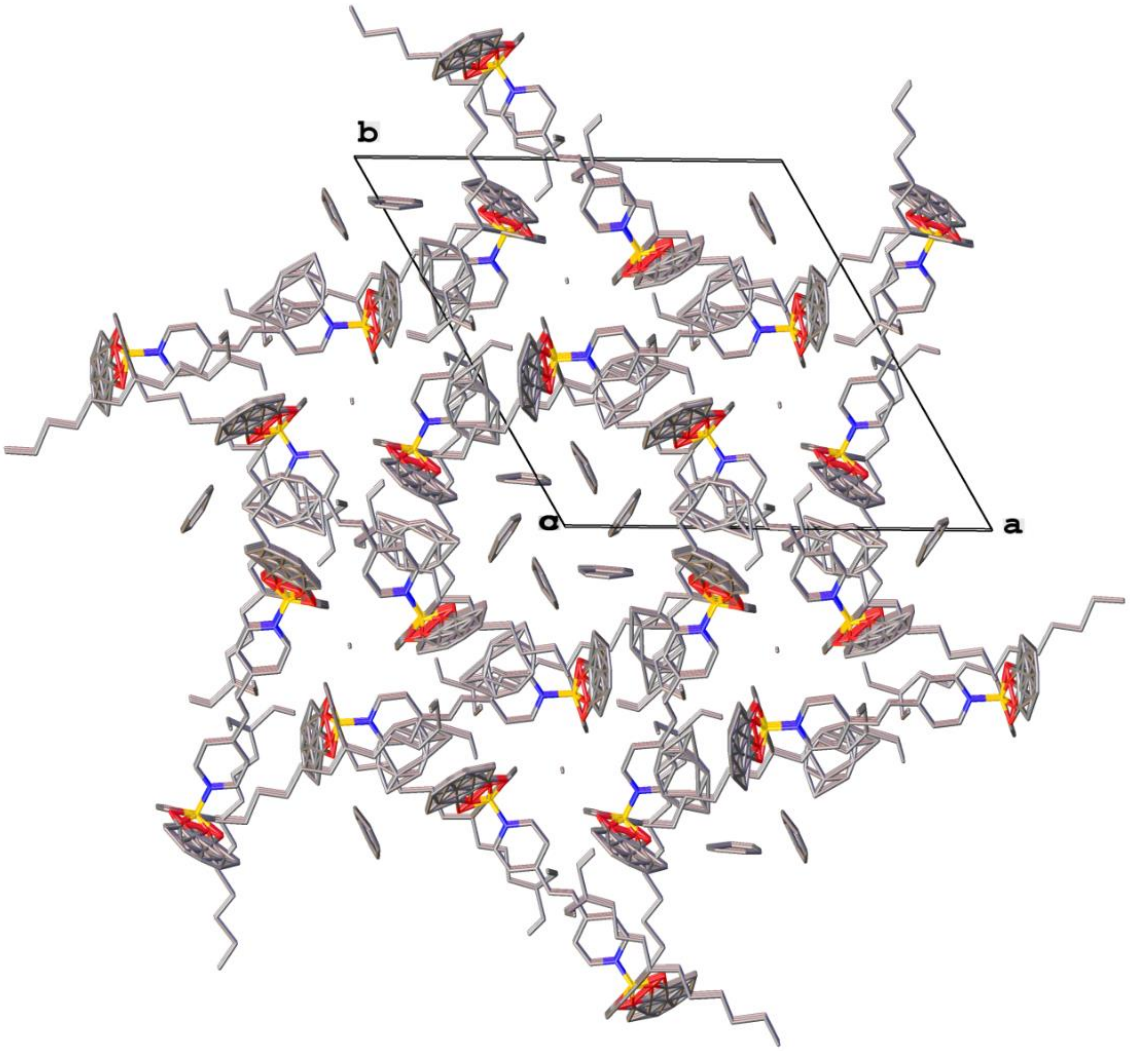

Figure 3.4: Hexagonal packing. The view is down the hexagonal c axis, parallel to the chain direction. Too simplify the view, benzene was used as disordered solvent located between chains instead of toluene.

view for CP2 also forms a pincer like wave but is not as square **Figure 3.3**. Due to the high disorder of the toluene guest, the true amount of toluene guest molecules per repeat unit is unknown. The dihedral angle between the fluorene and dipyridyl ethylene is 103.82° which like seen in CP1, CP2 also has angle strain at this juncture. This angle can be seen between C4, B1, and N1 in **(Figure 3.2)**. The respective boron nitrogen bond length is 1.704 Å. The dihedral angle of dipyridyl ethylene is evaluated is 180° and is measured using the nitrogen atoms and the two carbon atoms that form the alkene between the

aromatics. CP2 crystals consist of hexagonal plates that are yellow in color. The crystal system is hexagonal with a $P6_3/m$ space group with a repeat unit volume of 10,997.9 $Å^3$, and a density of 0.682 grams per cubic centimeter.

Interestingly the flat hexagonal plates when seen as larger single crystals also reflects the crystal system. This packing **(Figure 3.4)** is displayed using benzene molecules as guest molecules instead of toluene to show less disorder. It should be stated that this solvent guest location is just a representation of how the molecules could orient themselves. In the past, this crystal structure was considered "mysterious" because it was very rare to be the only crystalline phase present in the vials that they were grown in. The other phase is a macrocycle that will be discussed later in this chapter. Due to this, further analysis such as TGA could not be used because a pure hexagonal phase crystallization had been so elusive. One crystallization that took place with highly concentrated boronate diester 1 and dipyridyl ethylene in toluene did show that this product did seem to be mostly pure phase CP2 which gives the expectation that this is the kinetic product versus the thermodynamic product of macrocycle that's pure in phase crystalizes over larger amounts of time (weeks).

3.2.4: Experimental

Crystals of CP1 created in benzene were placed in a Kugelrohr under reduced pressure at 110 °C for one hour to which all benzene guest was removed. A four-dram vial was charged with the guest solvent free coordinated polymer (102mg, 0.135 mmol). The vial was heated and stirred while toluene (3 mL) was slowly added drop wise. Upon cooling, yellow crystal clusters appeared rapidly with no red crystals seen leading to an

expectation that the product was pure in phase. The sample was sent to the crystallographer for single crystal XRD. Diffraction data showed that the sample was in fact the rare hexagonal phase.

3.3: Dioxane Coordinated Polymer (CP3)

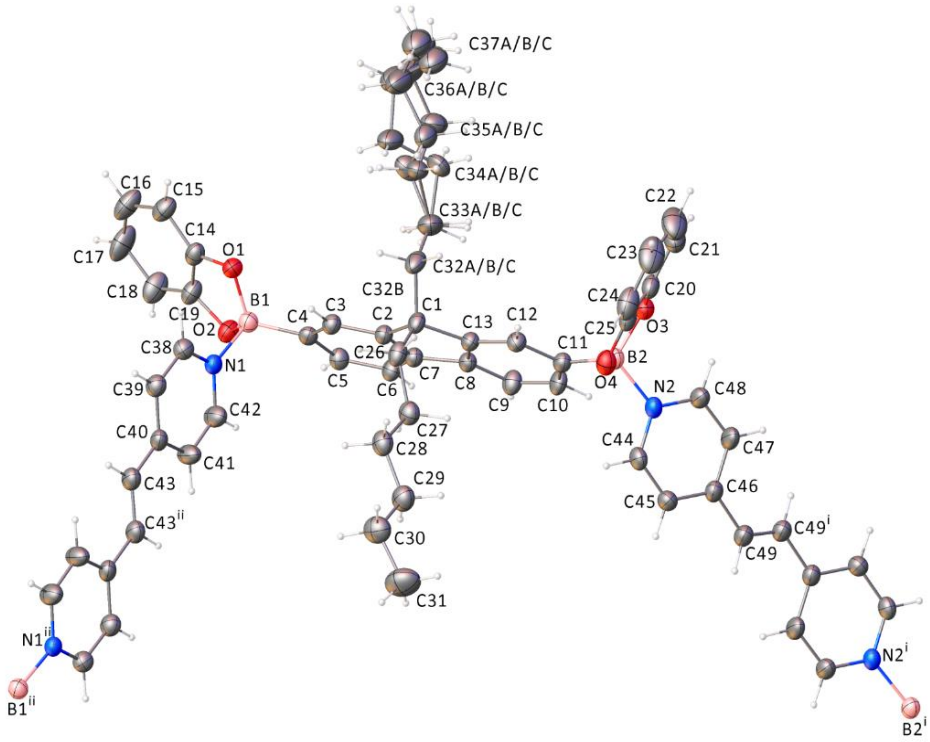

Figure 3.5: Fragment of the polymeric chain repeating unit. Displacement ellipsoids drawn at the 40% probability level.

3.3.2: Results

XRD was performed on the CP3 crystals, and the compound crystallizes in the triclinic system. The space group *P*-1 was confirmed by structure solution. The asymmetric unit consists of one $C_{37}H_{40}B_2O_4$ component of the polymeric $(C_{37}H_{40}B_2O_4)(C_{12}H_{10}N_2)$ chain, half each of two independent $C_{12}H_{10}N_2$ components, each located on a crystallographic inversion center and 1.5 dioxane molecules. One dioxane is located on a crystallographic

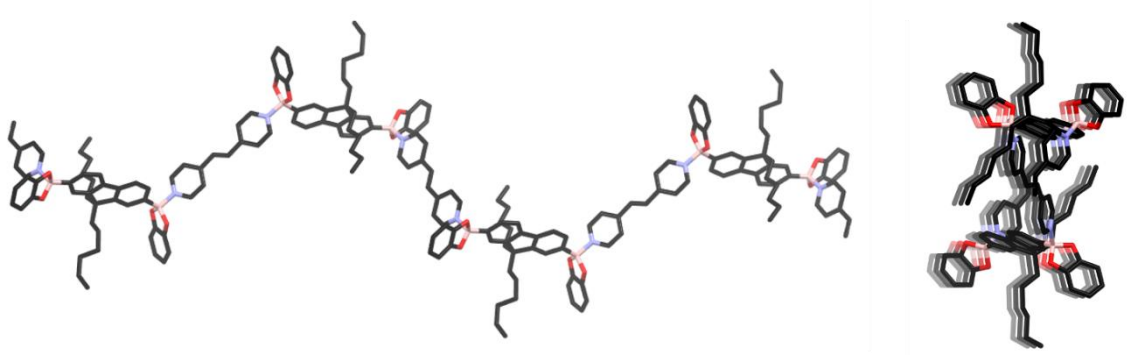

Figure 3.6: Left: Front view of the dioxane coordination polymer with DE1 linked with dipyridyl ethylene showing its direction alternating symetrically on its inversion center. Right: Side view of the coordination polymer showing a one dimensional infinite chain.

inversion center, and only half is present per asymmetric unit. The second independent dioxane is disordered and was modeled with three components. The total disordered dioxane population was constrained to sum to one.

3.3.3: Discussion

The dioxane coordination polymer CP3 is a one-dimensional polymer that alternates in the same up and down wave while also alternating direction from left to right symmetrically mirroring its inversion center **(Figure 3.5, Figure 3.6)**. This significantly lengthens the frequency of the polymer structure repeating itself versus just viewing its crystal repeat unit by its inversion center which has not been seen in what has been previously discussed. CP3 also contains 1.5 dioxane guests per crystal repeat unit. This has commonality to CP1 and CP2 in the sense that it is one-dimensional except when viewing the side, CP3 differs to which it not only is repeating vertically but horizontally as well **(Figure 3.6, Right)**. This difference may be because dioxane's intermolecular interactions are very different than the solvents used in CP1 and CP2 since dioxane is not aromatic, takes up more space, and has two lone pairs on each oxygen. It is expected

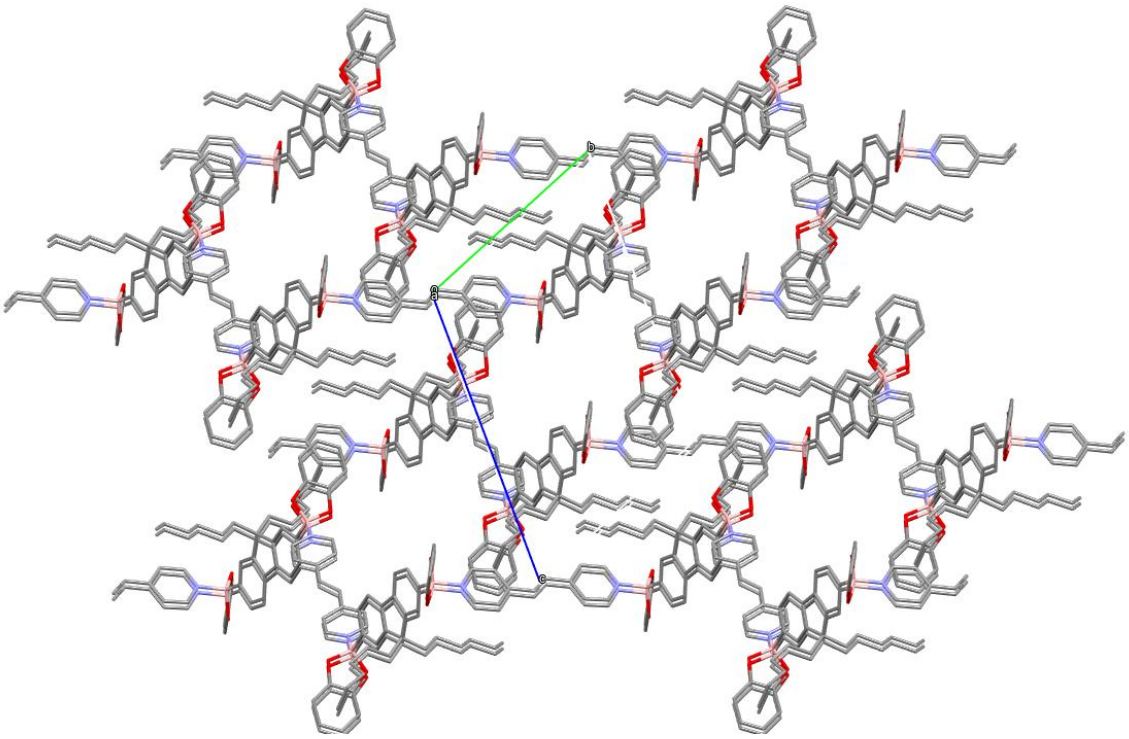

Figure 3.7: View of the dioxane coordinated polymer's packing showing that the dihexyl chains of adjacent polymer chains interacting with one another.

that the large amount of space that dioxane takes up as a guest within the crystal structure's repeat unit, forces the inversion center to repeat in a newly seen horizontal manner. This also may be the reason that there are less solvent guest molecules per repeat unit within this structure when compared to CP1. Dioxane clearly takes up more space than benzene and the dipyridyl ethylene monomers have more dimensional freedom from the DE1 repeat units when compared to CP1. The changes in size do seem to show a trend as the solvent guests in CP1, and CP3 are larger as the coordination polymer's labeling numbers become higher. The dihedral angles between the fluorene and dipyridyl ethylene for CP3 are 107.22° and 109.13° which has much less angle strain as seen in previous coordination polymers at this juncture. This angle can be seen between C4, B1, and N1 in Figure 18. The respective boron nitrogen bond lengths are

1.675 Å and 1.635 Å. CP3 crystals consist of blocks that are orange in color. The crystal system is triclinic with a P-1 space group with a repeat unit volume of 2,383.59 $Å^3$ and a density of 1.233 grams per cubic centimeter.

Commonalities that the three mentioned coordinated polymers have when compared to one another is that they have the same type or intermolecular interactions in which the dihexyl chains of adjacent chains have a lamellar like interaction with their neighbors. The aromatic regions of the polymer chains all interact with their neighboring aromatics regions as well (**Figure 3.7)**.

3.3.4: Experimental

The CP3 crystals originated from a CP1 crystal vapor study which dioxane was meant to only interact as a vapor. This was to see if dioxane vapor might replace the benzene guest and undergo an SCSC transition to which the crystal structure may be different based on XRD data if a change had occurred. A one-dram vial was charged with of CP1 crystals containing benzene guest (50 mg, 0.055 mmol). The one dram was then placed in a four dram with dioxane solvent (7 mL) and capped. The intention of this study was to only allow dioxane vapor to interact with the CP1 crystals but after the four-dram vial was sealed, it was accidently knocked over. This caused the CP1 crystals to become submerged within the dioxane solution. Due to this error, the vial was still left with CP1 crystals still in dioxane solution to find out if new crystals would grow with a dioxane guest as the CP1 crystals slowly dissolved. Over two weeks the vial was left to sit and single crystals did end up growing in the shape of small orange blocks but still large enough to be analyzed by XRD. The sample vial was then sent to the crystallographer for single

crystal XRD.

3.4: Hexanes/Hexanes and Dichloromethane Coordination Polymer (CP4)

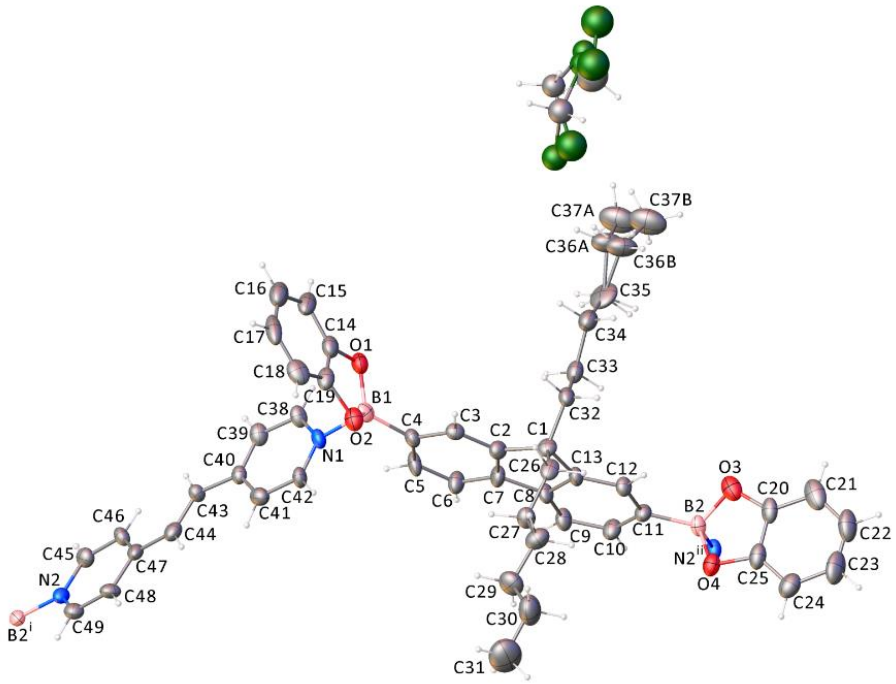

Figure 3.8: Asymmetric unit of the crystal. One polymeric repeat unit. Displacement ellipsoids drawn at the 40% probability level. Superscripts denote symmetry-equivalent atoms. Disordered CH_2Cl_2 atoms not labeled.

3.4.2: Results

XRD was performed on the CP4 crystals, and the compound crystallized in the trigonal system. The pattern of systematic absences in the intensity data was consistent with the enantiomorphous space group pairs $P3_1/P3_2$ and $P3_121/P3_221$. A reasonable and stable solution in $P3_1$ was eventually obtained, giving an absolute structure (Flack) parameter from the final model of -0.02(3). From refinement trials, the crystal is a merohedral twin emulating the higher Laue group (-3*m*). Including the twin matrix (0 1 0 / 1 0 0 / 0 0 -1) in the refinement decreased the *R*1-value from 0.084 to 0.056. The major twin fraction refined to 0.580(4). Solution attempts in the space group $P3_121$, suggested

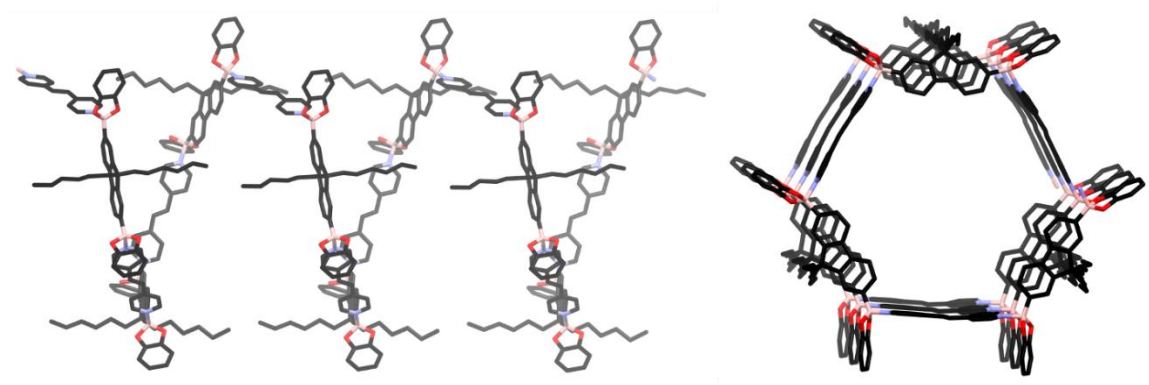

Figure 3.9: Left: Front view of the hexanes/hexanes and dichloromethane coordination polymer with DE1 linked with dipyridyl ethylene showing its direction alternating symetrically on its inversion center. Right Side view of the coordination polymer showing a one dimensional helical infinite chain.

by ADDSYM, were inferior and suggested pseudosymmetry. The best refinement in $P3_121$ converged at $R1/wR2 = 0.074 / 0.201$, but resulted in enlarged displacement ellipsoids for many atoms, especially those corresponding to the hexyl group substituents and atoms C16/C23 and C17/C22 of the dioxo-phenyl substituent in the $P3_1$ model. This suggests that these parts of the structure are incompatible with the two-fold axis imposed by $P3_121$. The CH_2Cl_2 disorder also could not be reasonably modeled in $P3_121$. The achievement of a crystallographically stable twin refinement in $P3_1$ with lower residuals and a reasonable solvent disorder model therefore provides good support for $P3_1$ as the correct space group choice. The asymmetric unit in $P3_1$ consists of one $(C_{37}H_{40}B_2O_4)(C_{12}H_{10}N_2)$ repeating unit and a region of disordered solvent modeled as dichloromethane. The CH_2Cl_2 disorder was modeled using three components having freely refined occupancies of 0.22(1), 0.18(1) and 0.13(1).

3.4.3: Discussion

Coordination Polymer 4 (CP4) exists as yellow wedges which is interesting because

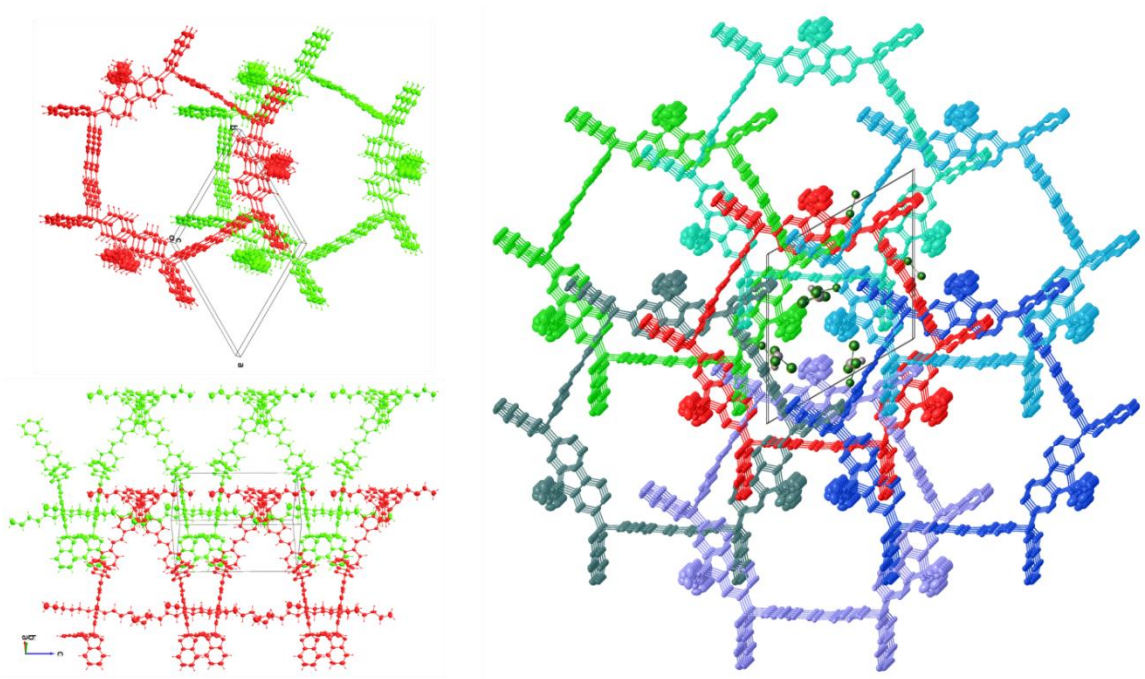

Figure 3.10: Left: Adjacent helices (green, red) interdigitate with neighboring helices. Right: One central helix (red) surrounded by six interdigitated helices (greens / blues). CH_2Cl_2 solvent also shown. Dichloromethane guest molecules can be seen within the red center helix and if only hexanes was used the strucure would be the same except without dichloromethane solvent.

the nature of its structure is different as it is the only true helical structure seen. It should also be noted that the structure is the same if crystallized in hexanes alone or with different ratios of hexanes and dichloromethane. There are no hexanes solvent guests within the structure which is expected to be due to hexanes having more than one isomer as opposed to CP1 and CP3 derived in dioxane which is only one. Hexanes is also not aromatic which is believed to be a driving force for solvent guest inclusion seen with benzene in CP1. Though its not a guest, hexanes is still the driving force for the structure because it dominates the architecture even with dichloromethane present, which is small enough to be held as a guest within the small pores where it can fit **(Figure 3.8, Figure 3.9)**. CP4 does follow the same trend as all other coordination polymers in which the aromatic areas of the repeat unit interact with others as well as the hexyl chains seem to

also interact and tether the crystal structure together. The hexyl chains **(Figure 3.10)** seen in the red helix are interdigitated within surrounding helixes which would give even more structural integrity to the crystalline system than just lamellar like tethering interactions seen in earlier coordinated polymers discussed. The robust nature and size of the single crystals also give evidence to this. Even when any excess solvent or guest has been removed, though with less refinement, single crystal XRD was still able to be performed which proved the original structure was still intact. Of all coordinated polymers seen from these building blocks, CP4 has densely bound structure because of the interdigitating chains, and all intermolecular forces keeping the structure together are from the repeat units of the helix's interaction to one another. What this means is that there is no solvent guest other than dichloromethane if it were to be added during synthesis. The dihedral angles between the fluorene and dipyridyl ethylene for CP4 are 107.4° and 112.82° which has angle strain just above and also below the standard sp^3 bond angle of 109.5°. This angle can be seen between C4, B1, and N1 in **(Figure 3.8)**. The respective boron nitrogen bond lengths are 1.708 Å and 1.620 Å and the dihedral angle of dipyridyl ethylene is evaluated is 172.34° and is measured using the nitrogen atoms and the two carbon atoms that form the alkene between the aromatics. CP4 crystals are pyramidal in shape and yellow in color. The crystal system is trigonal with a $P3_1$ space group with a repeat unit volume of 3,442.1 $Å^3$ and a density of 1.154 grams per cubic centimeter.

3.4.4: Experimental

Crystals of CP1 created in benzene were placed in a Kugelrohr under reduced pressure at 110 ºC for one hour to ensure all benzene guest had been removed. A four-

dram vial was charged with the guest free coordinated polymer (24.8 mg, 0.33 mmol) and dissolved in hexanes (5 mL). Overnight the vial contained larger than average yellow wedge crystals that normally are not seen in such a short time. The sample was sent to the crystallographer for single crystal XRD. Later, larger amounts of the VCP1 were dissolved in hexanes and ratio of dichloromethane and hexanes up to 75:25 percent. Single crystal XRD showed that the only change to the crystal structure was the addition of dichloromethane as a guest in the space of small pores within the helical structure between areas of interdigitated dihexyl chains from other adjacent helixes.

3.5: Vacuum Oven Pyrolysis Coordination Polymer (CPV)

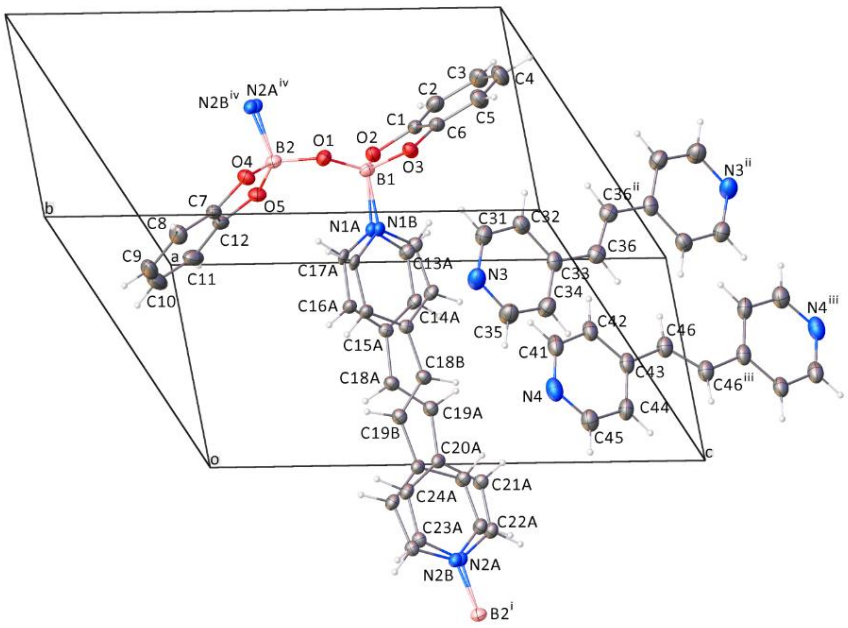

Figure 3.11: Components of the structure, some expanded by symmetry. Superscripts denote symmetry-equivalent atoms. 1,2-bpe linker of the polymeric chains is disordered. Both non-bonded guest 1,2-bpe molecules are on crystallographic inversion centers. Displacement ellipsoids drawn at the 50% probability level.

3.5.2: Results

XRD was performed on the CPV crystals, and the compound crystallizes in the

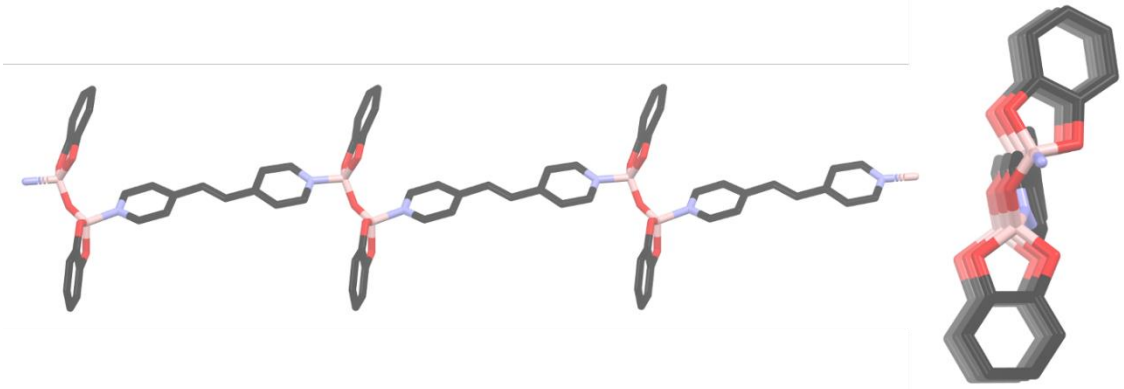

Figure 3.12: Left: Front view of the vacuum oven pyrolysis coordination polymer with dipyrocatechol borate linked with dipyridyl ethylene. Right: Side view of the coordination polymer showing a one dimensional infinite chain.

triclinic system. The pattern space group *P*-1 (No. 2) was confirmed by structure solution. The asymmetric unit consists of one $[(C_6H_4O_2BOBO_2C_6H_4)(C_{12}H_{10}N_2)]$ polymeric repeating unit and half each of two crystallographically independent $C_{12}H_{10}N_2$ molecules, both located on crystallographic inversion centers. The fluorene moiety in DE1 is not present. The $C_{12}H_{10}N_2$ part of the polymer is disordered over two orientations, by an approximate two-fold rotation about the N1-N2 vector.

3.5.3: Discussion

The vacuum melt crystallization experiment was done to possibly discover the crystal structure of VCP1 represented only by PXRD because single crystal XRD analysis is not possible. This is because once all benzene guest is evacuated under reduced pressure and heat, the products become polycrystalline during the structural shift. This effort did produce crystals but with unexpected results because coordination polymerization occurred but was very different. Though the two monomers were added in equal molar ratios, the DE1 underwent a form of pyrolysis in which all of it seemed to break down into a black film degrading into the smaller compound, dipyrocatechol borate. In the crystal

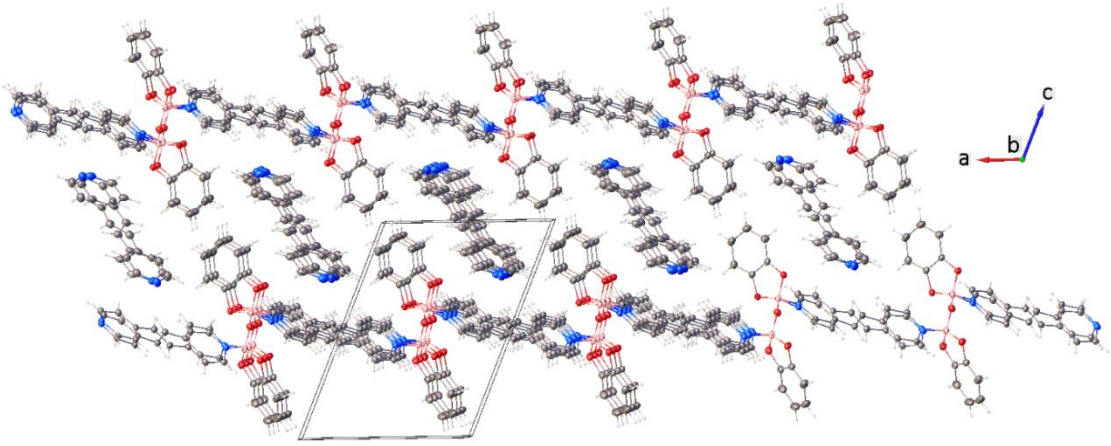

Figure 3.13: Infinite polymeric chains with dipyridyl ethylene molecules encapsulated in interstitial pockets. Components of the structure, some expanded by symmetry. Superscripts denote symmetry-equivalent atoms. dipyridyl ethylene of the polymeric chains is disordered. Both non-bonded guest dipyridyl ethylene molecules are on crystallographic inversion centers. Displacement ellipsoids drawn at the 50% probability level.

structure, the fluorene component of DE1 is completely absent and some of the diboronate ester that decomposed was able to supply the oxygen to the dipyrocatechol borate to allow a bridging oxygen between the two boronate esters still seen. Since the reaction occurred in vacuum this would mean that fully decomposed DE1 would be the only supply for the oxygen as well. Further evidence of this is because not only is the coordinated polymer still linked together by dipyridyl ethylene, but there are also two excess unlinked dipyridyl ethylene guests for every polymer repeat unit that are not bonded to anything **(Figure 3.11, Figure 3.12)**. The fact that there are technically three dipyridyl ethylene molecules for every one polymer repeat unit shows that though molar ratios of monomer were initially equal, the dipyrocatechol borate from the diboronate ester precursor is only shown to be a molar ratio compared to dipyridyl ethylene seen in the crystal structure. The dihedral angles between the fluorene and dipyridyl ethylene for the vacuum pyrolysis coordination polymer are 105.09° and 107.49° which has angle

strain lower than the standard sp^3 bond angle of 109.5°. This angle can be seen between C4, B1, and N1 in **(Figure 3.13)**. The respective boron nitrogen bond lengths are 1.639 Å and 1.635 Å. This new coordination polymer's crystals form as needles yellow in color. The crystal system is triclinic with a P-1 space group with a repeat unit volume of 1,509.53 $Å^3$ and a density of 1.360 grams per cubic centimeter.

3.5.4: Experimental

A round bottom flask was charged with DE1 (103 mg, 0.180 mmol) and dipyridyl ethylene (34.0 mg, 0.187 mmol) and the flask was then placed in a porcelain mortar within a vacuum oven. The oven was placed under reduced pressure (12 mmHg) and heated to 170-200 ˚C. The two compounds melted overnight and crystals grew on the upper sided of the flask. The mortar was used to transfer heat from the bottom of the oven and temperature was monitored with a thermometer at the oven's base. Crystals were then given to the crystallographer for analysis.

3.6: Macrocycle Produced in Toluene

3.6.2: Results

XRD was performed on the macrocycle crystals and the compound crystallizes in the triclinic system. The space group *P*-1 (No. 2) was confirmed by structure solution. The asymmetric unit consists of half of one $[(C_{37}H_{40}B_2O_4)_2(C_{12}H_{10}N_2)_2]$ molecule located on a crystallographic inversion center, and three independent regions of electron density modeled reasonably well as disordered, fractionally occupied toluene molecules. Toluene molecules C54-C60 and C75-C81 are disordered about inversion centers. The site occupancy of C54-C60 refined freely to about 50% and was fixed at half-occupancy for the

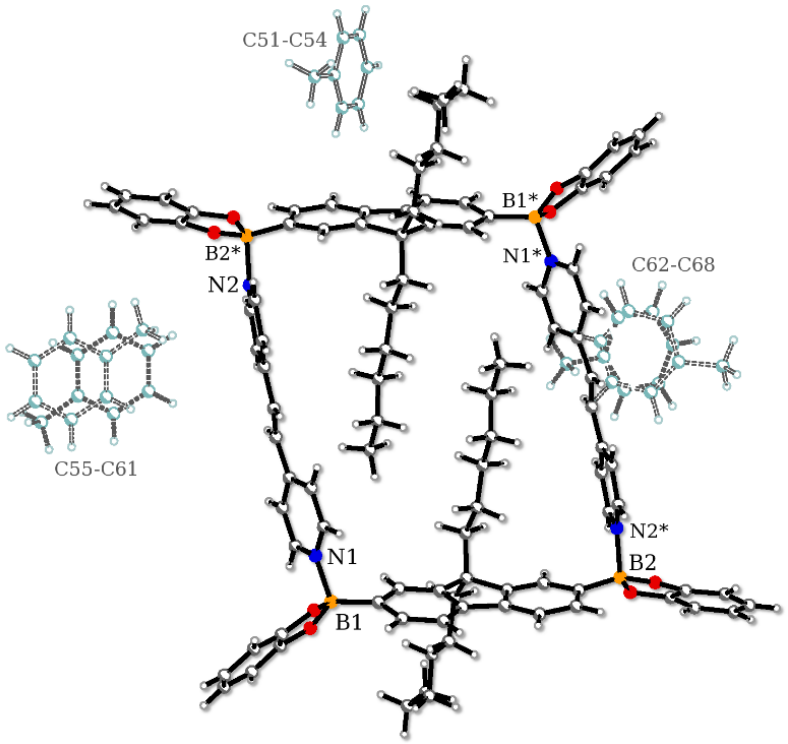

Figure 3.14: Components of the structure. Centrosymmetric molecule $(C_{37}H_{40}B_2O_4)_2(C_{12}H_{10}N_2)_2$ and 3.6 disordered toluene guests.

final cycles. Toluene molecules C61-C67 and C68-C74 are disordered over two orientations on a general position with refined populations of 0.543(6) and 0.457(6), respectively, which were constrained to sum to one. The disorder and occupancy of C75-C80 is linked with that of C61-C67/C68-C74 such that when component C61-C67 is present in a given asymmetric unit, both disordered components of C75-C80 are absent for steric reasons. The C75-C80 occupancy was therefore fixed at half the occupancy of C61-C67. The toluene molecules were refined as rigid hexagons and distance restraints were applied to the methyl groups. Both unique hexyl chains are disordered over two orientations starting with the third carbon from the fluorene base.

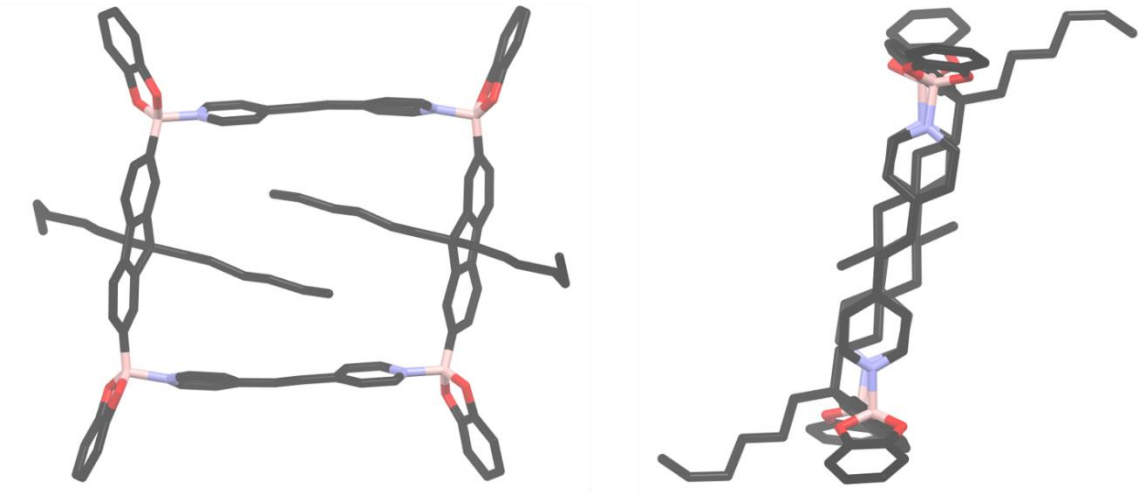

Figure 3.15: Front view of the macrocycle produced in dilluted toluene with DE1linked with dipyridyl ethylene showing it is created with two of equivalents of each starting material and symmetric on its inversion center. Right: Side view of macrocycle.

3.6.3: Discussion

As seen when discussing CP2 coordination polymer made from toluene, another product also forms when the crystallization occurs. The macrocycle that forms is the only product from toluene that has shown to be pure except in one instance. In this structure there are roughly 3.6 toluene guest molecules of toluene per repeat unit **(Figure 3.14)**. The macrocycle does make an intrinsic pore but the four hexyl chains (two per fluorene) fill it **(Figure 3.15)**. As seen in all previous coordinated polymers, the dihexyl chains in the macrocycle also interact in a lamellar like way with the same chains of adjacent macrocycles effectively tethering the crystal structure together, but in a different way. The macrocycles appear to stack like towers with the dihexyl chains intrinsically filling the pore within the cycle directionally above and below the aromatic and rigid aromatic scaffolding. Due to this, the dihexyl chains between macrocycles interact with one hexyl chain from a singular macrocycle in which one of the dihexyl chains is pointed up vertically interacting with the dihexyl chain in the vertically down direction with the macrocycle

above it. At the same time in respect to the same macrocycle with its other hexyl chain facing vertically below where this chain interacts with macrocycle in the up position from the macrocycle below. These interactions create a lamellar like unit of intrinsic hexyl chains within the macrocycles that seem give structural integrity to the tower system as if there was one complete aliphatic tether throughout, essentially acting as mortar to hollow holed bricks where the holes were all aligned and filled and unified.

The macrocycle structure from the singular tower's perspective has been discussed but the stability of keeping the towers connected to one another is due to catechol derivative of the diboronate ester's interdigitation with other macrocyclic catechol entities from macrocycles of adjacent towers. To put this in view, a specific macrocycle vertical tower is adjacent to other towers that are positioned in such a way that they are shifted vertically which allows other catechol moieties to overlap. This overlap with interlocking macrocycle towers together which will be discussed in more detail **(Chapter 3)**.

Each of the dihedral angles between the fluorene and dipyridyl ethylene for the macrocycle are 105.20° and 108.77° which has angle strain lower than the standard sp^3 bond angle of 109.5°. This angle can be seen between the fluorene carbon, B1, and N1 and the fluorene carbon, B2, and N2 in **(Figure 3.14).** The respective boron nitrogen bond lengths are 1.676 Å and 1.646 Å and the dihedral angle of dipyridyl ethylene is evaluated is 171.85° and is measured using the nitrogen atoms and the two carbon atoms that form the alkene between the aromatics. The macrocycles crystals are diamond in shape and

red in color. The crystal system is triclinic with a P-1 space group with a repeat unit volume of 2,616.5 $Å^3$ and a density of 1.162 grams per cubic centimeter.

3.6.4: Experimental

A round bottom flask was charged with boronate ester DE1 (0.298 g, 0.522 mmol) and DPE (0.1004 g, 0.551 mmol) and dissolved in toluene (250 mL). Crystallization occurred over two weeks and produced large red diamond prisms along with crystal clusters. The sample was given to the crystallographer for XRD analysis and PXRD was also performed to show that the sample was pure in phase.

3.7: Naphthalene Diol Coordination Polymer

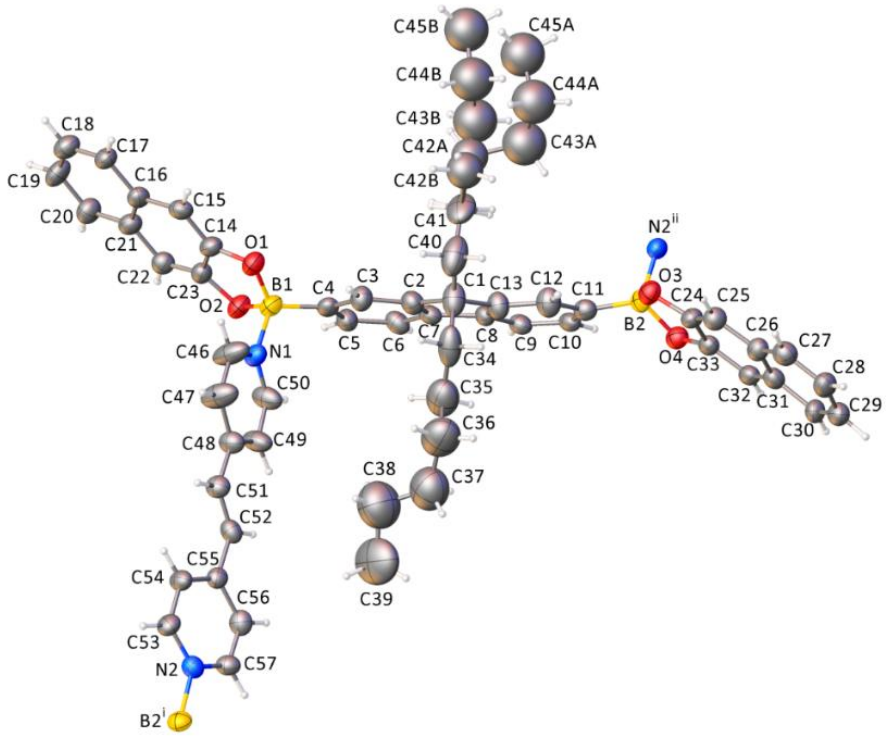

Figure 3.16: Asymmetric unit of the crystal. Displacement ellipsoids drawn at the 30% probability level. Superscripts denote symmetry-equivalent atoms. Two-fold disorder of one hexyl chain (C42-C45).

3.7.2: Results

XRD was performed on naphthalene diol coordination polymer crystals, and the compound crystallizes in the cubic system. The pattern of systematic absences in the intensity data was uniquely consistent with the space group *Pa*-3 (No. 205). The asymmetric unit consists of one crystallographically independent $(C_{45}H_{44}B_2O_4)(C_{12}H_{10}N_2)$ polymeric repeating unit and a large volume of disordered benzene. Two-fold disorder of the outer four atoms of one hexyl sidechain (C42-C45) was modeled with two equally populated components.

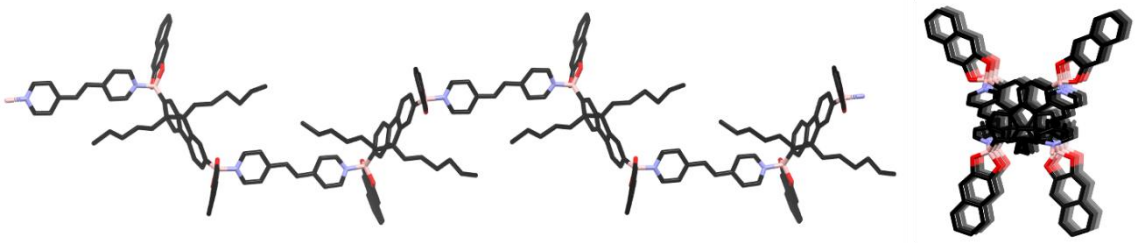

Figure 3.17: Left: Front view of the naphthalene diol coordination polymer synthesised with naphthalene DE1 linked with dipyridyl ethylene showing its direction alternating symetrically on its inversion center. Right: Side view of the coordination polymer showing a one dimensional infinite chain.

3.7.3: Discussion

A naphthalene diol was chosen to create a diboronate ester due to its extended resonance. In theory it can better stabilize a charge which could have a direct effect on boron's empty p orbitals being filled by a nucleophile within the naphthalene diol diboronate ester synthesized. The naphthalene diol coordination polymer crystallized much like CP1 in benzene solution to which robust crystals formed overnight. With this similarity, their color, shape, and crystal structure were very different. The naphthalene diol polymer formed large orange cubes that also reflect the cubic crystal structure solved

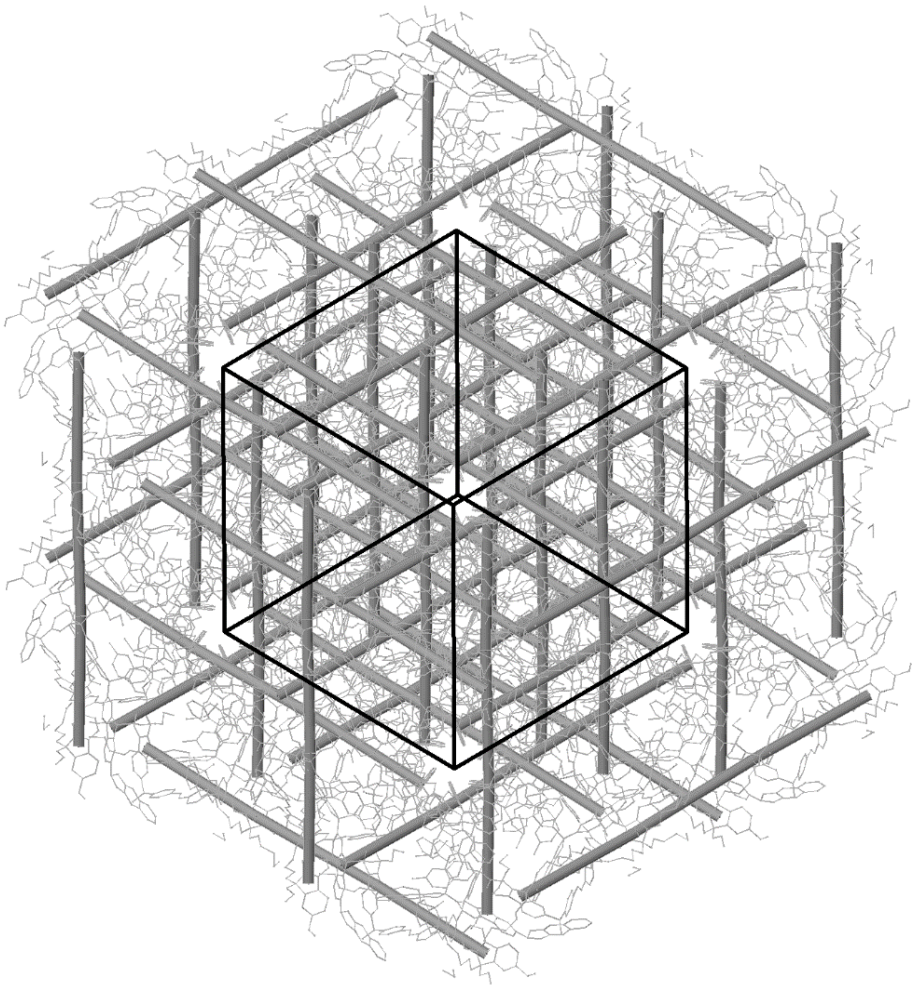

Figure 3.18: View down the 3-fold axis of the cubic unit cell ([111] direction). Chain directions highlighted by heavy grey rods. Unit cell outline in dark black.

by XRD single crystal analysis **(Figure 3.16)**. The polymer exists in infinite one dimensional chains but unlike many other crystalline polymers, the chains exist in the x, y, and z axis as opposed to all chains pointing in the same direction **(Figure 3.17, Figure 3.18)**. This seems to weave them together in a way that makes them stable when not in solution due to their long chain cooperative motion. It is also expected that the crystal size gives evidence of this stability as well. Within the woven polymer chains there are large cavities that hold large amounts of disordered solvent and take up 31% of the total cell volume.

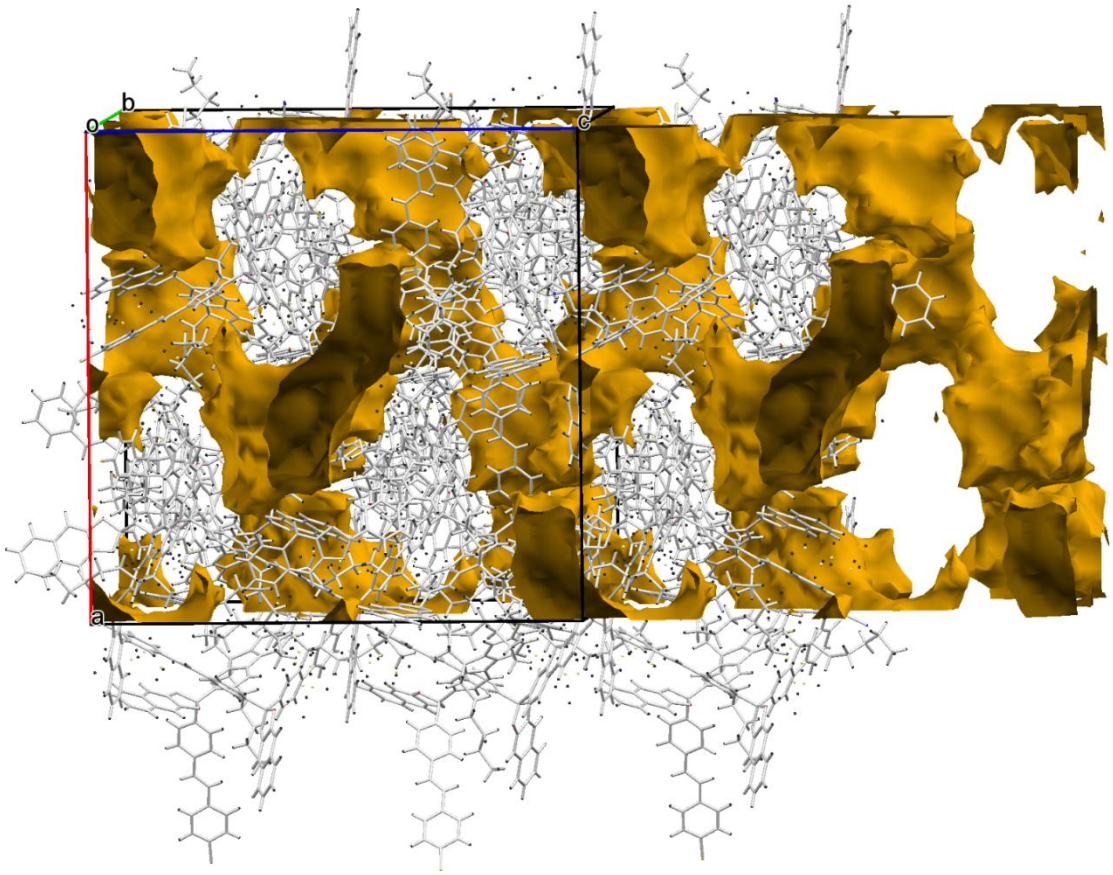

Figure 3.19: The unit cell contains large cavities (31% of total cell volume) filled with badly disordered solvent (benzene) species, which could not be modeled and were removed from the structure computationally with the Squeeze technique. The solvent-filled cavities are drawn as yellow surfaces.

Interestingly the naphthalene diol coordinated polymer could possibly have use in isolating specific types of organic solvents/compounds since these cavities are accessible. The naphthalene diol coordination polymer's dihedral angles between the fluorene and dipyridyl ethylene for the are 106.50° and 109.03° which has angle strain lower than the standard sp^3 bond angle of 109.5°. This angle can be seen between the fluorene carbon, B1, and N1 and the fluorene carbon, B2, and N2 in **(Figure 3.16)**. The respective boron nitrogen bond lengths are 1.634 Å and 1.623 Å and the dihedral angle of dipyridyl ethylene is evaluated is 173.40° and is measured using the nitrogen atoms and the two carbon atoms that form the alkene between the aromatics. The polymer's crystals grow as cubes

and are orange in color. The crystal system is cubic with a Pa-3 space group with a repeat unit volume of 36, 563 $Å^3$ and a density of 0.866 grams per cubic centimeter.

3.7.4: Experimental

Naphthalene Diol Diboronate Ester

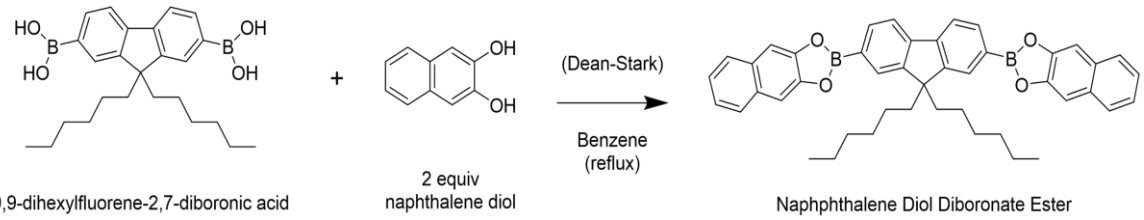

Scheme 3.1: 9,9-dihexylfluorene and two equivalents of naphthalene diol are refluxed in benzene with a Dean-Stark trap to produce the Naphthalene Diol Diboronate Ester through a condensation reaction.

A round bottom flask was charged with 9,9-dihexylfluorene-2,7-diboronic acid (300.7 mg, 0.712 mmol) and naphthalene diol (250.9 mg, 1.566 mmol) and dissolved in benzene (250 mL). Heat activated 3Å sieves and benzene (10 mL) were added to a Dean Stark trap that was then attached to the reaction flask. Initially reactants did not go into solution but upon heating to reflux the solution became clear and colorless. Reaction was allowed to reflux for 24 hours while stirring under a nitrogen atmosphere. The solution was then purified through hot gravity filtration before isolation in which benzene was removed by rotary evaporation. Short path distillation was performed on the resulting white solid product was put under reduced pressure sublimation (Kuglerohr) at 125°C for two hours to remove excess naphthalene diol (260.2 mg, >100% (excess naphthalene impurity)).

^{1}H NMR (300 MHz, CD3Cl3): δ 8.223 (d, J=0.84 Hz, 1H), 8.198 (d, J=0.98 Hz, 1H), 8.179 (s, 2H), 7.979 (d, J=0.43 Hz, 1H), 7.952 (d, J=0.48 Hz, 1H), 7.933-7.9014 (m, 4H), 7.718 (s, 4H), 7.507-7.475 (m, 4H), 2.209-2.156 (m, J=7.94 Hz, 4H), 1.149-1.007 (m, 12H), 0.755 (m,

J=6.88, 6H), 0.700-0.622 (m, 4H). All solvent and water peaks are omitted.

Naphthalene Diol Coordination Polymer

A round bottom flask was charged with naphthalene diol boronate ester (83.3 mg, 0.124 mmol) and dipyridyl ethylene (24.0 mg, 0.132 mmol) and dissolved in benzene (125 mL). Crystallization occurred over night and produced large orange cubes along with crystal clusters. The sample was given to the crystallographer for XRD.

3.8: Nitrocatechol Coordination Polymer

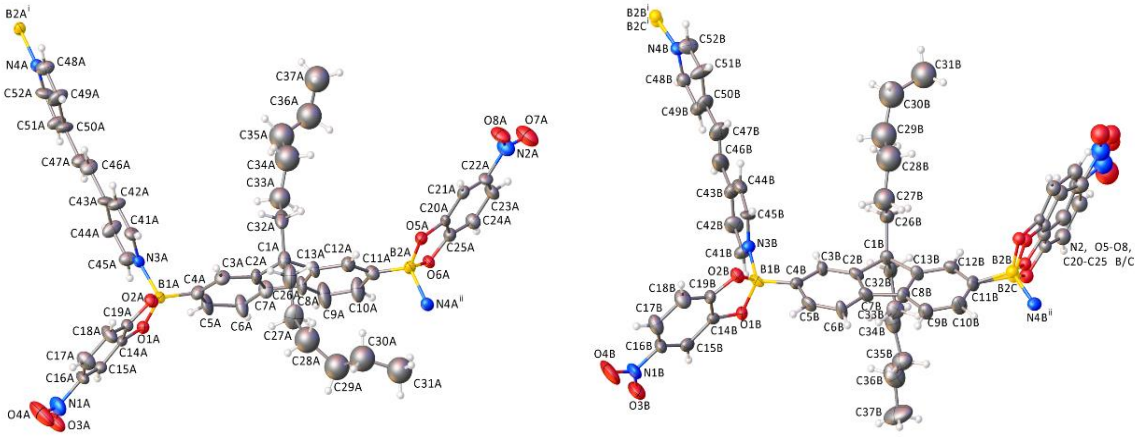

Figure 3.20: Displacement ellipsoid plots with atom numbering schemes of the repeating units of the two independent polymeric chains. Displacement ellipsoids drawn at the 20% probability level.

3.8.2: Results

XRD was performed on the nitrocatechol coordination polymer, and the compound crystallizes in the monoclinic system. The pattern of systematic absences in the intensity data was consistent with the space groups $P2_1$ and $P2_1/m$; intensity statistics suggested an acentric structure. The space group $P2_1$ was eventually confirmed by structure solution and was further verified using the ADDSYM program on the ordered part of the structure.[5] ADDSYM found no missed symmetry elements. The structure is

severely disordered, and an approximate, heavily restrained disorder model was refined. The identifiable contents of the asymmetric unit consist of two crystallographically independent $\{C_{49}H_{48}B_2N_4O_8\}$ polymeric chain repeat units.

3.8.3: Discussion

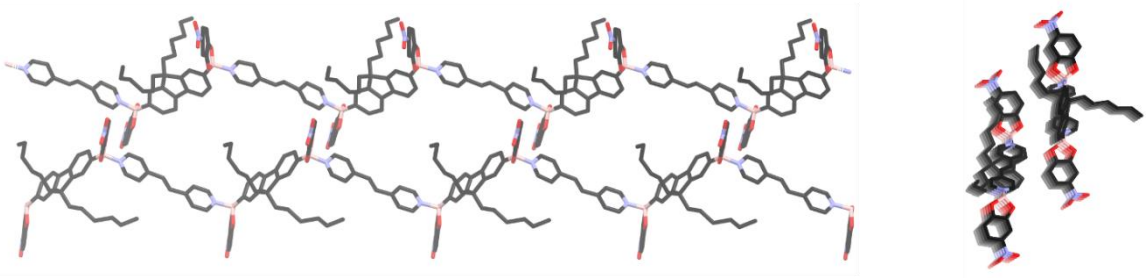

Figure 3.21: Front view of the nitrocatechol coordination polymer synthesised with nitrochatechol diboronate ester linked with dipyridyl ethylene showing its direction alternating symetrically on its inversior center. Right: Side view of the coordination polymer showing a one dimensional infinite chain.

4-Nitrocatechol was explored due to the large electron withdrawing effect this substituent. This in effect would pull electron density away from the empty p orbital of boron within the boronate ester once synthesized and create a much stronger bond once it has interacted with a nucleophile. When the nitrocatechol diboronate ester was reacted with dipyridyl ethylene this proven to be the case. Unlike every coordinated polymer synthesized in solvent already mentioned, the two starting materials were so reactive that dissolving them into virtually any solvent would cause an instantaneous reaction with looked more like a plastic and did not form crystals. Finally, dichloromethane was used in the array of test solutions and overnight crystals had formed. It is expected that a solvent as polar as dichloromethane was needed to interact with the nitro moieties on the boronate ester as well the empty π orbital on boron. If the chlorine lone pairs on dichloromethane were able to interact with this orbital enough, it

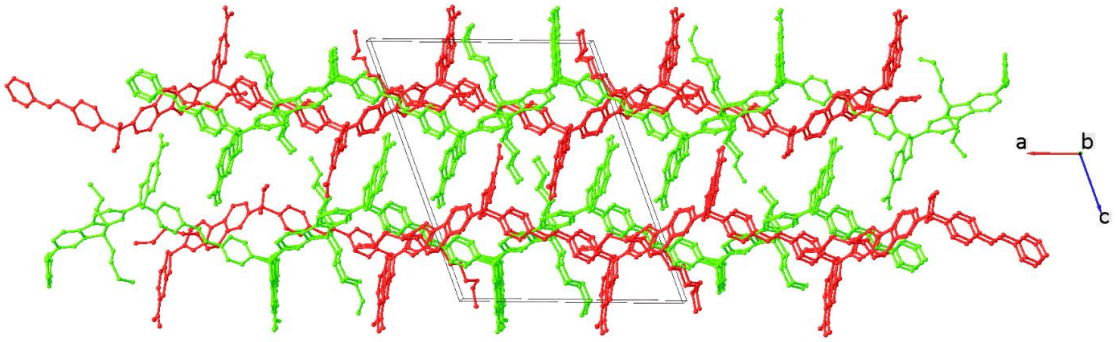

Figure 3.22: The nitrocatechol coordination polymer exists as two separate chain both facing in the a-axis but alternate with one another. Each of the two distinct chains pack directly over an under another chain with the same repeating pattern seen as red for one chain and green for the other. Packing of chains viewed along the chain direction (a axis). Chain "A" = red, "B" = green in right image.

would slowly block the chance for the dipyridyl ethylene to do a nucleophile. Over time the dipyridyl linker did overcome the dichloromethane's interaction but it took long enough that both reactants were able to be dissolved once added to solution and crystallization was capable of occurring. The crystals formed were capable of XRD single crystal analysis but once pulled from solution their single crystallinity was short lived. It seems that the dichloromethane molecules that existed within the crystals themselves, then went quickly from liquid state to gas causing the crystals to go from a translucent yellow to opaque in less than a minute. Though the single crystal turning opaque is indicative of it becoming polycrystalline, the sample was added fast enough that the crystal structure could be calculated **(Figure 3.20, Figure 3.21)**. To combat this problem with keeping crystallinity after crystallization in dichloromethane, other solvents were added slowly in the expectation that they may replace the dichloromethane guest to help stabilize the single crystals in air. When done for each solvent, crystals slowly became opaque while still in solution, which did not prove to be usable for XRD.

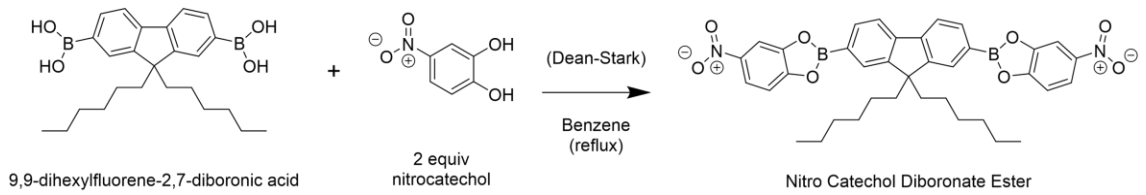

Scheme 3.2: 9,9-dihexylfluorene and two equivalents of catechol are refluxed in benzene with a Dean-Stark trap to produce the Nitrocatechol Diboronate Ester through a condensation reaction.

Unlike all previous coordination polymers discussed, the nitrocatechol coordination polymer exists as two separate concatenated chains that both run in the same direction **(Figure 3.22)** and are labeled Chain A and B. The nitrocatechol coordination polymer's dihedral angles between the fluorene and dipyridyl ethylene for the are 108.68° and 108.97° for chain A and 109.64° and 109.94° for chain B which has least angle strain of any other previously mentioned coordination polymers also the macrocycle. This angle can be seen between the fluorene carbon, B1, and N1 and the fluorene carbon, B2, and N2 in **(Figure 3.20)**. The respective boron nitrogen bond lengths are 1.664 Å and 1.685 Å for chain A and 1.641 Å and 1.622 Å. The dihedral angle of dipyridyl ethylene is evaluated is 169.46° and is measured using the nitrogen atoms and the two carbon atoms that form the alkene between the aromatics. The nitrocatechol coordination polymer's crystals grow as blocks and yellow in color. The crystal system is cubic with a Pa-3 space group with a repeat unit volume of 36, 563 $Å^3$ and a density of 0.866 grams per cubic centimeter.

3.8.4: Experimental

Nitrocatechol Diboronate Ester

A round bottom flask was charged with 9,9-dihexylfluorene-2,7-diboronic acid (1.0013g, 2.372 mmol) and nitrocatechol (821.3 mg, 5.295 mmol) and dissolved in benzene (400 mL). Heat activated 3Å sieves and 10 mL Benzene were added to a Dean

Stark trap that was then attached to the reaction flask. Initially reactants did not go into solution but upon heating to reflux the solution became clear and colorless. Reaction was allowed to reflux for 24 hours while stirring under a nitrogen atmosphere. The solution was then purified through hot gravity filtration before isolation in which benzene was removed by rotary evaporation. Short path distillation was performed on the resulting white solid product with reduced pressure sublimation (Kuglerohr) at 110°C for two hours to remove excess nitrocatechol (1.487 g, 95.0%).

^{1}H NMR (300 MHz, CD3Cl3): δ 8.271 (d, J=2.01 Hz, 2H), 8.2466 (d, J=2.37 Hz, 1H), 8.2198 (d, J=2.37 Hz, 1H), 8.179 (s, 1H), 8.1534 (s, 1H), 8.1342 (s, 2H), 7.9732 (s, 1H), 7.9495 (s, 1H), 7.4835 (s, 1H), 7.4547 (s, 1H), 2.191-2.135 (m, J=8.01 Hz, 4H), 1.515-1.03 (m, 12H), 0.783-0.735 (m, J=6.13 Hz, 6H), 0.687-0.587 (m, J=15.55 Hz, 4H). All solvent and water peaks are omitted.

Nitrocatechol Coordination Polymer

A four-dram vial was charged with nitrocatechol diboronate ester (5.0 mg, 0.008 mmol) and dipyridyl ethylene (1.38 mg, 0.008 mmol) and dichloromethane (5 mL) was added. The nitrocatechol diboronate ester did not immediately dissolve but once sonicated the solution was a translucent yellow. The vial was left to and yellow block crystals grew overnight. The sample was then given to the crystallographer for analysis.

3.9.1: X-ray Diffraction Data for Coordination Polymers and Macrocycle

Structure Label	Benzene Derived Coordination Polymer 1	Toluene Derived Coordination Polymer 2	Dioxane Derived Coordination Polymer 3	Hexanes/Hexanes and Dichloromethane Derived Coordination Polymer 4
Empirical formula	C61H62B2N2O4	$C_{49}H_{50}B_2N_2O_4$	C55H62B2N2O7	C49.53H51.06B2Cl1.06N2O4
Crystal habit and color	wedge; yellow	hexagonal plate; yellow	block; orange	pyramidal; yellow
Formula weight	908.74	752.53	884.68	797.42
Temperature/K	100(2)	173(2)	200(2)	100(2)
Crystal system	monoclinic	hexagonal	triclinic	trigonal
Space group	P21/n	$P6_3/m$	P-1	P31
a/Å	13.8410(7)	22.5615(9)	12.2648(5)	14.7550(7)
b/Å	21.5251(12)	22.5615(9)	12.3331(5)	14.7550(7)
c/Å	16.8118(9)	24.948(2)	17.9650(10)	18.2565(10)
α/°	90	90	107.113(2)	90
β/°	95.807(2)	90	102.374(2)	90
γ/°	90	120	104.8590(10)	120
Volume/Å3	4983.0(5)	10997.9(12)	2383.59(19)	3442.1(4)
Z	4	6	2	3
ρcalcg/cm3	1.211	0.682	1.233	1.154
Crystal size/mm3	0.22 × 0.18 × 0.14	0.54 × 0.5 × 0.48	0.2 × 0.1 × 0.08	0.36 × 0.26 × 0.22
Reflections collected	160659	64617	59670	71612
Goodness-of-fit on F2	1.029	1.352	1.058	1.075
Final R indexes [I>=2σ (I)]	R1 = 0.0549, wR2 = 0.1212	R_1 = 0.1028, wR_2 = 0.3177	R1 = 0.0613, wR2 = 0.1482	R1 = 0.0558, wR2 = 0.1424
Largest diff. peak/hole / e Å-3	0.65/-0.23	0.32/-0.46	0.60/-0.42	0.44/-0.28
Dihedral angles between the fluorene and dipyridyl ethylene	105.51°, 107.84°	103.82°	107.22°, 109.13°	107.4°, 112.82°
Boron nitrogen bond lengths (Å)	1.670, 1.658	1.704	1.675, 1.635	1.708, 1.620

Table 3.1: X-ray diffraction data of single crystal coordination polymers derived in benzene, toluene, acetonitrile, and hexes/hexanes and dichloromethane. Also shown is the dihedral bond angles and crystal habit and color.

3.9.2: X-ray Diffraction Data for Coordination Polymers and Macrocycle

Structure Label	Vacuum Pyrolysis Coordination Polymer	Toluene Derived Macrocycle	Naphthalene Diol Coordination Polymer	Nitrocatechol Coordination Polymer
Empirical formula	$C_{36}H_{28}B_2N_4O_5$	$C_{122.77}H_{128.3}B_4N_4O_8$	$C_{57}H_{54}B_2N_2O_4$	$C_{49}H_{48}B_2N_4O_8$
Crystal habit and color	needle; yellow	irregular, yellow-orange	cube; orange	block; yellow
Formula weight	618.24	1831.07	852.64	842.53
Temperature/K	100(2)	100(2)	100(2)	301(2)
Crystal system	triclinic	triclinic	cubic	monoclinic
Space group	P-1	P-1	Pa-3	$P2_1$
a/Å	10.4681(4)	11.6224(6)	33.1906(10)	18.421(3)
b/Å	11.6641(5)	13.4837(7)	33.1906(10)	16.398(2)
c/Å	13.9848(6)	17.1974(8)	33.1906(10)	22.799(3)
α/°	100.7860(16)	82.409(3)	90	90
β/°	107.7760(17)	82.900(3)	90	110.275(3)
γ/°	104.4005(16)	79.972(3)	90	90
Volume/Å^3	1509.53(11)	2616.6(2)	36563(3)	6460.5(15)
Z	2	1	24	4
ρ_{calc}g/cm^3	1.360	1.162	0.929	0.866
Crystal size/mm^3	0.26 × 0.08 × 0.05	0.22 × 0.12 × 0.1	0.32 × 0.28 × 0.24	0.48 × 0.4 × 0.06
Reflections collected	48391	76761	160261	40223
Goodness-of-fit on F^2	1.047	1.038	1.464	0.995
Final R indexes [I>=2σ (I)]	R_1 = 0.0395, wR_2 = 0.0767	R_1 = 0.0456, wR_2 = 0.1072	R_1 = 0.1076, wR_2 = 0.3243	R_1 = 0.0851, wR_2 = 0.2281
Largest diff. peak/hole / e Å^{-3}	0.22/-0.21	0.39/-0.30	0.85/-0.39	0.33/-0.38
Dihedral angles between the fluorene and dipyridyl ethylene	105.09°, 107.49°	105.20°, 108.77°	106.65°, 109.03°	A: 108.68°, 108.97° B: 109.64°, 109.94°
Boron nitrogen bond lengths (Å)	1.639, 1.635	1.676, 1.646	1.634, 1.623	A: 1.664, 1.685 B: 1.641, 1.622

Table 3.2: X-ray diffraction data of single crystal coordination polymers derived vacuum, created with a naphthalene diboronate ester, created with a nitrocatechol diboronate ester, and the macrocycle also created from toluene. Also shown is the dihedral bond angles and crystal habit and color. The vacuum pyrolysis coordination polymer does not have a fluorene carbon. The dihedral bond angles represented are from the oxygen that bridges the dipyrocatechol borate to the boron to the dipyridyl ethylene.

3.10: Conclusion

As seen earlier **(Chapter 2)**, the coordination polymer, CP1, forms when DE1 and DPE are mixed in equal ratios which induces the growth of yellow wedge crystals **(Figure 2.2)**. For CP1 to form, the solvent is benzene which also becomes a guest within the crystal repeat unit, leading to the expectation that it must play a role in the formation of the polymer's crystal structure. There are two total benzene guest molecules but they technically exist as three entities in which one total benzene molecule exists within the repeat unit and two other benzenes are cut in half, meaning the other half of their molecules are part of an adjacent repeat unit **(Figure 2.1)**. To investigate this hypothesis, the same two monomers, DE1 and DPE were dissolved in the same manner as CP1 but in different solvents. An array of solvents were experimented with and some either had no crystallization occur or if a crystallization occurred then it may have precipitated as a crude powder and was not capable of characterization. Other solvents that did create stable single crystal coordination polymers from DE1 and DPE were toluene, dioxane, and hexanes/hexanes and dichloromethane mixtures. Toluene was the first choice to experiment with because it is identical to benzene except for having on methyl group in the place of a hydrogen. This small change actually led to an elusive coordination polymer, CP2 **(Figure 3.2, Figure 3.3)**, that was rare to form as pure in phase but when seen as a large single crystal it grew as a yellow hexagonal plate. Though these plates were large single crystals, diffraction remained poor and the amount of toluene solvent in the crystal structure has yet to be elucidated. CP2 was rare because the macrocycle also formed in toluene **(Figure 3.14, Figure 3.15)** as a red triangular prism which was the

dominant product. Once XRD analysis had been performed at room temperature it was shown to have phase purity over long periods of crystal growth in more dilute conditions which had not yet been proven for over a decade. The third coordination polymer, CP3, to crystallize did so in dioxane **(Figure 3.5, Figure 3.6)** and was a one-dimensional chain in which single crystals grew as orange blocks. CP3's chain repeats itself on it's inversion center, but instead of repeating in just an up/down nature like CP1 and CP2, it also does so in a left/right direction which lengthens the frequency of its total repeat unit when viewed as the points where it replicates its pattern. Lastly, hexanes and mixtures of hexanes with dichloromethane also produce a coordination polymer, CP4 **(Figure 3.8, Figure 3.8)**, that exists as yellow wedges when seen as a large single crystal. The one-dimensional chain has more commonality with CP3 than CP1 and CP2 because it also has more dimension freedom in how the chain extends but stands alone due to it helix formation. This is the only helical polymer seen with these same starting materials used for coordination polymers CP1-CP4. The helixes are interdigitated with adjacent chains leaving little access for solvents to exist as guests. More interesting is that even if hexanes and dichloromethane are used together in a 75:25 ratio, hexanes is still the driving force and the same structure exists has hexane alone with the exception that dichloromethane does act as a guest within the small pockets within the helix and interdigitated dihexyl chains from neighboring chains **(Figure 3.10)**.

Seen previously **(Chapter 2)** is that when CP1 vacant of benzene guest, it has fully transitioned to VCP1 in which is polycrystalline which means that XRD analysis cannot be performed. In an effort to possibly produce the structure for VCP1 in single crystal form,

an experiment was designed to effectively create a molten polymer crystallization with DE1 and DPE with reduced pressure (12 mmHg) at a temperature between 170-200 °C. A vacuum oven coordination polymer **(Figures 3.5.1, 3.5.2)** with large single crystals did occur in the form of yellow needles, but after XDR analysis was performed, the results were incredibly unexpected. It seems that two thirds of the DE1 monomer had degraded completely into a black film while also supplying the oxygen for the remaining third of the DE1 reactant. This remaining amount of DE1 also underwent a form of pyrolysis in which the fluorene backbone of DE1 was cleaved of the two boronate esters, and those esters were seen newly bridge by an oxygen only possible from the fully degraded DE1. This new oxygen bridged diboronate ester formed a new monomer material of dipyrocatechol borate which was still able to coordinate with DPE into a one-dimensional polymer with two DPE molecules as guests within the crystal structure.

To explore new coordination polymers two new diboronate efforts were synthesized. One compound used to synthesize a new diboronate derivative was naphthalene diol due to its extended resonance and the other compound was nitrocatechol for its strong electron withdrawing effects. When the naphthalene diol diboronate ester and DPE were mixed in benzene in an equal molar ratio, a highly crystalline coordination polymer **(Figure 3.18, Figure3.19)** grew over night in the form of large orange cubes. After XRD analysis had been performed, it was seen that the use of the naphthalene diol derivative had produced a not yet seen characteristic in which the polymer chains were still one-dimensional polymers but existed in an interwoven manner in the x, y, and z axis which also produced large crystalline cavities **(Figure 3.18, Figure**

3.18) that took up 31% and filled with disordered solvent. Lastly, when the nitrocatechol diboronate ester was mixed with an equal molar ratio of DPE, the only solvent found to form a single crystalline coordination polymer **(Figure 3.20, Figure 3.21)** was dichloromethane. Without this solvent, the two reactants would precipitate rapidly resulting in an unusable or characterizable material. These single crystals grew as yellow blocks and deteriorated rapidly once pulled from solvent. Still, XRD analysis was able to be performed and it was seen like all polymers mentioned thus far, naphthalene diol coordination polymer also existed as one-dimensional with the exception that the crystal repeat unit consisted as two separate and different polymers that extended in a concatenated fashion on the same axis **(Figure 3.22)**.

Many coordinated polymeric crystal structures have been produced in which four have been created from the same starting material in different solvents. In just the case for CP1 through CP4 all crystal repeat units had many of the same qualities but were also highly unique. For instance, though they were all one-dimensional chains, the manner in which each repeat unit extends in dimensional space on its central axis based on how the inversion center moved forward was very diverse. This can be highlights as CP1 extending in a square wave square wave, CP2 extending in a similar fashion with a larger frequency with a different crystal system, CP3 extending with a much larger frequency due to its inversion center having more dimensional freedom, and CP4 due to its interdigitated helical nature. These polymers came in different colors, shapes, and a range in the amount of guest molecules contained within their host. This diversity seen in characteristics has large impact because it highlights how just two starting materials can

produce such different qualities in a robust and crystalline form. This argument is only strengthened when also discussing the vacuum pyrolysis, naphthalene diol and nitrocatechol coordination polymers because it sheds light on the idea that whether the original DE1 monomer was changed from heat or small and simple new diboronate ester derivatives are used, different products with virtually any combination of characteristic could be made in the future.

3.11 References

(1) Stephens, A. J.; Scopelliti, R.; Tirani, F. F.; Solari, E.; Severin, K. Crystalline Polymers Based on Dative Boron–Nitrogen Bonds and the Quest for Porosity. *American Chemical Society Materials Letters* **2019**, *1* (1), 3–7. https://doi.org/10.1021/acsmaterialslett.9b00054.

(2) Christinat, N.; Croisier, E.; Scopelliti, R.; Cascella, M.; Röthlisberger, U.; Severin, K. Formation of Boronate Ester Polymers with Efficient Intrastrand Charge-Transfer Transitions by Three-Component Reactions. *European Journal of Inorganic Chemistry* **2007**, *2007* (33), 5177–5181. https://doi.org/https://doi.org/10.1002/ejic.200700723.

(3) Luisier, N.; Bally, K.; Scopelliti, R.; Fadaei, F. T.; Schenk, K.; Pattison, P.; Solari, E.; Severin, K. Crystal Engineering of Polymeric Structures with Dative Boron–Nitrogen Bonds: Design Criteria and Limitations. *Crystal Growth & Design* **2016**, *16* (11), 6600–6604. https://doi.org/10.1021/acs.cgd.6b01292.

(4) Gao, W.-X.; Feng, H.-J.; Guo, B.-B.; Lu, Y.; Jin, G.-X. Coordination-Directed Construction of Molecular Links. *Chemical Reviews* **2020**, *120* (13), 6288–6325. https://doi.org/10.1021/acs.chemrev.0c00321.

(5) Foo, M. L.; Matsuda, R.; Kitagawa, S. Functional Hybrid Porous Coordination Polymers. *Chemistry of Materials* **2014**, *26* (1), 310–322. https://doi.org/10.1021/cm402136z.

(6) Folmer-Andersen, J. F.; Aït-Haddou, H.; Lynch, V. M.; Anslyn, E. v. 2,6-Di(Pyrimidin-4-Yl)Pyridine Ligands with Nitrogen-Containing Auxiliaries: The Formation of Functionalized Molecular Clefts upon Metal Coordination. *Inorganic Chemistry* **2003**, *42* (26), 8674–8681. https://doi.org/10.1021/ic034823b.

(7) Cubberley, M. S.; Iverson, B. L. 1H NMR Investigation of Solvent Effects in Aromatic Stacking Interactions. *Journal of the American Chemical Society* **2001**, *123* (31), 7560–7563. https://doi.org/10.1021/ja015817m.

(8) Bear, J. C.; Cockcroft, J. K.; Williams, J. H. Influence of Solvent in Crystal Engineering: A Significant Change to the Order–Disorder Transition in Ferrocene. *Journal of the American Chemical Society* **2020**, *142* (4), 1731–1734. https://doi.org/10.1021/jacs.9b11895.

(9) Liu, J.; Lavigne, J. J. *Boronic Acids*, Second.; Hall, D. G., Ed.; Wiley-VCH Verlag GmbH & Co. KGaA: Weinheim, Germany, 2011; Vol. 2. https://doi.org/10.1002/9783527639328.

(10) Rambo, B. M.; Tilford, R. W.; Lanni, L. M.; Liu, J.; Lavigne, J. J. Boronate-Linked Materials: Ranging from Amorphous Assemblies to Highly Structured Networks. In *Macromolecules Containing Metal and Metal-Like Elements*; Abd-El-Aziz, A. S., Carraher Jr., C. E., Pittman Jr., C. U., Zeldin, M., Eds.; John Wiley & Sons, Inc.: Hoboken, NJ, USA, 2009; Vol. 9, pp 255–294. https://doi.org/10.1002/9780470527085.ch6.

(11) Maynor, M. S.; Nelson, T. L.; O'Sulliva, C.; Lavigne, J. J. A Food Freshness Sensor Using the Multistate Response from Analyte-Induced Aggregation of a Cross-Reactive Poly(Thiophene). *Organic Letters* **2007**, *9* (17), 3217–3220. https://doi.org/10.1021/ol071065a.

(12) Cai, M.; Daniel, S. L.; Lavigne, J. J. Conjugated Bis and Poly(Dioxaborole)s for Optical Sensing of Lewis Bases Based on Main-Chain Perturbations. *Chemical Communications* **2013**, *49* (58), 6504–6506. https://doi.org/10.1039/C3CC41189C.

CHAPTER 4: SINGLE CRYSTAL TO SINGLE CRYSTAL TRANSITIONS OF TOLUENE DERIVED MACROCYCLE PRECURSORAMOLECULAR POROSITY

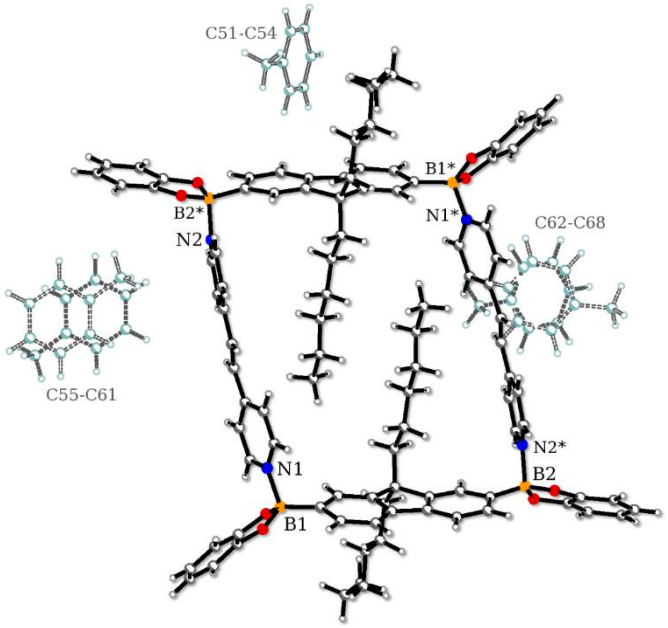

Figure 4.1: Components of the structure. Centrosymmetric molecule $(C_{37}H_{40}B_2O_4)_2(C_{12}H_{10}N_2)_2$ and 3.6 disordered toluene guests. XRD analysis was performed at room temperature (301 K).

4.1: Introduction

Post-synthetic modification of products is a growing field that includes SCSC transitions which are when a guest compound within a crystalline host can be added, removed or even exchanged through a liquid or vapor. [1–3] Other types of these SCSC transitions that will not be focused on in this text but still occur are topochemical polymerizations stereoselective isomerization, both which are mainly induced by wavelength or heat.[4,5] As seen previously **(Chapter 2)** we proved we were able to perform three SCSC transitions to CP1, a coordination polymer made from DE1 and DPE in

benzene, to which one was an overnight liquid SCSC transition with styrene and the two others were vapor SCSCtransitions with acetonitrile and fluorobenzene.[6–13] Of these transitions in which all solvents used replaced benzene as a guest, fluorobenzene caused no change to the crystalline polymer repeat unit, styrene induced small changes to the repeat unit, and drastic changes occurred when acetonitrile caused the crystal system to change from monoclinic to triclinic. The acetonitrile transition also gave the one-dimensional chain more dimensional degrees of freedom which extended the frequency of translation symmetry of the chain repeat unit when not viewing it from its inversion center but its spatial representationBecause these SCSC transitions were observed, the next question we asked was, since the macrocycle seems to be the dominant crystalline phase made when DE1 and DPE are mixed in equal molar ratio in toluene **(Chapter 3)** could it also undergo and SCSC transition?

4.2: Toluene Derived Macrocycle

The macrocycle is one of two crystal structures seen when DE1 and DPE are added to toluene in equal molar ratios **(Chapter 3)**. The coordination polymer, CP2, is the kinetic product seen only as pure in phase when it crystalized rapidly in highly concentrated conditions. The macrocycle is viewed as the thermodynamic product due to it being the dominant crystal structure that, though takes significantly longer time to crystallize, is much easier to synthesize as single crystals that are phase pure, as seen by PXRD data. Each macrocycle has 3.6 toluene guests per crystalline repeat unit and single crystals are red triangular prisms.

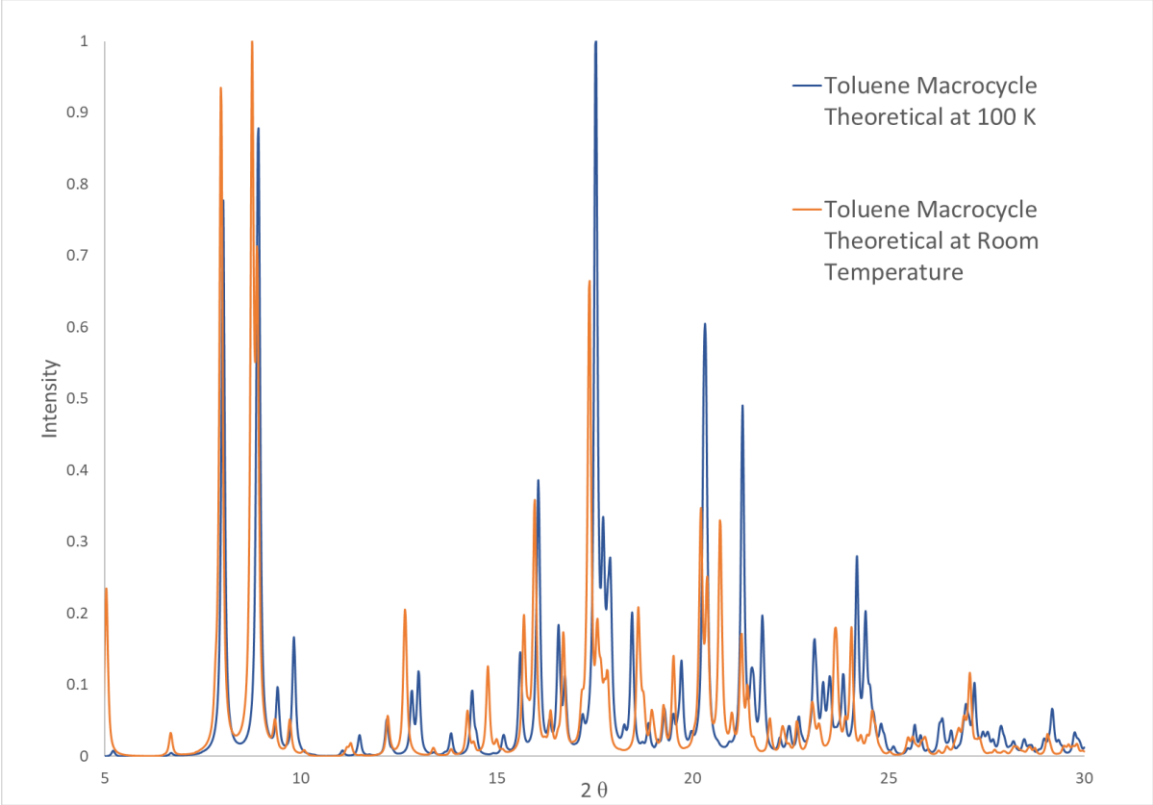

Figure 4.2: **Blue** Theoretical PXRD of toluene macrocycle from XRD data at 100 K. **Orange** Theoretical PXRD of toluene macrocycle from XRD data at room temperature (301 K).

4.2.2: Results

For many years it proved cumbersome to determine whether there was a pure phase of the macrocycle made from toluene or if it was the coordinated polymer CP2. When darker red diamond prism crystals were grown in toluene solution and it seemed pure from intuition do to color and shape based on samples submitted for XRD analysis, the PXRD would still not match the theoretical PXRD given from single crystal XRD data. We hypothesized that that lower at temperatures which XRD is normally performed at, the macrocycle might have a different conformation than at room temperature. Once XRD had been performed at room temperature it was seen that there were clear differences when comparing the two theoretical PXRD spectra to one another, that they

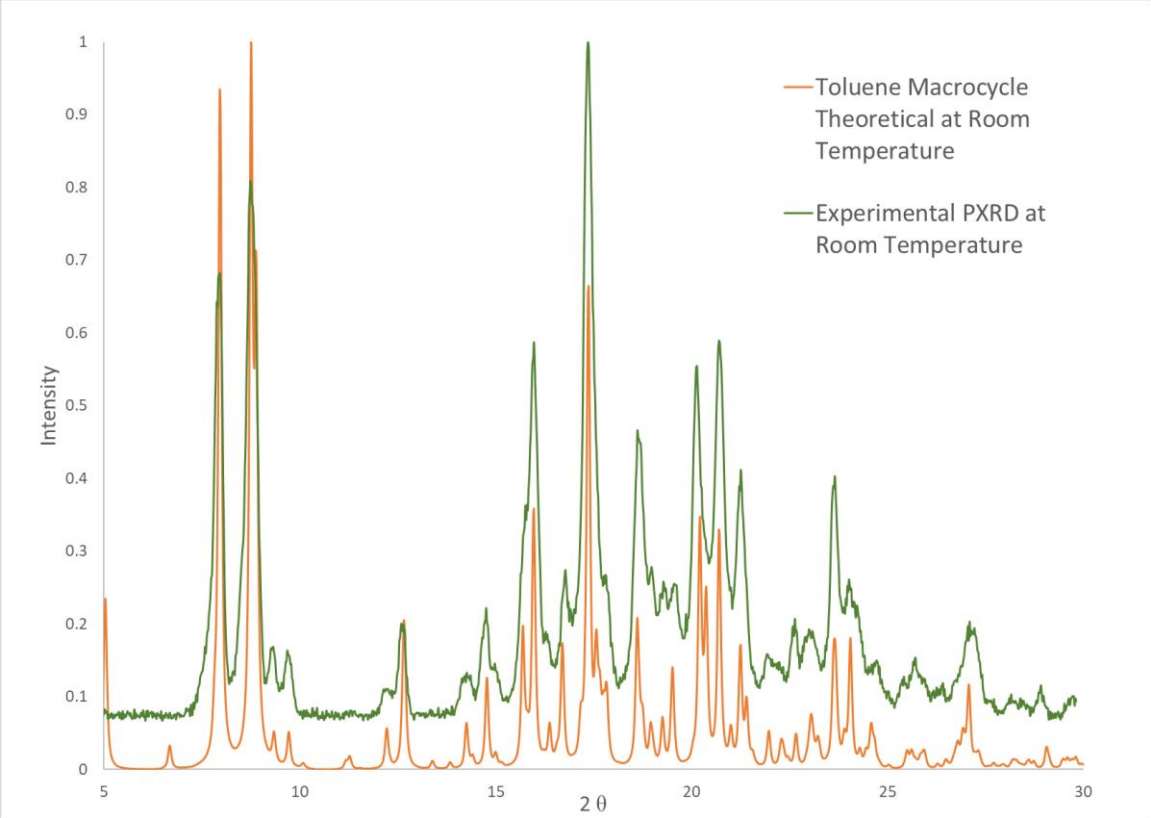

Figure 4.3: Orange: Theoretical PXRD of toluene derived macrocycle from XRD data at room temperature (301 K). Green: Experimental PXRD of toluene derived macrocycle showing phase purity proving that macrocycle was the dominant crystal phase when crystals were grown in more dillute conditions over longer periods of time.

were very different **(Figure 4.2)**.

4.2.3: Discussion

Though PXRD is not viewed as critical as XRD analysis, it is still paramount in crystal research because the theoretical PXRD spectra given from XRD data yields a "fingerprint" that can be used to determine if the product is pure in phase. The possibility of two different PXRD patterns based on the temperature XRD analysis **(Figure 4.3)** could be viewed as crippling to a research project even if the problem existed for a product that

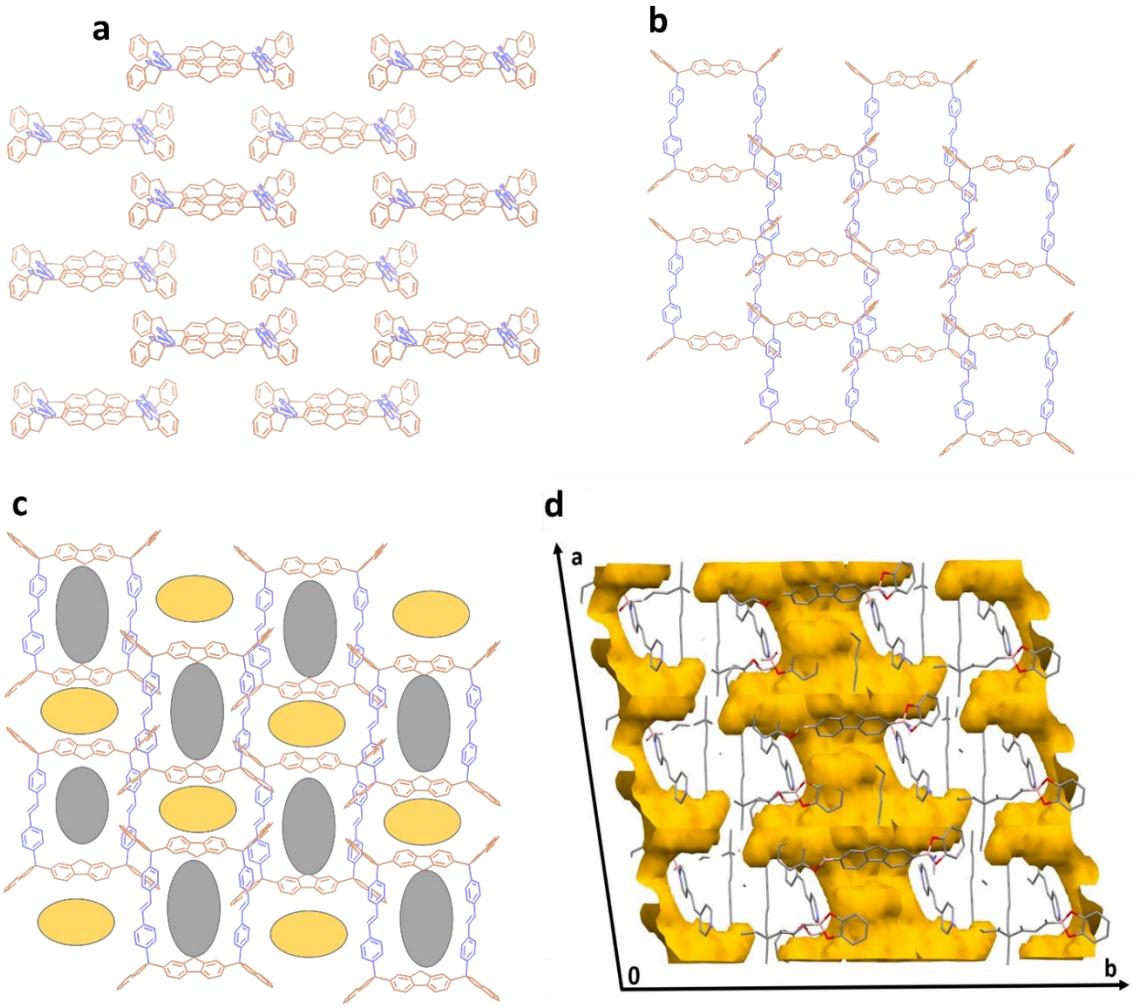

Figure 4.4: **a.** Front view showing the way the macrocycles stack into "towers" with the omission of the dihexyl chains for clarity. The adjacent towers are shifted vertically such that the catechol moieties overlap in and over under fashion. **b.** Top view of the towers viewable in figure (a). **c.** The same figure as in (b) but with grey ovals representing where the dihexl chains of each macrocycle are withn the pores and yellow ovals showing the extrinsic area of the crystal structure where the extrinsic porosity created by macrocycle cage overlap in which is home to the toluene guest moleules in the crystal repeat unit. **d.** With the use of z-clipping in the Mercury program that is part of the CCDC software package, the extrinsice porosity show as void space (yellow) which also highlights how an SCSC transitions to be discussed can occur since there is tunneling access throughout the crystals fornew possible guests to be hosted with open access for movement.

always grows as just one phase. In the case of the macrocycle and the polymer, the room temperature of XRD resolved an issue that had been very problematic in the past. When it was elucidated that one crystal structure alone had been grown many times for macrocycle **(Figure 4.2)** and the issue was temperature, two very different PXRD spectra

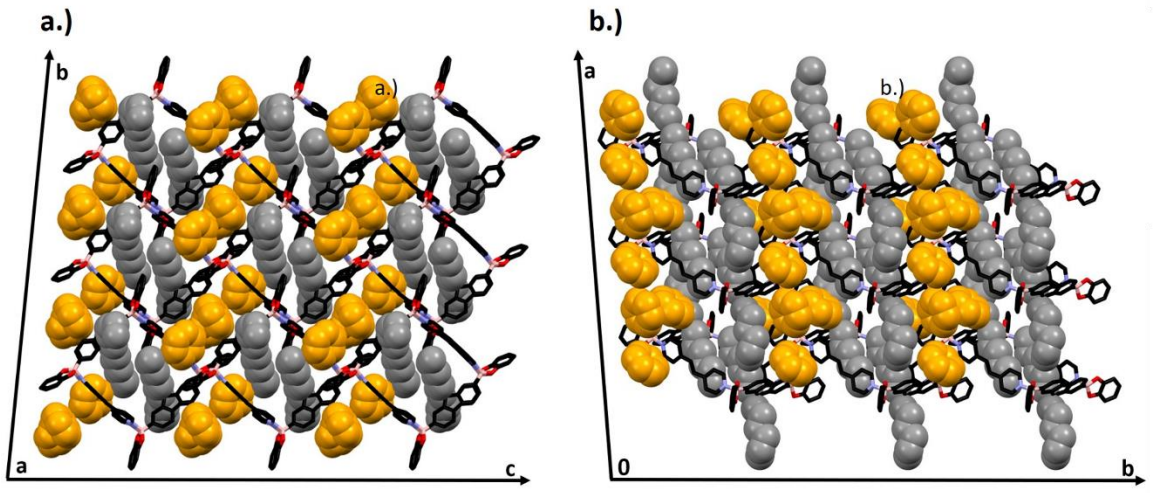

Figure 4.5: When viewing the crystal structure in a different manner, it is easier to see how the hexyl chains interact in a lamellar like way. Seen in **a.** is a top view of the macrocycle. Instead of showing toluene as a guest which has more disorder, benzene is shown in yellow and in the space-fill style for clarity. Seen in **b.** is a side view which gives a better perspective in highlighting the grey hexyl chains, in the space-fill style, acting as tethers which illustrates the way they tether the crystal network throughout.

were finally resolved proving that macrocycle does in fact grow pure in phase over longer periods of time in more dilute conditions.

The macrocycles stack on top of one another in which the dihexyl chains for each of the two DE1 units intrinsically exist facing above and below the macrocycle when viewing a macrocycle's aromatic backbone as flat. The intrinsic dihexyl chains act as aliphatic tethers inside the tower like stacks of macrocycles holding them together throughout the network. Each tower is shifted vertically to the adjacent ones such that they overlap in an interdigitated manner **(Figure 4.4)**.

The dihexyl chains are omitted for clarity to help elucidate CH-π and π–π interactions of the rigid aromatic backbone of adjacent cages and cages above and below one another **(Figure 4.4, a, b, c)**. These interactions cause all cages to be interdigitated with one another increasing the stability of the single crystal framework. Seen above are

the side view of four cage columns in view (with slight tilt for more depth) **(Figure 4.4, a)**, the top view of eight cage columns in view **(Figure 4.4, b)**, and the identical image seen in figured 4.2.4.b. but filled with yellow and grey ovals **(Figure 4.4, c)**. These grey ovals represent the aliphatic dihexyl chains (not explicitly shown) that interact with one another to stitch the cage columns together. Yellow ovals represent extrinsic porosity created by aromatic interaction and interdigitation **(Figure 4.4, d)**. The void space of extrinsic porosity can be seen to show the how large the pores are that hold solvent guests. These extrinsic channel-like pores that hold toluene guest makes it seem a possible route for another solvent guest to penetrate the framework in an SCSC transition. These channels can also be seen when replacing the toluene guest with benzene for less disorder and clarity, seen in yellow **(Figure 4.5)**. The benzene guests in these pores are illustrated in space fill style along with the with hexyl chains, seen in grey. From these two perspectives the space fill makes it easier to see lamellar like tethering of the dihexyl chains when intermolecularly interacting with ones that are neighboring them. These interactions of tethering effectively help with stabilizing the system when viewed as holding the macrocycle stacked towers together, but when adding the perspective of towers interdigitating with one another, all molecular interactions compound on one another. It seems that when looking at the guest aromatic CH-π and the π- π interactions with one another, and the macrocyclic framework, the lamellar like tethering, and the macrocycle like tower interdigitation, the framework would not change much if any post-synthetic modification were to occur.

The room temperature conformation of the macrocycle with toluene as a guest

had many differences when compared to the one in which XRD was performed at 100 K. Each of the dihedral angles between the fluorene and dipyridyl ethylene for the room temperature macrocycle are 104.75° and 108.77° which has more angle strain than the conformation at 100 K. This angle can be seen between the fluorene carbon, B1, and N1 and the fluorene carbon, B2, and N2 in **(Figure 3.14)**. The respective boron nitrogen bond lengths are 1.689 Å and 1.655 Å and the dihedral angle of dipyridyl ethylene is evaluated is 172.47° and is measured using the nitrogen atoms and the two carbon atoms that form the alkene between the aromatics. The macrocycles crystals are diamond in shape and red in color. The crystal system is triclinic with a P-1 space group with a repeat unit volume of 2,710.80 $Å^3$ and a density of 1.117 grams per cubic centimeter. The density did not change but the unit cell volume was larger than the conformation when in cryogenic conditions.

4.2.3: Experimental

A round bottom flask was charged with DE1 (52.3 mg, 0.092 mmol) and DPE (31.86 mg, 1.74 mmol) and dissolved in toluene (40 mL). Crystallization occurred over two weeks and produced large red diamond prisms along with crystal clusters. There were not any yellow hexagon plates seen in the sample which means that from the eye view it was pure in phase. Part of the sample was then given to the crystallographer for analysis and PXRD was performed on what remained of the sample. The spectra showed the sample to be pure phase.

4.3: Benzene Vapor SCSC Transition from Toluene Derived Macrocycle Precursor

As was discussed previously **(Chapter 2)**, benzene was proven to have a high

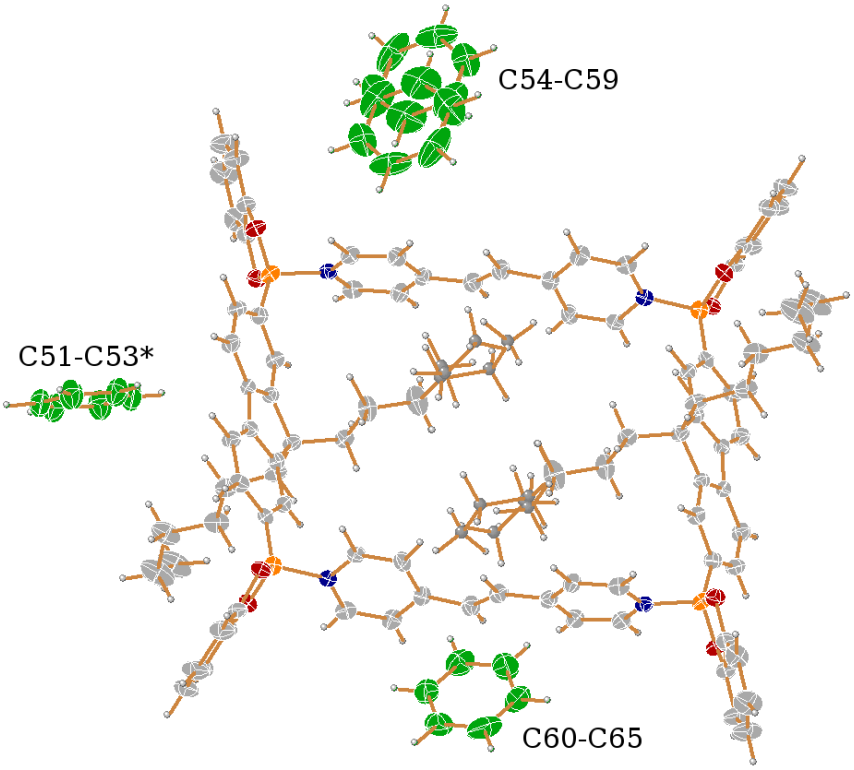

Figure 4.6: Once the toluene guest macrocycle is placed in the presence of benzene vapor, the SCSC transition occurs over night to which the benzene replaces the toluene as a guest within the macrocycle crystal structure. Counterintuitively, the benzene guest macrocycle has a better refinement from XRD analysis than its predessor even when XRD was performed on the same sample before the transition.

affinity to selectively reabsorb into VCP1 which was a reversible process in which PXRD could be performed, giving evidence that the process was highly repeatable. With this reasoning, benzene solvent as a vapor seemed to the best choice for exploring an SCSC transition to the toluene macrocycle precursor.

4.3.2 Results

The compound transitions in the triclinic system. The space group *P*-1 (No. 2) was confirmed by structure solution. The asymmetric unit consists of half of one $[(C_{37}H_{40}B_2O_4)_2(C_{12}H_{10}N_2)_2]$ complex located on a crystallographic inversion center, and three independent benzene molecules. Benzene C51-C53 is located on a crystallographic

inversion center and only half is present per asymmetric unit. Benzene C54-C60 is disordered about an inversion center and was refined with half-occupancy with all C-C distances restrained to be similar (SHELX SADI). Benzene C61-C66 is ordered on a general position.

4.3.3: Discussion

When the benzene vapor SCSC transition occurred to the toluene macrocycle precursor, qualitative analysis was not possible as seen previously **(Chapter 2)** in which a color change would occur in a single crystal. Though staying translucent, it either became paler in color or had a viewable change in reflected wavelength. After performing NMR and XRD after the toluene macrocycle was sealed in the presence of benzene overnight, it was observed that the benzene had replaced the original toluene molecule equivalency in virtually the same locations in the crystal repeat unit. When viewed by the naked eye, no change could be noticed when looking at the sample to find if it was more opaque than the previous day before being placed within a benzene vapor environment. Interestingly, XRD analysis of the transitioned crystal showed that the refinement was actually better with the benzene as a guest than the same sample previously hosting toluene. In the words of the crystallographer, “it seems that benzene is able to have a better fit”, which would mean that as a guest it provides less disorder. What is more counterintuitive is that when DE1 and DPE are mixed in equal molar ratio with benzene as solvent, the only product is a one-dimensional polymer as opposed to a macrocycle. From this new data, we have a benzene guest SCSC transition with better refinement than its toluene precursor all the while you cannot create macrocycle by crystallization in benzene solvent

alone using the methodology described herein. This is a perfect example of using post synthetic modification to get a product that is not attainable in the normal paradigm of organic chemistry. Interestingly, when discussed at the end of this chapter, it may show that even with better refinement seen, using benzene as a guest within the macrocycle still may not be the best crystalline confirmation when the toluene precursor is left in benzene vapor longer than just overnight or longer than forty-eight hours.

The transitioned benzene macrocycle's dihedral angles between the fluorene and dipyridyl ethylene for the are 105.20° and 108.77° which has slightly more angle strain of than the toluene derived precursor. This angle can be seen between the fluorene carbon and respective boron nitrogen bond angle **(Figure 4.6)**. The respective boron nitrogen bond lengths are 1.645 Å and 1.685 Å. The dihedral angle of dipyridyl ethylene is evaluated is 171.85° and is measured using the nitrogen atoms and the two carbon atoms that form the alkene between the aromatics. The macrocycles crystals are diamond in shape and red in color. The crystal system is triclinic with a P-1 space group with a repeat unit volume of 2,620.41 $Å^3$ and a density of 1.152 grams per cubic centimeter. Overall, it seems that the macrocycle framework did not change much when the benzene SCSC transition occurred.

4.3.4: Experimental

A one-dram vial was charged with toluene derived macrocycle single crystals (25 mg, 0.057 mmol). The one dram was then placed in a four dram with benzene solvent (7 mL) and sealed. This was done to ensure that only benzene vapor could interact with the sample. Within a day the translucent red crystals had not changed and after 48 hours the

sample vial was then sent to the crystallographer for single crystal XRD.

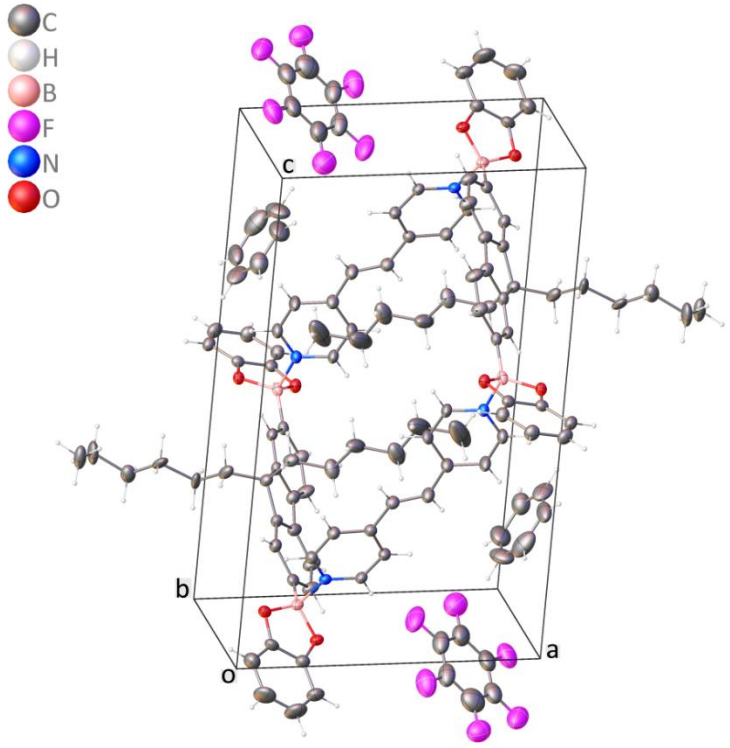

Figure 4.7: Like seen previously, the macrocoy cycle is symmetrically mirored on it's crystallographic inversion center, with minor disorder of one hexyl chain. Half of the benzene molecules were replaced by hexafluorobenzene. Both C_6H_6 and C_6F_6 molecules are disordered over two closely spaced positions. Displacement ellipsoids drawn at the 40% probability level.

4.4 SCSC Hexafluorobenzene Vapor SCSC Transition of Benzene Transitioned Macrocycle

Once the overnight benzene vapor transition had been characterized with a better refinement, the next question to be asked, was could we do it again with another solvent vapor? Historically, literature has reported that when benzene and hexafluorobenzene were mixed with one another in equal molar ratios, both with the exact same boiling point of 80.1 °C, they form a clear and colorless crystal within just a few hours.[14,15] This is because of their opposite quadrupoles. Due to this knowledge, hexafluorobenzene seemed like the perfect solvent for the next vapor SCSC transition.

4.4.1: Results

The compound crystallizes in the triclinic system. The space group *P*-1 (No. 2) was confirmed by structure solution. The asymmetric unit consists of half of one [$(C_{37}H_{40}B_2O_4)_2(C_{12}H_{10}N_2)_2$)] cycle located on a crystallographic inversion center, one hexafluorobenzene molecule and one benzene molecule. The hexyl substituent C26-C31 is disordered over two positions with fractional occupancies A/B = 0.614(5)/0.386(5), which were constrained to sum to one. C-C bond distances in the disordered part of the chain were restrained to be similar to one another using SHELX SADI restraints. A spherical restraint was applied to the anisotropic displacement parameters of the terminal hexyl chain atoms C35-C37 (SHELX ISOR). Both the hexafluorobenzene (C51-C56/F51-F56) and the benzene (C61-C66) molecules are disordered over two closely spaced positions each with occupancies of C51-C56/F51-F56 A/B = 0.702(5)/0.298(5) and C61-C66 A/B = 0.51(1)/0.49(1), also constrained to sum to one. The C_6 rings of each molecule were refined as rigid hexagons with *d*(C-C) = 1.39 Å. C-F distances were restrained to be similar (SADI). The geometry of the minor component was restrained to be similar to that of the major using a SAME instruction. Displacement parameters for nearly superimposed atoms of all disorder components were held equal. Non-hydrogen atoms were refined with anisotropic displacement parameters.

4.4.2: Discussion

As stated repeatedly, the benzene guest transition had better refinement than its toluene guest precursor and did not seem to change its translucent nature in the least

after the transition occurred. Optically, this infers that the benzene transitioned sing crystal did not seem to have become opaque which would be indicative of losing single crystallinity. Hexafluorobenzene has an almost completely opposite quadrupole when compared to benzene and because of this, when the two liquids are mixed together they become crystalline due to their intermolecular forces attracting one another in an organized manner. With this knowledge, hexafluorobenzene was chosen as a prime candidate for a second SCSC transition due to the expectation that it seemed likely to interact with the system while also at the same time, if a transition occurred, it would be interesting to learn if hexafluorobenzene would replace the benzene guest completely, not at all, or reflect historic literature as an interaction within the macrocycle host and with one another.[14,15] It turns out that the third option occurred in which only half of the benzene guest was replaced, and did in fact interact with benzene within the porous extrinsic channels throughout the crystal.

The transitioned hexafluorobenzene/benzene macrocycle's dihedral angles between the fluorene and dipyridyl ethylene for the are 103.72° and 108.89°. This angle can be seen between the fluorene carbon and respective boron nitrogen bond angle **(Figure 4.7)**. The respective boron nitrogen bond lengths are 1.698 Å and 1.644 Å. The dihedral angle of dipyridyl ethylene is evaluated is 176.01° and is measured using the nitrogen atoms and the two carbon atoms that form the alkene between the aromatics. The crystals are the original triangular shaped when seen as large single crystals but are much darker in nature and to which it almost has an orange purple hue. Interestingly, CP1 was also exposed to hexafluorobenzene and the same color change occurred but only on

the surface since XRD proved it did not interpenetrate into the crystal structure. Because of this it leads to the idea that hexafluorobenzene is directly correlated to this color change. In the case for the polymer, the color only changed on the surface. Though an SCSC transition to CP1 did not occur, it certainly had an impact on the optoelectronic characteristics on the outside of the single crystals. The crystal system is triclinic with a P-1 space group with a repeat unit volume of 26,630.3 $Å^3$ and a density of 1.284 grams per cubic centimeter which is slightly higher than the toluene and benzene macrocycles.

4.4.3: Experimental

A one-dram vial was charged with benzene transitioned macrocycle single crystals (25 mg, 0.057 mmol). The one dram was then placed in a four dram with hexafluorobenzene solvent (7 mL) and sealed. This was done to ensure that only hexafluorobenzene vapor could interact with the sample. Within a day the translucent red crystals started to turn orange-purple but stayed translucent. Over two weeks the vial was left to sit and the crystals had become slightly opaque but stayed mostly translucent and were darker in color than seen when only left in hexafluorobenzene vapor for twenty-four hours. The sample vial was then sent to the crystallographer for single crystal XRD.

4.5: Irreversibility Studies to find if the SCSC Transitions of The Original Toluene Derived Precursor

After the XRD analysis had been performed, we investigated two questions, are these processes reversible and, could the intermediate process be skipped? As in, could benzene and hexafluorobenzene solvents contained in separate vials be sealed in a larger

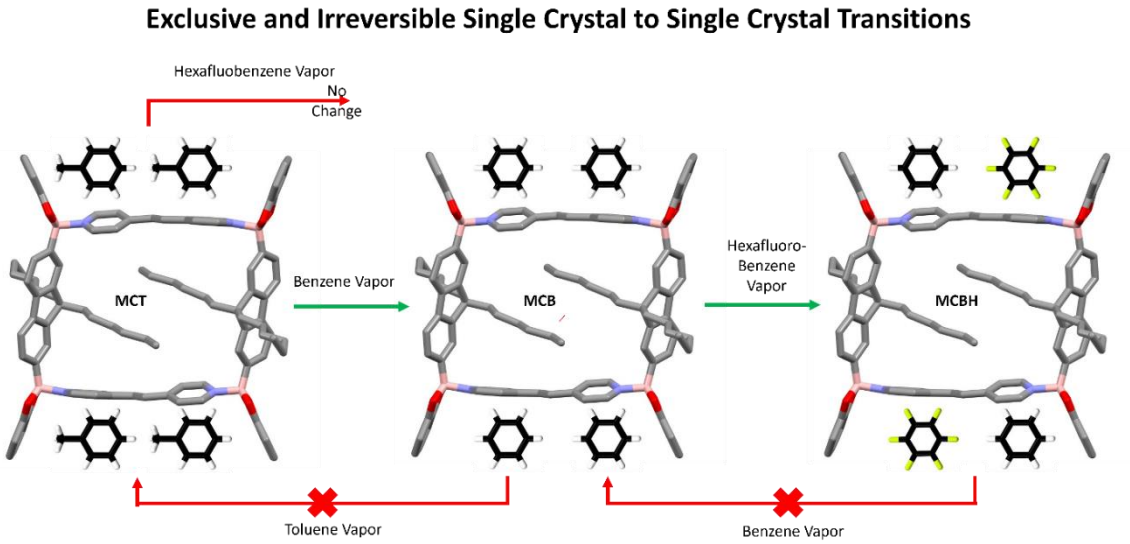

Figure 4.8: Representation of the cascade effect that proved that both vapor transitions on the toluene derived precursor followed by the benzene transitioned macrocyle were not reversible. In fact, they hac to happen in a stepwise process in which the benzene vapor transition had to occur first followed by the hexafluorobenzene transition. Both transitioned samples were placed within a sealed environment of thei previous solvents and over time, XRD analysis proved that their transition was not reversible. It was also seen that the toluene derived precursor could not undergo a SCSC vapor transition without the benzene transition occuring first. It also could not be experimentally performed with and equal molar mixture o benzene and hexafluorobenzene because the two solvents meant to only interact as vapor from the solvenent outside the sample vial would crystallize within a few hours.

one in which single crystals of the toluene derived macrocycle would only be exposed to both vapors at the same time essentially skipping the benzene transition step? To answer the second question quickly, the experiment would either be very hard to perform if not impossible because even if the effort was made to ensure both solvents could not mix together, and it was ensured that when sealed the toluene macrocycles were only exposed to both vapors there would be no evidence that the transition had not been a stepwise process. Essentially meaning that it would be unknown if the benzene vapor SCSC transition occurred first and was followed by the hexafluorobenzene vapor transition. Therefore, the third question to be asked was, could toluene macrocycle single crystals undergo an SCSC transition with hexafluorobenzene vapor alone?

4.5.2: Results

Benzene transitioned single crystals were sealed in the presence of toluene vapor and hexafluorobenzene transitioned crystals were sealed in a vial with benzene vapor for two weeks. XRD analysis showed that no guest exchange had occurred for both vials and were therefore both SCSC transitions were considered to be irreversible processes. Toluene derived macrocycle was also sealed in the presence of hexafluorobenzene vapor for two weeks and XRD analysis shows that toluene guests had not been replaced and there was no change in diffraction from the original sample.

4.5.3: Discussion

Since the processes showed to be irreversible it would be inferred that after the transitions occurred, the enthalpy of binding for the new guests was much stronger than it was for toluene guests in the original macrocycle precursor. When comparing the benzene vapor transitioned single crystals, it was seen that there was better refinement and less disorder than when XRD analysis was performed on the toluene guest sample before the transition. It is expected that this is because benzene had a better fit within the intrinsic pores due to being smaller. The fact that the hexafluorobenzene transitioned crystals were irreversible leads to the expectation that benzene and hexafluorobenzene molecules had much stronger intermolecular interactions with one another compared to just the CH-π and the π-π bonding were only held by the guests of the same species within the framework.[14,16] This can be seen when viewing the orientations of guests comparing

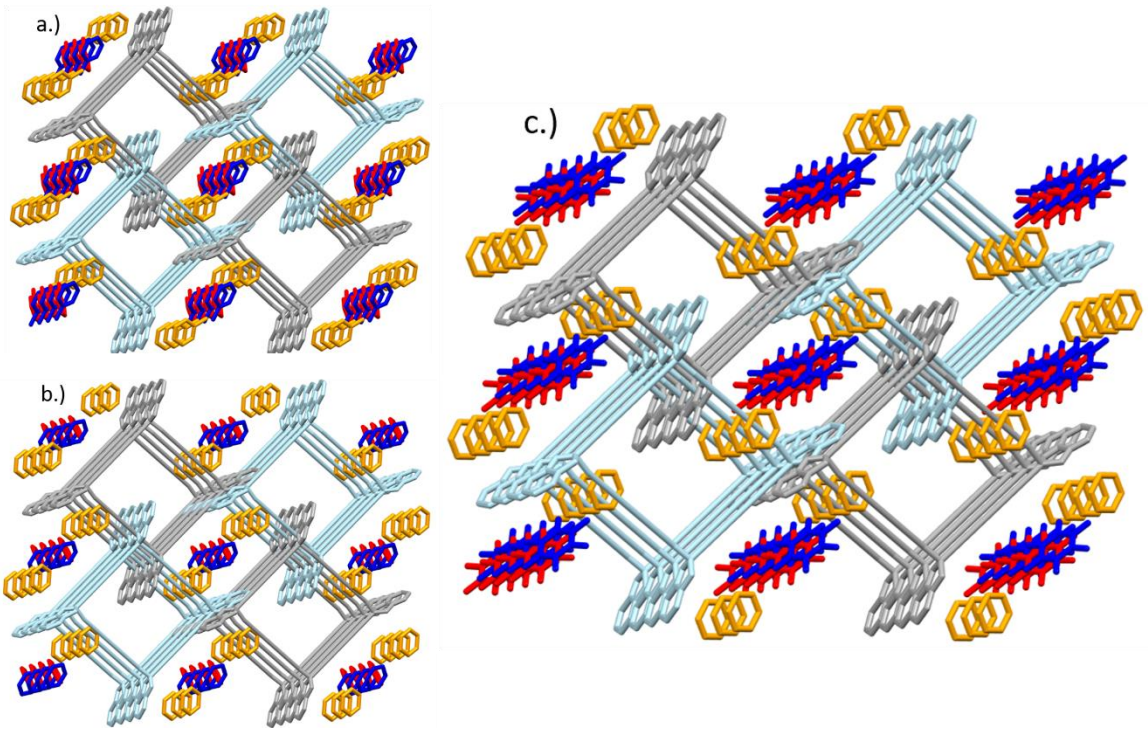

Figure 4.9: Most of the aromatic atoms, all the aliphatic atoms, and hydrogens were omitted for clarity. The molecules in red and blue and yellow highlight these orientations and where they are located throughout the structure. Red and blue guests exist within the extrinsic porous channel created outside of the macrocycles while yellow are located in between the DPE linkers as macrocycles stack on top of one another. Seen above are, **a.**, The toluene derived macrocycle, **b.**, the benzene transitioned macrocycle, and, **c.**, the hexafluorobenzene transitioned macrocycle. Seen in **c.** is benzene in yellow and hexafluorobenzene in red and blue. Macrocycles are shown in light blue and grey for clarity in showing the interdigitated manner the "tower" like stacks are arranged.

their intermolecular interactions to one another within the three crystal structures **(Figure 4.9)**. Most of the aromatic atoms, all the aliphatic atoms, and hydrogens were omitted for clarity. Red, yellow, and blue molecules are shown to highlight the three guest orientations seen within the three crystal structures. Red and blue guests exist within the extrinsic porous channel created outside of the macrocycles while yellow are located in between the DPE linkers as macrocycles stack on top of one another. Seen above are the toluene derived macrocycle **(Figure 4.9, a.)**, the benzene transitioned macrocycle **(Figure 4.9, b.)**, and the hexafluorobenzene transitioned macrocycle **(Figure**

4.9, a. and b). When viewing the toluene and benzene guests within the figure, only CH-π and π-π interactions are occurring. The orientations occur because of their interaction as guests with one another and their interactions with the host system. The hexafluorobenzene orientations exist in a manner where benzene (yellow) is located between the macrocycles and hexafluorobenzene in (red and blue) are located within the extrinsic channels and are oriented in an offset manner while also interacting with the benzene's location **(Figure 4.9 c.)**. It is expected that benzene and hexafluorobenzene having quadrupoles opposite of one another, making their interactions much stronger than that of the benzene and toluene guests alone. This is seen in literature and this illustrates how strong the intermolecular forces are between benzene and hexafluorobenzene because, though they have the same boiling point, when mixed together they crystallize at room temperature, exemplifying the strength of the π-π interaction.[14,15] Hexafluorobenzene is another highlight of this work because it is yet another example of post-synthetic modification creating a product that is not attainable directly by standard procedures typically performed. When DE1 and DPE are dissolved in hexafluorobenzene alone, they never crystallize even if left for months. An uncharacterizable precipitate does occur if DE1 and DPE forced at high concentrations which means that still with either approach, single crystals cannot be attained via the benzene intermediate.

Found to be more interesting, is that while the process is already known to be irreversible, a single crystal of toluene macrocycle could not be transitioned with hexafluorobenzene vapor alone which showed that these two SCSC transitions must

occur in a stepwise manner. Even though toluene's quadrupole having a higher electrostatic potential due to hyperconjugation, the melting point of the dimer toluene and hexafluorobenzene create is room temperature (301K).[17] Therefore, because hexafluorobenzene has a weaker interaction with toluene than benzene it would be expected that the strength of the intermolecular interaction would not occur, thus inhibiting molecular transport and the direct displacement of toluene by hexafluorobenzene. It seems this irreversibility and forced stepwise process could possibly open the door for future research on the cascade effect of post-synthetic modification not only being capable of creating products incapable of being created in a standard way but also allowing for other step(s) to occur after, that may have the characteristics needed for the end goal.

4.6 X-ray Diffraction Data for SCSC Transitions from Toluene Precursor

Structure Label	Toluene Derived Macrocycle at 100K	Single Crystal to Single Crystal Benzene Vapor Transition of Toluene Derived Macrocycle	Single Crystal to Single Crystal Hexafluorobenzene Vapor Transition of Toluene Derived Macrocycle	Toluene Derived Macrocycle at 301K
Empirical formula	C122.77H128.3B4N4O8	C122H128B4N4O8	C122H112B4F12N4O8	C122.2H127.66B4N4O8
Crystal habit and color	irregular; yellow-orange	irregular; yellow-orange	irregular; yellow	block; orange
Formula weight	1831.07	1817.48	2033.39	1823.58
Temperature/K	100(2)	100(2)	100(2)	301(2)
Crystal system	triclinic	triclinic	triclinic	triclinic
Space group	*P*-1	*P*-1	*P*-1	*P*-1
a/Å	11.6224(6)	11.5851(3)	11.4836(8)	11.6037(6)
b/Å	13.4837(7)	13.4695(3)	13.0982(9)	13.5369(7)
c/Å	17.1974(8)	17.2578(4)	17.9150(13)	17.7832(9)
α/°	82.409(3)	82.5370(10)	82.719(2)	83.227(2)
β/°	82.900(3)	82.8110(10)	83.912(2)	83.324(2)
γ/°	79.972(3)	80.7410(10)	81.075(2)	79.061(2)
Volume/Å3	2616.6(2)	2620.41(11)	2630.3(3)	2710.8(2)
Z	1	1	1	1
ρcalcg/cm3	1.162	1.152	1.284	1.117
Crystal size/mm3	0.22 × 0.12 × 0.1	0.3 × 0.12 × 0.1	0.28 × 0.22 × 0.12	0.6 × 0.42 × 0.24
Reflections collected	76761	76203	29757	83948
Goodness-of-fit on F2	1.038	1.033	1.018	1.046
Final R indexes [I>=2σ (I)]	R_1 = 0.0456, wR_2 = 0.1072	R_1 = 0.0494, wR_2 = 0.1178	R_1 = 0.0628, wR_2 = 0.1479	R_1 = 0.0738, wR_2 = 0.2206
Largest diff. peak/hole / e Å-3	0.39/-0.30	0.54/-0.56	0.39/-0.33	0.56/-0.30
Dihedral angles between the fluorene and dipyridyl ethylene	105.20°, 108.77	105.00°, 108.50°	103.72°, 108.89°	104.75°, 108.27°
Boron nitrogen bond lengths (Å)	1.676, 1.646	1.685, 1.645	1.698, 1.644	1.689, 1.655

Table 4.1: X-ray diffraction data of the toluene derived macrocycle at 100K,the benzene vapor SCSC transition, the hexafluorobenzene vapor SCSC transition and the toluene derived macrocycle at room temperature (301 K).

4.7 Thermodynamic Event when Toluene Derived Macrocycle Left in the Presence of Benzene Vapor

Figure 4.10: While it is seen that benzene vapor can replace toluene as a guest in the macrocycle, if left over time in benzene vapor a visible transition occurs. At a specific feature, and over time, the color changes from red to yellow quickly and then the yellow color transitions across the crystal.

4.7.2: Results

The transition that occurs when the toluene derived macrocycle is placed in the presence of benzene can happen overnight. But not discussed is the changes that occur when it stays sealed with benzene vapor over longer periods of time. The red diamond prism single crystals stay the same in size and shape but the red dramatically changes to yellow **(Figure 4.10)**.

4.7.3: Discussion

Foreshadowed earlier in this chapter, is that though the benzene guest has better refinement than that of its toluene guest predecessor, it still may not be the preferred conformation. This is because when left in benzene vapor for longer periods of time, an extraordinary change occurs that started as early as three days. It is believed that a

"thermodynamic event" occurs in which there is a spontaneously change at a very specific point of the single crystal from which a chain reaction occurs that can be seen visually. At one very small region of a single crystal of the benzene vapor SCSC transitioned macrocycle, the red changes to yellow and the yellow starts cascading across the crystal as if someone were pulling a yellow sheet over it. Until photos were taken with a microscope daily, this information would go against the early hypothesis that when toluene macrocycle crystals were left in the presence of benzene vapor that the change was homogenous in which the entire crystal would transition from red to yellow. As in, the red over the entirety of the crystal would slowly fade in to the yellow color. But once this was not seen to be the case, the expectation was a major polymorphic shift occurring based on the clearly seen radial heterogenous transformation in which a clear line between the red color from the beginning and the yellow seen at the end of the transition.[18]

Once the event was finished and the crystal had completely turned yellow, it seemed that, though still highly crystalline, it unfortunately did not diffract well enough to examine the structure with single crystal XRD. However, the diffraction rings seen did show that it polycrystalline. Though more data is still needed as evidence, the hypothesis is that that a topochemical polymerization occurred to which the dipyridyl linkers are able to break away from their boron dative bond and swing up, performing a nucleophilic exchange to boron of a macrocycle directly above it in the stack.[5,19] The attack would cause another DPE to leave propagating the chain reaction. There is evidence that the length of DPE is very close to the same length needed between the two boron's above

and below for this to occur. If this was to be true it could be inferred that the chain reaction could be seen visually happening as the single crystals slowly become yellow **(Figure 4.10)**. Furthermore, this change in visual wavelength reflected could certainly be used in the future for optical sensing and detection of benzene.

4.7.4: Experimental

Single crystals of toluene derived macrocycle were placed on a matte black microscope slide specifically made for imaging**.** The slide was then placed in a petri dish on top of a spacer to raise its elevation. This was done to make sure that the single crystals were never exposed to benzene as a liquid when was pipetted daily onto the base of the petri dish and covered. Because it was not a perfect seal, benzene would slowly escape as vapor. When the slighted change of color at a specific point of one crystal, the petri dish was handled with extreme care to have only slight changes to their orientation on the slide and were photographed daily.

4.8: Discussion

The macrocycle that was derived in toluene had interesting results **(Figure 4.1)**. It was finally able to be proven pure in phase once XRD analysis was performed at room temperature (301 K) **(Figure 4.3)**. This had been a very problematic issue for studying these crystals because the theoretical PXRD from XRD analysis was done at 100 K, its theoretical was very different from that at room temperature **(Figure 4.2)**.

It, like CP1 **(Chapter 2)**, was able to undergo an SCSC transition when left over night in the presences of benzene **(Figure 4.6)**. When this change occurred, it did not have much change to its crystal structure. XRD analysis demonstrated that overnight the

benzene was able to replace the toluene guest within the host framework and counterintuitively, the refinement for the diffraction was better than that of its toluene guest predecessor. It was also found to be an irreversible process. Furthermore, a second SCSC transition took place with hexafluorobenzene vapor **(Figure 4.7)**. In this instance the hexafluorobenzene was able to replace half of the benzene guest within the structure and was also an irreversible process. This was expected to be due to the strong intermolecular forces that benzene and hexafluorobenzene have in which they will form a crystal at room temperature.[14,15] Interestingly, when SCSC transitions occurred to CP1 single crystals, there was no change to the polymer, small changes, or in the case of being exposed to acetonitrile vapor, a drastic change. When compared to transitions that took place for the macrocycle, there were differences to bond angle and lengths but not dramatic enough to make changes to the crystal structure overall. It is expected that the lamellar like tethers that holds the stacked macrocycle vertically and the interdigitation the adjacent towers have with one another caused the frameworks to not have much freedom to move **(Figure 4.5)**.

Once the toluene derived macrocycle was left in the presence of benzene vapor over days, there was a dramatic change that occurs in which a very specific point of the red crystal turns yellow. Once this change starts, over just a few days, the yellow spreads over the crystal until it is a bright yellow. To be clear, this is not a slow change in shade from red to yellow but a very heterogenous transformation in which a clear line between the red color from the beginning and the yellow seen at the end of the transition. This seems to be a “thermodynamic event” that spontaneously starts at a single point of the

crystal, propagating a chain reaction that moves through entirety of the single crystal.[18,19] Furthermore, this change seen from red to yellow, even if the mechanism in not know could have application in the optical sensing of benzene in the vapor form.

4.9: References

(1) Zhang, Y.-B.; Su, J.; Furukawa, H.; Yun, Y.; Gándara, F.; Duong, A.; Zou, X.; Yaghi, O. M. Single-Crystal Structure of a Covalent Organic Framework. *Journal of the American Chemical Society* **2013**, *135* (44), 16336–16339. https://doi.org/10.1021/ja409033p.

(2) Sindt, A. J.; Smith, M. D.; Berens, S.; Vasenkov, S.; Bowers, C. R.; Shimizu, L. S. Single-Crystal-to-Single-Crystal Guest Exchange in Columnar Assembled Brominated riphenylamine Bis-Urea Macrocycles. *Chemical Communications* **2019**, *55* (39), 5619–5622. https://doi.org/10.1039/C9CC01725A.

(3) Xiao, W.; Hu, C.; Ward, M. D. Guest Exchange through Single Crystal–Single Crystal Transformations in a Flexible Hydrogen-Bonded Framework. *Journal of the American Chemical Society* **2014**, *136* (40), 14200–14206. https://doi.org/10.1021/ja507689m.

(4) Chu, Q.; Swenson, D. C.; MacGillivray, L. R. A Single-Crystal-to-Single-Crystal Transformation Mediated by Argentophilic Forces Converts a Finite Metal Complex into an Infinite Coordination Network. *Angewandte Chemie International Edition* **2005**, *44* (23), 3569–3572. https://doi.org/https://doi.org/10.1002/anie.200500400.

(5) Xu, W. L.; Smith, M. D.; Krause, J. A.; Greytak, A. B.; Ma, S.; Read, C. M.; Shimizu, L. S. Single Crystal to Single Crystal Polymerization of a Self-Assembled Diacetylene Macrocycle Affords Columnar Polydiacetylenes. *Crystal Growth & Design* **2014**, *14* (3), 993–1002. https://doi.org/10.1021/cg401380a.

(6) Rambo, B. M.; Tilford, R. W.; Lanni, L. M.; Liu, J.; Lavigne, J. J. Boronate-Linked Materials: Ranging from Amorphous Assemblies to Highly Structured Networks. In *Macromolecules Containing Metal and Metal-Like Elements*; Abd-El-Aziz, A. S., Carraher Jr., C. E., Pittman Jr., C. U., Zeldin, M., Eds.; John Wiley & Sons, Inc.: Hoboken, NJ, USA, 2009; Vol. 9, pp 255–294. https://doi.org/10.1002/9780470527085.ch6.

(7) Liu, J.; Lavigne, J. J. *Boronic Acids*, Second.; Hall, D. G., Ed.; Wiley-VCH Verlag GmbH & Co. KGaA: Weinheim, Germany, 2011; Vol. 2. https://doi.org/10.1002/9783527639328.

(8) Stephens, A. J.; Scopelliti, R.; Tirani, F. F.; Solari, E.; Severin, K. Crystalline Polymers Based on Dative Boron–Nitrogen Bonds and the Quest for Porosity. *American Chemical Society Materials Letters* **2019**, *1* (1), 3–7. https://doi.org/10.1021/acsmaterialslett.9b00054.

(9) Luisier, N.; Bally, K.; Scopelliti, R.; Fadaei, F. T.; Schenk, K.; Pattison, P.; Solari, E.; Severin, K. Crystal Engineering of Polymeric Structures with Dative Boron–Nitrogen Bonds: Design Criteria and Limitations. *Crystal Growth & Design* **2016**, *16* (11), 6600–6604. https://doi.org/10.1021/acs.cgd.6b01292.

(10) Christinat, N.; Croisier, E.; Scopelliti, R.; Cascella, M.; Röthlisberger, U.; Severin, K. Formation of Boronate Ester Polymers with Efficient Intrastrand Charge-Transfer Transitions by Three-Component Reactions. *European Journal of Inorganic Chemistry* **2007**, *2007* (33), 5177–5181. https://doi.org/https://doi.org/10.1002/ejic.200700723.

(11) Bear, J. C.; Cockcroft, J. K.; Williams, J. H. Influence of Solvent in Crystal Engineering: A Significant Change to the Order–Disorder Transition in Ferrocene. *Journal of the American Chemical Society* **2020**, *142* (4), 1731–1734. https://doi.org/10.1021/jacs.9b11895.

(12) Gao, W.-X.; Feng, H.-J.; Guo, B.-B.; Lu, Y.; Jin, G.-X. Coordination-Directed Construction of Molecular Links. *Chemical Reviews* **2020**, *120* (13), 6288–6325. https://doi.org/10.1021/acs.chemrev.0c00321.

(13) Foo, M. L.; Matsuda, R.; Kitagawa, S. Functional Hybrid Porous Coordination Polymers. *Chemistry of Materials* **2014**, *26* (1), 310–322. https://doi.org/10.1021/cm402136z.

(14) Edwards, A. J.; Mackenzie, C. F.; Spackman, P. R.; Jayatilaka, D.; Spackman, M. A. Intermolecular Interactions in Molecular Crystals: What's in a Name? *Faraday Discussions* **2017**, *203*, 93–112. https://doi.org/10.1039/C7FD00072C.

(15) PATRICK, C. R.; PROSSER, G. S. A Molecular Complex of Benzene and Hexafluorobenzene. *Nature* **1960**, *187* (4742), 1021. https://doi.org/10.1038/1871021a0.

(16) Nishio, M. CH/π Hydrogen Bonds in Crystals. *CrystEngComm* **2004**, *6* (27), 130–158. https://doi.org/10.1039/B313104A.

(17) Cockcroft, J. K.; Li, J. G. Y.; Williams, J. H. Influence of Methyl-Substitution on the Dynamics of the C–H···F–C Interaction in Binary Adducts. *CrystEngComm* **2019**, *21* (37), 5578–5585. https://doi.org/10.1039/C9CE00541B.

(18) Krishnan, B. P.; Sureshan, K. M. A Spontaneous Single-Crystal-to-Single-Crystal Polymorphic Transition Involving Major Packing Changes. *Journal of the American Chemical Society* **2015**, *137* (4), 1692–1696. https://doi.org/10.1021/ja512697g.

(19) Dou, L.; Zheng, Y.; Shen, X.; Wu, G.; Fields, K.; Hsu, W.-C.; Zhou, H.; Yang, Y.; Wudl, F. Single-Crystal Linear Polymers Through Visible Light–Triggered Topochemical Quantitative Polymerization. *Science (1979)* **2014**, *343* (6168), 272–277. https://doi.org/10.1126/science.1245875.

CHAPTER 5: A NEW APPROACH IN SYNTHESIZING A FULLY CONJUGATED COVALENT ORGANIC FRAMEWORKS WITH SEMICONDUCTOR POTENTIAL

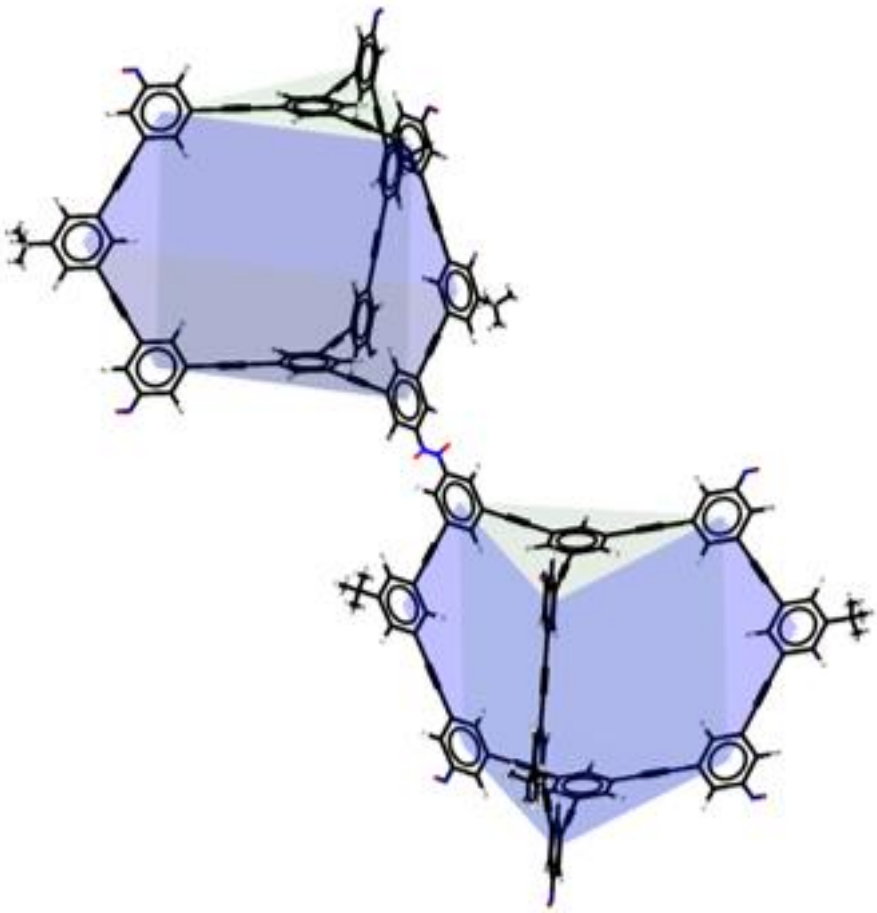

Figure 5.1: Two synthesized conjugated bicyclic cages bridges by an azodioxide π bond where electron communication exists throughout.

5.1: Introduction

Over the past decades, focus has accelerated in predesigned self-assembling structures for many classes of materials that can be optimized before, during, and after

synthesis, yielding characteristics that may not be attainable within the standard paradigm of organic synthesis.[1] Structures of this nature include, but are not limited to covalent organic frameworks (COFs), metal organic frameworks (MOFs), nanoparticles, and new advances in the production of graphene. [2–13]

Previously discussed **(Chapter 1)** is how reticular design can be very helpful when planning to achieve an end goal when creating materials that will interact in a manner such that the overall product's framework will be known before synthesis. It has also been seen that the thermodynamics of the system have so many physical forces at play that it can lead to pitfalls where having a well thought plan and expectation can then still yield unexpected product. This can be due to solvent driven interactions, IPN, and many other variables and forces working with one another in the reaction matrix which usually ends up with a product that is lowest in energy.[14]

Also discussed previously is the idea of electron transport through a conjugated framework, a new field for carbon based, organic, supramolecular and highly porous materials where synthetic modification would be incredibly useful. It would be especially useful in having the ability to dope molecules that range in characteristics of virtually any kind because the changes it would effectively be able to change the abilities of the host in way that could be fashioned to meet many desired products.[1,15,16]

Therefore, to achieve these desired characteristics and capabilities, it would be advantageous to create a framework that is not only capable of electronic communication, but can communicate in all directions through a three-dimensionally linked network. Modification post-polymerization could be used to fine-tune the

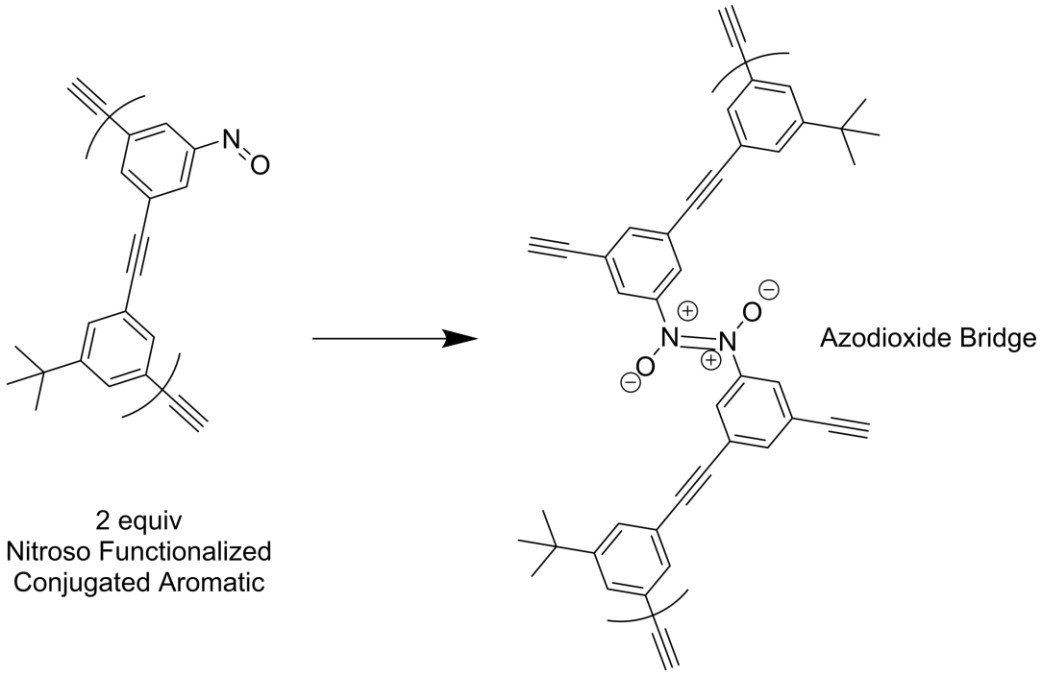

Scheme 5.1: Synthetic scheme of two equivalents of a nitroso functionalized derivative that is capable of dynamically bonding to form an azodioxide bridge. This bridge is capable of extending conjugation between the building blocks.

material's properties towards a diverse array of applications. For this to occur, the possible pitfalls of reticular synthetic design would also need to be resolved:

5.2: A New Approach to Reticular Chemistry

Herein we have devised a new approach for the creation of 3-D conjugated frameworks with persistent pores derived from bicyclic molecular cage building blocks. It is expected that significant advances will arise upon covalently linking cages in a manner that allows electronic communication between these building blocks, thereby creating a completely bonded three-dimensional and crystalline COF. Connecting the conjugated cages via pi-conjugated bridges affords the type of networking that will result in a completely conjugated 3-D COF (ConCOF). This new material would be highly porous and readily functionalized while still being capable of hosting diverse guests, resulting in "the-first-of-its-kind" material because it is porous, conjugated and tunable. The innovation

herein addresses the pertinent challenges by using starting materials that follow these rules:

1) The self-assembling building blocks must be three dimensional macrocyclic cages with their connective moieties facing outward. This ensures that the starting material is already porous in itself.

2.) The carbon bond angles responsible for the proposed cage must consist of sp and sp^2 hybridizations for three reasons. The first is because the bond strength would give more rigidity which would allow less conformational changes that are not wanted when planning a design in a reticular way. The second is that these hybridizations consist of bond angles of 180˚ and 120˚ degrees. These angles make it much easier to work with because the use of linear and trigonal planar entities when predesigning in this reticular manner, allows for greater predictability in the final product. For example, COF-18 utilized the trigonal planar building blocks in which benzene-1,3,5-triboronic acid dynamically bonded with tetrahydroxybenzene, a two-dimensional COF was formed.[3] While on the topic of the connectivity of these angles, for instance in sp^2 bonding, it only takes two angles of 120˚ degrees to end up in the same direction as started if the angles between building blocks were trans. It could be argued that in the effort to create a ConCOF with a predictable final product, that the use of the two-dimensional COF-18 is a poor example, but this thought process would forget that single bonds between the alkenes and alkynes can freely rotate. If phenyl rings are part of the design and are used for all the connectivity, the conformation could end up with one of the rings orthogonal to the other as opposed COF-18 that is completely planar. This orthogonal connectivity

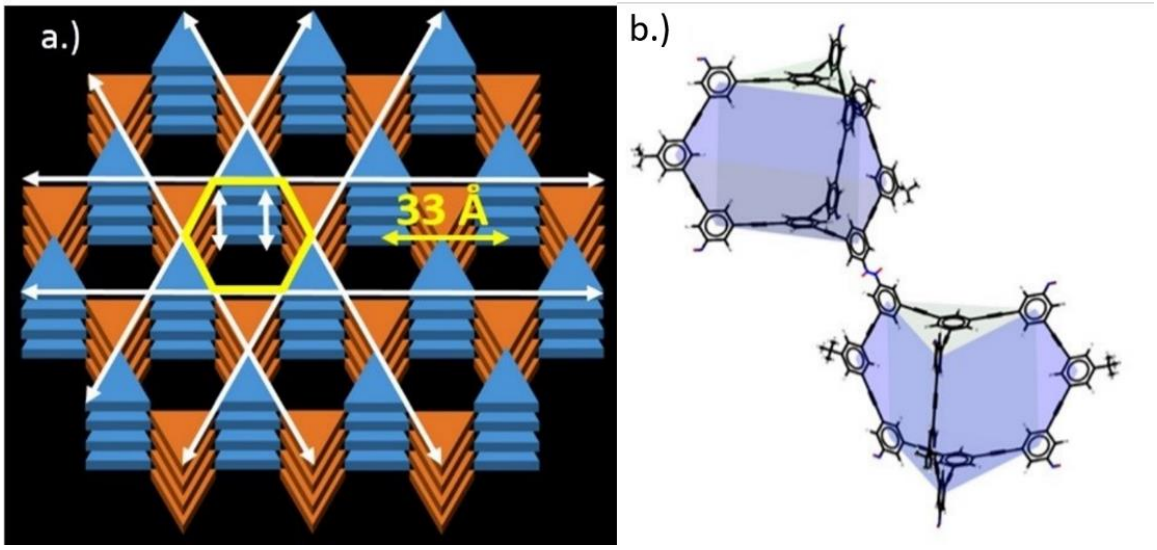

Figure 5.2: a.) Top view of AC1 highlighting the large hexagonal pores produced upon three dimensionally cross-linking.Alsohighlighted (Yellow) is the multiscale porosity of the system to which the cages are also porous and the vectors of networking (White) giving strength to the structure.b.) Overlay of triangular prism and bifrustum cages showing why AC1 is the expected networked structure.

is key to three-dimensional building blocks. The third reason is that when the dynamically bonding moieties on the outside self-assemble in a way that it forms an alkene or an alkyne, then linear directional connectivity can be obtained. The only outcome that would not adhere to this is if the formation of an alkene was cis which is not favorable because the building blocks would already have to be large due to statements previously mentioned.

3.) The building block must be completely conjugated throughout which is now already fulfilled by the second rule above. Because all connectivity is sp and sp^2 hybridized, this conjugation is already taking place

4.) When predesigning something that follows these requirements, it must also be capable of avoiding interpenetration. The reason the term cage, instead of macrocycle, has been repeated is that if the starting material only existed as a single macrocycle, IPN would be much more possible as opposed to a bimacrocyclic (bicyclic)

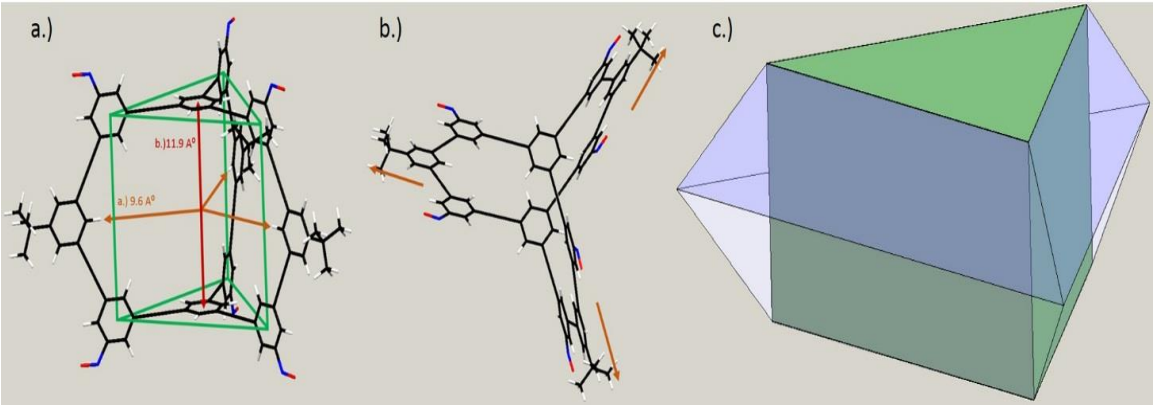

Figure *5*.3: a.) Side view of the six nitroso-functionalized cage; the green triangular prism highlights the macrocycle cavity, while the red and orange arrows indicate the cavity dimensions with a height of 11.9 Å between the top and bottom faces and 9.6 Å from the center axis to the three diethynylbenzene side-arms. b.) Top view of the cage showing the C3-symmetric design with diethynylbenzene side-arms containing a protruding t-butyl moiety (indicated with orange arrows). c.) Schematic of the green triangular prism of the cage cavity and the blue triangular bifrustum macrocyclic shell resulting from connecting each triangular face of the macrocycle with the t-butyl-functionalized diethynylbenzene side-arms. These side-arms produce a bulging affect that limits how these cages may assemble when crosslinked through the dimerization of nitroso-groups at the corners of the triangular faces to form azodioxide bonds.

cage. This also ensures that the building block is three dimensional which means it already holds a large pore within itself along with having more structural integrity in its own right, meaning that as the network rigidly forms it would only make the framework stronger. Once the building blocks have been synthesized, we planned to pursue two routes to obtain azodioxide-bridged products, that ensures a π bond between cages, essentially allowing electron transportation in the expectation of a ConCOF single crystal or completely conjugated thin film. It is also expected that either outcome would be capable of an array of potential applications. The intent of this new endeavor is to demonstrate the utility of this approach and establish a reference for the capabilities of such a paradigm. Based on precedent regarding COF synthesis, it has been challenging thus far to obtain single-crystalline materials.[17] This is unfortunately due to the inherently higher reproducibility of properties exhibited by such a single crystal COF.[14,16] Therefore, the

fabrication of a completely conjugated nano-scaffold structure that is cross-linked in all three dimensions is an attractive concept. Such a material would provide an avenue into the realm of 3-D self-assembled semi-conducting materials.

4.3: Post-Polymerization Plans

After analyzing different design possibilities, a multi-angled polyhedral shape was chosen. Specifically, a triangular bifrustum macrocyclic shell **(Figure 5.2)**, represents an independent building block capable of distributing the crystal packing stresses evenly across all directions.[10,18] This symmetric cage results from connecting each triangular face of the macrocycle with *t*-butyl-functionalized diethynylbenzene side-arms. Consequently, the conjugated cage can be viewed as two geometric elements where, in one view, the cage is its own structural entity, and in the other it is the location of the bondable vectors of the nitroso groups **(Figure 5.2 c)**.

The macrocyclic nature of building block reduces the possibilities of IPN because of simple steric considerations while maintaining the large cavity size and shape. In addition, the *t*-butyl groups appended to the side edges help reduce the likelihood of face-to-face or edge-to-edge assembly by effectively blocking this motif while simultaneously directing assembly towards the corners. Therefore, combining the concepts of a triangular bifrustum cage created by Moore,[18] with precedent set by Wuest to create completely networked, covalently linked organic single crystals, we are generating a completely conjugated, covalent framework. Interestingly the expected crystal structure to be discussed would be a three-dimensional tessellation to which the pores created in the expected multi-scale porous system would exist as void space with the same volume

of the cage itself. The cavity within this cage is 11.9Å between the top and bottom faces and 9.6 Å from the center axis to the three diethynylbenzene side-arms (**Figure 5.2 a, b**). Modest alterations to the original design of Moore will produce a cage decorated with six chlorobenzene groups.[18] The chlorides can be converted to nitroso-groups capable of dynamic bonding to form azodioxide bridges which allow electronic communication between cages **(Figure 5.1, 5.3)**.[14] Upon obtaining the desired cage, we will pursue two routes to create extended network forms. The first is to grow single crystals and the second is based on azodioxide crosslinked thin films with varying degrees of cross-linking.

5.4: Results

Preliminary Studies: Ground state equilibrium geometries were calculated using DFT (BY3LP 6-31G**) in vacuum. The electron density map shows that the six nitroso moieties are the expected electron rich nodes in which the dynamic bonding is to occur **(Figure 5.3 a)**. HOMO and LUMO orbital energies were also evaluated using DFT (BY3LP 6-31G*) for a singular cage along with two cages linked through a trans azodioxide bond.[14,19] It is evident that the isolated cage itself can pass electron density between orbitals from just the initial HOMO/LUMO calculations indicating the HOMO is dispersed within the *t*-butyl phenyl acetylene linkages of the cage **(Figure 5.3 b)**, as opposed to its transfer to the six nitroso moieties in the LUMO **(Figure 5.3 c)**. It should be noted that the top three HOMOs are degenerate as are the bottom five LUMOs **(Figure 5.3 b)**. This is particularly encouraging as this behavior is commonly observed among semi-

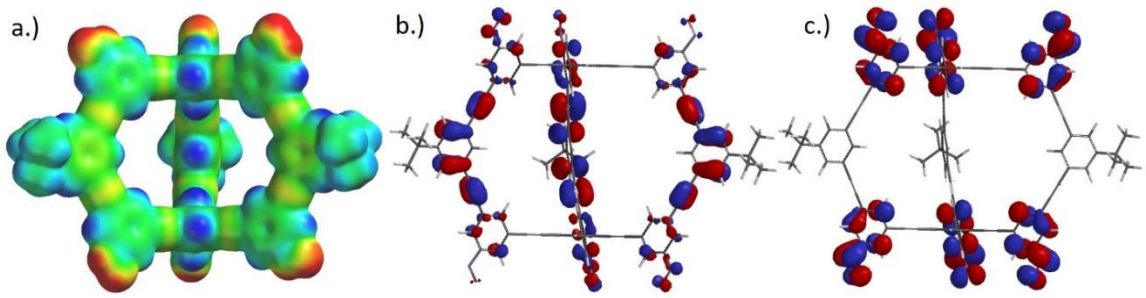

Figure 5.4 a.) Electrostatic potential map of the six nitroso-functionalized cage highlighting the charge distribution observed in the molecule (energy map: -100 kJ $mole^{-1}$ to 100 kJ $mole^{-1}$). b.) Visualization of the HOMO indicating orbital density localized on the three t-butyl-functionalized diethynylbenzene side-arms. c.) Visualization of the LUMO showing electron density overlapping of the six degenerate orbitals of the same energy. Equilibrium ground state geometries were directly calculated using DFT BY3LP level of theory with 6-31G** basis set in vacuum.

conducting materials.[20] Given that all phenyl connections are in the meta position, simple resonance arguments could be made discrediting complete conjugation. However, literature reports that in the excited state, not only does electron delocalization occur through meta-linked groups but is actually improved during electron transfer as opposed to para-linkages. The band gap for a single cage is 3.24 eV which was lowered significantly to 2.77 eV after two of the cages were connected through an azodioxide adduct, providing evidence of electronic communication via spyro-conjugation between orthogonal phenyl rings connected by acetylene linkages.[21,22]

The creation of a polyhedral bicyclic cage has been demonstrated by Moore. A new chlorine outfitted cage has been in the process of being synthesized over 26 steps following successive Sonogashira couplings, deprotections, and unmasking of aryl iodides which lead to the essential connecting of the largest pieces **(Scheme 7, 8)** that is then capable of cyclization (**Scheme 11,)**. A single modification of the starting materials previously used will replace 3-bromoaniline with 3-bromo-5-chloroaniline. The chloride will provide the site for introduction of the nitroso-group as well as other desired

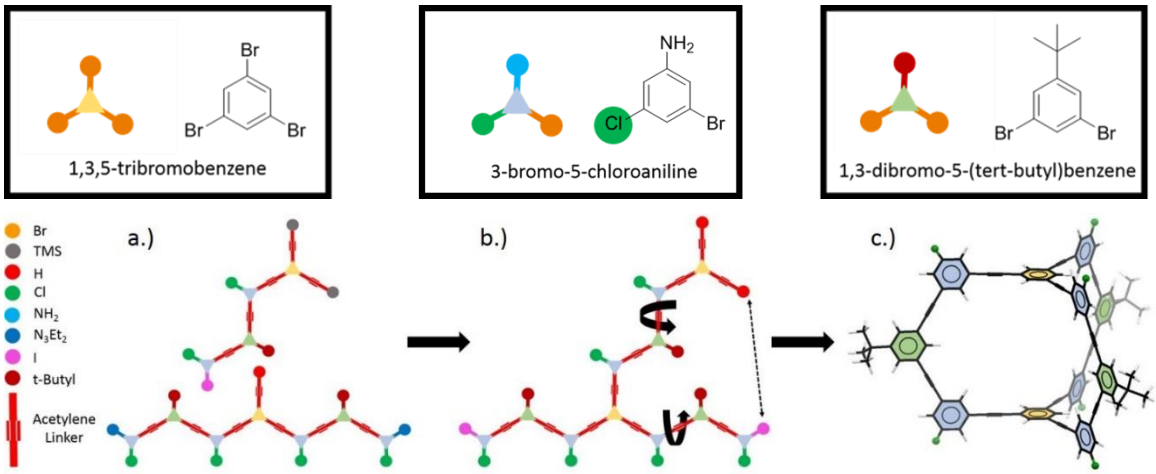

Scheme 5.2: Depiction of the last five steps in the synthesis of the chlorine outfitted cage. a.) Connecting the last two branches. b.) Showing how sigma bonds are capable of rotating to allow cyclization to occur. c.) The chlorine outfitted bicyclic cage product. Blue, green and beige phenyl rings represent the three different starting materials.

functionality. While this chloride is ideal for introduction of the prerequisite amine it is expected to be inert to the Sonogashira couplings used to assemble the cage framework as well as when "unmasking" the aryl iodide from the 3,3-diethyltyriazine protecting groups.[23] In fact, this small change in design of the cage is predicted to improve overall activity, selectivity and yields observed throughout the synthesis while directing the six unreacted chlorine atoms to symmetrically face outward from the cage which is imperative for the azodioxide crosslinking to take place **(Figure 4c)**[14,19].

Once the new cage derivative is synthesized, the Wuest protocol will be used to convert the chlorides to nitroso-groups capable of dynamic bonding to form 3D cross-linked conjugated single crystals. Interestingly, this approach has also demonstrated the ability to grow single crystals homogenous in size.[14,19]

5.5: Discussion

All derivatives created, depending on how many phenyl rings were connected by

ethynyl linkers range from oils to more viscous products based on in how many phenyl rings were connected in a chain. Compounds 1, 3, 4, and 6 were all oils that were very fluid in nature. The colors did range in which C1 and C3 were colorless, and C4 and C6 ranged pale yellow to red depending on how pure they were. C7 was also very fluid but a reddish purple while C2 had a slight hint of pale green but was more viscous like an oil due to the extra trimethylsilylacetylene moiety attached when compared to C1. When it came to connecting the compounds to form derivatives in which more than one phenyl ring were linked together, products became much more viscous the larger the product became. For instance, B0 was green and a very thick oil and B1 and B1D were like amorphous wax or like taffy. B2 and B3 were amorphous solids in which B2 was yellow and B3 was orange. So far, B2 and B3 have been synthesized. For instance, what we have learned is as follows. Every reaction seemed to have a different process and finesse, but each knowledge about purifying each derivative has been attained. Compared to the work that took place previously **(Chapters 2-4)**, this was all a completely new set of syntheses. The one drawback of all these derivatives, whether called compounds or branches, is that none of them were able to be crystallized which would have been very helpful for isolation. In fact, it seems the longer the derivatives became, the less chance there was for crystallization due to the number of conformations the branches may have that ranges on how many connected phenyl rings there are. Toward the end of this chapter, there is a new reticular design for the for the creation of the cage that hopefully will significantly shorten the number of reactions and also force new derivatives, not yet discussed, to have higher symmetry in which would allow crystallization to occur. This is

expected to be useful, because from an already common knowledge fact in chemistry, compounds that are the same in conformation crystallize with more ease.

5.5.2: Synthetic Issues that have been Resolved

Diethyltriazene Reaction

What was expected to be one of the easier reactions was the reactions of 3-bromo-5-chloroaniline into C6 in which the aniline was undergoes a Sandmeyer diazonium intermediate to the end as a diethyltriazene functional group upon the addition of diethyl amine and sodium carbonate. The problematic issue that occurred was in the first step when 6M hydrochloric acid was added to the starting material while dissolved in acetonitrile. The reactant immediately precipitated as a slurry in which the stir bar was not able to continue. Solvent after solvent was exchanged and it was found that even the starting material would only dissolve in acetonitrile and the slurry in nothing. It was finally determined that the slurry was caused by the protonation of aniline and that if a wider stir bar was used it would have enough angular momentum to continue stirring within the slurry. Once the aqueous sodium nitrite solution was added dropwise, the slurry immediately went directly back into solution.[18]

3-bromo-5-ethynyl t-butylbenzene

As it turns out, 1,3,5 tribromobenzene and C3 travels through a silica gel column at almost the exact same rate. Even more problematic is that 1,3,5-tribromobenzene is barely visible in the UV wavelength when performing TLC. This meant that effort when spotting each test tube in a grid could end up with a researcher using TLC as evidence that

it was pure but when all tubes were added together and isolated with rotary evaporation, the NMR showed that there was still starting material. It also did not help that the electron donation of the t-butyl group was not favorable for the reaction. With that being said, there was a solution that came in the form of two new changes.[18,23]

The first was intentionally "short changing" the yield in the understanding that more would still be isolated as pure product and for almost every reaction that takes place for this project it is important because the amount of side products created when not pure would make larger derivative side products, further increasing difficult in isolation. The first solution found was to add 1.2-1.4 molar equivalents of trimethylsilyl acetylene instead of just one which accounted for terminal acetylene homocoupling but also and intentionally created two products instead of one. This ensured that virtually all starting material had reacted in which in which 3,5-dibromo t-butyl benzene became monosubstituted or disubstituted. It turns out that that this intentional "sabotage" was highly effective because when performing flash chromatography in hexanes (an already an incredibly nonpolar solvent), while the starting material and monosubstituted traveled virtually at the same speed, the mono and disubstituted did not. Therefore, isolating pure C3 came in higher yield and in less time. The second resolution was not trusting UV TLC for the test tubes blotted when the first rows showed to have absorption. For the most part none of the rows were trusted by TLC. Instead, NMR analysis-was performed on test tubes, in which each isolated with rotary evaporation in sets of two or three. The reason NMR was used is because it is a quantitative absolute answer instead of the qualitative form of thin layer chromatography.

Diethyltriazene Isolation

This did not become a pertinent issue that needed to be resolved until derivatives became larger because every bit of product lost from isolation came with a tax in the form of the number of reactions it took to create along with how much in monetary amount it cost fiscally and physically. It was not even fully understood as a correlative issue until 800 mg of Branch Two that already seemed mostly pure from NMR spectra, still had impure residual and since B2 takes fourteen reactions as a predecessor, it is incredibly problematic to have it lost after flash chromatography. With the use of chemical intuition and graduate student soul search, eventually there was a correlation in which the derivatives that had a diethyltriazene functionality always seemed to be less in yield and the yield became lower the larger the derivative was in size. After speaking with three professors, it was decided that considering that diethyltriazene has three lone pairs, the it must be binding directly to the silica gel because its affinity as a Lewis acid. This was then majorly corrected by the silica gel in a column with the solvent intended for use and a small concentration of triethyl amine (much like the precursor reactant causing our recent issues). Triethyl amine was used instead of other amine choices because it had commonality with diethyl triazene structure that was the issue. This treatment was then purged with diethyl amine free solvent in the expectation that it would rid any excess and all Lewis acid parts of the gel surface area would already be coordinated with.

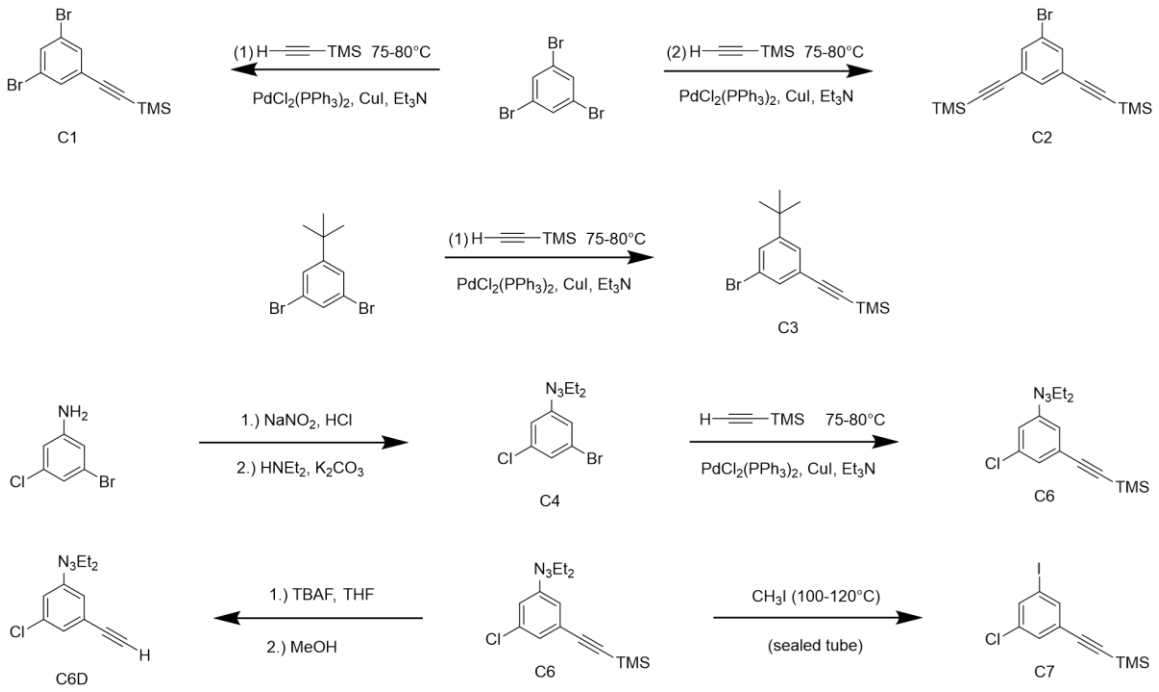

Scheme 5.3: Using three starting materials: 1,3,5-tribromobenzene, 1,3-dibromotbutylbenzene, and 3-bromo-5-chloroaniline, the derivatives needed (compounds 1-4 and 1-7) to be synthesized together can be formed. The only modified compound from the cage when created in 1992 is the chlorine added to 3-bromoaniline to which we are using 3-bromo-5chloroaniline.

Unmasking of Aryl Iodide

When following procedure from literature to unmask the aryl iodide from its diethyltriazene precursor, only two to six hours were needed for the reaction to come to completion.[24] A pressure tube needed to be charged with diethyl triazene and iodomethane and upon being sealed, it was heated to 120°C and stirred. The issue, now resolved, was that the reaction eventually needed to be left running over a weekend to finish to completion. This was not so much a problem of product purity but considered as time wasted. Finally, it was noticed that though the base of the tube with iodomethane and the diethyltriazene derivative was stirring was stirring, and both the solvent line within the tube and the solvent line of the silica oil used for heating were equal, the tube

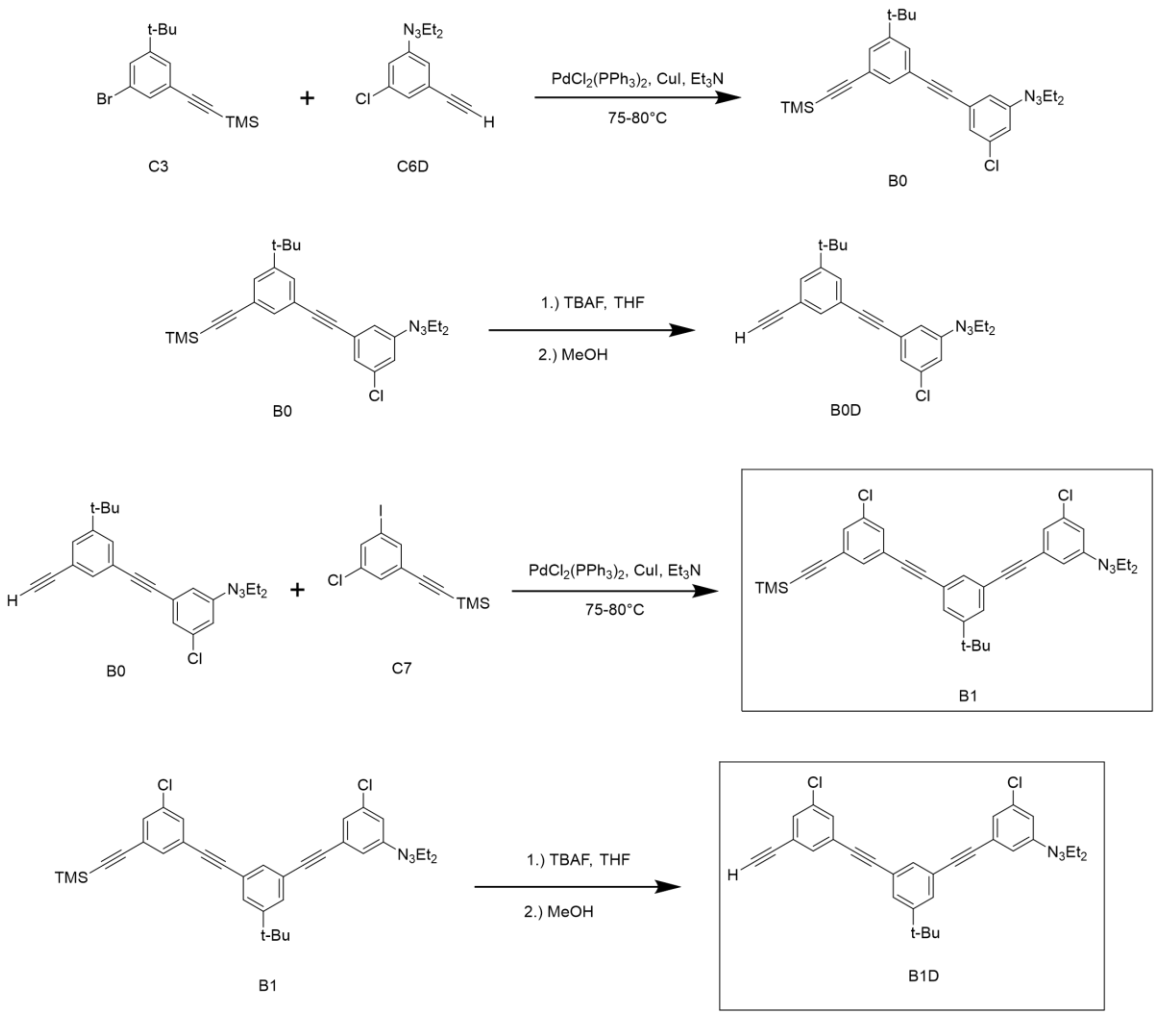

Scheme 5.4: With the derivatives made, they will be reacted with one another to make Branch Zero (B0), Branch 1 (B1), And Branch One Deprotected (B1D). Highlighted in squares are the materials needed to make Branch Two and Three.

seemed to be refluxing at the top. If the idea of a sealed tube is to create high pressures and a reflux can be seen, it would mean that the tube technically was potentially not getting to the pressure level that is possibly needed for the kinetics of the reaction to occur at the same speed as seen in literature. Therefore, the empty head space that existed in the tube had too much volume/height and was being cooled down by the environment and allowing the reflux. The solution to speed up the reaction kinetics was simply to use a smaller tube with a height of four inches instead of eight or ten. It was

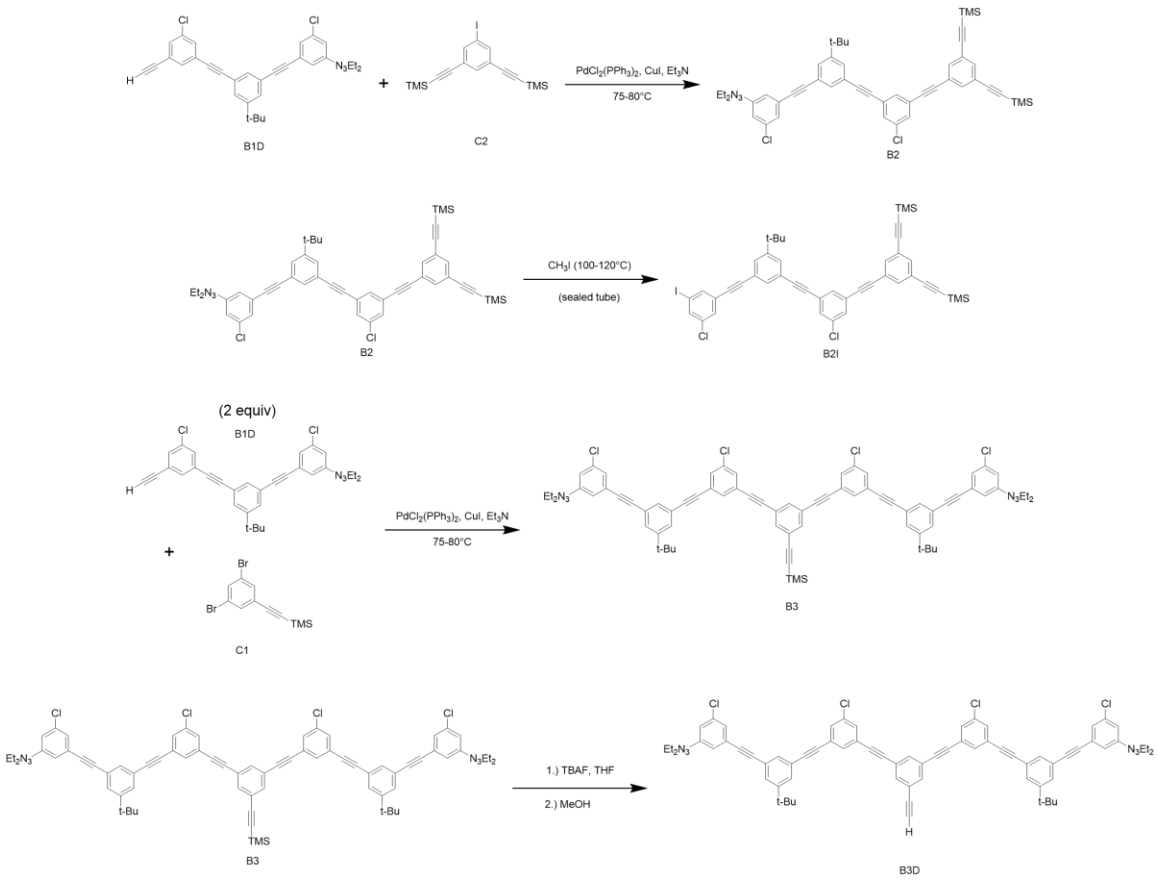

Scheme 5.5: Full synthesis scheme to create Branch 2 (B2) and Branch 3 (B3) from Branch 1 and Branch 1 Deprotected derivatives.

clear that this small change was getting to a much higher pressure than previously because once the reflux climbed to the top of the tube, the pressure kept building and soon there was no reflux occurring and the reaction barely came to a boil. Once this had taken place, the reaction completed based on the procedure used.

Glaser Coupling

Even when Sonogashira coupling reactants had been in reduced pressure overnight, triethyl amine had freshly been distilled, and a freeze pump was repeated three times and the reaction was started under a sealed nitrogen atmosphere,

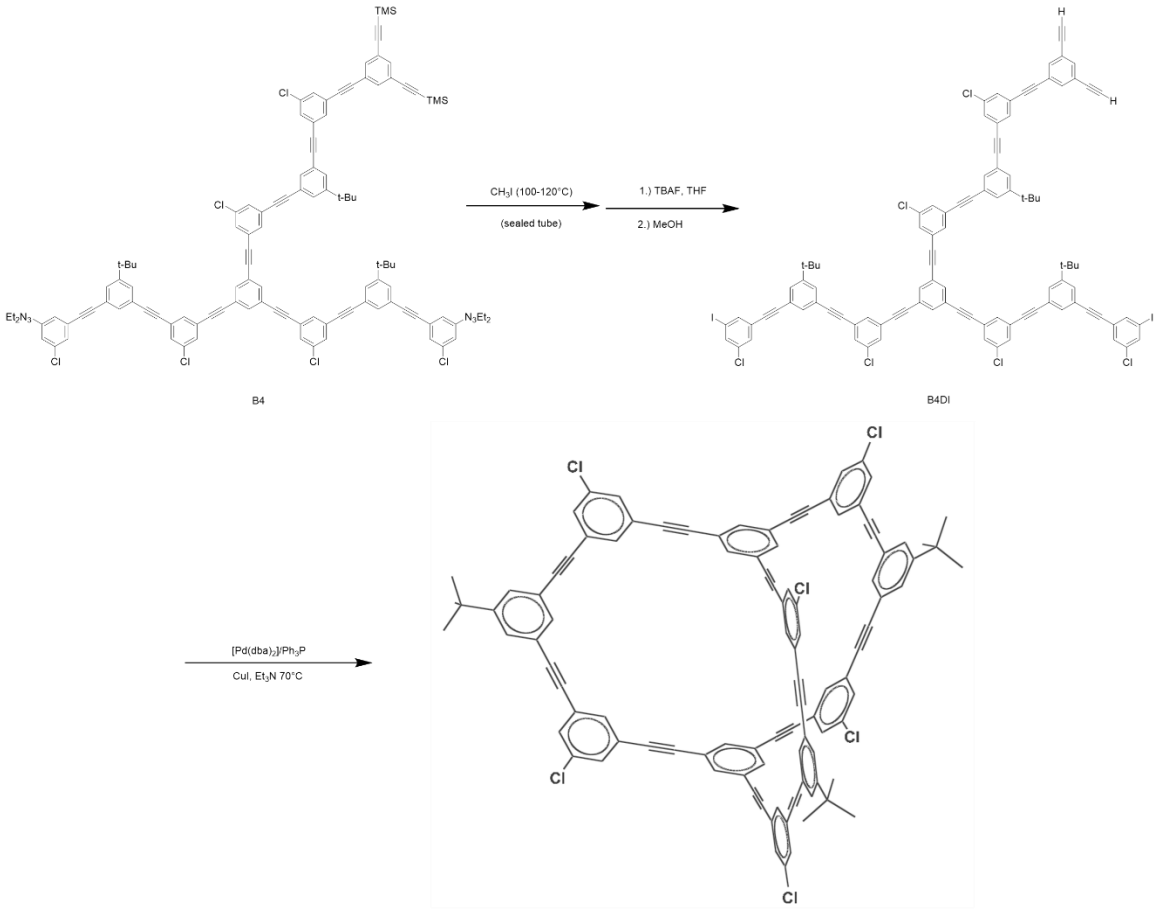

Scheme 5.6: Synthetic scheme of the bicyclic cage from Branch 1 and Branch 2 derivatives.

homocoupling of terminal acetylenes would still occur.[25] This became problematic in the sense that as the compound became larger, it meant that more and more reactions had taken place previously to get to that point. When deprotecting these branches for an additional coupling to get to the next product, homocoupling would still occur in which two of the branches would couple with one another as opposed to heterocoupling with the new derivative to extend the branch to its next form. This also made isolation via flash chromatography much more tedious to perform. Later in this chapter, a new reticular synthetic design to synthesize the cage which should make this problem negligible significantly shorten the number of reactions needed. The bicyclic nano-

scaffold cage synthesis consists of four reactions done in a repeated manner. These reactions are as follows: Sonogashira coupling, deprotecting a trimethylsilyl group from acetylene, transforming aniline to diethyltriazene, and unmasking diethyltriazene into a convenient aryl iodide. This may be received as a task when viewed as just four reactions but the number of total reactions was very extensive **(Scheme 8, 9, 10)**. The original design by Moore was very clever to which as one acetylene was deprotected and a Sonogashira coupling was then performed, an aryl iodide could be unmasked from the diethyl triazine functionality. This conveniently yielded a highly reactive aryl halide to be coupled with the next derivative which shows that the diethyltriazene moiety was an effective mask during the previous syntheses that would not have worked if a halide had been in the same location.[18]

5.5.4: Reaction Schemes Followed to Synthesize the Cage

5.6: Experimental

General Sonogashira Coupling Procedure: 5-trimethylsilylacetynyl-1,3-dibromobenzene

A Schlenk tube was charged with 1,3,5-tribromobenzene (2.00 g, 6.353 mmol), copper iodide (0.1210 g, 0.635 mmol), and bis(triphenylphosphine)palladium (II) chloride (0.2323 g, 0.314 mmol) followed by distilled triethyl amine (32 mL), benzene (9.2 mL), and trimethylsilyl acetylene (1.1 mL, 7.624 mmol). Oxygen was removed via freeze, pump, thaw which was then performed three times and replaced with a nitrogen atmosphere.

Acetylene derivatives containing at least one phenyl ring would undergo a separate freeze, pump, thaw within addition funnel to be added dropwise to which the

benzene equivalent would be the solvent used. The reaction was heated between 75-80 °C and stirred for 48 hours. Once the reaction had completed, most of the triethyl amine benzene were allowed to evaporate from the mixture. The remaining solution was then purified via silica plug to remove ammonium salts and catalyst with hexanes. After removal of solvent by rotary evaporation the solution was then purified by column chromatography, using hexanes as the eluent. The resulting product was a clear oil (1.76 g, 83 %)

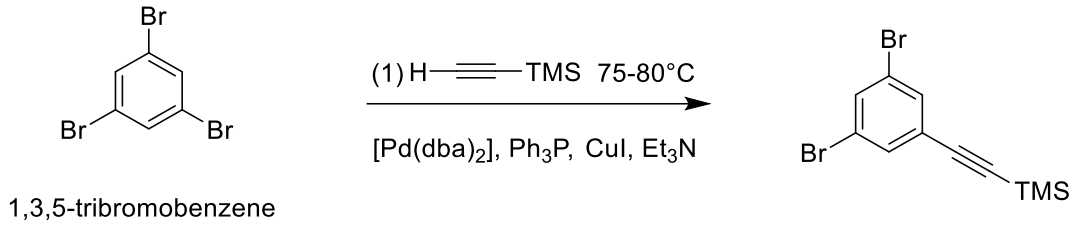

1,3,5-tribromobenzene

Scheme 5.7: Compound 1

^{1}H NMR (300 MHz, CHCl3): δ 7.6178 (t, J =1.676 Hz, 1H), 7.5434 (d, J=0.809 Hz, 2H), 0.2500 (s, 9H).

All solvent and water peaks are omitted.

Compound 2 (C2):

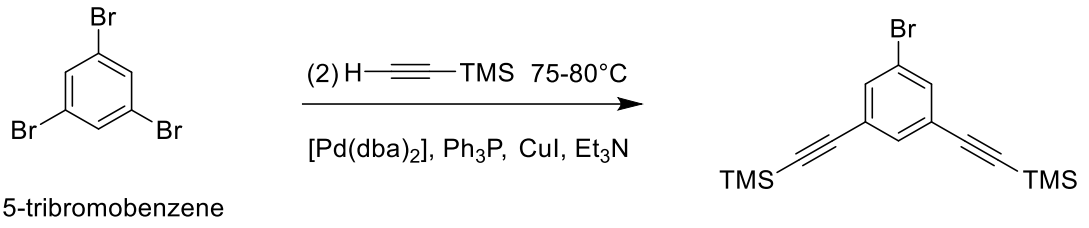

1,3,5-tribromobenzene

Scheme 5.8: Compound 2

^{1}H NMR (400 MHz, CDCl3): δ 7.4697-7.4819 (m, 2H), 7.3433 (t, J=1.414 Hz, 1H), 3.7573 (q, J= 10.664 Hz, 4H), 1.2618 (t, J=5.587 Hz, 6H), 0.2425 (s, 18H). All solvent and water peaks are omitted.

Compound 3 (C3):

Compound 3 was prepared by a Sonogashira coupling of 3,5-dibromo t-butyl benzene and trimethylsilylacetylene. (yield 37.67%)

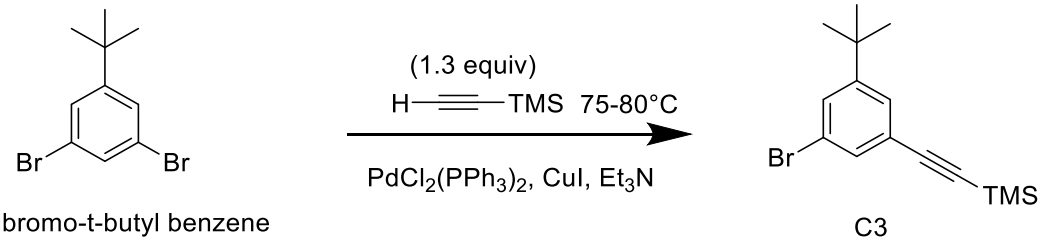

3,5-dibromo-t-butyl benzene

C3

Scheme 5.9: Compound 3

^{1}H NMR (400 MHz, CDCl3): δ 7.4379-7.4668 (m, 2H), 7.4040 (t, J=1.421 Hz, 1H), 1.3207 (s, 9H), 0.2597 (s, 9H). All solvent and water peaks are omitted.

General Diethyltriazene Synthesis Procedure: 1-(3-bromo-5-chlorophenyl)-3,3-diethyltriaz-1-ene (C4)

A boiling flask was charged with acetonitrile (60 mL) and 3-bromo-5-chloroaniline

(3.00g, 14.6 mmol) with magnetic stirring. 6M HCl (28 mL) was added slowly with vigorous stirring, then the flask was placed in a salt and ice bath. Sodium nitrite (3.26g, 47.3 mmol) was dissolved in water (4 mL) and added drop wise to the flask, maintaining a temperature < 5 ºC. The solution was left to stir for 30 min before being transferred into an ice jacketed addition funnel. A boiling flask was charged with potassium carbonate (26.2g, 189 mmol), water (13 mL), and diethylamine (12 mL, 116 mmol). The round bottom was placed in a salt and ice bath. The addition funnel solution was added drop wise to the flask with vigorous stirring. After 30 minutes the flask was removed from the ice bath and allowed to warm to room temperature. The organic layer was then isolated via separation funnel from which the aqueous layer was washed with hexanes. The hexanes and organic layer were combined and concentrated by rotary evaporation. The solution was then extracted in diethyl ether washed deionized water and salt brine before being treated with anhydrous magnesium sulfate, filtered, concentrated, and purified by silica plug, yielding **C4**. The product was a translucent yellow oil (3.8975g, 92.32%).

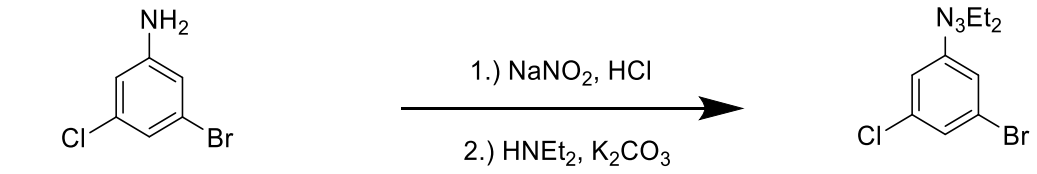

3-bromo-5-chloroaniline C4

Scheme 5.10: Compound 4

^{1}H NMR (400 MHz, CDCl3): δ 7.4663 (t, J=1.674, 1 H), 7.3486 (t, J=1.650 Hz, 1 H), 7.2327 (t, J=1.815 Hz, 1H), 3.7731 (q, J=10.902 Hz, 4H), 1.2292-1.3189 (m, 6H). All solvent and water peaks are omitted.

Compound 6 (C6):

Compound 6 was prepared by a Sonogashira coupling of Compound 4 and trimethylsilylacetylene. (yield 94.37%)

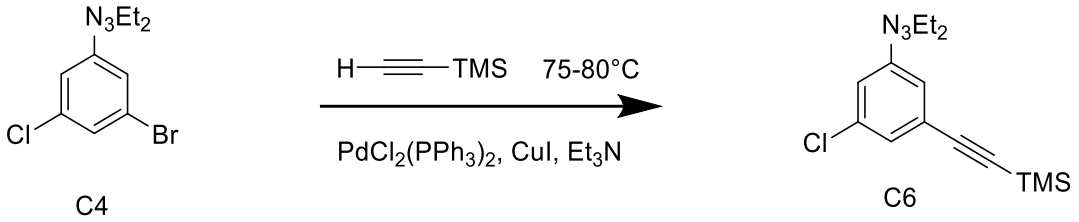

Scheme 5.11: Compound 6

^{1}H NMR (300 MHz, CDCl3): δ 7.3759-7.40832 (m, 2H), 7.1950 (t, J=1.701 Hz, 1H), 3.7672 (q, J= 10.674 Hz, 4H), 1.2515-1.2977 (m, 6H), 0.2525 (s, 9H). All solvent and water peaks are omitted.

General Procedure for Deprotection of Trimethylsilylacetylene: Compound 6 D

A round bottom flask was charged with Compound 6 (1.00 g, 3.25 mmol) and tetrahydrofuran (17 mL) and stirred. Once dissolved, 1M tetrabutylammonium fluoride (4 mL) was added drop wise to the flask and then left to stir for 30 minutes. Large excess of methanol was then added to quickly quench the reaction and rotary evaporation was used to remove tetrahydrofuran and methanol from the crude product to ensure that it was not miscible in water. The crude deprotected acetylene derivative was isolated via separation funnel using diethyl ether and deionized water. Once the organic layer had been dried with a salt brine wash followed by treatment with magnesium sulfate, it was concentrated down using rotary evaporation. This yielded a crude brown product that

became paler in color after undergoing vacuum filtration through a silica plugged frit. The resulting product was a pale-yellow oil (0.51 g, 92.20%).

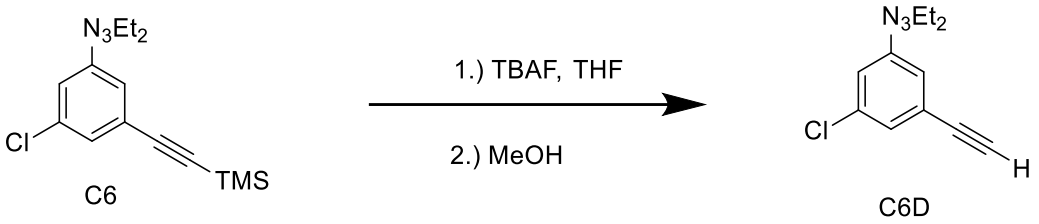

Scheme 5.12: Compound 6 Deprotected

1H NMR (300 MHz, CDCl3): δ 7.4109-7.4343 (m, 2H), 7.2129 (t, J=1.436 Hz, 1H), 3.7722 (q, J=10.574 Hz, 4H), 3.0782 (s, 1H), 1.2522-1.3666 (m, 6H). All solvent and water peaks omitted.

General Procedure for Unmasking of Aryl Iodide: Compound 7

A sealed tube was charged with Compound 6 (1.022 g, 3.32 mmol) with excess iodomethane and a stir bar. The sealed tube was stirred overnight at 120 °C. After 12+ hours the solution was much darker and a solid had developed. The excess solvent was then removed through rotary evaporation and the crude oil was isolated via separatory funnel with diethyl ether, washed with aqueous sodium thiosulfate, and dried with a salt brine before being treated with anhydrous magnesium sulfate, filtered and concentrated via rotary evaporation. The resultant product was then purified through a silica plug with hexanes and concentrated via rotary evaporation, resulting with a pale-yellow oil (0.92 g, 82.56%).

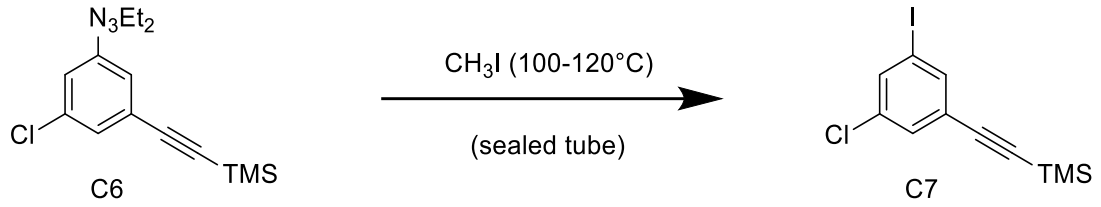

Scheme 5.13: Compound 7

^{1}H NMR (300 MHz, CDCl3): δ 7.6969 (s, 1H), 7.6545 (s, 1H), 7.4122 (s, 1H), 0.2463 (s, 9H). All solventand water peaks are omitted.

Branch Zero

Branch Zero was prepared by a Sonogashira coupling of Compound 3 and Compound 6 Deprotected (yield 57.03%).

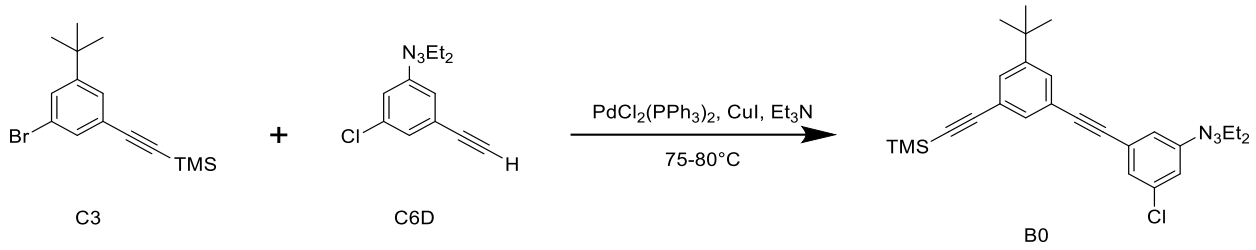

Scheme 5.14: Branch Zero

^{1}H NMR (400 MHz, CD2Cl2): δ 7.5329 (t, J=1.647 Hz, 1H),7.4734 (t, J=1.694 Hz, 1H),7.4503 (t, J=1.588 Hz, 1H), 7.4382 (t, J=1.429 Hz, 1H), 7.3995 (t, J=1.906 Hz, 1H), 7.2383 (t, J= 1.588 Hz, 1H), 3.7792 (q, J=9.838 Hz, 4H), 1.3057-1.3618 (m, 15H), 0.2538 (s, 9H). All solvent and water peaks are omitted.

Branch Zero Deprotected (B0D):

Branch Zero Deprotected was prepared by deprotection of trimethylsilylacetylene (yield 57.03%).

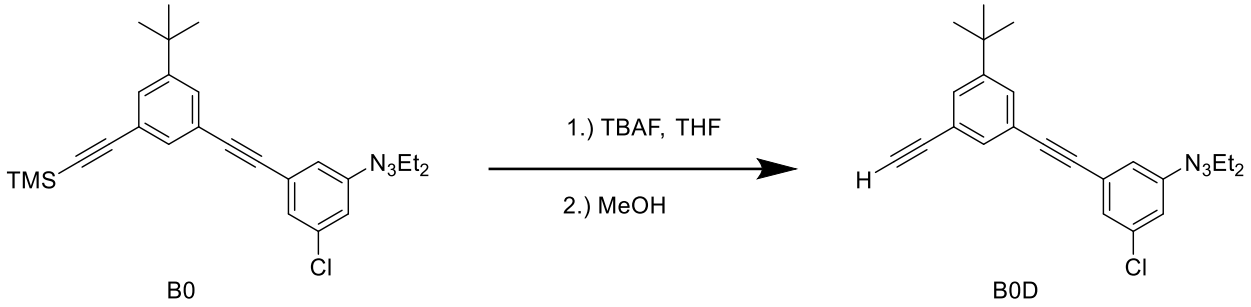

Scheme 5.15: Branch Zero Deprotected

^{1}H NMR (300 MHz, CD2Cl2): δ 7.5817 (t, J= 1.480 Hz, 1H), 7.5285 (t, J=1.563 Hz, 1H), 7.4671-7.4869 (m, 2H), 7.4161 (t, J=1.837 Hz, 1H), 7.2584 (t, J=1.515 Hz, 1H), 3.7821 (q, J= 10.521 Hz, 4H), 3.1495(s, 1H), 1.2340-1.3628 (m, 15H). All solvent and water peaks are omitted.

Branch 1 (B1):

Branch One was prepared by a Sonogashira coupling of Branch Zero Deprotected and Compound 7 (yield 82.44%).

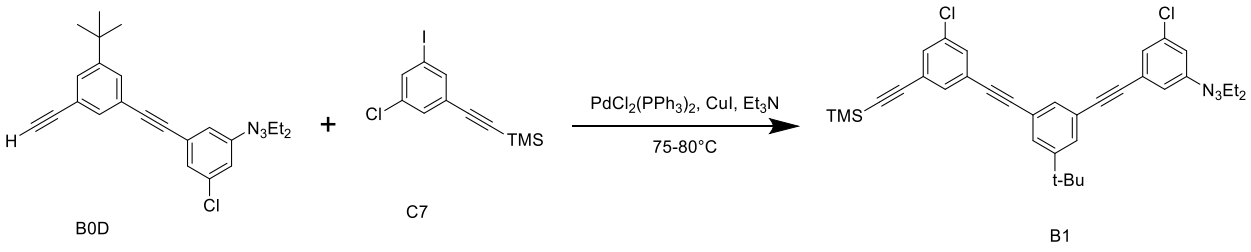

Scheme 5.16: Branch 1

^{1}H NMR (400 MHz, CD2Cl2): δ 7.5865 (t, J=1.572 Hz, 1H), 7.5608 (t, J=1.708 Hz, 1H), 7.5125-7.5315 (m, 2H), 7.4906 (t, J=1.504 Hz, 1H), 7.4728 (t, J=1.551 Hz, 1H), 7.4074-

7.4243 (m, 2H), 7.2614 (t, J=1.583 Hz, 1H), 3.7835 (q, J=9.990 Hz, 4H), 1.1935-1.3521 (m, 15H), 0.2558 (s, 9H). All solvent and

water peaks are omitted.

Branch 1 Deprotected (B1D):

Branch 1 Deprotected was prepared by deprotection of trimethylsilylacetylene (yield 88.10%).

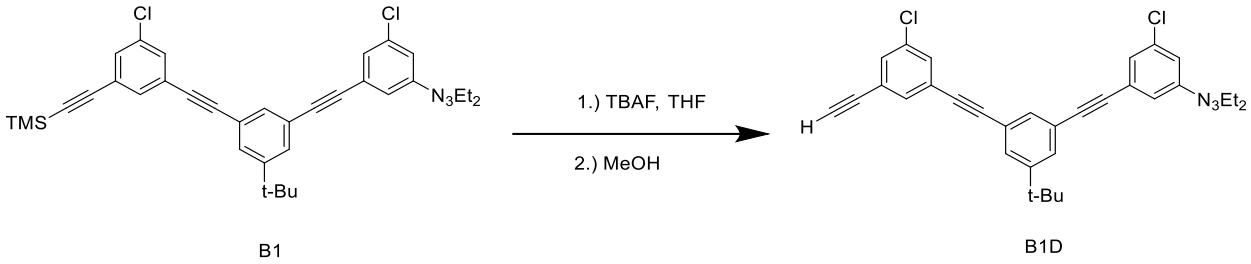

B1 B1D

Scheme 5.17 Branch 1 Deprotected

^{1}H NMR (300 MHz, CD2Cl2): δ 7.5799-7.6096 (m, 1H), 7.5606-7.5721 (m, 2H), 7.5177-7.5479 (m, 2H), 7.4541-7.4804 (m, 2H), 7.4113 (t, J=1.924 Hz, 1H), 3.7846 (q, J=10.250 Hz, 4H), 3.2308 (s, 1H),

Branch 2 (B2):

Branch 2 was prepared by a Sonogashira coupling of Branch 1 Deprotected and Compound 2 (yield 65.40%).

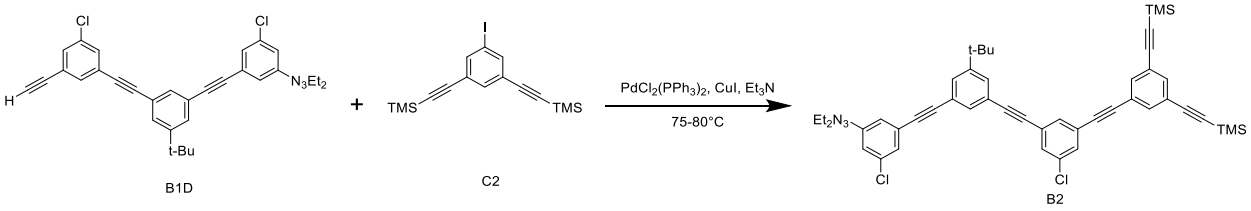

Scheme 5.18: Branch 2

^{1}H NMR (400 MHz, CD2Cl2): δ 7.5808-7.6095 (m, 3H), 7.5634 (d, J=0.432 Hz, 2H), 7.5231-7.5346 (m,3H), 7.4707-7.4964 (m, 2H), 7.4121 (t, J=1.838 Hz, 1H), 7.2642 (t, J=1.526 Hz, 1H), 3.7841 (q, J= 8.511Hz, 4H), 1.2184-1.3587 (m, 15H), 0.2492 (s, 18H). All solvent and water peaks are omitted.

Branch 3 (B3):

Branch 3 was prepared by a Sonogashira coupling of Branch 1 Deprotected and Compound 2 (yield 82.85%).

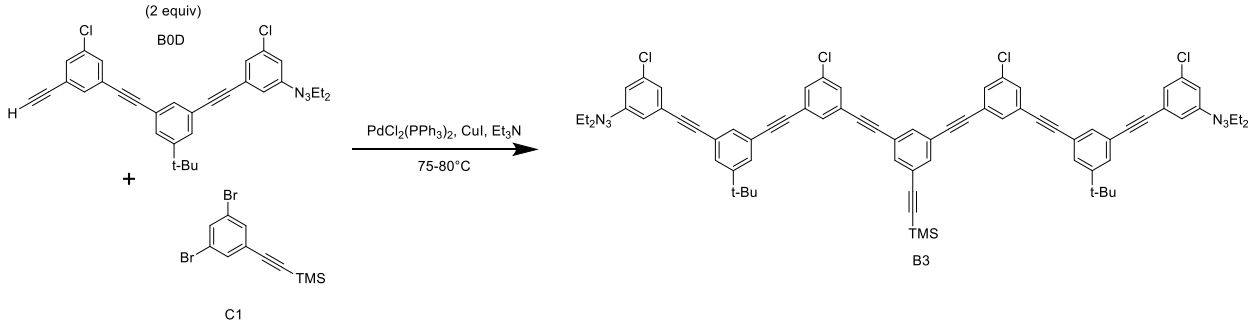

Scheme 5.19 Branch 3

^{1}H NMR (400 MHz, CD2Cl2): δ 7.6623-7.6693 (m, 1H), 7.6249 (d, J=0.654 Hz, 3H), 7.5827-7.5934 (m,5H), 7.5155-7.5495 (m, 6H), 7.4722 (t, J=1.661 Hz, 2H), 7.4086 (t, J=1.957 Hz, 2H), 7.2614 (t, J=1.763Hz, 2H), 3.7694-3.7915 (m, 8H), 1.3561 (s, 18H), 1.2124-1.2859 (m, 12H), 0.2288-0.2663 (m, 9H). All solvent and water peaks are omitted.

5.6: Future Reticular Synthetics Design

Throughout this project we have been trying to think of new ways to create the bicyclic cage in a manner that would allow better yields and less reactions. There was one pivotal step that made the reticular design that we feel has recently been solved. With the use of derivatives already made, we can move forward with this new method. With a new compound, 1,3,5-diiodobenzene, we plan to couple three C6D derivatives that make a new and large tri-C6D

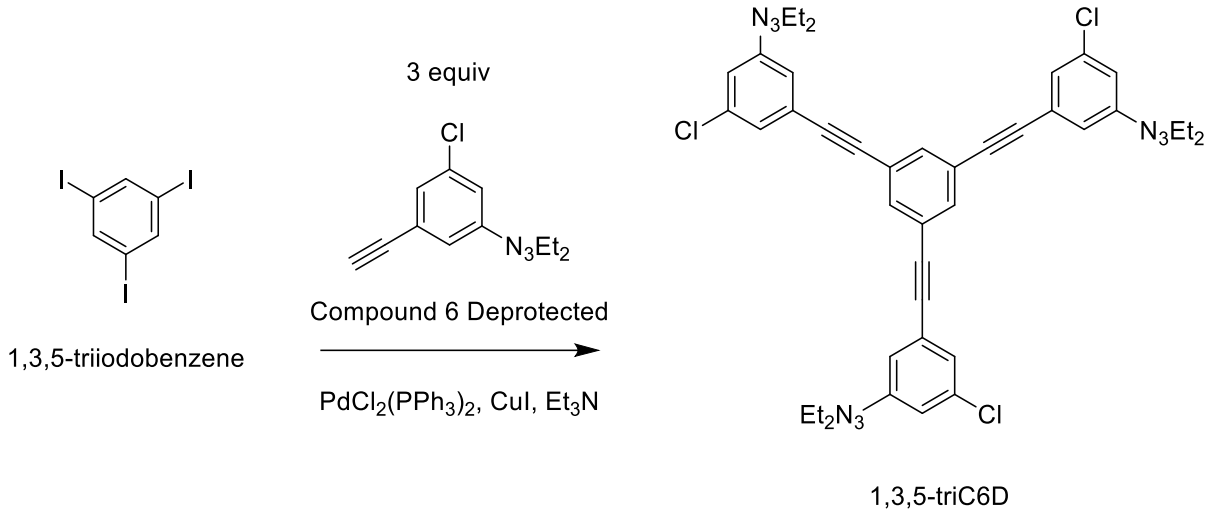

Scheme 5.20: 1,3,5-tri Compound 6D

branch. The expectation is that if we tried to react three B1D derivatives, it would have less chance of reacting due to its size. TriC6D will then have all three diethyltriazene groups unmasked to become aryl iodides (1,3,5-triC7 Branch) which are much more reactive than the bromine that C6D reacted with in the first design **(Scheme 25).**

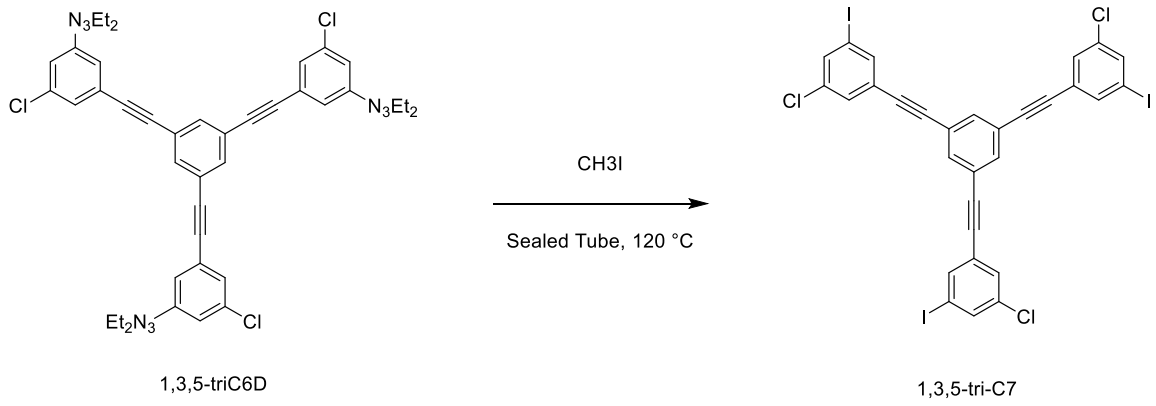

Scheme 5.201 1.3.5-trie Compound 7

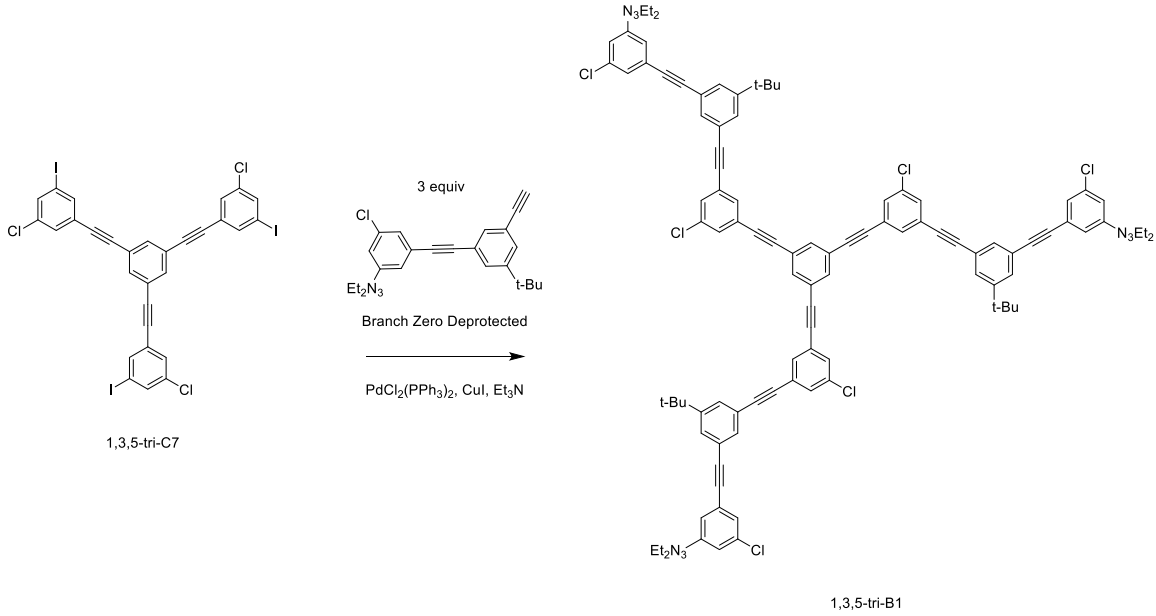

Scheme 22: 1,3,5-tri Branch 1

Three equivalents of B0D will then be couple to 1,3,5-tri-C7 which will form a new large branch (1,3,5-triB1). Because we are adding more symmetry to the compounds in this new route we expect less conformations which is expected to make crystallizing the product for isolation much more attainable. This is because the tri substituted branches would have less degrees of rotation which was not seen on branches synthesized previously.

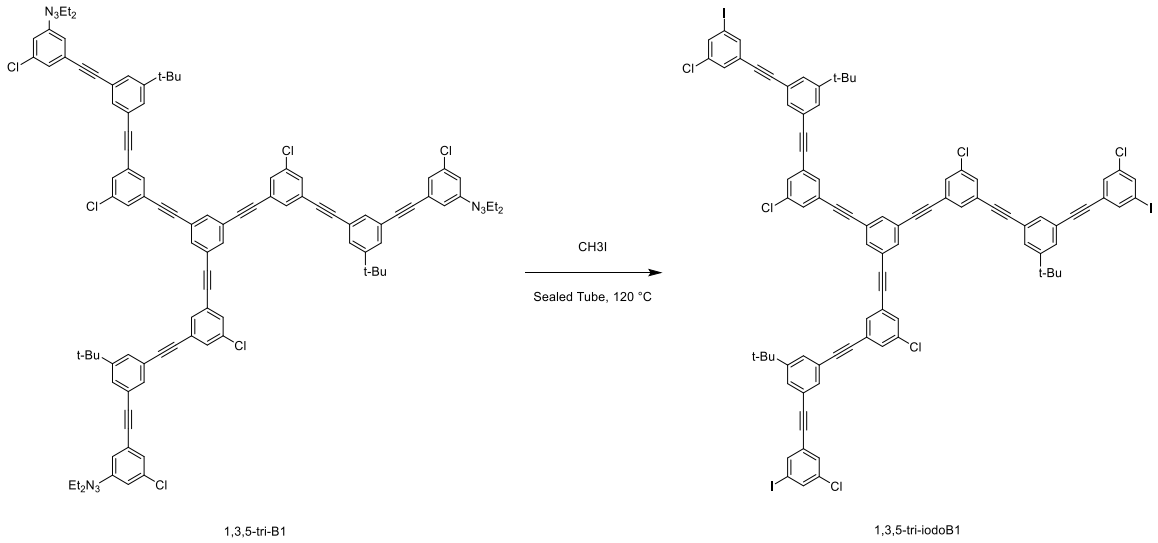

Scheme 5.23: 1,3,5-tri Iodo Branch 1

Another unmasking of three aryl iodides will occur from the three diethyltriazenes located on 1,3,5-tri-B1, a new branch will be formed, 1,3,5-triiodo-B1. It should be noted that this new reticular design that has aryl iodides on the new branches as they are made which will prevent the Glazer homocoupling that occurred previously. Because of this, the homocoupling that can occur will only be smaller derivatives which will save much on enthalpic tax of creating the bicyclic cage.

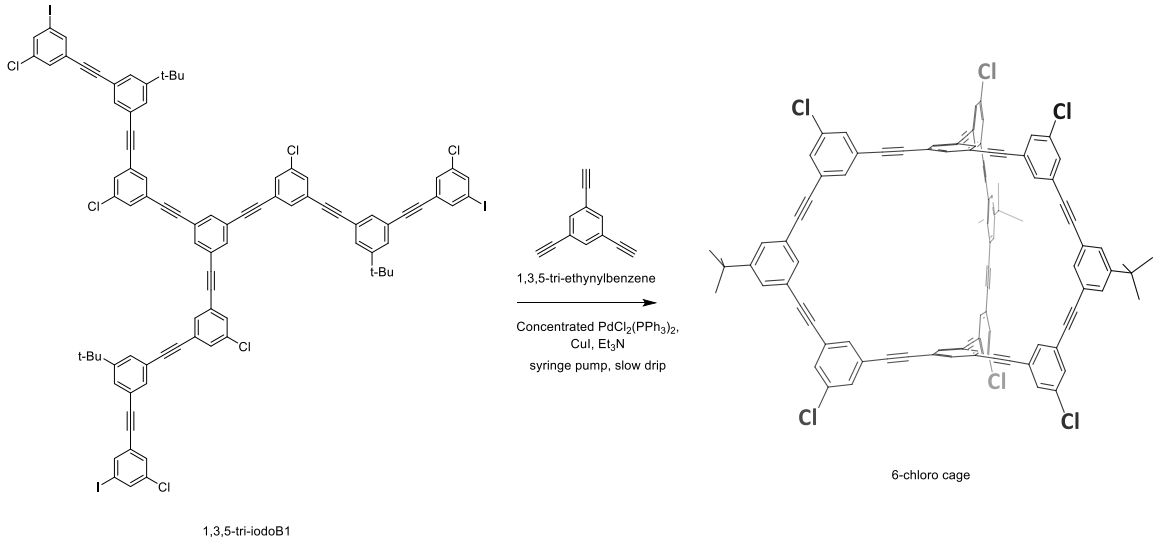

Scheme 5.24: Bicyclic Cage

Finally, a new derivative that has already been made with ease is 1,3,5-triethynylbenzene. This was where the pitfall in our new design had shortcomings when trying to create it in the past because controlling the reaction becomes questionable, but if done in the proper conditions it could work. By coupling 1,3,5-triiodoB1 with 1,3,5-triethynl benzene the question that came to mind is how would the coupling would be controlled. The answer came later with a new synthetic method. If each were added dropwise into a solution with the same Sonogashira coupling method used throughout except that both catalysts would be in much higher percentage and the ratio of triethylamine was larger when compared to the original one, then it is possible to cyclize the cage faster. Under these new changes in condition, it is expected that the 1,3,5-triethynylbenzene derivative will only couple one of its terminal acetylenes when only one aryl iodide the 1,3,5-triiodoB1. When this occurs, it will essentially create the last branch needed from the original reticular synthesis design which will already be in the reactive environment that allows the double cyclization and continue forward into becoming the bicyclic cage we plan to create.

5.7: References

(1) Fracaroli, A. M.; Siman, P.; Nagib, D. A.; Suzuki, M.; Furukawa, H.; Toste, F. D.; Yaghi, O. M. Seven Post-Synthetic Covalent Reactions in Tandem Leading to Enzyme-like Complexity within Metal–Organic Framework Crystals. *Journal of the American Chemical Society* **2016**, *138* (27), 8352–8355. https://doi.org/10.1021/jacs.6b04204.

(2) Feng, X.; Ding, X.; Jiang, D. Covalent Organic Frameworks. *Chemical Society Reviews* **2012**, *41* (18), 6010–6022. https://doi.org/10.1039/C2CS35157A.

(3) Tilford, R. W.; Mugavero III, S. J.; Pellechia, P. J.; Lavigne, J. J. Tailoring Microporosity in Covalent Organic Frameworks. *Advanced Materials* **2008**, *20* (14), 2741–2746. https://doi.org/https://doi.org/10.1002/adma.200800030.

(4) Zhang, Y.-B.; Su, J.; Furukawa, H.; Yun, Y.; Gándara, F.; Duong, A.; Zou, X.; Yaghi, O. M. Single-Crystal Structure of a Covalent Organic Framework. *Journal of the American Chemical Society* **2013**, *135* (44), 16336–16339. https://doi.org/10.1021/ja409033p.

(5) Kim, S.; Choi, H. C. Recent Advances in Covalent Organic Frameworks for Molecule-Based Two-Dimensional Materials. *American Chemical Society Omega* **2020**, *5* (2), 948–958. https://doi.org/10.1021/acsomega.9b03549.

(6) AU - Karagiaridi, O.; AU - Bury, W.; AU - Sarjeant, A. A.; AU - Hupp, J. T.; AU - Farha, O. K. Synthesis and Characterization of Functionalized Metal-Organic Frameworks. *JoVE* **2014**, No. 91, e52094–e52094. https://doi.org/doi:10.3791/52094.

(7) Kwon, E. H.; Kim, M.; Lee, C. Y.; Kim, M.; Park, Y. D. Metal–Organic-Framework-Decorated Carbon Nanofibers with Enhanced Gas Sensitivity When Incorporated into an Organic Semiconductor-Based Gas Sensor. *American Chemical Society Applied Materials & Interfaces* **2022**, *14* (8), 10637–10647. https://doi.org/10.1021/acsami.1c24740.

(8) Rice, A. M.; Leith, G. A.; Ejegbavwo, O. A.; Dolgopolova, E. A.; Shustova, N. B. Heterometallic Metal–Organic Frameworks (MOFs): The Advent of Improving the Energy Landscape. *American Chemical Society Energy Letters* **2019**, *4* (8), 1938–1946. https://doi.org/10.1021/acsenergylett.9b00874.

(9) Shustova, N. B.; Cozzolino, A. F.; Dincă, M. Conformational Locking by Design: Relating Strain Energy with Luminescence and Stability in Rigid Metal–Organic Frameworks. *Journal of the American Chemical Society* **2012**, *134* (48), 19596–19599. https://doi.org/10.1021/ja3103154.

(10) Yoo, H.; Millstone, J. E.; Li, S.; Jang, J.-W.; Wei, W.; Wu, J.; Schatz, G. C.; Mirkin, C. A. Core−Shell Triangular Bifrustums. *Nano Letters* **2009**, *9* (8), 3038–3041. https://doi.org/10.1021/nl901513g.

(11) Yoo, J. J.; Balakrishnan, K.; Huang, J.; Meunier, V.; Sumpter, B. G.; Srivastava, A.; Conway, M.; Mohana Reddy, A. L.; Yu, J.; Vajtai, R.; Ajayan, P. M. Ultrathin Planar Graphene Supercapacitors. *Nano Letters* **2011**, *11* (4), 1423–1427. https://doi.org/10.1021/nl200225j.

(12) Rice, A. M.; Dolgopolova, E. A.; Shustova, N. B. Fulleretic Materials: Buckyball- and Buckybowl-Based Crystalline Frameworks. *Chemistry of Materials* **2017**, *29* (17), 7054–7061. https://doi.org/10.1021/acs.chemmater.7b02245.

(13) Dunlap, J. H.; Loszko, A. F.; Flake, R. A.; Huang, Y.; Benicewicz, B. C.; Greytak, A. B. Multiply-Binding Polymeric Imidazole Ligands: Influence of Molecular Weight and Monomer Sequence on Colloidal Quantum Dot Stability. *The Journal of Physical Chemistry C* **2018**, *122* (46), 26756–26763. https://doi.org/10.1021/acs.jpcc.8b08984.

(14) Beaudoin, D.; Maris, T.; Wuest, J. D. Constructing Monocrystalline Covalent Organic Networks by Polymerization. *Nature Chemistry* **2013**, *5* (10), 830–834. https://doi.org/10.1038/nchem.1730.

(15) Wang, H.; Shao, Y.; Mei, S.; Lu, Y.; Zhang, M.; Sun, J.; Matyjaszewski, K.; Antonietti, M.; Yuan, J. Polymer-Derived Heteroatom-Doped Porous Carbon Materials. *Chemical Reviews* **2020**, *120* (17), 9363–9419. https://doi.org/10.1021/acs.chemrev.0c00080.

(16) Uribe-Romo, F. J.; Hunt, J. R.; Furukawa, H.; Klöck, C.; O'Keeffe, M.; Yaghi, O. M. A Crystalline Imine-Linked 3-D Porous Covalent Organic Framework. *Journal of the American Chemical Society* **2009**, *131* (13), 4570–4571. https://doi.org/10.1021/ja8096256.

(17) Nguyen, V.; Grünwald, M. Microscopic Origins of Poor Crystallinity in the Synthesis of Covalent Organic Framework COF-5. *Journal of the American Chemical Society* **2018**, *140* (9), 3306–3311. https://doi.org/10.1021/jacs.7b12529.

(18) Wu, Z.; Lee, S.; Moore, J. S. Synthesis of Three-Dimensional Nanoscaffolding. *Journal of the American Chemical Society* **1992**, *114* (22), 8730–8732. https://doi.org/10.1021/ja00048a073.

(19) Vancik, H.; Simunic-Meznaric, V.; Mestrovic, E.; Halasz, I. Nitrosobenzene Dimerizations as a Model System for Studying Solid-State Reaction Mechanisms. *The Journal of Organic Chemistry* **2004**, *69* (14), 4829–4834. https://doi.org/10.1021/jo049537b.

(20) Terao, J.; Tsuji, Y. New Synthetic Methods of π-Conjugated Inclusion Complexes with High Conductivity. *Journal of Inclusion Phenomena and Macrocyclic Chemistry* **2014**, *80* (3), 165–175. https://doi.org/10.1007/s10847-014-0381-y.

(21) Thompson, A. L.; Ahn, T.-S.; Thomas, K. R. J.; Thayumanavan, S.; Martínez, T. J.; Bardeen, C. J. Using Meta Conjugation To Enhance Charge Separation versus Charge Recombination in Phenylacetylene Donor−Bridge−Acceptor Complexes. *Journal of the*

American Chemical Society **2005**, *127* (47), 16348–16349. https://doi.org/10.1021/ja054543q.

(22) Bischof, P.; Gleiter, R.; Haider, R. Through-Bond Interaction of Two Mutually Perpendicular .Pi. Systems. A Comparison with Spiroconjugation. *Journal of the American Chemical Society* **1978**, *100* (4), 1036–1042. https://doi.org/10.1021/ja00472a003.

(23) Gottardo, C.; Kraft, T. M.; Hossain, M. S.; Zawada, P. v; Muchall, H. M. Linear Free-Energy Correlation Analysis of the Electronic Effects of the Substituents in the Sonogashira Coupling Reaction. *Canadian Journal of Chemistry* **2008**, *86* (5), 410–415. https://doi.org/10.1139/v08-038.

(24) Moore, J. S.; Weinstein, E. J.; Wu, Z. A Convenient Masking Group for Aryl Iodides. *Tetrahedron Letters* **1991**, *32* (22), 2465–2466. https://doi.org/https://doi.org/10.1016/S0040-4039(00)74354-1.

(25) Eglinton, G.; Galbraith, A. R. 182. Macrocyclic Acetylenic Compounds. Part I. Cyclotetradeca-1 :3-Diyne and Related Compounds. *Journal of the Chemical Society (Resumed)* **1959**, 889. https://doi.org/10.1039/jr9590000889.

CHAPTER 6: FUTURE DIRECTIONS

As the research taken place concludes, there are many parts to the projects that have been discussed that need further investigation. This is to provide insight to future graduate and undergraduate researchers.

6.1: Future CP1 Benzene Guest Studies

When it comes to CP1 made from DE1 and DPE, there is still a lot that is needed for a better understanding of the system. For instance, though the binding energy of the benzene guest with in the host polymer framework was calculated using data from TGA and DSC, it is still unknown which of the two benzene guests leaves the system first. It is known that benzene guest leaves very slowly when CP1 single crystals are placed in reduced pressure over time and even though twenty days have passed but when the single crystals are heated to 110 °C under the same conditions, the guest is removed within and hour. Further investigation should use proton NMR, carbon NMR and XRD analysis on samples placed in reduced pressure at different temperatures over time. This data could elucidate rate determining energies of benzene leaving while possibly yield information on when of the two guests leaves first. This is important because it is unknown if the guests leave at the same rate of if one must leave before another. Another route is to place CP1 single crystals in the presence of deuterated benzene. The reason

for this is because deuterium when compared to hydrogen has the ability to have a stronger non-covalent bonding affinity in a noncovalent intramolecular manner.[1] Based on past studies, deuterated benzene vapor would be able to fully replace benzene as a guest within CP1 in which new experimental data can be analyzed. It is expected that deuterated benzene will have a stronger binding affinity to the host framework due to the neutron giving it a larger molecular moment than just the proton alone. If this is the case, then it will take more energy (higher temperature) to vacate them deuterated benzene from the polymer. This could also cause one of the two guests to vacate before the other which would give evidence to which benzene guests leaves first on the original CP1. The same discussed methods discussed previously using TGA, DSC, and XRD would be used to characterize the deuterated benzene guest within CP1 as well.

6.2: Styrene Vapor SCSC Transition on CP1

As stated previously, there was an SCSC transition that occurred to which styrene solvent replaced the benzene quest within CP1 and caused slight changes to the crystal structure. CP1 crystals should also be placed in just styrene vapor to see if the same transition occurs.

6.3: The Use of Supercritical CO_2 on CP1 to Transition to VCP1 that is Capable of XRD Analysis

When CP1 is placed under reduced pressure at 110 °C, the benzene guest leaves the framework and the crystals transition to VCP1. Though PXRD shows that the product is a still highly crystalline and a new structure, the samples lose single crystallinity which is problematic because this does not allow the new transitioned structure to be analyzed

by XRD. Supercritical CO_2 has been used in literature to solve this issue in which the CO_2 can displace the benzene guest based on equilibrium.[2] Since the CO_2 so much smaller in size when compared to benzene, as it slowly is allowed to be released, it could leave the CP1 and transition to VCP1 while still staying single crystalline. If this were to occur, it would give understanding on why the CP1 transition to VCP1 is highly reversible.

6.4: In Situ Spectroscopic Study of VCP1 using ATR-IR/FTIR with Benzene Vapor

With the use of surface spectroscopy, benzene vapor can flow over VCP1 and while infrared absorption is observed. As benzene enters the VCP1 and starts the transition back to CP1, the benzene absorption peaks may narrow and even shift.[3,4] It may also show two separate peaks since the two benzene guest environments are different which was also seen in carbon NMR for CP1. If this were to occur, one peak might show up earlier than the other which could answer speculation of the transition of VCP1 to CP1 in which its questioned if one guest has to enter the framework to allow the second guest.

6.5: Develop Protocol for Synthesizing Pure Phase Macrocycle and Get Repeated PXRD After the Topochemical Transformation that Occurs when Left in Benzene Vapor for Longer Periods of Time

In order to prove whether or not macrocycle in the presence of benzene has a topochemical polymerization occur in which the red crystals turn yellow and possibly transition to CP1, protocol must be experimented with in which pure phase macrocycle crystals can be grown quickly and efficiently. It has been seen that the macrocycle can occur as phase pure when the crystals are grown in dilute conditions and also the polymer occurs when reactants are more concentrated. Other method expected to get

macrocycle as phase pure is changing the molar ratios of to DE1 and DPE such that one is double the amount than the other. It is surmised that this could have an effect on the dynamic nature of the bonds formed between the nitrogen and boron to which it will allow the lower energy crystal structure to be grown and not the higher. Another route to explore is temperature controlled cooling of the solution over different amount of time.

Once this protocol has been created and it works, macrocycle crystals will be left in the presence of benzene vapor until they have changed from red to yellow and PXRD will be performed to find out if it matches the PXRD for CP1, thus proving an expected topochemical polymerization or not.

6.7: References

(1) Wade, D. Deuterium Isotope Effects on Noncovalent Interactions between Molecules. *Chemico-Biological Interactions* **1999**, *117* (3), 191–217. https://doi.org/10.1016/S0009-2797(98)00097-0.

(2) Zhang, X.; Chang, D.; Liu, J.; Luo, Y. Conducting Polymer Aerogels from Supercritical CO2 Drying PEDOT-PSS Hydrogels. *Journal of Materials Chemistry* **2010**, *20* (24), 5080. https://doi.org/10.1039/c0jm00050g.

(3) Tan, S.; Williams, C. T. An In Situ Spectroscopic Study of Prochiral Reactant–Chiral Modifier Interactions on Palladium Catalyst: Case of Alkenoic Acid and Cinchonidine in Various Solvents. *The Journal of Physical Chemistry C* **2013**, *117* (35), 18043–18052. https://doi.org/10.1021/jp403273c.

(4) Sun, X.; Williams, C. T. In-Situ ATR-IR Investigation of Methylcinnamic Acid Adsorption and Hydrogenation on Pd/Al2O3. *Catalysis Communications* **2012**, *17*, 13–17. https://doi.org/10.1016/j.catcom.2011.09.040.

BIBLIOGRAPHY

AU - Karagiaridi, O.; AU - Bury, W.; AU - Sarjeant, A. A.; AU - Hupp, J. T.; AU - Farha, O. K. Synthesis and Characterization of Functionalized Metal-Organic Frameworks. JoVE 2014, No. 91, e52094–e52094. https://doi.org/doi:10.3791/52094.

Avens, H. J.; Unice, K. M.; Sahmel, J.; Gross, S. A.; Keenan, J. J.; Paustenbach, D. J. Analysis and Modeling of Airborne BTEX Concentrations from the Deepwater Horizon Oil Spill. Environmental Science & Technology 2011, 45 (17), 7372–7379. https://doi.org/10.1021/es200963x.

Bear, J. C.; Cockcroft, J. K.; Williams, J. H. Influence of Solvent in Crystal Engineering: A Significant Change to the Order–Disorder Transition in Ferrocene. *Journal of the American Chemical Society* 2020, 142 (4), 1731–1734. https://doi.org/10.1021/jacs.9b11895.

Beaudoin, D.; Maris, T.; Wuest, J. D. Constructing Monocrystalline Covalent Organic Networks by Polymerization. Nature Chemistry 2013, 5 (10), 830–834. https://doi.org/10.1038/nchem.1730.

Bischof, P.; Gleiter, R.; Haider, R. Through-Bond Interaction of Two Mutually Perpendicular .Pi. Systems. A Comparison with Spiroconjugation. Journal of the American Chemical Society 1978, 100 (4), 1036–1042. https://doi.org/10.1021/ja00472a003.

Bojdys, M. J.; Briggs, M. E.; Jones, J. T. A.; Adams, D. J.; Chong, S. Y.; Schmidtmann, M.; Cooper, A. I. Supramolecular Engineering of Intrinsic and Extrinsic Porosity in Covalent Organic Cages. *Journal of the American Chemical Society* 2011, 133 (41), 16566–16571. https://doi.org/10.1021/ja2056374.

Cai, M.; Daniel, S. L.; Lavigne, J. J. Conjugated Bis and Poly(Dioxaborole)s for Optical Sensing of Lewis Bases Based on Main-Chain Perturbations. Chemical Communications 2013, 49 (58), 6504–6506. https://doi.org/10.1039/C3CC41189C.

Chadha, R.; Arora, P.; Saini, A.; Jain, D. S. Solvated Crystalline Forms of Nevirapine: Thermoanalytical and Spectroscopic Studies. AAPS American Association of Pharmaceutical Scientists 2010, 11 (3), 1328–1339. https://doi.org/10.1208/s12249-010-9511-z.

Christinat, N.; Croisier, E.; Scopelliti, R.; Cascella, M.; Röthlisberger, U.; Severin, K. Formation of Boronate Ester Polymers with Efficient Intrastrand Charge-Transfer Transitions by Three-Component Reactions. European Journal of Inorganic Chemistry 2007, 2007 (33), 5177–5181. https://doi.org/https://doi.org/10.1002/ejic.200700723.

Chu, Q.; Swenson, D. C.; MacGillivray, L. R. A Single-Crystal-to-Single-Crystal Transformation Mediated by Argentophilic Forces Converts a Finite Metal Complex into an Infinite Coordination Network. Angewandte Chemie International Edition 2005, 44 (23), 3569–3572. https://doi.org/https://doi.org/10.1002/anie.200500400.

Cockcroft, J. K.; Li, J. G. Y.; Williams, J. H. Influence of Methyl-Substitution on the Dynamics of the C–H···F–C Interaction in Binary Adducts. CrystEngComm 2019, 21 (37), 5578–5585. https://doi.org/10.1039/C9CE00541B.

Cubberley, M. S.; Iverson, B. L. 1H NMR Investigation of Solvent Effects in Aromatic Stacking Interactions. *Journal of the American Chemical Society* 2001, 123 (31), 7560–7563. https://doi.org/10.1021/ja015817m.

DeHaven, B. A.; Liberatore, H. K.; Greer, A.; Richardson, S. D.; Shimizu, L. S. Probing the Formation of Reactive Oxygen Species by a Porous Self-Assembled Benzophenone Bis-Urea Host. *American Chemical Society* Omega 2019, 4 (5), 8290–8298. https://doi.org/10.1021/acsomega.9b00831.

Dou, L.; Zheng, Y.; Shen, X.; Wu, G.; Fields, K.; Hsu, W.-C.; Zhou, H.; Yang, Y.; Wudl, F. Single-Crystal Linear Polymers Through Visible Light–Triggered Topochemical Quantitative Polymerization. Science (1979) 2014, 343 (6168), 272–277. https://doi.org/10.1126/science.1245875.

Dunlap, J. H.; Loszko, A. F.; Flake, R. A.; Huang, Y.; Benicewicz, B. C.; Greytak, A. B. Multiply-Binding Polymeric Imidazole Ligands: Influence of Molecular Weight and Monomer Sequence on Colloidal Quantum Dot Stability. The Journal of Physical Chemistry C 2018, 122 (46), 26756–26763. https://doi.org/10.1021/acs.jpcc.8b08984.

Edwards, A. J.; Mackenzie, C. F.; Spackman, P. R.; Jayatilaka, D.; Spackman, M. A. Intermolecular Interactions in Molecular Crystals: What's in a Name? Faraday Discussions 2017, 203, 93–112. https://doi.org/10.1039/C7FD00072C.

Eglinton, G.; Galbraith, A. R. 182. Macrocyclic Acetylenic Compounds. Part I. Cyclotetradeca-1 :3-Diyne and Related Compounds. Journal of the Chemical Society (Resumed) 1959, 889. https://doi.org/10.1039/jr9590000889.

Feng, X.; Ding, X.; Jiang, D. Covalent Organic Frameworks. Chemical Society Reviews 2012, 41 (18), 6010–6022. https://doi.org/10.1039/C2CS35157A.

Folmer-Andersen, J. F.; Aït-Haddou, H.; Lynch, V. M.; Anslyn, E. v. 2,6-Di(Pyrimidin-4-Yl)Pyridine Ligands with Nitrogen-Containing Auxiliaries: The Formation of Functionalized Molecular Clefts upon Metal Coordination. Inorganic Chemistry 2003, 42 (26), 8674–8681. https://doi.org/10.1021/ic034823b.

Foo, M. L.; Matsuda, R.; Kitagawa, S. Functional Hybrid Porous Coordination Polymers. Chemistry of Materials 2014, 26 (1), 310–322. https://doi.org/10.1021/cm402136z.

Fracaroli, A. M.; Siman, P.; Nagib, D. A.; Suzuki, M.; Furukawa, H.; Toste, F. D.; Yaghi, O. M. Seven Post-Synthetic Covalent Reactions in Tandem Leading to Enzyme-like Complexity within Metal–Organic Framework Crystals. Journal of the American Chemical Society 2016, 138 (27), 8352–8355. https://doi.org/10.1021/jacs.6b04204.

Gao, W.-X.; Feng, H.-J.; Guo, B.-B.; Lu, Y.; Jin, G.-X. Coordination-Directed Construction of Molecular Links. Chemical Reviews 2020, 120 (13), 6288–6325. https://doi.org/10.1021/acs.chemrev.0c00321.

Geer, M. F.; Walla, M. D.; Solntsev, K. M.; Strassert, C. A.; Shimizu, L. S. Self-Assembled Benzophenone Bis-Urea Macrocycles Facilitate Selective Oxidations by Singlet Oxygen. The Journal of Organic Chemistry 2013, 78 (11), 5568–5578. https://doi.org/10.1021/jo400685u.

Goodlett, D. W.; Sindt, A. J.; Hossain, M. S.; Merugu, R.; Smith, M. D.; Garashchuk, S.; Gudmundsdottir, A. D.; Shimizu, L. S. From Incident Light to Persistent and Regenerable Radicals of Urea-Assembled Benzophenone Frameworks: A Structural Investigation. The Journal of Physical Chemistry A 2021, 125 (6), 1336–1344. https://doi.org/10.1021/acs.jpca.0c08953.

Gottardo, C.; Kraft, T. M.; Hossain, M. S.; Zawada, P. v; Muchall, H. M. Linear Free-Energy Correlation Analysis of the Electronic Effects of the Substituents in the Sonogashira Coupling Reaction. Canadian Journal of Chemistry 2008, 86 (5), 410–415. https://doi.org/10.1139/v08-038.

Gounder, R.; Moini, A. Automotive NOx Abatement Using Zeolite-Based Technologies. Reaction Chemistry & Engineering 2019, 4 (6), 966–968. https://doi.org/10.1039/C9RE90030F.

Kim, S.; Choi, H. C. Recent Advances in Covalent Organic Frameworks for Molecule-Based Two-Dimensional Materials. *American Chemical Society* Omega 2020, 5 (2), 948–958. https://doi.org/10.1021/acsomega.9b03549.

Kim, S.; Choi, H. C. Recent Advances in Covalent Organic Frameworks for Molecule-Based Two-Dimensional Materials. American Chemical Society Omega 2020, 5 (2), 948–958. https://doi.org/10.1021/acsomega.9b03549.

Kittikhunnatham, P.; Som, B.; Rassolov, V.; Stolte, M.; Würthner, F.; Shimizu, L. S.; Greytak, A. B. Fluorescence Polarization Measurements to Probe Alignment of a Bithiophene Dye in One-Dimensional Channels of Self-Assembled Phenylethynylene Bis-Urea Macrocycle Crystals. The Journal of Physical Chemistry C 2017, 121 (33), 18102–18109. https://doi.org/10.1021/acs.jpcc.7b07136.

Krishnan, B. P.; Sureshan, K. M. A Spontaneous Single-Crystal-to-Single-Crystal Polymorphic Transition Involving Major Packing Changes. *Journal of the American Chemical Society* 2015, 137 (4), 1692–1696. https://doi.org/10.1021/ja512697g.

Kumar, P.; Vahidzadeh, E.; Thakur, U. K.; Kar, P.; Alam, K. M.; Goswami, A.; Mahdi, N.; Cui, K.; Bernard, G. M.; Michaelis, V. K.; Shankar, K. C3N5: A Low Bandgap Semiconductor Containing an Azo-Linked Carbon Nitride Framework for Photocatalytic, Photovoltaic and Adsorbent Applications. *Journal of the American Chemical Society* 2019, 141 (13), 5415–5436. https://doi.org/10.1021/jacs.9b00144.

Kwon, E. H.; Kim, M.; Lee, C. Y.; Kim, M.; Park, Y. D. Metal–Organic-Framework-Decorated Carbon Nanofibers with Enhanced Gas Sensitivity When Incorporated into an Organic Semiconductor-Based Gas Sensor. *American Chemical Society* Applied Materials & Interfaces 2022, 14 (8), 10637–10647. https://doi.org/10.1021/acsami.1c24740.

Kwon, E. H.; Kim, M.; Lee, C. Y.; Kim, M.; Park, Y. D. Metal–Organic-Framework-Decorated Carbon Nanofibers with Enhanced Gas Sensitivity When Incorporated into an Organic Semiconductor-Based Gas Sensor. American Chemical Society Applied Materials & Interfaces 2022, 14 (8), 10637–10647. https://doi.org/10.1021/acsami.1c24740.

Li, H.; Chavez, A. D.; Li, H.; Li, H.; Dichtel, W. R.; Bredas, J.-L. Nucleation and Growth of Covalent Organic Frameworks from Solution: The Example of COF-5. *Journal of the American Chemical Society* 2017, 139 (45), 16310–16318. https://doi.org/10.1021/jacs.7b09169.

Li, X.-Z.; Tian, C.-B.; Sun, Q.-F. Coordination-Directed Self-Assembly of Functional Polynuclear Lanthanide Supramolecular Architectures. Chemical Reviews 2022, 122 (6), 6374–6458. https://doi.org/10.1021/acs.chemrev.1c00602.

Liu, J.; Lavigne, J. J. Boronic Acids, Second.; Hall, D. G., Ed.; Wiley-VCH Verlag GmbH & Co. KGaA: Weinheim, Germany, 2011; Vol. 2. https://doi.org/10.1002/9783527639328.

Luisier, N.; Bally, K.; Scopelliti, R.; Fadaei, F. T.; Schenk, K.; Pattison, P.; Solari, E.; Severin, K. Crystal Engineering of Polymeric Structures with Dative Boron–Nitrogen Bonds: Design Criteria and Limitations. Crystal Growth & Design 2016, 16 (11), 6600–6604. https://doi.org/10.1021/acs.cgd.6b01292.

Maynor, M. S.; Nelson, T. L.; O'Sulliva, C.; Lavigne, J. J. A Food Freshness Sensor Using the Multistate Response from Analyte-Induced Aggregation of a Cross-Reactive Poly(Thiophene). Organic Letters 2007, 9 (17), 3217–3220. https://doi.org/10.1021/ol071065a.

Millini, R.; Bellussi, G. Chapter 1. Zeolite Science and Perspectives; 2017; pp 1–36. https://doi.org/10.1039/9781788010610-00001.

Moore, J. S.; Weinstein, E. J.; Wu, Z. A Convenient Masking Group for Aryl Iodides. Tetrahedron Letters 1991, 32 (22), 2465–2466. https://doi.org/https://doi.org/10.1016/S0040-4039(00)74354-1.

Moosavi, S. M.; Nandy, A.; Jablonka, K. M.; Ongari, D.; Janet, J. P.; Boyd, P. G.; Lee, Y.; Smit, B.; Kulik, H. J. Understanding the Diversity of the Metal-Organic Framework Ecosystem. Nature Communications 2020, 11 (1), 4068. https://doi.org/10.1038/s41467-020-17755-8.

Nguyen, V.; Grünwald, M. Microscopic Origins of Poor Crystallinity in the Synthesis of Covalent Organic Framework COF-5. *Journal of the American Chemical Society* 2018, 140 (9), 3306–3311. https://doi.org/10.1021/jacs.7b12529.

Nguyen, V.; Grünwald, M. Microscopic Origins of Poor Crystallinity in the Synthesis of Covalent Organic Framework COF-5. Journal of the American Chemical Society 2018, 140 (9), 3306–3311. https://doi.org/10.1021/jacs.7b12529.

Nikolayenko, V. I.; Heyns, A.; Barbour, L. J. Threading the Needle: Guest Transport in a Versatile 0D Porous Molecular Crystal. Chemical Communications 2017, 53 (82), 11306–11309. https://doi.org/10.1039/C7CC06676G.

Nishio, M. CH/π Hydrogen Bonds in Crystals. CrystEngComm 2004, 6 (27), 130–158. https://doi.org/10.1039/B313104A.

Niu, W.; Smith, M. D.; Lavigne, J. J. Self-Assembling Poly(Dioxaborole)s as Blue-Emissive Materials. *Journal of the American Chemical Society* 2006, 128 (51), 16466–16467. https://doi.org/10.1021/ja065986c.

Ogoshi, T.; Yamagishi, T. Chapter 1. Historical Background of Macrocyclic Compounds; 2015; pp 1–22. https://doi.org/10.1039/9781782622321-00001.

PATRICK, C. R.; PROSSER, G. S. A Molecular Complex of Benzene and Hexafluorobenzene. Nature 1960, 187 (4742), 1021. https://doi.org/10.1038/1871021a0.

Percástegui, E. G.; Ronson, T. K.; Nitschke, J. R. Design and Applications of Water-Soluble Coordination Cages. Chemical Reviews 2020, 120 (24), 13480–13544. https://doi.org/10.1021/acs.chemrev.0c00672.

Pingitore, V.; Gugliuzza, A. Fabrication of Porous Semiconductor Interfaces by PH-Driven Assembly of Carbon Nanotubes on Honeycomb Structured Membranes. The Journal of Physical Chemistry C 2013, 117 (50), 26562–26572. https://doi.org/10.1021/jp405969b.

Rambo, B. M.; Tilford, R. W.; Lanni, L. M.; Liu, J.; Lavigne, J. J. Boronate-Linked Materials: Ranging from Amorphous Assemblies to Highly Structured Networks. In Macromolecules Containing Metal and Metal-Like Elements; Abd-El-Aziz, A. S., Carraher Jr., C. E., Pittman Jr., C. U., Zeldin, M., Eds.; John Wiley & Sons, Inc.: Hoboken, NJ, USA, 2009; Vol. 9, pp 255–294. https://doi.org/10.1002/9780470527085.ch6.

Rice, A. M.; Dolgopolova, E. A.; Shustova, N. B. Fulleretic Materials: Buckyball- and Buckybowl-Based Crystalline Frameworks. Chemistry of Materials 2017, 29 (17), 7054–7061. https://doi.org/10.1021/acs.chemmater.7b02245.

Rice, A. M.; Leith, G. A.; Ejegbavwo, O. A.; Dolgopolova, E. A.; Shustova, N. B. Heterometallic Metal–Organic Frameworks (MOFs): The Advent of Improving the Energy Landscape. *American Chemical Society* Energy Letters 2019, 4 (8), 1938–1946. https://doi.org/10.1021/acsenergylett.9b00874.

Sharma, R. K.; Yadav, P.; Yadav, M.; Gupta, R.; Rana, P.; Srivastava, A.; Zbořil, R.; Varma, R. S.; Antonietti, M.; Gawande, M. B. Recent Development of Covalent Organic Frameworks (COFs): Synthesis and Catalytic (Organic-Electro-Photo) Applications. Materials Horizons 2020, 7 (2), 411–454. https://doi.org/10.1039/C9MH00856J.

Shustova, N. B.; Cozzolino, A. F.; Dincă, M. Conformational Locking by Design: Relating Strain Energy with Luminescence and Stability in Rigid Metal–Organic Frameworks. Journal of the American Chemical Society 2012, 134 (48), 19596–19599. https://doi.org/10.1021/ja3103154.

Sindt, A. J.; Smith, M. D.; Berens, S.; Vasenkov, S.; Bowers, C. R.; Shimizu, L. S. Single-Crystal-to-Single-Crystal Guest Exchange in Columnar Assembled Brominated riphenylamine Bis-Urea Macrocycles. Chemical Communications 2019, 55 (39), 5619–5622. https://doi.org/10.1039/C9CC01725A.

Stephens, A. J.; Scopelliti, R.; Tirani, F. F.; Solari, E.; Severin, K. Crystalline Polymers Based on Dative Boron–Nitrogen Bonds and the Quest for Porosity. *American Chemical Society* Materials Letters 2019, 1 (1), 3–7. https://doi.org/10.1021/acsmaterialslett.9b00054.

Sun, X.; Williams, C. T. In-Situ ATR-IR Investigation of Methylcinnamic Acid Adsorption and Hydrogenation on Pd/Al2O3. Catalysis Communications 2012, 17, 13–17. https://doi.org/10.1016/j.catcom.2011.09.040.

Tan, S.; Williams, C. T. An In Situ Spectroscopic Study of Prochiral Reactant–Chiral Modifier Interactions on Palladium Catalyst: Case of Alkenoic Acid and Cinchonidine in Various Solvents. The Journal of Physical Chemistry C 2013, 117 (35), 18043–18052. https://doi.org/10.1021/jp403273c.

Teo, Y. C.; Lai, H. W. H.; Xia, Y. Synthesis of Ladder Polymers: Developments, Challenges, and Opportunities. Chemistry – A European Journal 2017, 23 (57), 14101–14112. https://doi.org/https://doi.org/10.1002/chem.201702219.

Terao, J.; Tsuji, Y. New Synthetic Methods of π-Conjugated Inclusion Complexes with High Conductivity. Journal of Inclusion Phenomena and Macrocyclic Chemistry 2014, 80 (3), 165–175. https://doi.org/10.1007/s10847-014-0381-y.

Thompson, A. L.; Ahn, T.-S.; Thomas, K. R. J.; Thayumanavan, S.; Martínez, T. J.; Bardeen, C. J. Using Meta Conjugation To Enhance Charge Separation versus Charge Recombination in Phenylacetylene Donor−Bridge−Acceptor Complexes. Journal of the American Chemical Society 2005, 127 (47), 16348–16349. https://doi.org/10.1021/ja054543q.

Tilford, R. W.; Mugavero III, S. J.; Pellechia, P. J.; Lavigne, J. J. Tailoring Microporosity in Covalent Organic Frameworks. Advanced Materials 2008, 20 (14), 2741–2746. https://doi.org/https://doi.org/10.1002/adma.200800030.

Uribe-Romo, F. J.; Hunt, J. R.; Furukawa, H.; Klöck, C.; O'Keeffe, M.; Yaghi, O. M. A Crystalline Imine-Linked 3-D Porous Covalent Organic Framework. *Journal of the*

American Chemical Society 2009, 131 (13), 4570–4571. https://doi.org/10.1021/ja8096256.

Vancik, H.; Simunic-Meznaric, V.; Mestrovic, E.; Halasz, I. Nitrosobenzene Dimerizations as a Model System for Studying Solid-State Reaction Mechanisms. The Journal of Organic Chemistry 2004, 69 (14), 4829–4834. https://doi.org/10.1021/jo049537b.

Wade, D. Deuterium Isotope Effects on Noncovalent Interactions between Molecules. Chemico-Biological Interactions 1999, 117 (3), 191–217. https://doi.org/10.1016/S0009-2797(98)00097-0.

Wang, H.; Shao, Y.; Mei, S.; Lu, Y.; Zhang, M.; Sun, J.; Matyjaszewski, K.; Antonietti, M.; Yuan, J. Polymer-Derived Heteroatom-Doped Porous Carbon Materials. Chemical Reviews 2020, 120 (17), 9363–9419. https://doi.org/10.1021/acs.chemrev.0c00080.

Wu, Z.; Lee, S.; Moore, J. S. Synthesis of Three-Dimensional Nanoscaffolding. *Journal of the American Chemical Society* 1992, 114 (22), 8730–8732. https://doi.org/10.1021/ja00048a073.

Xiao, W.; Hu, C.; Ward, M. D. Guest Exchange through Single Crystal–Single Crystal Transformations in a Flexible Hydrogen-Bonded Framework. *Journal of the American Chemical Society* 2014, 136 (40), 14200–14206. https://doi.org/10.1021/ja507689m.

Xu, W. L.; Smith, M. D.; Krause, J. A.; Greytak, A. B.; Ma, S.; Read, C. M.; Shimizu, L. S. Single Crystal to Single Crystal Polymerization of a Self-Assembled Diacetylene Macrocycle Affords Columnar Polydiacetylenes. Crystal Growth & Design 2014, 14 (3), 993–1002. https://doi.org/10.1021/cg401380a.

Xu, Y.; Smith, M. D.; Krause, J. A.; Shimizu, L. S. Control of the Intramolecular [2+2] Photocycloaddition in a Bis-Stilbene Macrocycle. The Journal of Organic Chemistry 2009, 74 (13), 4874–4877. https://doi.org/10.1021/jo900443e.

Yoo, H.; Millstone, J. E.; Li, S.; Jang, J.-W.; Wei, W.; Wu, J.; Schatz, G. C.; Mirkin, C. A. Core−Shell Triangular Bifrustums. Nano Letters 2009, 9 (8), 3038–3041. https://doi.org/10.1021/nl901513g.

Yoo, J. J.; Balakrishnan, K.; Huang, J.; Meunier, V.; Sumpter, B. G.; Srivastava, A.; Conway, M.; Mohana Reddy, A. L.; Yu, J.; Vajtai, R.; Ajayan, P. M. Ultrathin Planar Graphene Supercapacitors. Nano Letters 2011, 11 (4), 1423–1427. https://doi.org/10.1021/nl200225j.

Zhang, X.; Chang, D.; Liu, J.; Luo, Y. Conducting Polymer Aerogels from Supercritical CO2 Drying PEDOT-PSS Hydrogels. Journal of Materials Chemistry 2010, 20 (24), 5080. https://doi.org/10.1039/c0jm00050g.

Zhang, Y.-B.; Su, J.; Furukawa, H.; Yun, Y.; Gándara, F.; Duong, A.; Zou, X.; Yaghi, O. M. Single-Crystal Structure of a Covalent Organic Framework. *Journal of the American Chemical Society* 2013, 135 (44), 16336–16339. https://doi.org/10.1021/ja409033p.

APPENDIX A: SINGLE CRYSTAL DATA

A.1 Single Crystal Information for Benzene Derived CP1

[(C37H40B2O4)(C12H10N2)]·1.82(1)C6H6·0.18(1)(C6H4F2) (SAS78162.10)

X-ray intensity data from an irregular yellow crystal were collected at 100(2) K using a Bruker D8 QUEST diffractometer equipped with a PHOTON-100 CMOS area detector and an Incoatec microfocus source (Mo Kα radiation, λ = 0.71073 Å). The raw area detector data frames were reduced and corrected for absorption effects using the Bruker APEX3, SAINT+ and SADABS programs.[1,2] Final unit cell parameters were determined by least-squares refinement of 9793 reflections taken from the data set. The structure was solved with SHELXT.[3] Subsequent difference Fourier calculations and full-matrix least-squares refinement against F^2 were performed with SHELXL-2018[3] using OLEX2.[4]

The compound crystallizes in the monoclinic system. The pattern of systematic absences in the intensity data was consistent with the space group $P2_1/n$, which was confirmed by solution. The asymmetric unit consists of one polymeric $[(C_{37}H_{40}B_2O_4)(C_{12}H_{10}N_2)]$ repeat unit, half each of two benzene molecules located on inversion centers (C50-C52 and C53-C55), and another complete benzene molecule (C56-C61). One hexyl substituent (C33-C37) is disordered over two conformations (A/B) with a refined major population fraction of 0.609(4). The disorder was modeled with the aid of

same-distance (SHELX SADI) C-C distance restraints to maintain a chemically reasonable geometry. Atoms in close proximity to their disorder component counterparts were assigned equal displacement parameters. The residual electron density map near two of the three independent benzene molecules (C50-C52 and C56-C61) was consistent with partial occupation by 1,4-difluorobenzene. Occupancies refined to: C50A-C52A/C50B-F51B = 0.888(8)/0.112(8) (x 0.5) and C56-C61/C56B-F59B = 0.873(4)/0.127(4). Total site occupancies were constrained to sum to one. Same-distance restraints were applied to appropriate C-F pairs. All non-hydrogen atoms were refined with anisotropic displacement parameters except for the minor component $C_6H_4F_2$ atoms (isotropic). Hydrogen atoms bonded to carbon were placed in geometrically idealized positions and included as riding atoms with *d*(C-H) = 0.95 Å and *U*iso(H) = 1.2*U*eq(C) for aromatic hydrogen atoms, d(C-H) = 0.99 Å and Uiso(H) = 1.2Ueq(C) for methylene hydrogen atoms, and d(C-H) = 0.98 Å and Uiso(H) = 1.5Ueq(C) for methyl hydrogens. The methyl hydrogens were allowed to rotate as a rigid group to the orientation of maximum observed electron density. The largest residual electron density peak in the final difference map is 0.43 e-/Å3, located 1.28 Å from H53.

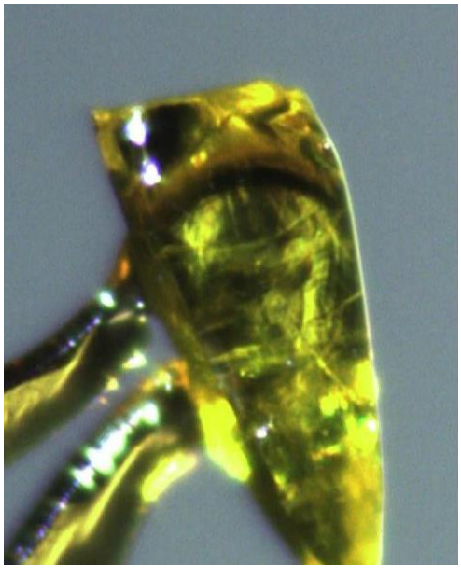

Figure A.1: Single crystal of CP1 used for XRD.

(1) APEX3 Version 2016.5-0 and SAINT+ Version 8.37A. Bruker AXS, Inc., Madison, Wisconsin, USA, 2016.
(2) SADABS-2016/2: Krause, L., Herbst-Irmer, R., Sheldrick G.M. and Stalke D. *J. Appl. Cryst.* 2015, *48*, 3-10.
(3) (a) SHELXT: Sheldrick, G.M. *Acta Cryst*. 2015, *A71*, 3-8. (b) SHELXL: Sheldrick, G.M. *Acta Cryst*. 2015, *C71*, 3-8.
(4) OLEX2: a complete structure solution, refinement and analysis program. Dolomanov, O. V., Bourhis, L. J., Gildea, R. J., Howard J. A. K. and Puschmann, H. *J. Appl. Cryst.* 2009, *42*, 339-341.

Identification code	SAS7816210
Empirical formula	$C_{61}H_{61.63}B_2F_{0.36}N_2O_4$
Formula weight	915.31
Temperature/K	100(2)
Crystal system	monoclinic
Space group	$P2_1/n$
a/Å	13.8375(6)
b/Å	21.5046(9)
c/Å	16.8476(7)
α/°	90
β/°	95.903(2)
γ/°	90
Volume/Å^3	4986.8(4)
Z	4
ρ_{calc}g/cm^3	1.219
μ/mm^{-1}	0.075
F(000)	1948.0
Crystal size/mm^3	0.4 × 0.24 × 0.16
Radiation	MoKα (λ = 0.71073)
2Θ range for data collection/°	4.442 to 50.336
Index ranges	-16 ≤ h ≤ 16, -25 ≤ k ≤ 25, -20 ≤ l ≤ 20
Reflections collected	132080
Independent reflections	8914 [R_{int} = 0.0916, R_{sigma} = 0.0407]
Data/restraints/parameters	8914/45/660
Goodness-of-fit on F^2	1.120
Final R indexes [I>=2σ (I)]	R_1 = 0.0628, wR_2 = 0.1394
Final R indexes [all data]	R_1 = 0.0972, wR_2 = 0.1528
Largest diff. peak/hole / e Å^{-3}	0.43/-0.20

Table A.1: Single crystal data of CP1

A.2 Single Crystal Information for CP1 After SCSC Styrene Transition

X-ray intensity data from a yellow wedge-shaped crystal were collected at 100(2) K using a Bruker D8 QUEST diffractometer equipped with a PHOTON-100 CMOS area detector and an Incoatec microfocus source (Mo Kα radiation, λ = 0.71073 Å). The raw area detector data frames were reduced and corrected for absorption effects using the Bruker APEX3, SAINT+ and SADABS programs.[1,2] Final unit cell parameters were determined by least-squares refinement of 9862 reflections taken from the data set. The structure was solved with SHELXT.[3] Subsequent difference Fourier calculations and full-matrix least-squares refinement against F^2 were performed with SHELXL-2017[3] using OLEX2.[4]

The compound crystallizes in the monoclinic system. The pattern of systematic absences in the intensity data was consistent with the space groups $P2_1$ and $P2_1/m$; intensity statistics suggested a non-centrosymmetric structure. A reasonable and stable solution and refinement was obtained in $P2_1$, which was the space group identified by SHELXT. A check of the finished structure with the ADDSYM program found no missed symmetry elements.[5] The asymmetric unit consists of one $C_{49}H_{50}B_2N_2O_4$ polymeric repeat unit and two crystallographically independent styrene molecules. The two sets of like bonds in the $–CHCH_2$ substituent of the styrene molecules were restrained to be similar using SHELX SADI instructions. All non-hydrogen atoms were refined with anisotropic displacement parameters. Hydrogen atoms bonded to carbon were located in Fourier difference maps before being placed in geometrically idealized positions and included as riding atoms with *d*(C-H) = 0.95 Å and *U*iso(H) = 1.2*U*eq(C) for aromatic hydrogen atoms,

d(C-H) = 0.99 Å and *U*iso(H) = 1.2*U*eq(C) for methylene hydrogen atoms, and *d*(C-H) = 0.98 Å and *U*iso(H) = 1.5*U*eq(C) for methyl hydrogens. The methyl hydrogens were allowed to rotate as a rigid group to the orientation of maximum observed electron density. The largest residual electron density peak in the final difference map is 0.44 $e^-/Å^3$, located 1.27 Å from H53. Because of the absence of heavy atoms in the crystal, the absolute structure (Flack) parameter is not reliable, and the absolute structure was not established.

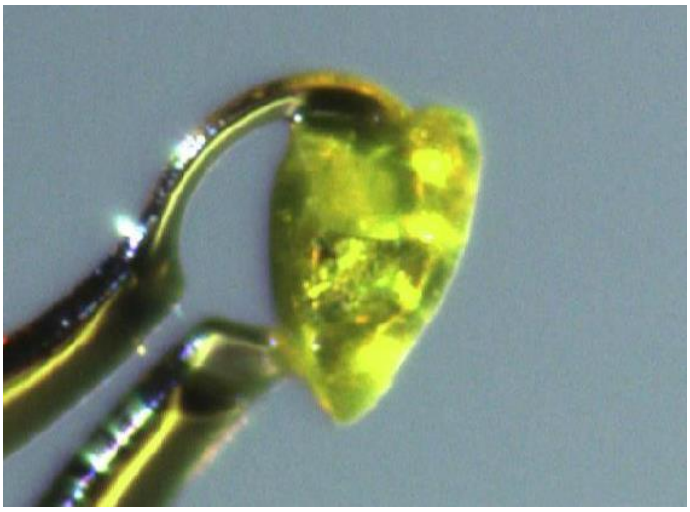

Figure A.2: Single Crystal Information for CP1 After SCSC Fluorobenzene Transition

ed on diffractometer at 100 K.
(1) APEX3 Version 2016.5-0 and SAINT+ Version 8.37A. Bruker AXS, Inc., Madison, Wisconsin, USA, 2016.
(2) SADABS-2016/2: Krause, L., Herbst-Irmer, R., Sheldrick G.M. and Stalke D. *J. Appl. Cryst.* 2015, *48*, 3-10.
(3) (a) SHELXT: Sheldrick, G.M. *Acta Cryst*. 2015, *A71*, 3-8. (b) SHELXL: Sheldrick, G.M. *Acta Cryst*. 2015, *C71*, 3-8.
(4) OLEX2: a complete structure solution, refinement and analysis program. Dolomanov, O. V., Bourhis, L. J., Gildea, R. J., Howard J. A. K. and Puschmann, H. *J. Appl. Cryst.* 2009, *42*, 339-341.
(5) (a) LePage, Y. *J. Appl. Crystallogr.* 1987, *20*, 264-269. (b) Spek, A. L. *J. Appl. Crystallogr.*, 1988, *21*, 578-579. (c) Spek, A. L. *Acta Crystallogr., Sect A* 1990, *46*, C34. (d) PLATON: Spek, A.L. *Acta Cryst.,* 2009, *D65*, 148-155.

Identification code	SAS78117sty
Empirical formula	$C_{65}H_{66}B_2N_2O_4$
Formula weight	960.81
Temperature/K	100(2)
Crystal system	monoclinic
Space group	$P2_1$
a/Å	10.7153(6)
b/Å	21.4490(13)
c/Å	11.9226(7)
α/°	90
β/°	105.384(2)
γ/°	90
Volume/Å^3	2642.0(3)
Z	2
ρ_{calc}g/cm^3	1.208
μ/mm^{-1}	0.074
F(000)	1024.0
Crystal size/mm^3	0.24 × 0.18 × 0.12
Radiation	MoKα (λ = 0.71073)
2Θ range for data collection/°	4.376 to 50.848
Index ranges	-12 ≤ h ≤ 12, -25 ≤ k ≤ 25, -14 ≤ l ≤ 14
Reflections collected	54743
Independent reflections	9701 [R_{int} = 0.0471, R_{sigma} = 0.0415]
Data/restraints/parameters	9701/3/661
Goodness-of-fit on F^2	1.045
Final R indexes [I>=2σ (I)]	R_1 = 0.0525, wR_2 = 0.1268
Final R indexes [all data]	R_1 = 0.0724, wR_2 = 0.1367
Largest diff. peak/hole / e Å^{-3}	0.44/-0.39

Table A.2: Single crystal data of styrene SCSC transitioned CP1.

A.3 Single Crystal Information for CP1 After SCSC Acetonitrile Transition

X-ray intensity data from an irregular orange crystal were collected at 100(2) K using a Bruker D8 QUEST diffractometer equipped with a PHOTON-100 CMOS area detector and an Incoatec microfocus source (Mo Kα radiation, λ = 0.71073 Å). The raw area detector data frames were reduced and corrected for absorption effects using the Bruker APEX3, SAINT+ and SADABS programs.[1,2] Final unit cell parameters were determined by least-squares refinement of 9923 reflections taken from the data set. The structure was solved with SHELXT.[3] Subsequent difference Fourier calculations and full-matrix least-squares refinement against F^2 were performed with SHELXL-2017[3] using OLEX2.[4]

The compound crystallizes in the triclinic system. The space group *P*-1 (No. 2) was confirmed by structure solution. The asymmetric unit consists of one [$C_{49}H_{50}B_2N_2O_4$] polymeric repeat unit and one acetonitrile molecule. There are half each of two independent 1,2-dipyridylethene (*dpe*) ligands within the polymeric repeat unit, each bound to the central $C_{37}H_{40}B_2O_4$ subunit. The *dpe* ligands are located on crystallographic

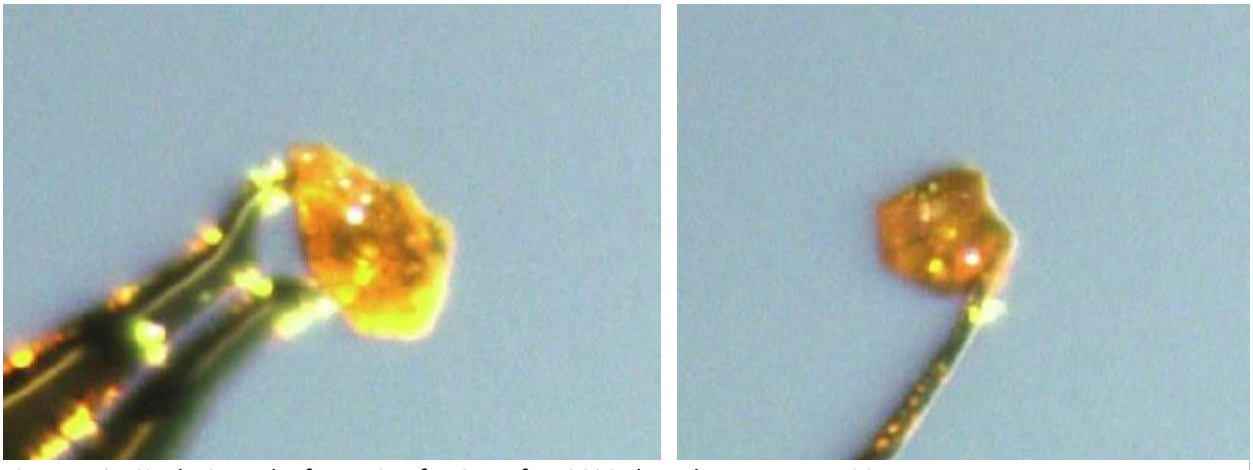

Figure A.3: Single Crystal Information for CP1 After SCSC Fluorobenzene Transition

inversion centers. All non-hydrogen atoms were refined with anisotropic displacement parameters. Hydrogen atoms were located in Fourier difference maps before being placed in geometrically idealized positions and included as riding atoms with *d*(C-H) = 0.95 Å and *U*iso(H) = 1.2*U*eq(C) for aromatic hydrogen atoms, *d*(C-H) = 0.99 Å and *U*iso(H) = 1.2*U*eq(C) for methylene hydrogen atoms, and *d*(C-H) = 0.98 Å and *U*iso(H) = 1.5*U*eq(C) for methyl hydrogens. The methyl hydrogens were allowed to rotate as a rigid group to the orientation of maximum observed electron density. The largest residual electron density peak in the final difference map is 0.25 $e^-/Å^3$, located 0.77 Å from C46.

(1) APEX3 Version 2016.5-0 and SAINT+ Version 8.37A. Bruker AXS, Inc., Madison, Wisconsin, USA, 2016.
(2) SADABS-2016/2: Krause, L., Herbst-Irmer, R., Sheldrick G.M. and Stalke D. *J. Appl. Cryst.* 2015, *48*, 3-10.
(3) (a) SHELXT: Sheldrick, G.M. *Acta Cryst*. 2015, *A71*, 3-8. (b) SHELXL: Sheldrick, G.M. *Acta Cryst*. 2015, *C71*, 3-8.
(4) OLEX2: a complete structure solution, refinement and analysis program. Dolomanov, O. V., Bourhis, L. J., Gildea, R. J., Howard J. A. K. and Puschmann, H. *J. Appl. Cryst.* 2009, *42*, 339-341.

Identification code	AMF7548_2
Empirical formula	$C_{51}H_{53}B_2N_3O_4$
Formula weight	793.58
Temperature/K	100(2)
Crystal system	triclinic
Space group	P-1
a/Å	12.1958(7)
b/Å	12.6787(7)
c/Å	16.1666(9)
α/°	106.600(2)
β/°	104.804(2)
γ/°	106.584(2)
Volume/Å^3	2135.8(2)
Z	2
ρ_{calc}g/cm^3	1.234
μ/mm^{-1}	0.077
F(000)	844.0
Crystal size/mm^3	0.16 × 0.1 × 0.08
Radiation	MoKα (λ = 0.71073)
2Θ range for data collection/°	4.952 to 51.36
Index ranges	-14 ≤ h ≤ 14, -15 ≤ k ≤ 15, -19 ≤ l ≤ 19
Reflections collected	52801
Independent reflections	8117 [R_{int} = 0.0727, R_{sigma} = 0.0627]
Data/restraints/parameters	8117/0/545
Goodness-of-fit on F^2	1.017
Final R indexes [I>=2σ (I)]	R_1 = 0.0471, wR_2 = 0.0897
Final R indexes [all data]	R_1 = 0.0941, wR_2 = 0.1045
Largest diff. peak/hole / e Å^{-3}	0.25/-0.24

Table A.3: Single crystal data of styrene SCSC transitioned CP1.

A.4 Single Crystal Information for Toluene Derived CP2

[(C37H40B2O4)(C12H10N2)]·unknown solvate (JEL27a, VMD066-78)

The compound crystallized as large (occasionally > 3 mm) yellow hexagonal plates, which were often intergrown. Several such crystals were surveyed from different reactions and crystal growth attempts, and similar difficulties were encountered in selecting a suitable data crystal. Despite the large crystal size, diffraction patterns from this material were characterized by very intense low-angle diffraction which degraded rapidly with increasing 2ϑ, resulting in no observable high-angle diffraction above $2\vartheta_{max}$ ~ 40º. This behavior was reproduced from several crystals and at temperatures from 100 K to room temperature. Extensive polymer and solvent disorder in the crystal (described below) is the reason for these observations. The best dataset came from a yellow irregular chunk cleaved from a massive hexagonal crystal. Data were collected at 173(2) K using a Bruker SMART APEX diffractometer (Mo K radiation, = 0.71073 Å).[1] The raw area detector data frames were reduced and corrected for absorption effects using the SAINT+ and SADABS programs.[1] Data were truncated at $2\vartheta_{max}$ = 40º. Final unit cell parameters were determined by least-squares refinement of 8417 reflections taken from the data set in the angular range 4.48º < 2ϑ < 37.92º. The structure was solved by direct methods with SHELXS.[2] Subsequent difference Fourier calculations and full-matrix least-squares refinement against F^2 were performed with SHELXL-2013/4[2] using OLEX2.[3]

The compound crystallizes in the hexagonal system. The space groups $P6_3$ and $P6_3/m$ were suggested by the pattern of systematic absences in the intensity data. The

best refinement was achieved in the centrosymmetric group $P6_3/m$ (No. 176). The asymmetric unit consists of half each of the two polymer strand components $C_{37}H_{20}B_2O_4$ and $C_{12}H_{10}N_2$, and a large, featureless volume of electron density, assumed to be disordered solvent species. The $C_{37}H_{20}B_2O_4$ component is located on a mirror plane and the $C_{12}H_{10}N_2$ component is situated about an inversion center. Two-fold disorder of the $-BO_2C_6H_4$ grouping was observed and was modeled with two equally populated positions. Disorder of part of one hexyl group (C20-C25) across the mirror plane was also observed and modeled using two independent conformations A/B per asymmetric unit, generating a total of four positions throughout the unit cell. Only atoms C23-C25 are affected. The total population for this group was constrained to full site occupancy. A total of 61 distance restraints were used to maintain chemically reasonable geometries for the disordered species. Non-hydrogen atoms were refined with anisotropic displacement parameters except for disordered atoms (isotropic). Hydrogen atoms were placed in geometrically idealized positions and included as riding atoms. No chemically reasonable model could be found for the disordered solvent guests, which presumably are the crystallization solvent toluene. This electron density was removed from the structure factors using the Squeeze program in PLATON.[4] Squeeze calculated a solvent-accessible volume of 4888.9 $Å^3$ (44.5% of the total unit cell volume), enclosing the equivalent of 1207 electrons per unit cell. The electron count suggests four toluene molecules per formula unit. The reported F.W., d_{calc} and $F(000)$ reflect known unit cell contents only. The largest residual electron density peak in the final difference map is 0.32 $e^-/Å^3$, located 0.56 Å from C11A. While the general features of the structure (polymeric nature and

connectivity) are well-established, the extensive crystal disorder reduces the precision of the refinement, and the finer details of the structure (bond distances and angles, displacement parameters) should therefore be regarded as approximate.

(1) SMART Version 5.631, SAINT+ Version 6.45a and SADABS Version 2.10. Bruker Analytical X-ray Systems, Inc., Madison, Wisconsin, USA, 2003.
(2) Sheldrick, G.M. *Acta Cryst*. 2008, A64, 112-122.
(3) Dolomanov, O. V., Bourhis, L. J., Gildea, R. J., Howard J. A. K. and Puschmann, H. OLEX2: a complete structure solution, refinement and analysis program. *J. Appl. Cryst.* 2009, *42*, 339-341.
(4) (a) Sluis, P. v.d.; Spek, A. L. *Acta Crystallogr., Sect. A* 1990, *46*, 194-201. (b) PLATON: Spek, A. L. *J. Appl. Cryst.* 2003, *36*, 7-13; www.cryst.chem.uu.nl/platon/.

Identification code	jel27aqz_sq_s
Empirical formula	$C_{49}H_{50}B_2N_2O_4$
Formula weight	752.53
Temperature/K	173(2)
Crystal system	hexagonal
Space group	$P6_3/m$
a/Å	22.5615(9)
b/Å	22.5615(9)
c/Å	24.948(2)
α/°	90
β/°	90
γ/°	120
Volume/Å^3	10997.9(12)
Z	6
ρ_{calc}mg/mm^3	0.682
m/mm^{-1}	0.042
F(000)	2400.0
Crystal size/mm^3	0.54 × 0.5 × 0.48
Radiation	MoKα (λ = 0.71073)
2Θ range for data collection	2.648 to 40.276°
Index ranges	-21 ≤ h ≤ 21, -21 ≤ k ≤ 21, -24 ≤ l ≤ 24
Reflections collected	64617
Independent reflections	3604 [R_{int} = 0.1727, R_{sigma} = 0.0616]
Data/restraints/parameters	3604/61/235
Goodness-of-fit on F^2	1.352
Final R indexes [I>=2σ (I)]	R_1 = 0.1028, wR_2 = 0.3177
Final R indexes [all data]	R_1 = 0.1427, wR_2 = 0.3636
Largest diff. peak/hole / e Å^{-3}	0.32/-0.46

Table A.4: Single crystal data of acetonitrile SCSC transitioned CP1.

A.5 Single Crystal Information for Dioxane Derived CP3

X-Ray Structure Determination, (C37H40B2O4)(C12H10N2)·(C4H8O2)1.5

(SAS7810423)

X-ray intensity data from an orange block were collected at 200(2) K using a Bruker D8 QUEST diffractometer equipped with a PHOTON-100 CMOS area detector and an Incoatec microfocus source (Mo K radiation, = 0.71073 Å). Crystals mounted at 100 K cracked and diffracted poorly. The raw area detector data frames were reduced and corrected for absorption effects using the Bruker APEX3, SAINT+ and SADABS programs.[1,2] Final unit cell parameters were determined by least-squares refinement of 9850 reflections taken from the data set. The structure was solved with SHELXT.[3] Subsequent difference Fourier calculations and full-matrix least-squares refinement against F^2 were performed with SHELXL-2017[3] using OLEX2.[4]

The compound crystallizes in the triclinic system. The space group *P*-1 was confirmed by structure solution. The asymmetric unit consists of one $C_{37}H_{40}B_2O_4$ component of the polymeric $(C_{37}H_{40}B_2O_4)(C_{12}H_{10}N_2)$ chain, half each of two independent $C_{12}H_{10}N_2$ components, each located on a crystallographic inversion center and 1.5 dioxane molecules. One dioxane is located on a crystallographic inversion center, and only half is present per asymmetric unit. The second independent dioxane is disordered and was modeled with three components. The total disordered dioxane population was constrained to sum to one. O-C and C-C distances were restrained to appropriate values. One of the hexyl side chains (C32-C37) is disordered and was modeled with three components (A-C). 1,2- and 1,3- C-C distances in the disordered hexyl groups were

restrained to be similar to those in the ordered hexyl chain (SHELX SAME). The total group population was constrained to sum to one, and refined to A/B/C = 0.344(3)/0.343(2)/0.313(3). All non-hydrogen atoms were refined with anisotropic displacement parameters except for disordered dioxane atoms (isotropic). Hydrogen atoms bonded to carbon were placed in geometrically idealized positions and included as riding atoms with *d*(C-H) = 0.95 Å and *U*iso(H) = 1.2*U*eq(C) for aromatic hydrogen atoms, *d*(C-H) = 0.99 Å and *U*iso(H) = 1.2*U*eq(C) for methylene hydrogen atoms, and *d*(C-H) = 0.98 Å and *U*iso(H) = 1.5*U*eq(C) for methyl hydrogens. The methyl hydrogens were allowed to rotate as a rigid group to the orientation of maximum observed electron density. The largest residual electron density peak in the final difference map is 0.60 $e^-/Å^3$, located 0.54 Å from C10S.

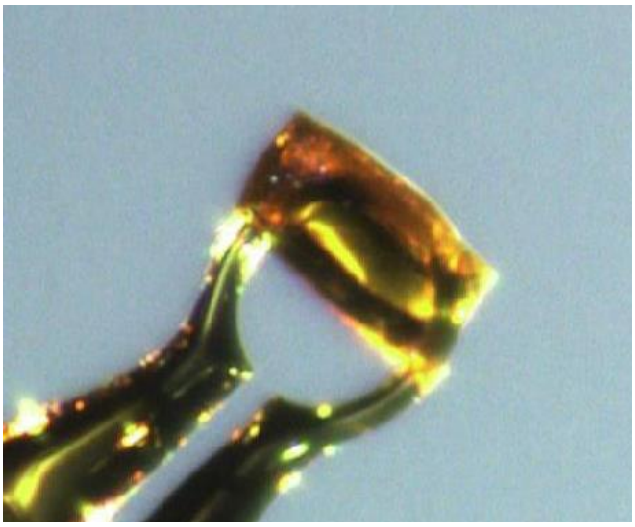

Figure A.4: Single Crystal Information of CP3

(1) APEX3 Version 2016.5-0 and SAINT+ Version 8.37A. Bruker AXS, Inc., Madison, Wisconsin, USA, 2016.
(2) SADABS-2016/2: Krause, L., Herbst-Irmer, R., Sheldrick G.M. and Stalke D. *J. Appl. Cryst.* 2015, *48*, 3-10.
(3) (a) SHELXT: Sheldrick, G.M. *Acta Cryst*. 2015, *A71*, 3-8. (b) SHELXL: Sheldrick, G.M. *Acta Cryst*. 2015, *C71*, 3-8.
(4) OLEX2: a complete structure solution, refinement and analysis program. Dolomanov, O. V., Bourhis, L. J., Gildea, R. J., Howard J. A. K. and Puschmann, H. *J. Appl. Cryst.* 2009, *42*, 339-341.

Identification code	SAS7810423
Empirical formula	$C_{55}H_{62}B_2N_2O_7$
Formula weight	884.68
Temperature/K	200(2)
Crystal system	triclinic
Space group	P-1
a/Å	12.2648(5)
b/Å	12.3331(5)
c/Å	17.9650(10)
α/°	107.113(2)
β/°	102.374(2)
γ/°	104.8590(10)
Volume/Å^3	2383.59(19)
Z	2
ρ_{calc}g/cm^3	1.233
μ/mm^{-1}	0.080
F(000)	944.0
Crystal size/mm^3	0.2 × 0.1 × 0.08
Radiation	MoKα (λ = 0.71073)
2Θ range for data collection/°	4.756 to 50.054
Index ranges	-14 ≤ h ≤ 14, -14 ≤ k ≤ 14, -21 ≤ l ≤ 21
Reflections collected	59670
Independent reflections	8418 [R_{int} = 0.0505, R_{sigma} = 0.0381]
Data/restraints/parameters	8418/73/669
Goodness-of-fit on F^2	1.058
Final R indexes [I>=2σ (I)]	R_1 = 0.0613, wR_2 = 0.1482
Final R indexes [all data]	R_1 = 0.0993, wR_2 = 0.1686
Largest diff. peak/hole / e Å^{-3}	0.60/-0.42

Table A.5: Single crystal data for dioxane derived CP3.

A.6 Single Crystal Information for Hexanes/Hexanes and Dichloromethane Derived CP4

X-Ray Structure Determination, (C37H40B2O4)(C12H10N2)·(CH2Cl2)0.53(2) SAS7896_10

X-ray intensity data from a yellow pyramidal prism were collected at 100(2) K using a Bruker D8 QUEST diffractometer equipped with a PHOTON-100 CMOS area detector and an Incoatec microfocus source (Mo K radiation, = 0.71073 Å). The raw area detector data frames were reduced and corrected for absorption effects using the Bruker APEX3, SAINT+ and SADABS programs.[1,2] Final unit cell parameters were determined by least-squares refinement of 9840 reflections taken from the data set. The structure was solved with SHELXT.[3] Subsequent difference Fourier calculations and full-matrix least-squares refinement against F^2 were performed with SHELXL-2016[3] using OLEX2.[4]

The compound crystallizes in the trigonal system. The pattern of systematic absences in the intensity data was consistent with the enantiomorphous space group pairs $P3_1/P3_2$ and $P3_121/P3_221$. A reasonable and stable solution in $P3_1$ was eventually obtained, giving an absolute structure (Flack) parameter from the final model of -0.02(3). From refinement trials, the crystal is a merohedral twin emulating the higher Laue group (-3*m*). Including the twin matrix (0 1 0 / 1 0 0 / 0 0 -1) in the refinement decreased the *R*1-value from 0.084 to 0.056. The major twin fraction refined to 0.580(4). Solution attempts in the space group $P3_121$, suggested by ADDSYM, were inferior and suggested pseudosymmetry. The best refinement in $P3_121$ converged at *R*1/*wR*2 = 0.074 / 0.201, but resulted in enlarged displacement ellipsoids for many atoms, especially those corresponding to the hexyl group substituents and atoms C16/C23 and C17/C22 of the

dioxo-phenyl substituent in the $P3_1$ model. This suggests that these parts of the structure are incompatible with the two-fold axis imposed by $P3_121$. The CH_2Cl_2 disorder also could not be reasonably modeled in $P3_121$. The achievement of a crystallographically stable twin refinement in $P3_1$ with lower residuals and a reasonable solvent disorder model therefore provides good support for $P3_1$ as the correct space group choice. The asymmetric unit in $P3_1$ consists of one $(C_{37}H_{40}B_2O_4)(C_{12}H_{10}N_2)$ repeating unit and a region of disordered solvent modeled as dichloromethane. The CH_2Cl_2 disorder was modeled using three components having freely refined occupancies of 0.22(1), 0.18(1) and 0.13(1). Distance restraints of *d*(C-Cl) = 1.75(2) Å and *d*(Cl-Cl) = 2.80(2) were applied to each component. The outer two atoms of one hexyl substituent (C36/C37) are disordered over two conformations with occupancies fixed at 50% each for stability, close to values obtained from trial refinements. 'Same-distance' restraints (SHELX SADI) were used for all C-C bonds involving the outer five atoms of the two hexyl groups (C27-C31 and C33-C37). Anisotropic displacement parameters were restrained to a spherical form for atom C31 (ISOR). Enhanced rigid-bond restraints (RIGU) were applied to the anisotropic displacement parameters of atoms C14-C19. All non-hydrogen atoms were refined with anisotropic displacement parameters. Hydrogen atoms bonded to carbon were placed in geometrically idealized positions and included as riding atoms with *d*(C-H) = 0.95 Å and *U*iso(H) = 1.2*U*eq(C) for aromatic hydrogen atoms, *d*(C-H) = 0.99 Å and *U*iso(H) = 1.2*U*eq(C) for methylene hydrogen atoms, and *d*(C-H) = 0.98 Å and *U*iso(H) = 1.5*U*eq(C) for methyl hydrogens. The methyl hydrogens were allowed to rotate as a rigid group to the

orientation of maximum observed electron density. The largest residual electron density peak in the final difference map is 0.44 $e^-/Å^3$, located 1.80 Å from H31B.

(1) APEX3 Version 2016.5-0 and SAINT+ Version 8.37A. Bruker AXS, Inc., Madison, Wisconsin, USA, 2016.
(2) SADABS-2016/2: Krause, L., Herbst-Irmer, R., Sheldrick G.M. and Stalke D. *J. Appl. Cryst.* 2015, *48*, 3-10.
(3) (a) SHELXT: Sheldrick, G.M. *Acta Cryst*. 2015, *A71*, 3-8. (b) SHELXL: Sheldrick, G.M. *Acta Cryst.* 2015, *C71*, 3-8.
(4) OLEX2: a complete structure solution, refinement and analysis program. Dolomanov, O. V., Bourhis, L. J., Gildea, R. J., Howard J. A. K. and Puschmann, H. *J. Appl. Cryst.* 2009, *42*, 339-341.

Identification code	SAS7898_10
Empirical formula	$C_{49.53}H_{51.06}B_2Cl_{1.06}N_2O_4$
Formula weight	797.42
Temperature/K	100(2)
Crystal system	trigonal
Space group	$P3_1$
a/Å	14.7550(7)
b/Å	14.7550(7)
c/Å	18.2565(10)
α/°	90
β/°	90
γ/°	120
Volume/Å^3	3442.1(4)
Z	3
ρ_{calc}g/cm^3	1.154
μ/mm^{-1}	0.131
F(000)	1267.0
Crystal size/mm^3	0.36 × 0.26 × 0.22
Radiation	MoKα (λ = 0.71073)
2Θ range for data collection/°	4.462 to 50.128
Index ranges	-17 ≤ h ≤ 17, -17 ≤ k ≤ 17, -21 ≤ l ≤ 21
Reflections collected	71612
Independent reflections	8124 [R_{int} = 0.0516, R_{sigma} = 0.0291]
Data/restraints/parameters	8124/107/559
Goodness-of-fit on F^2	1.075
Final R indexes [I>=2σ (I)]	R_1 = 0.0558, wR_2 = 0.1424
Final R indexes [all data]	R_1 = 0.0683, wR_2 = 0.1519
Largest diff. peak/hole / e Å^{-3}	0.44/-0.28
Flack parameter	-0.02(3)

Table A.6: Single crystal data for hexanes/ hexanes and dichloromethane derived CP4.

A.7 Single Crystal Information for Vacuum Pyrolysis CP

[(C6H4O2BOBO2C6H4)(C12H10N2)](C12H10N2) **(** SAS78157, yellow crystals)

X-ray intensity data from a yellow needle were collected at 100(2) K using a Bruker D8 QUEST diffractometer equipped with a PHOTON-100 CMOS area detector and an Incoatec microfocus source (Mo Kα radiation, λ = 0.71073 Å). The raw area detector data frames were reduced and corrected for absorption effects using the Bruker APEX3, SAINT+ and SADABS programs.[1,2] Final unit cell parameters were determined by least-squares refinement of 9840 reflections taken from the data set. The structure was solved with SHELXT.[3] Subsequent difference Fourier calculations and full-matrix least-squares refinement against F^2 were performed with SHELXL-2018[3] using OLEX2.[4]

The compound crystallizes in the triclinic system. The pattern space group *P*-1 (No. 2) was confirmed by structure solution. The asymmetric unit consists of one $[(C_6H_4O_2BOBO_2C_6H_4)(C_{12}H_{10}N_2)]$ polymeric repeating unit and half each of two crystallographically independent $C_{12}H_{10}N_2$ molecules, both located on crystallographic inversion centers. The $C_{12}H_{10}N_2$ part of the polymer is disordered over two orientations, by an approximate two-fold rotation about the N1-N2 vector. The major disorder component occupancy refined to 0.756(2). The geometry of the minor component was restrained to be similar to that of the major using a SHELX SAME instruction (35 restraints). All non-hydrogen atoms were refined with anisotropic displacement parameters. Hydrogen atoms bonded to carbon were in general located in difference Fourier maps before being placed in geometrically idealized positions and included as

riding atoms with *d*(C-H) = 0.95 Å and *U*iso(H) = 1.2*U*eq(C). The largest residual electron density peak in the final difference map is 0.22 $e^-/Å^3$, located 1.06 Å from O1.

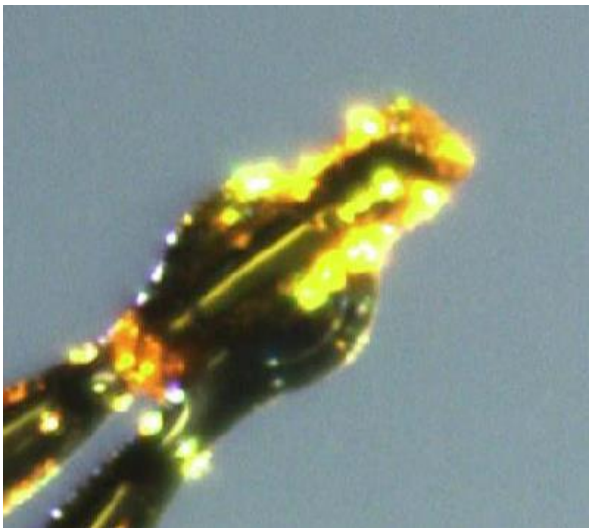

Figure A.5: Single crystal of vacuum pyrolysis CP.

(1) APEX3 Version 2016.5-0 and SAINT+ Version 8.38A. Bruker AXS, Inc., Madison, Wisconsin, USA, 2016.
(2) SADABS-2016/2: Krause, L., Herbst-Irmer, R., Sheldrick G.M. and Stalke D. *J. Appl. Cryst.* 2015, *48*, 3-10.
(3) (a) SHELXT: Sheldrick, G.M. *Acta Cryst*. 2015, *A71*, 3-8. (b) SHELXL: Sheldrick, G.M. *Acta Cryst*. 2015, *C71*, 3-8.
(4) OLEX2: a complete structure solution, refinement and analysis program. Dolomanov, O. V., Bourhis, L. J., Gildea, R. J., Howard J. A. K. and Puschmann, H. *J. Appl. Cryst.* 2009, *42*, 339-341.

Identification code	SAS78157
Empirical formula	$C_{36}H_{28}B_2N_4O_5$
Formula weight	618.24
Temperature/K	100(2)
Crystal system	triclinic
Space group	P-1
a/Å	10.4681(4)
b/Å	11.6641(5)
c/Å	13.9848(6)
α/°	100.7860(16)
β/°	107.7760(17)
γ/°	104.4005(16)
Volume/Å^3	1509.53(11)
Z	2
ρ_{calc}g/cm^3	1.360
μ/mm^{-1}	0.091
F(000)	644.0
Crystal size/mm^3	0.26 × 0.08 × 0.05
Radiation	MoKα (λ = 0.71073)
2Θ range for data collection/°	4.182 to 50.186
Index ranges	-12 ≤ h ≤ 12, -13 ≤ k ≤ 13, -16 ≤ l ≤ 16
Reflections collected	48391
Independent reflections	5366 [R_{int} = 0.0668, R_{sigma} = 0.0405]
Data/restraints/parameters	5366/35/468
Goodness-of-fit on F^2	1.047
Final R indexes [I>=2σ (I)]	R_1 = 0.0395, wR_2 = 0.0767
Final R indexes [all data]	R_1 = 0.0723, wR_2 = 0.0886
Largest diff. peak/hole / e Å^{-3}	0.22/-0.21

Table A.7: Single crystal data for vacuum pyrolysis CP.

A.8 Single Crystal Information for Toluene Derived Macrocycle (100K)

X-ray intensity data from an irregular yellow-orange crystal were collected at 100(2) K using a Bruker D8 QUEST diffractometer equipped with a PHOTON-100 CMOS area detector and an Incoatec microfocus source (Mo Kα radiation, λ = 0.71073 Å). The data crystal was cleaved from a large aggregation, which appeared red in color when thick, then orange when moderately thick and then yellow when thinner. The raw area detector data frames were reduced and corrected for absorption effects using the Bruker APEX3, SAINT+ and SADABS programs.[1,2] The structure was solved with SHELXT.[3] Subsequent difference Fourier calculations and full-matrix least-squares refinement against F^2 were performed with SHELXL-2018[3] using OLEX2.[4]

The compound crystallizes in the triclinic system. The space group *P*-1 (No. 2) was confirmed structure solution. The asymmetric unit consists of half of one [(C37H40B2O4)2(C12H10N2)2] complex located on a crystallographic inversion center, and three independent regions of electron density modeled reasonably well as disordered, fractionally occupied toluene molecules. Toluene molecules C51-C54 and C55-C61 are disordered about inversion centers; C62-C68 is disordered over two orientations (A/B) on a general position with refined populations of A/B = 0.538(3) / 0.462(3). The disorder and occupancy factor of C51-C54 is linked with that of C62-C68 (A/B) such that when component C62A-C68A is present in a given asymmetric unit, C51-C54 is also present with the same occupancy; conversely when component C62B-C68B is present, C51-C54 is absent. The toluene molecules were refined as rigid hexagons and

distance restraints were applied to the methyl groups. Hydrogen atoms bonded to carbon were located in difference Fourier maps before being placed in geometrically idealized positions and included as riding atoms with *d*(C-H) = 0.95 Å and *U*iso(H) = 1.2*U*eq(C) for aromatic hydrogen atoms, *d*(C-H) = 0.99 Å and *U*iso(H) = 1.2*U*eq(C) for methylene hydrogen atoms, and *d*(C-H) = 0.98 Å and *U*iso(H) = 1.5*U*eq(C) for methyl hydrogens. The methyl hydrogens were allowed to rotate as a rigid group to the orientation of maximum observed electron density. All non-hydrogen atoms were refined with anisotropic displacement parameters. Enhanced rigid-bond restraints (SHELX RIGU) and isotropic restraints (ISOR) were applied to the anisotropic displacement parameters of the disordered toluene atoms. The largest residual electron density peak in the final difference map is 0.39 $e^-/Å^3$, located 0.83 Å from H60.

Figure: A.6: Single crystal of toluene Macrocycle.

1) APEX3 Version 2018.1-0 and SAINT+ Version 8.38A. Bruker AXS, Inc., Madison, Wisconsin, USA, 2016.

(2) SADABS-2016/2: Krause, L., Herbst-Irmer, R., Sheldrick G.M. and Stalke D. *J. Appl. Cryst.* 2015, *48*, 3-10.

(3) (a) SHELXT: Sheldrick, G.M. *Acta Cryst*. 2015, *A71*, 3-8. (b) SHELXL: Sheldrick, G.M. *Acta Cryst*. 2015, *C71*, 3-8.

(4) OLEX2: a complete structure solution, refinement and analysis program. Dolomanov, O. V., Bourhis, L. J., Gildea, R. J., Howard J. A. K. and Puschmann, H. *J. Appl. Cryst.* 2009, *42*, 339-341.

Identification code	SAS781615
Empirical formula	$C_{122.77}H_{128.3}B_4N_4O_8$
Formula weight	1831.07
Temperature/K	100(2)
Crystal system	triclinic
Space group	P-1
a/Å	11.6224(6)
b/Å	13.4837(7)
c/Å	17.1974(8)
α/°	82.409(3)
β/°	82.900(3)
γ/°	79.972(3)
Volume/Å^3	2616.6(2)
Z	1
ρ_{calc}g/cm^3	1.162
μ/mm^{-1}	0.071
F(000)	977.0
Crystal size/mm^3	0.22 × 0.12 × 0.1
Radiation	MoKα (λ = 0.71073)
2Θ range for data collection/°	2.402 to 50.224
Index ranges	-13 ≤ h ≤ 13, -16 ≤ k ≤ 16, -20 ≤ l ≤ 20
Reflections collected	76761
Independent reflections	9282 [R_{int} = 0.0635, R_{sigma} = 0.0308]
Data/restraints/parameters	9282/228/707
Goodness-of-fit on F^2	1.038
Final R indexes [I>=2σ (I)]	R_1 = 0.0456, wR_2 = 0.1072
Final R indexes [all data]	R_1 = 0.0625, wR_2 = 0.1172
Largest diff. peak/hole / e Å^{-3}	0.39/-0.30

Table A.8: Single crystal data for toluene derived macrocycle (100 K).

A.9 Single Crystal Information for Naphthalene Diol CP

X-Ray Structure Determination, {(C45H44B2O4)(C12H10N2)}n·unknown solvate

(SAS078-49)

The compound crystallized as orange cubes, generally intergrown and twinned, exhibiting no extinctions under polarized light. The crystals crack under oil after a few hours, but were stable enough for successful quick transfer to the diffractometer cold stream for low-temperature data collection. X-ray intensity data from a crystal of approximate dimensions 0.24 x 0.28 x 0.32 mm^3 were collected at 100(2) K using a Bruker D8 QUEST diffractometer equipped with a PHOTON-100 CMOS area detector and an Incoatec microfocus source (Mo K radiation, = 0.71073 Å). The diffraction pattern was characterized by strong low-angle reflections which fell off rapidly in intensity at higher 2ϑ values. No significant intensity was observed above $2\vartheta_{max}$ ~ 40°, at which point the dataset was truncated. This value (d = 1.04 Å) was actually chosen after examination of the intensity statistics using the Bruker XPREP program, and corresponds to the resolution shell where the R(sigma) indicator rose above 0.35. The raw area detector data frames were reduced and corrected for absorption effects using the Bruker APEX3, SAINT+ and SADABS programs.[1,2] Final unit cell parameters were determined by least-squares refinement of 9835 reflections taken from the data set. The structure was solved readily by direct methods with SHELXS.[3] Subsequent difference Fourier calculations and full-matrix least-squares refinement against F^2 were performed with SHELXL-2016[3] using OLEX2.[4]

The compound crystallizes in the cubic system. The pattern of systematic absences in the intensity data was uniquely consistent with the space group *Pa*-3 (No. 205). The asymmetric unit consists of one crystallographically independent $(C_{45}H_{44}B_2O_4)(C_{12}H_{10}N_2)$ polymeric repeating unit and a large volume of disordered species, presumably the crystallization solvent toluene. Two-fold disorder of the outer four atoms of one hexyl sidechain (C42-C45) was modeled with two equally populated components. Disordered atom occupancies were fixed and 0.5, and 1,2- and 1,3- C-C distance restraints of 1.54 Å and 2.5 Å, respectively, were applied. Disordered atoms were refined with fixed isotropic displacement parameters of 0.175 $Å^2$ (C42) or 0.25 $Å^2$ (C43-C45). Additional 'rigid-bond' anisotropic displacement parameter restraints were applied to hexyl group atoms C34-C41 (SHELX RIGU) and to atoms of the pyridyl group N1/C46-C50 (DELU/SIMU). All non-hydrogen atoms were refined with anisotropic displacement parameters except where noted above. Hydrogen atoms bonded to carbon were located in Fourier difference maps before being placed in geometrically idealized positions and included as riding atoms with *d*(C-H) = 0.95 Å and *U*iso(H) = 1.2*U*eq(C) for aromatic hydrogen atoms, *d*(C-H) = 0.99 Å and *U*iso(H) = 1.2*U*eq(C) for methylene hydrogen atoms and *d*(C-H) = 0.98 Å and *U*iso(H) = 1.5*U*eq(C) for methyl hydrogens. The disordered solvent guests could not be modeled reasonably and were accounted for with the Squeeze technique implemented in PLATON.[5] The solvent-accessible volume per unit cell was calculated to be 11251 $Å^3$ (31% of the total cell volume), and to contain the equivalent of 2355 electrons per unit cell. The electron count per unit cell computes to about 2 toluene per formula unit. The scattering contribution of the electron density in the solvent volume was added to the structure

factors computed from the known part of the structure during refinement. The reported crystal density and *F.W*. are calculated from the known part of the structure only. The largest residual electron density peak in the final difference map is 0.85 $e^-/Å^3$, located 1.40 Å from H39A near the disordered hexyl groups. It likely indicates further hexyl disorder in this region, possibly combined with disordered solvent.

(1) APEX3 Version 2016.5-0 and SAINT+ Version 8.37A. Bruker AXS, Inc., Madison, Wisconsin, USA, 2016.
(2) SADABS-2016/2: Krause, L., Herbst-Irmer, R., Sheldrick G.M. and Stalke D. *J. Appl. Cryst.* 2015, *48*, 3-10.
(3) (a) SHELXS: Sheldrick, G.M. *Acta Cryst*. 2015, *A71*, 3-8. (b) SHELXL: Sheldrick, G.M. *Acta Cryst*. 2008, A64, 112-122.
(4) OLEX2: a complete structure solution, refinement and analysis program. Dolomanov, O. V., Bourhis, L. J., Gildea, R. J., Howard J. A. K. and Puschmann, H. *J. Appl. Cryst.* 2009, *42*, 339-341.
(5) (a) Sluis, P. v.d.; Spek, A. L. *Acta Crystallogr., Sect. A* 1990, *46*, 194-201. (b) PLATON SQUEEZE: Spek, A. L. *Acta Cryst.* 2015, *C71*, 9-18.

Identification code	sas078_049_sq
Empirical formula	$C_{57}H_{54}B_2N_2O_4$
Formula weight	852.64
Temperature/K	100(2)
Crystal system	cubic
Space group	Pa-3
a/Å	33.1906(10)
b/Å	33.1906(10)
c/Å	33.1906(10)
α/°	90
β/°	90
γ/°	90
Volume/Å^3	36563(3)
Z	24
ρ_{calc}g/cm^3	0.929
μ/mm^{-1}	0.057
F(000)	10848.0
Crystal size/mm^3	0.32 × 0.28 × 0.24
Radiation	MoKα (λ = 0.71073)
2Θ range for data collection/°	4.252 to 39.95
Index ranges	-31 ≤ h ≤ 28, -31 ≤ k ≤ 31, -31 ≤ l ≤ 28
Reflections collected	160261
Independent reflections	5669 [R_{int} = 0.1106, R_{sigma} = 0.0293]
Data/restraints/parameters	5669/140/569
Goodness-of-fit on F^2	1.464
Final R indexes [I>=2σ (I)]	R_1 = 0.1076, wR_2 = 0.3243
Final R indexes [all data]	R_1 = 0.1426, wR_2 = 0.3634
Largest diff. peak/hole / e Å^{-3}	0.85/-0.39

Table A.9: Single crystal data for naphthalene diol CP.

A.10 Single Crystal Information for Nitrocatechol CP

X-Ray Structure Determination, C49H48B2N4O8·unknown solvate (SAS078_43)

The compound crystallizes as abundant, well-formed yellow blocks, which proved to be unusually unstable. Efforts to handle crystals under paratone-N oil were not successful. The crystals crack, become cloudy and lose crystallinity essentially immediately after removal from the mother liquor. Attempts to 'net' a crystal with a Mitegen mesh while still in the mother liquor and transfer it directly into the cold stream also failed, resulting in several shattered crystals despite being in air for < 2 s. Eventually a crystal was sealed in a thin-walled glass capillary in the presence of the mother liquor for data collection at room temperature. Despite this treatment the crystals still cracked during the data collection, though visible solvent was still present. Fortunately, enough data with acceptable reflection redundancy were collected before crystal decomposition. Despite its large size, the data crystal did not diffract observably at higher angles. This is because of extensive disorder of the main polymeric part of the structure and of the large amount of guest solvent. Examination of the reflection data showed the mean $I/\sigma(I)$ fell below 1.5 at *ca*. 1.02 Å. The dataset was therefore truncated at that value ($2\theta_{max}$ = 40.8°).

X-ray intensity data were collected at 100(2) K using a Bruker D8 QUEST diffractometer equipped with a PHOTON-100 CMOS area detector and an Incoatec microfocus source (Mo K radiation, = 0.71073 Å). The raw area detector data frames were reduced and corrected for absorption effects using the Bruker APEX3, SAINT+ and SADABS programs.[1,2] Final unit cell parameters were determined by least-squares refinement of 9838 reflections taken from the data set. The structure was solved with

SHELXT.[3] Subsequent difference Fourier calculations and full-matrix least-squares refinement against F^2 were performed with SHELXL-2016[3] using OLEX2.[4]

The compound crystallizes in the monoclinic system. The pattern of systematic absences in the intensity data was consistent with the space groups $P2_1$ and $P2_1/m$; intensity statistics suggested an acentric structure. The space group $P2_1$ was eventually confirmed by structure solution, and was further verified using the ADDSYM program on the ordered part of the structure.[5] ADDSYM found no missed symmetry elements. The structure is severely disordered, and an approximate, heavily restrained disorder model was refined. The identifiable contents of the asymmetric unit consist of two crystallographically independent $\{C_{49}H_{48}B_2N_4O_8\}$ polymeric chain repeat units. These are comprised of one $C_{25}H_{32}(B_2O_2C_6H_3NO_2)_2$ grouping bonded to one $C_{12}H_{10}N_2$ ligand. Atoms of each independent chain were given atom label suffixes A or B. One $-BO_2C_6H_3NO_2$ substituent (B2B, N2B, O5B-O8B, C20B-C25B) of chain "B" is disordered over two orientations *via* a near-180° rotation about the C11B-B2B bond. Atoms of the second component of this group were given the label suffix C. Atoms of both components of these groups were refined isotropically with fixed occupancies of 50%. Both disorder components were restrained to be similar to an ordered group in chain "A" with SHELX SAME instructions. Three of the four hexyl substituents are disordered. Hexyl group C32B-C37B refined normally. Reasonable positions for atoms near the ends of the disordered hexyl chain were picked from Fourier maps. They could not be refined freely, and likely are scrambled over several different positions. For the final model, one orientation was refined. Hexyl group carbon atoms were restrained with C-C bond distance restraints of

1.54(2) Å and 1,3 C-C distance restraints of 2.6(2) Å. Some isotropic displacement parameters were fixed at the arbitrary value of 0.25 $Å^2$. All other non-hydrogen atoms were refined with anisotropic displacement parameters. Hydrogen atoms bonded to carbon were located in Fourier difference maps before being placed in geometrically idealized positions and included as riding atoms with *d*(C-H) = 0.95 Å and *U*iso(H) = 1.2*U*eq(C) for aromatic hydrogen atoms, *d*(C-H) = 0.99 Å and *U*iso(H) = 1.2*U*eq(C) for methylene hydrogen atoms and *d*(C-H) = 0.98 Å and *U*iso(H) = 1.5*U*eq(C) for methyl hydrogens. In addition to the disorder within the main part of the structure, a large volume of severely disordered electron density was located between the chains, assumed to be solvent guests. No reasonable disorder model could be achieved for these species, and they were accounted for using the Squeeze technique implemented in PLATON.[5] The solvent-accessible volume was calculated to be 2516 $Å^3$ per unit cell (39% of the total cell volume), containing the equivalent of 669 electrons per unit cell. The scattering contribution of this electron density was added to the structure factors computed from the known part of the structure during refinement. The reported crystal density and *F*.*W*. are calculated from the known part of the structure only. The largest residual electron density peak in the final difference map is 0.33 $e^-/Å^3$, located 0.88 Å from H31B. Because of the absence of heavy atoms in the crystal, the absolute structure was not established. The reported data clearly establishes the general structure of the material; however because of data quality limitations and the strongly disordered nature of the crystal, only the broader features of the structure, such as connectivity and dimensionality, are reliable.

(1) APEX3 Version 2016.5-0 and SAINT+ Version 8.37A. Bruker AXS, Inc., Madison, Wisconsin, USA, 2016.
(2) SADABS-2016/2: Krause, L., Herbst-Irmer, R., Sheldrick G.M. and Stalke D. *J. Appl. Cryst.* 2015, *48*, 3-10.
(3) (a) SHELXT: Sheldrick, G.M. *Acta Cryst*. 2015, *A71*, 3-8. (b) SHELXL: Sheldrick, G.M. *Acta Cryst*. 2008, A64, 112-122.
(4) OLEX2: a complete structure solution, refinement and analysis program. Dolomanov, O. V., Bourhis, L. J., Gildea, R. J., Howard J. A. K. and Puschmann, H. *J. Appl. Cryst.* 2009, *42*, 339-341.
(5) (a) Sluis, P. v.d.; Spek, A. L. *Acta Crystallogr., Sect. A* 1990, *46*, 194-201. (b) PLATON SQUEEZE: Spek, A. L. *Acta Cryst.* 2015, *C71*, 9-18.
Table 1 Crystal data and structure refinement for sas078_43_sq.

Identification code	sas078_43_sq
Empirical formula	$C_{49}H_{48}B_2N_4O_8$
Formula weight	842.53
Temperature/K	301(2)
Crystal system	monoclinic
Space group	$P2_1$
a/Å	18.421(3)
b/Å	16.398(2)
c/Å	22.799(3)
α/°	90
β/°	110.275(3)
γ/°	90
Volume/Å^3	6460.5(15)
Z	4
ρ_{calc}g/cm^3	0.866
μ/mm^{-1}	0.059
F(000)	1776.0
Crystal size/mm^3	0.48 × 0.4 × 0.06
Radiation	MoKα (λ = 0.71073)
2Θ range for data collection/°	4.298 to 40.776
Index ranges	-16 ≤ h ≤ 18, -16 ≤ k ≤ 16, -22 ≤ l ≤ 22
Reflections collected	40223
Independent reflections	12704 [R_{int} = 0.0618, R_{sigma} = 0.0720]
Data/restraints/parameters	12704/201/1039
Goodness-of-fit on F^2	0.995
Final R indexes [I>=2σ (I)]	R_1 = 0.0851, wR_2 = 0.2281
Final R indexes [all data]	R_1 = 0.1289, wR_2 = 0.2646
Largest diff. peak/hole / e Å^{-3}	0.33/-0.38

Table A.10: Crystal data for Nitrocatechol CP.

A.11 Single Crystal Information for Toluene Derived Macrocycle (301 K)

[(C37H40B2O4)2(C12H10N2)2]·(C7H8)3.46 (SAS78167_3xrd_RT)

X-ray intensity data from an orange blocklike crystal were collected at 301(2) K using a Bruker D8 QUEST diffractometer equipped with a PHOTON-100 CMOS area detector and an Incoatec microfocus source (Mo Kα radiation, λ = 0.71073 Å). The raw area detector data frames were reduced and corrected for absorption effects using the Bruker APEX3, SAINT+ and SADABS programs.[1,2] The structure was solved with SHELXT.[3] Subsequent difference Fourier calculations and full-matrix least-squares refinement against F^2 were performed with SHELXL-2018[3] using OLEX2.[4]

The compound crystallizes in the triclinic system. The space group *P*-1 (No. 2) was confirmed by structure solution. The asymmetric unit consists of half of one $[(C_{37}H_{40}B_2O_4)_2(C_{12}H_{10}N_2)_2]$ molecule located on a crystallographic inversion center, and three independent regions of electron density modeled reasonably well as disordered, fractionally occupied toluene molecules. Toluene molecules C54-C60 and C75-C81 are disordered about inversion centers. The site occupancy of C54-C60 refined freely to about 50% and was fixed at half-occupancy for the final cycles. Toluene molecules C61-C67 and C68-C74 are disordered over two orientations on a general position with refined populations of 0.543(6) and 0.457(6), respectively, which were constrained to sum to one. The disorder and occupancy of C75-C80 is linked with that of C61-C67/C68-C74 such that when component C61-C67 is present in a given asymmetric unit, both disordered components of C75-C80 are absent for steric reasons. The C75-C80 occupancy was therefore fixed at half the occupancy of C61-C67. The toluene molecules were refined as

rigid hexagons and distance restraints were applied to the methyl groups. Both unique hexyl chains are disordered over two orientations starting with the third carbon from the fluorene base. Appropriate 1,2- and 1,3-C-C distance restraints were applied to these atoms. Hydrogen atoms bonded to carbon were placed in geometrically idealized positions and included as riding atoms with *d*(C-H) = 0.95 Å and *U*iso(H) = 1.2*U*eq(C) for aromatic hydrogen atoms, *d*(C-H) = 0.99 Å and *U*iso(H) = 1.2*U*eq(C) for methylene hydrogen atoms, and *d*(C-H) = 0.98 Å and *U*iso(H) = 1.5*U*eq(C) for methyl hydrogens. All non-hydrogen atoms were refined with anisotropic displacement parameters except for the toluene atoms (isotropic). Enhanced rigid-bond restraints (SHELX RIGU) and isotropic restraints (ISOR) were applied to the anisotropic displacement parameters of the disordered hexyl group atoms. The largest residual electron density peak in the final difference map is 0.56 $e^-/Å^3$, located 0.70 Å from C54.

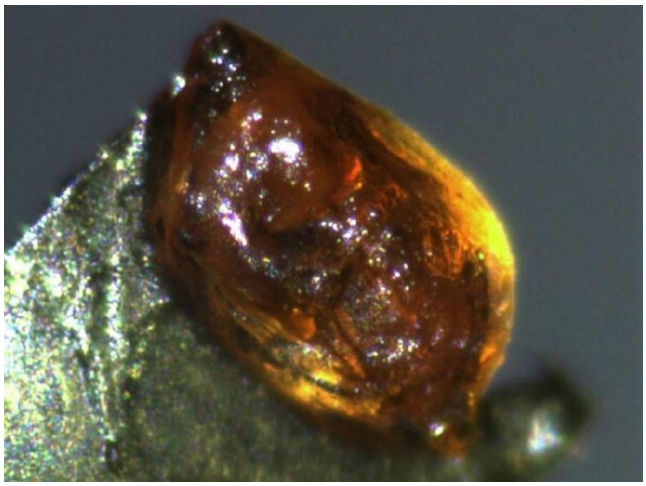

Figure A.7: Single crystal of Toluene Macrocycle (300K).

(1) APEX3 Version 2018.1-0 and SAINT+ Version 8.38A. Bruker AXS, Inc., Madison, Wisconsin, USA, 2016.
(2) SADABS-2016/2: Krause, L., Herbst-Irmer, R., Sheldrick G.M. and Stalke D. *J. Appl. Cryst.* 2015, *48*, 3-10.
(3) (a) SHELXT: Sheldrick, G.M. *Acta Cryst*. 2015, *A71*, 3-8. (b) SHELXL: Sheldrick, G.M. *Acta Cryst*. 2015, *C71*, 3-8.
(4) OLEX2: a complete structure solution, refinement and analysis program. Dolomanov, O. V., Bourhis, L. J., Gildea, R. J., Howard J. A. K. and Puschmann, H. *J. Appl. Cryst.* 2009, *42*, 339-341.

Identification code	SAS78167_3xrd
Empirical formula	$C_{122.2}H_{127.66}B_4N_4O_8$
Formula weight	1823.58
Temperature/K	301(2)
Crystal system	triclinic
Space group	P-1
a/Å	11.6037(6)
b/Å	13.5369(7)
c/Å	17.7832(9)
α/°	83.227(2)
β/°	83.324(2)
γ/°	79.061(2)
Volume/Å^3	2710.8(2)
Z	1
ρ_{calc}g/cm^3	1.117
μ/mm^{-1}	0.068
F(000)	973.0
Crystal size/mm^3	0.6 × 0.42 × 0.24
Radiation	MoKα (λ = 0.71073)
2Θ range for data collection/°	2.316 to 52.84
Index ranges	-14 ≤ h ≤ 14, -16 ≤ k ≤ 16, -22 ≤ l ≤ 22
Reflections collected	83948
Independent reflections	11088 [R_{int} = 0.0493, R_{sigma} = 0.0252]
Data/restraints/parameters	11088/130/600
Goodness-of-fit on F^2	1.046
Final R indexes [I>=2σ (I)]	R_1 = 0.0738, wR_2 = 0.2206
Final R indexes [all data]	R_1 = 0.0971, wR_2 = 0.2490
Largest diff. peak/hole / e Å^{-3}	0.56/-0.30

Table A.11: Single crystal data for toluene derived macrocycle (300 K).

A.12 Single Crystal Information for Benzene SCSC Transitioned from Toluene Derived Macrocycle

X-Ray Structure Determination, ⁅(C37H40B2O4)2(C12H10N2)2]·(C6H6)4 (SAS78161.3 BV)

X-ray intensity data from an irregular orange crystal were collected at 100(2) K using a Bruker D8 QUEST diffractometer equipped with a PHOTON-100 CMOS area detector and an Incoatec microfocus source (Mo Kα radiation, λ = 0.71073 Å). The data crystal was cleaved from a large aggregation, which appeared red in color in massive form, then orange when moderately thick and then yellow when thinner. The raw area detector data frames were reduced and corrected for absorption effects using the Bruker APEX3, SAINT+ and SADABS programs.[1,2] The structure was solved with SHELXT.[3] Subsequent difference Fourier calculations and full-matrix least-squares refinement against F^2 were performed with SHELXL-2018[3] using OLEX2.[4]

The compound crystallizes in the triclinic system. The space group *P*-1 (No. 2) was confirmed by structure solution. The asymmetric unit consists of half of one $[(C_{37}H_{40}B_2O_4)_2(C_{12}H_{10}N_2)_2]$ complex located on a crystallographic inversion center, and three independent benzene molecules. Benzene C51-C53 is located on a crystallographic inversion center and only half is present per asymmetric unit. Benzene C54-C60 is disordered about an inversion center and was refined with half-occupancy with all C-C distances restrained to be similar (SHELX SADI). Benzene C61-C66 is ordered on a general position. Hydrogen atoms bonded to carbon were located in difference Fourier maps before being placed in geometrically idealized positions and included as riding atoms with *d*(C-H) = 0.95 Å and *U*iso(H) = 1.2*U*eq(C) for arene hydrogen atoms, *d*(C-H) = 0.99 Å and

*U*iso(H) = 1.2*U*eq(C) for methylene hydrogen atoms and *d*(C-H) = 0.98 Å and *U*iso(H) = 1.5*U*eq(C) for methyl hydrogens. The methyl hydrogens were allowed to rotate as a rigid group to the orientation of maximum observed electron density. All non-hydrogen atoms were refined with anisotropic displacement parameters. The largest residual electron density peak in the final difference map is 0.39 $e^-/Å^3$, located 0.83 Å from H60.

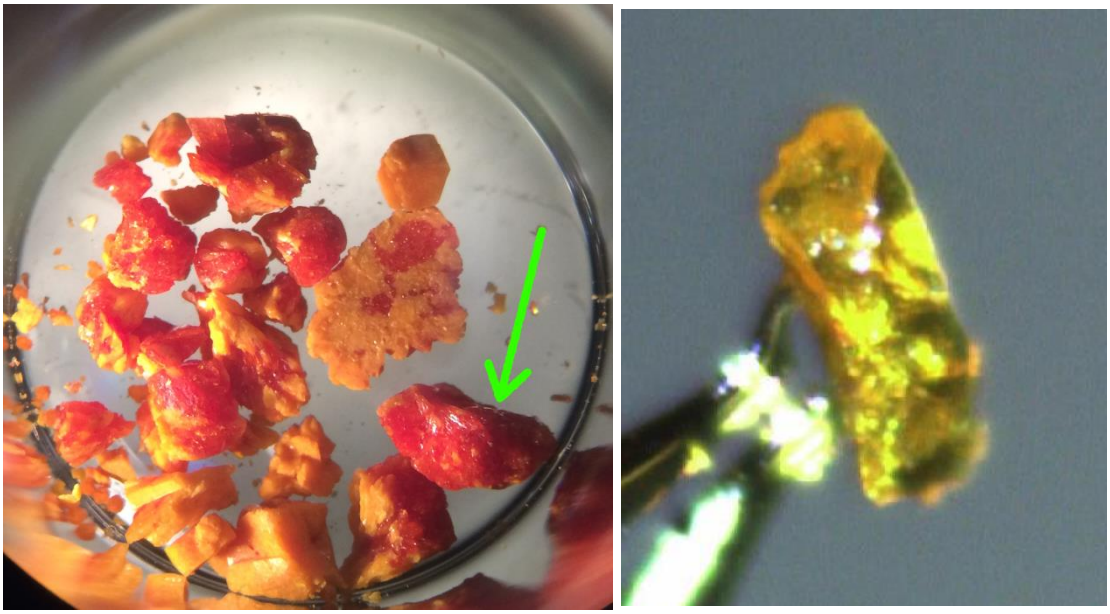

Figure A.8: Single crystal of benzene SCSC transitioned macrocycle originally derived in toluene. Sample as received. The crystal used for data collection (right) was cleaved from the red crystalline aggregation indicated by the green arrow in the left image.

(1) APEX3 Version 2018.1-0 and SAINT+ Version 8.38A. Bruker AXS, Inc., Madison, Wisconsin, USA, 2016.
(2) SADABS-2016/2: Krause, L., Herbst-Irmer, R., Sheldrick G.M. and Stalke D. *J. Appl. Cryst.* 2015, *48*, 3-10.
(3) (a) SHELXT: Sheldrick, G.M. *Acta Cryst*. 2015, *A71*, 3-8. (b) SHELXL: Sheldrick, G.M. *Acta Cryst*. 2015, *C71*, 3-8.
(4) OLEX2: a complete structure solution, refinement and analysis program. Dolomanov, O. V., Bourhis, L. J., Gildea, R. J., Howard J. A. K. and Puschmann, H. *J. Appl. Cryst.* 2009, *42*, 339-341.

Identification code	sas78163bv
Empirical formula	$C_{122}H_{124}B_4N_4O_8$
Formula weight	1817.48
Temperature/K	100(2)
Crystal system	triclinic
Space group	P-1
a/Å	11.5851(3)
b/Å	13.4695(3)
c/Å	17.2578(4)
α/°	82.5370(10)
β/°	82.8110(10)
γ/°	80.7410(10)
Volume/Å^3	2620.41(11)
Z	1
ρ_{calc}g/cm^3	1.152
μ/mm^{-1}	0.070
F(000)	968.0
Crystal size/mm^3	0.3 × 0.12 × 0.1
Radiation	MoKα (λ = 0.71073)
2Θ range for data collection/°	2.394 to 52.868
Index ranges	-14 ≤ h ≤ 14, -16 ≤ k ≤ 16, -21 ≤ l ≤ 21
Reflections collected	76203
Independent reflections	10771 [R_{int} = 0.0642, R_{sigma} = 0.0342]
Data/restraints/parameters	10771/15/652
Goodness-of-fit on F^2	1.033
Final R indexes [I>=2σ (I)]	R_1 = 0.0494, wR_2 = 0.1178
Final R indexes [all data]	R_1 = 0.0693, wR_2 = 0.1310
Largest diff. peak/hole / e Å^{-3}	0.54/-0.56

Table A.12: Single crystal data for benzene SCSC transitioned from toluene derived macrocycle.

A.13 Single Crystal Information for Hexafluorobenzene SCSC Transitioned from Benzene SCSC Transitioned Macrocycle

[(C37H40B2O4)2(C12H10N2)2]·(C6H6)2(C6F6)2 (SAS75102.13 hexafluorobenzene)

Crystals of the compound were generally orange-yellow in color, with the bulk sample appearing orange and individual crystals a lighter yellow when cleaved thin. All crystals showed extensive internal fracturing. The diffraction pattern indicated degraded crystallinity with broad and tailed peak shapes and faint powder rings at lower angles. Bragg intensities was strong at low angle but diminished rapidly at higher angles. Analysis of the dataset with the Bruker XPREP program showed the mean reflection $I/\sigma(I)$ fell below 2.0 at d = 0.95 Å (2ϑ = 43.9°), and the dataset was truncated at that value. X-ray intensity were collected at 100(2) K using a Bruker D8 QUEST diffractometer equipped with a PHOTON-100 CMOS area detector and an Incoatec microfocus source (Mo K radiation, = 0.71073 Å). The raw area detector data frames were reduced and corrected for absorption effects using the Bruker APEX3, SAINT+ and SADABS programs.[1,2] Final unit cell parameters were determined by least-squares refinement of 7397 reflections taken from the data set. The structure was solved with SHELXT.[3] Subsequent difference Fourier calculations and full-matrix least-squares refinement against F^2 were performed with SHELXL-2017[3] using OLEX2.[4]

The compound crystallizes in the triclinic system. The space group *P*-1 (No. 2) was confirmed by structure solution. The asymmetric unit consists of half of one $[(C_{37}H_{40}B_2O_4)_2(C_{12}H_{10}N_2)_2)]$ cycle located on a crystallographic inversion center, one hexafluorobenzene molecule and one benzene molecule. The hexyl substituent C26-C31

is disordered over two positions with fractional occupancies A/B = 0.614(5)/0.386(5), which were constrained to sum to one. C-C distances in the disordered part of the chain were restrained to be similar to one another using SHELX SADI restraints. A spherical restraint was applied to the anisotropic displacement parameters of the terminal hexyl chain atoms C35-C37 (SHELX ISOR). Both the hexafluorobenzene (C51-C56/F51-F56) and the benzene (C61-C66) molecules are disordered over two closely spaced positions each with occupancies of C51-C56/F51-F56 A/B = 0.702(5)/0.298(5) and C61-C66 A/B = 0.51(1)/0.49(1), also constrained to sum to one. The C_6 rings of each molecule were refined as rigid hexagons with *d*(C-C) = 1.39 Å. C-F distances were restrained to be similar (SADI). The geometry of the minor component was restrained to be similar to that of the major using a SAME instruction. Displacement parameters for nearly superimposed atoms of all disorder components were held equal. Non-hydrogen atoms were refined with anisotropic displacement parameters. Hydrogen atoms bonded to carbon were placed in geometrically idealized positions and included as riding atoms with *d*(C-H) = 0.95 Å and *U*iso(H) = 1.2*U*eq(C) for aromatic hydrogen atoms, *d*(C-H) = 0.99 Å and *U*iso(H) = 1.2*U*eq(C) for methylene hydrogen atoms, and *d*(C-H) = 0.98 Å and *U*iso(H) = 1.5*U*eq(C) for methyl hydrogens. The methyl hydrogens were allowed to rotate as a rigid group to the orientation of maximum observed electron density. The largest residual electron density peak in the final difference map is 0.39 $e^-/Å^3$, located 1.14 Å from F53B.

(1) APEX3 Version 2016.5-0 and SAINT+ Version 8.37A. Bruker AXS, Inc., Madison, Wisconsin, USA, 2016.
(2) SADABS-2016/2: Krause, L., Herbst-Irmer, R., Sheldrick G.M. and Stalke D. *J. Appl. Cryst.* 2015, *48*, 3-10.
(3) (a) SHELXT: Sheldrick, G.M. *Acta Cryst*. 2015, *A71*, 3-8. (b) SHELXL: Sheldrick, G.M. *Acta Cryst*. 2015, *C71*, 3-8.
(4) OLEX2: a complete structure solution, refinement and analysis program. Dolomanov, O. V., Bourhis, L. J., Gildea, R. J., Howard J. A. K. and Puschmann, H. *J. Appl. Cryst.* 2009, *42*, 339-341.

Identification code	SAS75102_13
Empirical formula	$C_{122}H_{112}B_4F_{12}N_4O_8$
Formula weight	2033.39
Temperature/K	100(2)
Crystal system	triclinic
Space group	P-1
a/Å	11.4836(8)
b/Å	13.0982(9)
c/Å	17.9150(13)
α/°	82.719(2)
β/°	83.912(2)
γ/°	81.075(2)
Volume/Å^3	2630.3(3)
Z	1
ρ_{calc}g/cm^3	1.284
μ/mm^{-1}	0.093
F(000)	1064.0
Crystal size/mm^3	0.28 × 0.22 × 0.12
Radiation	MoKα (λ = 0.71073)
2Θ range for data collection/°	4.444 to 43.928
Index ranges	-12 ≤ h ≤ 12, -13 ≤ k ≤ 13, -18 ≤ l ≤ 18
Reflections collected	29757
Independent reflections	6409 [R_{int} = 0.0770, R_{sigma} = 0.0559]
Data/restraints/parameters	6409/154/740
Goodness-of-fit on F^2	1.018
Final R indexes [I>=2σ (I)]	R_1 = 0.0628, wR_2 = 0.1479
Final R indexes [all data]	R_1 = 0.1076, wR_2 = 0.1748
Largest diff. peak/hole / e Å^{-3}	0.39/-0.33

Table A.13: Single crystal data for hexafluorobenzene SCSC transitioned from benzene SCSC transitioned macrocycle.